Assessment of the harmonic behaviour of a utility-scale photovoltaic plant

by
Jonathan Stephen Overett

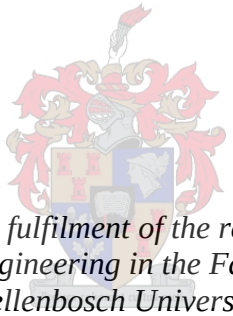

Thesis presented in partial fulfilment of the requirements for the degree Master of Science in Engineering in the Faculty of Engineering at Stellenbosch University

Supervisor: Prof. Hendrik Johannes Vermeulen
Department of Electrical & Electronic Engineering

December 2017

Declaration

- I have read and understand the Stellenbosch University Policy on Plagiarism and the definitions of plagiarism and self-plagiarism contained in the Policy [Plagiarism: The use of the ideas or material of others without acknowledgement, or the re-use of one's own previously evaluated or published material without acknowledgement or indication thereof (self-plagiarism or text-recycling)].
- I also understand that direct translations are plagiarism.
- Accordingly all quotations and contributions from any source whatsoever (including the internet) have been cited fully. I understand that the reproduction of text without quotation marks (even when the source is cited) is plagiarism.
- I declare that the work contained in this assignment is my own work and that I have not previously (in its entirety or in part) submitted it for grading in this module/assignment or another module/assignment.

J.S. Overett
December 2017

Abstract

The rapidly increasing deployment of utility-scale solar photovoltaic (PV) plants worldwide presents new technical challenges including the risk of unacceptably high harmonic voltage distortion in the utility network. PV plants affect the harmonic voltage distortion at their point of common coupling primarily by two distinct mechanisms: generation of harmonic currents due to switching action of the inverters and introduction of series and parallel resonances caused by connection of the plant to the network. The objective of this study is to investigate the harmonic behaviour of utility-scale PV plants based on the case-study of a 75 MW PV plant in the Northern Cape province of South Africa.

In this work, a harmonic simulation model of a PV plant is developed in DIgSILENT PowerFactory which represents the passive network components with sufficient accuracy to study the frequency response over the harmonic frequency band from 50 to 2500 Hz. 10-minute and 3-second aggregated harmonic measurement data and event-triggered waveform data were captured over a 12-day period using an IEC 61000-4-30 Class A power quality meter installed at the plant's 132 kV point of connection (POC). A quality assessment of harmonic measurement data shows that the accuracy of harmonic voltage and current measurements are likely to be significantly affected by quantisation and transducer error for even and higher-order harmonics. Analysis of the 3-second aggregated harmonic quantities indicates that their fluctuation during each 10-minute period is sufficiently small that the 10-minute average values adequately approximate the short-term and long-term behaviour of the plant.

The harmonic behaviour of the plant is investigated by considering the relationship between harmonic voltage and current emissions and active power, reactive power and time of day. Certain harmonic voltages increase with increasing plant active power output whilst others decrease but all harmonic currents remain constant or increase with increasing active power. It was not possible to quantify the relative impact of active and reactive power variation as the plant operates in voltage control mode. Brief periods of high harmonic current distortion were noted during start up and shut down of the plant. High harmonic currents at the 23rd harmonic order correspond with a series resonance identified in the model thus validating the POC frequency sweep simulation.

A comparative analysis of different published methods for assessment of the harmonic emissions contribution of the PV plant is performed. All methods show similar trends in identifying dominant harmonics and general harmonic behaviour but the magnitudes of the calculated emissions differ significantly in some instances. Where accurate frequency sweep data of the utility network and phasor measurement data are both available, the plant model enables application of the harmonic vector method to discriminate between utility and plant contributions. Simulated voltage emissions based using the manufacturer's quoted inverter current emissions do not closely match measured emissions due to the complexity of active source interactions within the real power system. Comparison of the mean, 75th percentile and 90th percentile emissions assessments demonstrate the effectiveness of percentile assessment in eliminating outlying high distortion periods from the assessed results.

Opsomming

Die vinnige toenemende implementering van grootskaalse sonkragfotovoltaïese (PV) aanlegte wêreldwyd, bied nuwe tegniese uitdagings, insluitende die risiko van onaanvaarbare hoë harmoniese spanningvervorming in die netwerk. PV aanlegte beïnvloed die harmoniese spanningvervorming by hul punt van algemene koppeling, hoofsaaklik deur twee afsonderlike meganismes: die opwekking van harmoniese strome as gevolg van die skakel aksie van die omkeerders en die inleiding van reeks en parallelle resonansies wat veroorsaak word deur die koppel van die kragstasie aan die netwerk. Die doel van hierdie studie is om die harmoniese gedrag van grootskaalse-PV aanlegte te ondersoek, gebaseer op die gevallestudie van 'n 75 MW PV kragstasie in die Noord-Kaaps provinsie van Suid-Afrika.

In hierdie werk word 'n harmoniese simulasiemodel van 'n PV-aanleg ontwikkel in DIgSILENT PowerFactory, wat die passiewe netwerk komponente verteenwoordig met voldoende akkuraatheid, om die frekwensieweergawe oor die harmoniese frekwensieband van 50 tot 2500 Hz te bestudeer. 10-minute en 3-sekonde geaggregeerde harmoniese metingsdata en gebeurtenisgeaktiveerde golfvormdata is oor 'n tydperk van 12 dae opgeneem met behulp van 'n IEC 61000-4-30 klas A kragkwaliteitsmeter geïnstalleer by die substasie se 132 kV punt van verbinding (POC). 'n Kwaliteitsbeoordeling van harmoniese metingsdata toon dat die akkuraatheid van harmoniese spanning en stroommetings waarskynlik aansienlik beïnvloed sal word deur kwantiserings en oorvormer foute vir ewe en hoër-orde harmonieke. Analise van die 3-sekonde geaggregeerde harmoniese waardes dui aan dat hul fluktuasie gedurende elke 10 minute tydperk klein genoeg is, sodat die 10-minute gemiddelde waardes die korttermyn- en langtermyngedrag van die aanleg ‘n voldoende benadering is.

Die harmoniese gedrag van die aanleg word ondersoek deur die verband tussen harmoniese spanning en stroom emissies en aktiewe krag, reaktiewe krag en tyd van die dag te oorweeg. Sekere harmoniese spannings verhoog met toenemende aktiewe kraguitset, terwyl ander afneem, maar alle harmoniese strome bly konstant of verhoog met toenemende aktiewe kraguitset. Dit was nie moontlik om die relatiewe impak van aktiewe en reaktiewe kragvariasie te kwantifiseer nie aangesien die aanleg in die spanningskontrolemodus funksioneer. Kort tydperke van hoë harmoniese stroomvervorming is tydens die aanvang en afsluiting van die aanleg opgemerk. Hoë harmoniese strome op die 23ste harmoniek stem ooreen met 'n reeks resonansie wat in die model geïdentifiseer is en dus valideer die POC-frekwensie sweep simulasie.

'n Vergelykende analise van verskillende gepubliseerde metodes vir die assessering van die harmoniese emissie bydrae van die PV-aanleg word uitgevoer. Alle metodes toon soortgelyke neigings in die identifisering van dominante harmonieke en algemene harmoniese gedrag, maar die groottes van die berekende emissies verskil in sommige gevalle beduidend. Waar akkurate frekwensie sweep data van die netwerk en fasor meting data albei beskikbaar is, maak die model dit moontlik vir die toepassing van die harmoniese vektor metode om te onderskei tussen netwerk en PV-aanleg bydraes. Gesimuleerde spanningsemissies gebaseer op die vervaardiger se verklaarde omkeerder-emissies, pas nie noukeurig ooreen met gemete emissies nie as gevolg van die kompleksiteit van aktiewe broninteraksies binne die werklike kragstelsel. Vergelyking van die gemiddelde 75ste persentiel- en 90ste persentielemissiesevaluasies toon die effektiwiteit van persentielassessering om die afgeleë hoë vervormingsperiode uit die geassesseerde resultate te elimineer.

Acknowledgements

The author gratefully acknowledges the contributions of the following people:

- My research supervisor, Prof. Johan Vermeulen, for his guidance in the research. His insights, good humour and pragmatic approach were invaluable in motivating and inspiring me to see the research through to its completion.
- My managers and colleagues at Aurecon for their support through the course of my studies and in acquiring metering data from the PV plant. Paul Nel, Jannie Meuter, Olaf von Abo, Duan Serfontein, Francois De Jager and the late Das Venter amongst others have all contributed in various ways to the research or to my knowledge and interest in the field in general.
- Willie van Wyk, Charl Marais and Jacobus van Zyl of CT Labs for assistance relating to the ImpedoDUO meters.
- Lindsay Collier for her continued support, encouragement and patience.
- My parents, Dan and Jenny Overett, for their continued love and support through the years.

Table of Contents

Declaration ..... **i**

Abstract ..... **ii**

Opsomming ..... **iii**

Acknowledgements ..... **iv**

Table of Contents ..... **v**

List of Figures ..... **ix**

List of Tables ..... **xiv**

1 Project description and motivation **1**

1.1 Introduction 1

1.2 Project motivation 2

1.3 Project description 4
1.3.1 Research objectives 4
1.3.2 Research methodology 5

1.4 Thesis structure 7

2 Literature review **9**

2.1 Overview 9

2.2 Solar PV background 9
2.2.1 Global solar PV market 9
2.2.2 Electricity market in South Africa 10
2.2.3 Solar PV in South Africa 11
2.2.4 Solar PV and quality of supply 12

2.3 Impact of harmonic distortion 12

2.4 Management of harmonic distortion and QoS standards 13
2.4.1 Basic principles of harmonic distortion management 13
2.4.2 Harmonic standards 15

2.5 Mitigation 18

2.6 Power system harmonic analysis overview 18
2.6.1 Fundamentals of harmonic analysis 18
2.6.2 Sequence component theory 21
2.6.3 Harmonic indices 23
2.6.4 Harmonic propagation, cancellation and attenuation 24

2.7 Harmonic resonance in power systems ... 25
2.7.1 Overview ... 25
2.7.2 Parallel resonance ... 25
2.7.3 Series resonance ... 27
2.7.4 Frequency dependence of impedance in power systems ... 28
2.7.5 Elimination of problematic harmonic resonant peaks ... 29

2.8 Solar PV plant technology ... 30
2.8.1 PV plant overview ... 30
2.8.2 Voltage source converter theory ... 32
2.8.3 Pulse-Width Modulation (PWM) ... 33
2.8.4 Harmonic behaviour of solar PV inverters ... 35
2.8.5 Harmonic control and mitigation strategies for inverters ... 37

2.9 Harmonic simulations ... 38

2.10 Analysis of harmonic measurements ... 40
2.10.2 Measurement-based methods for determination of emission contribution from an installation ... 41
2.10.3 Measurement-based methods for harmonic impedance estimation ... 45

2.11 Review of case studies related to power system harmonics and solar PV ... 46

2.12 Modelling techniques for harmonic simulations ... 47
2.12.1 Introduction ... 47
2.12.2 PWM solar inverters ... 48
2.12.3 Overhead lines ... 48
2.12.4 Cables ... 50
2.12.5 Power transformers ... 51
2.12.6 Capacitors, reactors and filter banks ... 53
2.12.7 Modelling of the utility network and network simplification ... 54
2.12.8 Load models ... 55

2.13 Software simulation tools ... 56
2.13.1 Introduction ... 56
2.13.2 DIgSILENT PowerFactory ... 56
2.13.3 Matlab/Simulink ... 57
2.13.4 Electromagnetic Transient Programs ... 57
2.13.5 Other Harmonic Analysis Programmes ... 57

2.14 Harmonic measurement ... 57
2.14.1 Quality of supply meters ... 58
2.14.2 Transducers ... 58

3 Frequency response of a solar PV plant ... 62

3.1 Simplified network model ... 62
3.1.1 Cable model ... 62
3.1.2 Transformer model ... 63

3.2 Cable frequency response ... 66

3.3 Park transformer frequency response ... 67
3.3.1 Primary terminals, secondary open circuit ... 67
3.3.2 Secondary terminals, primary open circuit ... 68
3.3.3 Primary terminals, secondary short circuit ... 69
3.3.4 Secondary terminals, primary short circuit ... 69

3.4 Inverter transformer frequency response 71
3.4.1 Primary terminals, secondary open circuit 71
3.4.2 Secondary terminals, primary open circuit 71
3.4.3 Primary terminals, secondary short circuit 71
3.4.4 Secondary terminals, primary short circuit 71

3.5 System frequency response 75
3.5.1 Point of connection, inverter terminals open circuit 75
3.5.2 Inverter terminals, point of connection open circuit 76
3.5.3 Point of connection, inverter terminals short circuit 77
3.5.4 Inverter terminals, point of connection short circuit 77
3.5.5 Point of connection, linear network impedance 79

3.6 Comparison of simplified model and complete PV plant frequency response 79
3.6.1 Point of connection, inverter terminals open circuit 82
3.6.2 Inverter terminals, point of connection open circuit 83
3.6.3 Point of connection, inverter terminals short circuit 83
3.6.4 Inverter terminals, point of connection short circuit 83
3.6.5 Point of connection, including external network 85
3.6.6 Inverter terminals, including external network 85

4 Analysis of harmonic measurements 87

4.1 Site description 87

4.2 Measurement data 88
4.2.1 Site power quality measurement installation 88
4.2.2 Measurement accuracy 90
4.2.2.1 Transducer error 90
4.2.3 Measurement trends 91
4.2.4 Comparison of the 3-second aggregated values and the 10-minute aggregated values 95
4.2.5 Extraction of harmonic components from event triggered waveform recordings 100
4.2.6 Conclusions from quality assessment of harmonic measurement data 104

4.3 Evaluation of plant harmonic behaviour 104
4.3.1 Variation of harmonic emissions with plant active power output 104
4.3.2 Variation of harmonic emissions with plant reactive power output 107
4.3.3 Variation of harmonic emissions with time of day 109

5 Comparative analysis of harmonic emission assessment calculation methods 111
5.1.1 Background harmonic emission calculation methodology 111

5.2 Background harmonic emission calculation results 114
5.2.1 Linear regression of harmonic voltage versus installation apparent power demand 114
5.2.2 Background harmonic voltage assessment 116

5.3 Current harmonic emissions for non-operational periods 120

5.4 Harmonic voltage emissions during plant operation 122
5.4.1 Phase components 122
5.4.2 Sequence Components 123

5.5 Harmonic current emissions during plant operation 125
5.5.1 Phase components 125
5.5.2 Sequence components 126

5.6 Comparative assessment of harmonic emissions calculation methods 128

5.6.1 Calculation method 1: Reverse application of the general summation law 128
5.6.2 Calculation method 2: Harmonic voltage phasor method 129
5.6.3 Calculation method 3: IEC 61000-3-6 long-duration simultaneous measurement of harmonic voltages and currents 134
5.6.4 Calculation method 4: Harmonic vector method 138
5.6.5 Calculation method 5: Harmonic load flow simulation 141
5.6.6 Comparison of calculation results for dominant harmonic orders 142
5.6.7 Comparison of mean, 75th percentile and 95th percentile emissions 144

6 Conclusions and recommendations 148

6.1 Introduction 148

6.2 Conclusions 148
6.2.1 Overview 148
6.2.2 Development of a harmonic simulation model of a solar PV plant and evaluation of the frequency response of the plant using the model 148
6.2.3 Quality assessment of harmonic measurement data captured at a utility-scale PV plant 149
6.2.4 Investigation of the harmonic behaviour of the PV plant based on trends in the recorded harmonic voltages and currents under different operating conditions of the plant 151
6.2.5 Comparative analysis of different methods of assessing the harmonic emissions contribution of the PV plant 151

6.3 Recommendations 155

7 References 157

Appendix A Scatter plots of POC harmonic voltage and current vs active and reactive power

Appendix B Scatter plots of POC harmonic voltage and current vs time of day

Appendix C Bar plots of mean background and operating harmonic voltages and currents

Appendix D Emissions calculation results for red, white and blue phases

List of Figures

Figure 2-1: REIPPP wind and solar PV projects – Round 1 to Round 3 (Compiled from [33] and [3]) 11
Figure 2-2: Harmonic disturbance, equipment immunity and compatibility levels [8] 14
Figure 2-3: Parallel resonance circuit 26
Figure 2-4: Frequency sweep of parallel resonant network 27
Figure 2-5: Series resonance circuit 27
Figure 2-6: Frequency sweep of series resonant network 28
Figure 2-7: Network impedance magnitude and angle plotted versus frequency [56] 29
Figure 2-8: Simplified PV plant architecture [65] 31
Figure 2-9: Three-phase, two-level voltage source inverter [69] 32
Figure 2-10: Sinusoidal pulse-width modulation (SPWM) [70] 33
Figure 2-11: Harmonic voltage vs amplitude modulation index for a SPWM inverter [70] 36
Figure 2-12: Harmonic voltage vs amplitude modulation index for a SVM inverter [70] 36
Figure 2-13: Calculation of background harmonic distortion based on linear regression of voltage harmonic distortion vs installation apparent power demand 42
Figure 2-14: Method for long-duration simultaneous measurement of harmonic voltages and currents 43
Figure 2-15: Harmonic voltage phasor method 44
Figure 2-16: Transmission line model 49
Figure 2-17: Fundamental frequency transformer model (T equivalent) [94] 51
Figure 2-18: Second order transformer model [94] 53
Figure 2-19: Shunt capacitor model 53
Figure 2-20: Harmonic impedance locus [136] 55
Figure 3-1: Aggregated PV plant model 62
Figure 3-2: Cable circuit equivalent circuit 63
Figure 3-3: Two-winding transformer equivalent circuit (a) including ideal transformer (b) secondary quantities referred to primary side 64
Figure 3-4: Cable circuit harmonic impedance characteristic – open circuit 66
Figure 3-5: Cable circuit harmonic impedance characteristic – short circuit 67
Figure 3-6: Park transformer harmonic impedance characteristic – primary terminals, secondary open circuit 68
Figure 3-7: Park transformer harmonic impedance characteristic – secondary terminals, primary open circuit 69
Figure 3-8: Park transformer harmonic impedance characteristic – primary terminals, secondary short circuit 70
Figure 3-9: Park transformer harmonic impedance characteristic – secondary terminals, primary short circuit 70
Figure 3-10: Inverter transformer harmonic impedance characteristic – primary terminals, secondary open circuit 72
Figure 3-11: Inverter transformer harmonic impedance characteristic – secondary terminals, primary open circuit 72

Figure 3-12: Inverter transformer harmonic impedance characteristic – primary terminals, secondary short circuit 73

Figure 3-13: Inverter transformer harmonic impedance characteristic – secondary terminals, primary short circuit 73

Figure 3-14: PV plant equivalent circuit 74

Figure 3-15: PV plant distribution network harmonic impedance characteristic – POC, inverter terminals open circuit..... 76

Figure 3-16: PV plant distribution network harmonic impedance characteristic – inverter terminals, POC open circuit..... 77

Figure 3-17 PV plant distribution network harmonic impedance characteristic – POC, inverter terminals short circuit 78

Figure 3-18: PV plant distribution network harmonic impedance characteristic – inverter terminals, POC short circuit 78

Figure 3-19: POC harmonic impedance characteristic with linear external grid impedance of varying short circuit capacity – inverter terminals open circuit..... 79

Figure 3-20: Full PV plant model of 75 MWac PV plant..... 80

Figure 3-21: Full PV plant distribution network harmonic impedance characteristic – POC, inverter terminals open circuit (with dashed trace of the simplified model characteristic) 82

Figure 3-22: PV plant distribution network harmonic impedance characteristic – inverter terminals, POC open circuit (with dashed trace of the simplified model characteristic) 83

Figure 3-23: PV plant distribution network harmonic impedance characteristic – POC, inverter terminals short circuit (with dashed trace of the simplified model characteristic) 84

Figure 3-24: PV plant distribution network harmonic impedance characteristic – inverter terminals, POC short circuit 84

Figure 3-25: POC harmonic impedance characteristic with simulated external grid impedance (provided by the utility) and linear external grid impedances for minimum and maximum POC short circuit currents – inverter terminals open circuit. Dashed lines represent corresponding network impedances prior to connection of PV plant. 86

Figure 3-26: Furthest inverter terminal harmonic impedance characteristic with simulated external grid impedance (provided by the utility) and linear external grid impedances for minimum and maximum POC short circuit currents..... 86

Figure 4-1: POC frequency sweep prior to connection of the PV plant compared to the linear sweeps for the minimum and maximum fault levels 87

Figure 4-2: Power quality meter installation schematic diagram 88

Figure 4-3: PV Plant fundamental frequency active and reactive power over the recording period..... 91

Figure 4-4: PV Plant fundamental frequency reactive power vs active power relationship..... 91

Figure 4-5: Mean, 95th percentile and maximum values of red-phase 10-minute aggregated secondary harmonic voltage (h = 1 to 25)..... 92

Figure 4-6: Red phase 132 kV VT secondary harmonic 10-minute aggregated voltages (h = 1 - 9) 93

Figure 4-7: Mean, 95th percentile and maximum values of red-phase 10-minute aggregated secondary harmonic current (h = 1 – 25) 94

Figure 4-8: Red phase 132 kV CT secondary 10-minute aggregated harmonic currents (h = 1 - 9)..... 95

Figure 4-9: Red phase 132 kV fundamental frequency current (Ia) – 3 s values and 10-min averages 96

Figure 4-10: Red phase 132 kV fundamental frequency voltage (Va) – 3 s values and 10-min averages 96

Figure 4-11: Standard deviation of 3-second aggregated 3rd harmonic voltages per 10-minute period plotted against the corresponding 10-minute aggregated values. 97

Figure 4-12: 3rd harmonic voltage on 19/04/2015. 3-second aggregated values vs 10-minute aggregated values. 97

Figure 4-13: 95th percentile of 3-second harmonic voltage standard deviation per 10-minute period vs 95th percentile of 10-minute harmonic voltages. 98

Figure 4-14: Standard deviation of 3-second aggregated 3rd harmonic currents per 10-minute period plotted against the corresponding 10-minute aggregated values. 98

Figure 4-15: 3rd harmonic current on 19/04/2015. 3-second aggregated values vs 10-minute aggregated values. 99

Figure 4-16: Standard deviation of 3-second aggregated harmonic currents per 10-minute period plotted against time of day (h = 2 – 10). 99

Figure 4-17: 95th percentile of 3-second harmonic current standard deviation per 10-minute period vs 95th percentile of 10-minute harmonic currents. 100

Figure 4-18: Temporal distribution of event-triggered event recordings. 101

Figure 4-19: Fundamental frequency active and reactive power of processed time-invariant events. 102

Figure 4-20: (a) 3-second aggregated reactive power measurements over full measurement period. Arrows indicate high reactive power output associated with plant start-up. (b) 3-second aggregated reactive power measurements for a 10-minute period during the plant start-up on 19 April 2015. 103

Figure 4-21: 10-minute harmonic voltage emissions vs plant active power generation (h = 2 – 10) Red, white and blue phases represented by red, green and blue dots respectively. 105

Figure 4-22: 10-minute harmonic voltage emissions vs plant active power generation trends based on active power bins of 25% of nominal power. Numbers in brackets in the legend indicate the number of 10-minute values within each power bin. 105

Figure 4-23: 10-minute harmonic current emissions vs plant active power generation (h = 2 – 10) Red, white and blue phases represented by red, green and blue dots respectively. 106

Figure 4-24: 10-minute harmonic current emissions vs plant active power generation trends based on active power bins of 25% of nominal power. Numbers in brackets in the legend indicate the number of 10-minute values within each power bin. 107

Figure 4-25: 10-minute harmonic voltage emissions vs plant reactive power output (h = 2 – 10) Red, white and blue phases represented by red, green and blue dots respectively. 107

Figure 4-26: 10-minute harmonic voltage emissions vs plant reactive power output trends based on 5 MVAr reactive power bins. Numbers in brackets in the legend indicate the number of 10-minute values within each reactive power bin. 108

Figure 4-27: 10-minute harmonic current emissions vs plant reactive power generation (h = 2 – 10) Red, white and blue phases represented by red, green and blue dots respectively. 108

Figure 4-28: 10-minute harmonic current emissions vs plant reactive power output trends based on 5 MVAr reactive power bins. Numbers in brackets in the legend indicate the number of 10-minute values within each reactive power bin. 109

Figure 5-1: Equivalent circuit for evaluation of individual harmonic emissions [58] 113

Figure 5-2: Linear regression of 10-minute voltages vs apparent power for (a) 7th, (b) 3rd and (c) 9th harmonic orders 116

Figure 5-3: Background harmonic voltage assessment results (Red Phase) 117

Figure 5-4: Effect of network and PV plant harmonic impedances in calculation of background harmonic impedance from harmonic measurements taken at night 117

Figure 5-5: Application of $PR_{agg,h} \geq 0.8$ criterion to phase components of calculated event background harmonic emissions 118

Figure 5-6: Calculated sequence components of background harmonic emissions showing application of $PR_{agg,h} \geq 0.8$ criterion 120

Figure 5-7: Mean red phase harmonic currents measured at the POC when the plant is not operating 121

Figure 5-8: Mean harmonic sequence currents measured at the POC when the plant is not operating 121

Figure 5-9: (a) Phase and (b) sequence component phasor diagrams of the third harmonic current in amperes 121

Figure 5-10: Mean red phase harmonic voltages from periods with P > 0 122

Figure 5-11: Mean positive sequence harmonic voltages from measurements during plant operation 124

Figure 5-12: Mean negative sequence harmonic voltages from measurements during plant operation 125

Figure 5-13: Mean red phase harmonic current from measurements during plant operation 125

Figure 5-14: Mean positive sequence harmonic currents from measurements during plant operation 127

Figure 5-15: Mean negative sequence harmonic currents from measurements during plant operation 127

Figure 5-16: Mean harmonic emissions (red phase) – Calculation 1: Reverse application of the general summation law 129

Figure 5-17: Mean harmonic emissions (red phase) – Calculation 2A: Harmonic voltage phasor method, Calculation 2B: Adapted harmonic voltage phasor method 130

Figure 5-18: Phasor diagrams showing individual events as dots, mean V_{poc} phasors as solid arrows and mean V_{bg} phasors as dashed arrows. (a) Normal events 7th harmonic, (b) Start-up events 7th harmonic, (c) Normal events 3rd harmonic 131

Figure 5-19: (a) Effect of small changes in mean of measured voltage magnitude on calculated emission for Method 2B. (b) Effect of changing background voltage level with constant harmonic emission. 134

Figure 5-20: Scatter plot of 7th harmonic 10-minute voltage vs current measurements with network and PV plant harmonic impedances. Red, green and blue lines indicate mean of all red, white and blue harmonic current measurement periods and corresponding mean voltage emissions calculated as $V_{pv} = I*Z_{nw}$. 135

Figure 5-21: Scatter plot of 7th harmonic 10-minute voltage vs current measurements with network and PV plant harmonic impedances. Red, green and blue lines indicate mean of operational red, white and blue phase harmonic current measurement periods (i.e. periods with P > 0) and corresponding mean voltage emissions calculated as $V_{pv} = I*Z_{nw}$ 135

Figure 5-22: Voltage vs current scatter plot of selected dominant harmonic orders 137

Figure 5-23: Red-phase PV plant mean voltage emissions calculated according to Method 3A and 3B 138

Figure 5-24: Thevenin equivalent circuit for evaluation of individual harmonic emissions [110] 138

Figure 5-25: Harmonic vector method [110] 139

Figure 5-26: Mean harmonic emissions (red phase) – Calculation 4: Harmonic vector method 139

Figure 5-27: 3rd harmonic emission calculation for Event 20 – Comparison of voltage phasor method (Method 2) and harmonic vector method (Method 4) 140

Figure 5-28: Inverter harmonic current emissions 141

Figure 5-29: Simulated PV plant harmonic voltage emissions at the POC 142

Figure 5-30: Comparison of calculation methods for normal operation (h = 5, Red phase) 143

Figure 5-31: Comparison of calculation methods for start-up operation (h = 5, Red phase) 143

Figure 5-32: Comparison of calculation methods for normal operation (h = 7, Red phase) 144

Figure 5-33: Comparison of calculation methods for start-up operation (h = 7, Red phase) 144
Figure 5-34: Comparison of mean, P75 and P90 emissions calculations for normal operation (h =5, Red phase) 145
Figure 5-35: Comparison of mean, P75 and P90 emissions calculations for start-up operation (h =5, Red phase) 146
Figure 5-36: Comparison of mean, P75 and P90 emissions calculations for normal operation (h =7, Red phase) 146
Figure 5-37: Comparison of mean, P75 and P90 emissions calculations for normal operation (h =7, Red phase) 147

List of Tables

Table 2-1: Summation exponents 14
Table 3-1: Park transformer and inverter transformer nameplate data 64
Table 3-2: Park transformer and inverter transformer equivalent circuit parameters 65
Table 3-3: Frequency sweep analysis scenarios for transformer harmonic analysis 67
Table 3-4: Frequency sweep analysis scenarios for system harmonic analysis 75
Table 3-5: Park transformer and inverter transformer nameplate data 81
Table 3-6: Park transformer and inverter transformer equivalent circuit parameters 81
Table 3-7: Calculated cable network parameters 81
Table 3-8: Frequency sweep analysis scenarios for system harmonic analysis 82
Table 4-1: Instrument transformer data 89
Table 4-2: Current probe data 89
Table 5-1: Methods for assessment of the harmonic contribution of the PV plant 111
Table 5-2: Methods for assessment of the background harmonic voltage 114
Table 5-3: R^2 values for Vh vs S linear regression 115
Table 5-4: Prevailing ratio, $PR_{agg,h}$, values for normal and start-up events 123
Table 5-5: Prevailing ratio, $PR_{agg,h}$, values for normal and start-up events 126
Table 5-6: Summation exponents 128
Table 5-7: Method 1 calculation data summary 128
Table 5-8: Calculation Method 2A Reliability Heatmap 132
Table 5-9: Calculation Method 2B Reliability Heatmap 133
Table 5-10: Calculation Method 4 Reliability Heatmap 141

1 Project description and motivation

1.1 Introduction

In recent years, the number of solar photovoltaic (PV) generation systems connected to electrical distribution networks worldwide has been rapidly increasing. Solar energy is widely available and PV power offers a clean, renewable energy source which does not emit pollutants during operation and consumes little to no water [1]. The rising cost of energy, technological improvements and rapidly falling costs of PV panels and other PV system components has accelerated the deployment of PV globally.

More solar PV capacity was built worldwide between 2010 and 2014 than in the preceding four decades and the cost of PV systems have reduced by a factor of three in the last six years, with the cost of PV modules reducing by a factor of five in the same period [1]. Deployment of PV generation is realised primarily through two different approaches: 1) multiple small to medium residential or commercial installations which are typically installed on rooftops and connected to the low voltage (LV) distribution network and, 2) large centralised utility-scale solar PV power stations, with multiple large inverters, which are connected to the medium voltage (MV) or high voltage (HV) network [2].

South Africa has recently seen the commissioning of its first utility-scale PV plants, constructed by independent power producer (IPP's) under the government's Renewable Energy Independent Power Producers Procurement Programme (REIPPPP). The programme procures power from privately owned renewable power plants (RPP's) selected in a competitive bidding process on the basis of twenty-year power purchase agreements (PPA's). The programme has to date awarded 79 projects with a combined capacity of 5243 MW. The bulk of the capacity is split between solar PV (39 projects, 1899 MW) and onshore wind projects (27 projects, 2660 MW) with the remaining capacity divided between concentrated solar power, small hydro, biomass and landfill gas generators [3].

The REIPPPP allows for solar PV projects with output power capacities of 5 – 75 MW. The capacity of many of the projects approaches the upper limit of this range with 19 awarded projects having a nominal AC power output capacity greater than 70 MW. Many of these projects are geographically clustered in the Northern Cape Province due to the region's excellent solar resource, low population density and the availability of land to accommodate the extensive arrays of PV cells that constitute the plants [3].

The integration of solar PV generation into the transmission or distribution network introduces several technical challenges, particularly in regions with high penetration of solar PV generation. Challenges to be considered include [4]:

- intermittency and low capacity factor of the solar PV resource. PV without storage cannot be dispatched,
- requirement for energy balancing from other fast response generation types (e.g. gas, hydro, other

renewables or energy storage) to balance PV plant power fluctuations or load fluctuations,

- control of reactive power flow and network voltage profiles,
- protection coordination and prevention of network islanding,
- transient stability and inverter fault ride through capabilities,
- power quality phenomena including voltage fluctuations, flicker and harmonics.

The rapid growth in deployment of utility-scale solar PV plants worldwide, and the ever-increasing capacity of such plants, warrants investigation of these technical challenges. Such investigations are especially relevant to the South African context where the government's REIPPPP programme has seen very rapid growth in renewable energy generation from a base of close to zero in 2011 to an allocation of 5243 MW of renewable energy – including 1899 MW of solar PV generation – due to be completed within the next few years.

1.2 Project motivation

The pulse-width modulation (PWM) inverters used within PV plants inject current harmonics into the distribution / transmission network. This may cause harmonic-sensitive equipment to malfunction if the level of harmonic distortion is too high [5]. The maloperation of control and protection equipment, overloading of power plant – notably power transformers – and the failure of power factor correction capacitors are well-known effects of power system harmonics [6].

Furthermore, harmonic current and voltage distortion can be exacerbated by the introduction of series and parallel resonances caused by connection of a solar PV plant to the network. If a resonant frequency coincides with a harmonic frequency present in the power system – generated by the PV plant or by an external harmonic source –the current or voltage distortion may be amplified, depending on the nature of the resonant impedance [7].

Various national and international standards exist to provide rules and guidelines for the management of power quality within electricity networks. In South Africa, the NRS 048 standard defines the basis for management of power quality [8]. Based on the standards, compatibility levels are defined as external standards for utilities, while planning levels define the utilities' internal power quality objectives. Planning levels in turn are used to determine the limits that are assigned to individual customers – both consumers and generators of electricity. These principles apply to a range of power quality phenomena including harmonic distortion.

Theoretically, the overall power quality performance of the system can be managed by assigning limits to customers and ensuring that they do not exceed their apportioned harmonic limits. In practice, it is often difficult to assess the actual harmonic current contribution of an individual customer. This is particularly true when the customer installation incorporates capacitive elements such as power factor correction capacitors or harmonic filters. A combination of measurements and simulations is therefore required to evaluate compliance [9].

Harmonic modelling of power systems can be difficult. Haplin [10] identifies the following key challenges for harmonic modelling of a new installation:

- Data for new equipment and installations are approximate and may change from initial design to as-built plant status.
- Utility systems are large and very complex so simplification and network reduction are required.
- Data for existing equipment may be limited to harmonic measurements at the Point of Connection (POC). Detailed data from existing customers are often not available.
- Utility network configurations and operating conditions as well as customer equipment operating conditions, configurations and procedures vary widely over time and are difficult to predict.

The ability to determine the harmonic emissions of an individual customer is important to both the utility and the customer. If the utility relies only on its measurement of the global harmonic voltage distortion at designated points in the network, high harmonic emissions from an individual installation may not be detected. This is because the sum of all contributions at the point of measurement may not exceed the utility planning levels even though one or more installation is exceeding its apportionment. The problem may become apparent only after connection of additional customers or after a change in the system configuration. In this case, the management of harmonic distortion will be reactive and customers may be adversely affected until a solution can be found.

Knowledge of the harmonic emissions is also beneficial to the customer so that he can demonstrate compliance to his apportioned limits and avoid penalties or disconnection that may result from violations. Additionally, mitigating measures – such as harmonic filters – can be designed timeously in consultation with the utility, should these be required. RPP's in South Africa are obligated to demonstrate compliance to the requirements of the RPP Grid Code by means of tests or studies, and to continuously monitor their compliance [11]. One of these requirements is that the harmonic current and voltage distortion emitted by the RPP do not exceed the emission limits apportioned by the Network Service Provider (NSP) – i.e. the utility.

As mentioned above, harmonic modelling and the evaluation of harmonic measurement data are the key components used in the evaluation of harmonic emissions from an individual installation. Several papers describe the modelling of individual PV systems to evaluate the PV system's harmonic distortion under various operating conditions [12] [13] [14] [15]. Simulation results are then compared to measurement data from the actual system in order to validate the model. These systems range in size from several kilowatts to 20 MW in the case of the PV plant described in [15]. Modelling has also been done to evaluate the impact of multiple small embedded PV systems, typically in the form of residential rooftop installations [16] [17].

Several other papers present an analysis of the harmonic emissions of solar PV systems based purely on measurement data, without modelling the system [18] [19]. Historically, the problems associated with harmonics generated by distributed generation and possible network resonances have seldom been investigated

[4] and there are few published results of the modelling and power quality investigation of a large utility-scale PV plants, although several studies have been conducted for large wind farms.

The problem of harmonic emissions from utility-scale solar PV plants, and the development of methodologies for assessment of such emissions, is becoming increasingly pertinent as the number and individual generating capacity of plants worldwide is growing rapidly. The issues are especially relevant in the South African context due to the rapid expansion of the solar PV industry and the significant number of large utility-scale generating plants which have recently been connected to the network or are due to be connected within the next few years. The proximity of some of these projects to one another, their remote location, far from major load centres, and the fact that they are often connected to relatively weak HV distribution systems are further factors that may influence the impact that these plants have on the harmonic distortion in the local distribution network.

This leads to the following research questions:

- How can a utility-scale solar PV plant be modelled to reasonably approximate its harmonic performance – in respect to both harmonic current sources within the plant and the harmonic impedance characteristic of the plant?
- Is the quality of data acquired from an HV-connected, utility-scale PV plant using typical power quality measurement apparatus adequate for harmonic emission assessment and analysis?
- How does the operating status of the plant impact the harmonic distortion measured at the POC?
- What measurement and analysis methods are suitable for determining the harmonic emissions of an operational plant?

The above background, overview and research questions describe several issues relating the modelling, measurements and assessment of harmonic distortion in large solar PV plants. The relevance of the work globally and within the South African context is highlighted and this gives rise to the project description in the following section.

1.3 Project description

1.3.1 Research objectives

The project background and motivation described in sections 1.1 and 1.2 give rise to the following research objectives:

- The development of a harmonic simulation model of a solar PV plant which represents both the harmonic sources within the plant and the harmonic impedance of the plant. This includes use of the model to evaluate the frequency response of the PV plant viewed from the POC and from the inverter terminals.
- The quality assessment of harmonic measurement data captured by power quality recording instruments installed at a utility-scale PV plant to determine its usefulness for the study of harmonic phenomena.

- The investigation of the harmonic behaviour of the PV plant based on trends in the recorded harmonic voltages and currents under different operating conditions of the plant.
- The comparative analysis of different methods described in the literature and predominant power quality standards in assessment of the harmonic emissions contribution of the PV plant.

1.3.2 Research methodology

These research objectives define the fundamental elements of the project. Each objective requires the execution of various research tasks to meet the requirements of the project. The tasks include the following:

- *Conduct a literature review:*

  The key focus areas of the literature review are as follows:

  - Fundamental theory of power system harmonics including phenomena such as resonance and harmonic propagation, amplification and cancellation.
  - National and international power quality standards and guidelines which define the measurement and assessment of harmonic emissions.
  - Harmonic generation mechanism and modelling of PWM solar PV inverters.
  - Modelling techniques for harmonic analysis including frequency-domain analysis and electromagnetic transient (EMT) simulations.
  - Harmonic behaviour and modelling of key network elements including transformers and medium voltage cables.
  - Harmonic measurement systems including an analysis of requirements for metering equipment and transducers.
  - Measurement-based methods for the assessment of the harmonic emission contribution of an installation.
  - Review of relevant case studies involving harmonic modelling and analysis with focus on applications involving solar PV, distributed generation and wind power.

- *Model the solar PV plant*

  A simplified, aggregated model of a typical PV plant will be built in DIgSILENT PowerFactory to aid in understanding of resonance mechanisms by means of harmonic frequency sweeps. Thereafter, a detailed model of the PV plant under study will be built. As-built drawings of the plant will be used together with manufacturer data sheets to ensure that the plant topology is accurately represented. Detailed harmonic representations of network elements are not typically considered in the engineering and design of a commercial plant and will be developed based on modelling techniques described in the literature.

Inverter harmonic spectra from the manufacturer's type test measurements will be considered in the modelling of the inverters as harmonic current sources. Wideband models of transformers and cables will be developed to account for the capacitive nature of these passive elements at high frequencies. Network data for the utility network in the region of the POC is not available. A pre-connection frequency sweep of the positive sequence harmonic impedance at the POC was provided by the utility and will be used in the simulation model. Equivalent linear network representations based on the expected minimum and maximum fault levels will also be considered.

- *Evaluate the frequency response of the PV plant using the simulation model*

  First, the harmonic impedance of the individual components of the PV plant distribution network – cables and transformers – will be assessed. Next detailed frequency sweep analyses will be conducted based on the simplified, aggregated model of the PV plant to identify the interactions which result in resonances in the PV plant harmonic impedance characteristic. Frequency sweep analyses will be conducted on the detailed model of the full PV plant to provide an indication of the actual resonances expected in the plant. The results will be compared to the results from the simplified model harmonic to understand the resonance mechanisms. Equivalent representations of the utility network will be assessed to evaluate the impact of the network on the harmonic impedance characteristics.

- *Assess the quality of measurement data captured at the PV plant POC*

  10-minute and 3-second aggregated harmonic voltage and current data from an IEC-61000-4-30 Class A [20] instrument installed at the POC of the PV plant will be analysed with the view to exploring instrument transformer accuracy and the quantization error of the meter in the context of the amplitudes of the measured harmonic components. The 10-minute values will subsequently be compared to 3-second values with the view to evaluate the temporal fluctuations in the harmonic distortion. Event-triggered waveform data is processed to extract the harmonic spectra of the voltages and currents for further analysis.

- *Evaluate the plant harmonic behaviour*

  The magnitudes of measured harmonic voltages and currents will be compared to the fundamental frequency active and reactive power and to time of day to investigate relationships between the operating conditions of the plant and network and the harmonic behaviour. Normal operation, plant start-up and non-operational periods will be considered. Where possible, correlations will be drawn between the simulated harmonic impedance and the observed harmonic behaviour.

- *Perform a comparative analysis of different methods of harmonic emission assessment*

  Various methods proposed in the literature and harmonic standards will be applied to the harmonic measurement data to gain further insight into the harmonic impact of the plant and to compare the assessment results of the different methods. The considered methods are:

  - Reverse application of the general summation law

- Harmonic voltage phasor method
- IEC 61000-3-6 long-duration simultaneous measurement of harmonic voltages and currents
- Harmonic vector method

The measurement-based methods will also be compared to emissions calculated using the DIgSILENT PowerFactory model.

1.4 Thesis structure

The remainder of this document is structured according to the following outline:

- *Chapter 2: Literature review*

  The relevant literature is reviewed. An overview of solar PV deployment in the global and South African energy markets and a summary of the impact of harmonic distortion provide background to the study. Methodologies and standards for management of harmonic distortion are outlined. Fundamentals of power system harmonic analysis and harmonic resonance are discussed to present the key theoretical concepts fundamental to the topic. Harmonic analysis techniques using measurement and simulation are discussed and accompanied by a review of relevant case studies. Detailed modelling techniques and simulation tools are discussed. Finally, harmonic measurement and components of measurement systems are reviewed.

- *Chapter 3: Frequency response of a solar PV plant*

  Development of a simplified, aggregated PV plant model in DIgSILENT Powerfactory using wideband harmonic models of transformers and cables is described. The harmonic impedance of the simplified model is simulated at the POC and at the inverter terminal with the opposite terminal alternatively open circuited and short circuited. The mechanisms of observed series and parallel resonances are identified. The simulations are repeated with a full model of the PV plant and the results compared to those of the aggregated model. The impact of an equivalent utility network on the harmonic impedance is also evaluated.

- *Chapter 4: Analysis of harmonic measurements*

  The acquisition of measurements from the POC of the PV plant is described. The quality of measurement data is evaluated considering the amplitude of the measured signals with respect to the quantisation error of the power quality meter and the accuracy of the voltage and current transducers. The 3-second aggregated measurement data is compared to the 10-minute aggregated data with a view to determining whether the 10-minute values are representative of both the short-term and long-term behaviour of the harmonic signals. A methodology for extracting harmonic components from event-triggered waveform recordings using the FFT is described.

- *Chapter 5: Comparative analysis of harmonic emission assessment calculation methods*

The harmonic emissions contribution is calculated – using aggregated measurement data and processed waveform data – according to four alternative methods described in the literature. The results of the methods are compared with each other and with harmonic load flow simulation results.

- *Chapter 6: Conclusions and recommendations*

  The study results are compared with the research objectives and conclusions are drawn. Recommendations are made for further related research.

2 Literature review

2.1 Overview

This chapter presents a survey of the literature relating to the impact of solar PV plants on network harmonic distortion and the methods for assessment of harmonic emissions from these plants. First the background of the global solar PV market, the historical and current status of the South African electricity market, and the development of solar PV generation plants in South Africa are described to contextualise the research. Then the general impact of harmonic distortion is described, followed by a discussion of management of harmonic distortion and harmonic mitigation techniques.

Thereafter attention is given to the fundamentals of harmonic analysis including relevant mathematical theory and issues related to harmonic resonance. Solar PV plant technology is discussed with emphasis on its impact on harmonic distortion whereafter practical simulation- and measurement-based techniques for harmonic evaluation and assessment are reviewed. The chapter concludes with a review of some of the more popular software tools used for harmonic analysis and a synopsis of key requirements for measurement of harmonic voltages and currents.

2.2 Solar PV background

2.2.1 Global solar PV market

There is an increasing recognition of the need to develop and deploy power generation technologies that address the issues of clean energy, sustainability and climate change [1]. The majority of electrical energy is presently generated by means of steam turbines which are powered by combustion of fossil fuels (coal, oil or natural gas) or by nuclear fission [21].

Burning of fossil fuels in the presence of air produces CO_2 which is widely recognised by scientists as the leading cause of climate change resulting in phenomena such as global warming, sea level rise, increasingly destructive storms and changes in rainfall patterns. Nuclear power plants do not emit CO_2 but they require special precautions to ensure the safe operation of plant and they produce radioactive waste which must be properly managed as it remains toxic for centuries [22]. Renewable energy is therefore regarded as a key technology to reduce CO_2 emissions from the energy system and in addition, to provide benefits in terms of social and economic development, energy access, energy security and reduction of negative health and environmental impacts [23].

The main commercially available renewable energy technologies are bioenergy, direct solar energy (PV and concentrating solar power (CSP)), geothermal energy, hydropower, ocean energy and wind energy (onshore and offshore) [23]. Of these technologies, hydropower, onshore wind and solar PV are considered most competitive on a global scale for the purpose of achieving CO_2 emission reduction objectives [24]. Installed

capacity of solar PV has increased rapidly in the last decade with a rate of deployment exceeding expectations and PV is therefore considered to be one of the most promising renewable technologies [1].

The market prices for solar PV dropped drastically over the five-year period from 2008 to 2013 – by a factor of five for PV modules and a factor of almost three for systems and continues to fall. The global new-built capacity in 2015 (50.6 GW) was more than seven times higher than the 2009 new-built capacity (7 GW). The cumulative installed capacity grew at an average annual rate of 49% in the ten-year period up to the year 2013 and had reached 229 GW by 2015 [25] [26]. Conservative estimates predict a global installed PV capacity of 500 GW by 2020, which will generate more than 2% of global electricity consumption. In a high-renewable forecast scenario, PV could generate 16% of global electricity by 2050 with an installed capacity exceeding 4600 GW [1].

2.2.2 Electricity market in South Africa

The majority of electricity in South Africa is produced by coal fired power stations. In 2008, 86 per cent of generation capacity was coal, 5 percent nuclear and the balance from conventional hydro, hydro pumped storage and gas / diesel. Eskom, a state-owned enterprise, produced 95 per cent of South African electricity, in addition to owning and operating the transmission network and large parts of the distribution network. Installed generation capacity was nearly 40GW with a peak demand of approximately 36GW, giving a narrow reserve margin [27].

Since 2007, as a result of this narrow reserve margin, South Africa has at times experienced a shortfall in electricity generation which resulted in widespread rolling blackouts, or load shedding [28]. In response to the crisis, the Department of Minerals and Energy and Eskom released a document entitled “Interventions to address electricity shortages” in January 2008 [29]. This outlined plans for short term interventions to increase reserve margin by adjustment of electricity prices, return to service of mothballed coal fired power stations, construction of new diesel-powered open cycle gas turbines, procurement of power from co-generators and various demand side management initiatives. Two new 4800MW coal power plants, Medupi and Kusile, were also included in the plan with their first 800MW units due to produce power in 2012 and 2013 respectively. The plan also states that “Renewable Energy (RE) options are being explored”, but only includes plans for 100 MW of wind power and 100 MW of solar power.

2.2.2.1 Integrated Resource Plan (IRP)

In March 2011, the government finalised the first version of the Integrated Resource Plan for Electricity 2010-2030 which is a more detailed document describing the proposed generation new build fleet for South Africa for the period 2010 to 2030. The plan considered a cost-optimal solution which would meet the CO2 emission constraints while also considering factors such as local job creation, water usage, security of supply and risk associated with new technologies. In addition to all existing and committed power plants, the plan included 9.6 GW of nuclear, 6.3 GW of coal, 17.8 GW of renewables and 8.9 GW of other generation sources [30].

2.2.2.2 Renewable Energy Independent Power Procurement Programme (REIPPP)

In 2009, the government began investigating feed-in tariffs (FIT's) for renewable energy. Feed-in tariffs are tariffs used in long term power purchase agreements (PPA's) which are intended to reflect the costs of different generation technologies, based on government analysis. In 2011 FIT's were abandoned in favour of a competitive tender model. Independent power producers (IPP's) are selected based on a score, 70 percent of which is determined by the bid energy price and 30 percent of which is related to economic and social development objectives [3]. The program is called the Renewable Energy Independent Power Procurement Program (REIPPP).

The programme has attracted a large number of domestic and international project developers and has been successful in adding a significant amount of renewable energy generation to the grid within a short space of time [3]. Four rounds of bidding have been completed to date and a total of 79 projects have been awarded with a combined capacity of 5243 MW. The bulk of the capacity is split between solar PV (39 projects, 1899 MW) and onshore wind projects (27 projects, 2660 MW) with the remaining capacity divided between concentrated solar power, small hydro, biomass and landfill gas generators [3] [31].

2.2.3 Solar PV in South Africa

39 solar PV projects have been awarded in the first four rounds of the REIPPPP, with a combined capacity of 1899 MW. The maximum AC power rating of solar PV plants built under the REIPPPP is limited to 75 MW, and many plants approach this ceiling, with 19 of the 45 Round 1 to 4 plants having a nominal capacity greater than 70 MW [32]. The size and distribution of solar PV plants, and wind farms, awarded up to REIPPPP Round 3, are shown in the Figure 2-1.

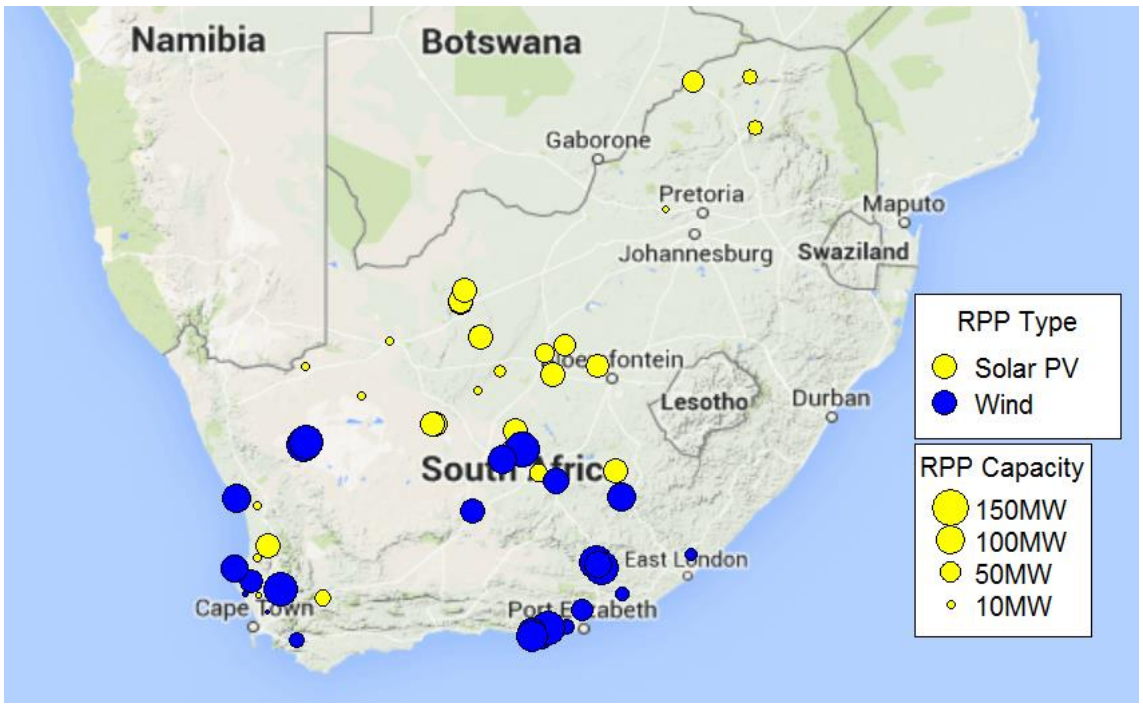

Figure 2-1: REIPPP wind and solar PV projects – Round 1 to Round 3 (Compiled from [33] and [3])

CSP, small hydro, biomass and other renewable technologies are omitted from the map – as are other thermal and hydro generation plants – since these employ conventional synchronous generators. Solar PV and wind turbines, however, use power electronic converter technology and therefore have greater influence on network harmonics performance.

It is clear from Figure 2-1, that the majority of the solar PV plants are situated in the Karoo, a semi-arid region in the central and northern part of the country. Many of the larger projects are clustered around transmission nodes near the towns of Kathu, Kimberley, De Aar and Prieska. In some instances, this has resulted in several hundred megawatts of PV generation being connected to a single transmission substation. Where the plants are not located in close proximity to a transmission substation, they are connected to the distribution network – typically the 132 kV network for larger plants. Due to the Karoo being a sparsely populated region, the electrical network is characterised by light loading and weak sub-transmission and distribution systems. Therefore, high concentrations of solar PV plants in these areas have the potential to significantly impact the quality of supply (QoS) in the region.

2.2.4 Solar PV and quality of supply

Solar PV installations have the potential to significantly impact the network quality of supply, particularly voltage fluctuations, flicker, harmonic distortion and high frequency disturbances [4] [34]. Voltage fluctuations and flicker are caused by power variations resulting from changes in solar irradiance caused by the movement of clouds and may be affected by factors including wind speed, the type and size of clouds, and the area covered by and layout of the solar panel array [35].

PV plants impact the harmonic performance of the network by injecting harmonic currents generated by the inverters into the network and by causing harmonic impedance resonances in the network due to capacitive elements within the plant. Harmonic performance of solar inverters is described in more detail in section 2.8.4, while the mechanisms of harmonic resonance are outlined in section 2.7. High frequency disturbances may also be caused by the high frequency switching of inverter power electronic devices [19].

2.3 Impact of harmonic distortion

Harmonic voltage distortion in the power network can have a negative impact on a variety of power system components including capacitor banks, transformers and motors due to overloading, overheating and increased losses [36]. Harmonic voltages, which increase the magnitude of voltage peaks, increase the dielectric stress on equipment insulation [6].

Harmonic can negatively impact the performance of electronic devices in many ways. Distorted voltage waveforms can increase the number of zero voltage crossings per cycle resulting in incorrect operation of devices which rely on zero crossing detection for timing or control purposes [37]. Voltage distortion may also cause unequal control angles of the switching devices in line commutated converters resulting in the generation of non-characteristic harmonics [38]. Electronic equipment and telecommunications lines may be affected by

electromagnetic interference resulting from emissions radiated at harmonic frequencies [38]. The accuracy of electromagnetic protection relays and energy meters can also be affected by harmonic distortion but modern digital devices are largely immune to such effects [36] [39].

Increased harmonic distortion also decreases power factor. Power factor is defined as the ratio of active to apparent power:

$$PF = \frac{P}{S} \tag{2.1}$$

The fundamental harmonic power factor, also called the displacement power factor (DPF), is defined as:

$$DPF = \frac{P_{(1)}}{S_{(1)}} = \frac{V_{(1)} I_{(1)} \cos\phi_{(1)}}{V_{(1)} I_{(1)}} = \cos\phi_{(1)} \tag{2.2}$$

where $P_{(1)}$ and $S_{(1)}$ are the active and apparent power of the fundamental harmonic and $V_{(1)}$, $I_{(1)}$ and $\phi_{(1)}$ are the voltage, current and phase angle of the fundamental harmonic.

For a distorted waveform, the total power factor is also influenced by the harmonic components of the waveform and will be less than the DPF [38]. If the voltage is sinusoidal, which may be a reasonable approximation for a network with a low source impedance, the total power factor can be calculated in terms of the DPF and current THD as:

$$PF = DPF \frac{1}{\sqrt{1 + THD_I^2}} \tag{2.3}$$

2.4 Management of harmonic distortion and QoS standards

2.4.1 Basic principles of harmonic distortion management

Power quality, including harmonic distortion, is typically managed by means of emission limits which are defined in power quality standards. The objective of such harmonic limits is to ensure that harmonic voltage and current levels in the network remain within ranges that are acceptable to utilities and their customers [40], and to ensure compatibility between end-user equipment and system equipment [36].

Harmonic distortion levels in the network typically exhibit a normal distribution and the immunity levels of customer equipment are also described by a normal distribution. The objective of power quality standards is to set compatibility levels such that the probability of them being exceeded at any time is low. In the case of the South African power quality specification, NRS 048, the compatibility levels are set to represent 95 % probability levels for the upper limit of the system disturbance levels – i.e. the 95th percentile of actual harmonic distortion must be less than the compatibility level [8]. The concepts of harmonic disturbance, equipment immunity and compatibility level are illustrated in Figure 2-2.

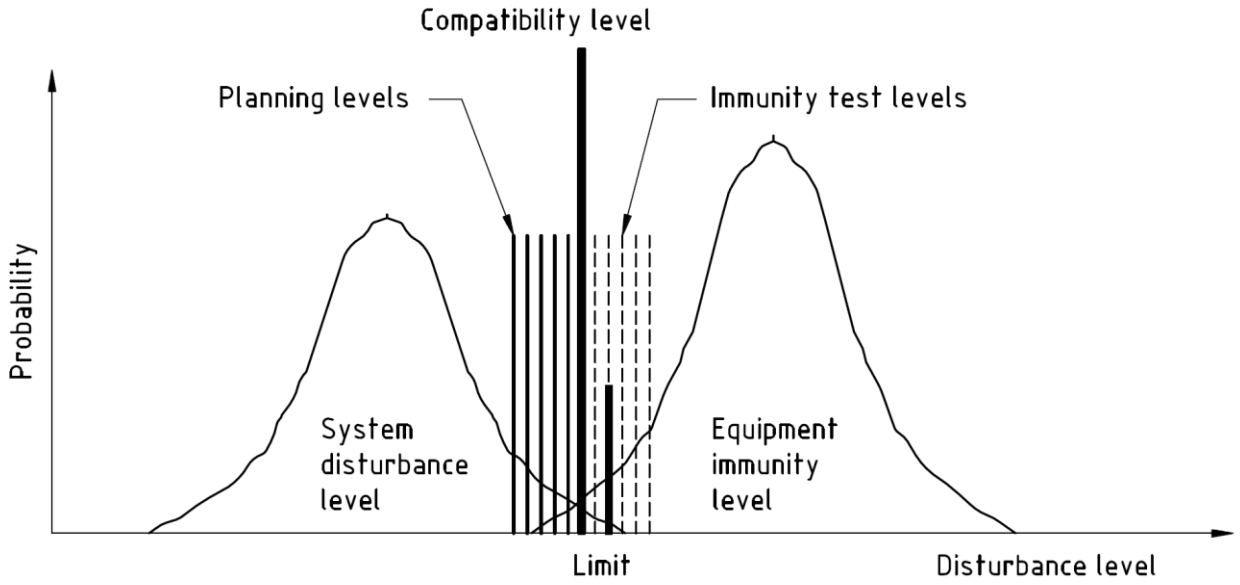

Figure 2-2: Harmonic disturbance, equipment immunity and compatibility levels [8]

Based on the compatibility levels, utilities can set planning levels, which represent internal quality objectives used to manage customer emissions and network characteristics, with the aim of ensuring that the compatibility levels are not exceeded [8]. Utilities in turn specify contractual limits applicable to large load and generation customers based on the maximum demand (load customers) / maximum export capacity (generators) of each installation and the system capacity at the point of connection. The harmonic contribution transferred from higher voltage levels must also be considered [41].

The NRS 048-4 guideline for large installations (maximum demand > 0.2 % of the network short circuit power at the point of common coupling (PCC)) is applicable to the calculation of emission limits for large solar farms in South Africa [41]. It states that the individual customer voltage emission limit is calculated as:

$$E_{U(h)i} = \sqrt[\alpha]{L_{U(h)}^{\alpha} - \left(T_{U(h)} \times L_{U(h)US}\right)^{\alpha}} \times \sqrt[\alpha]{\frac{S_i}{S_t}} \tag{2.4}$$

where:

$E_{U(h)i}$ is the individual customer harmonic voltage emission limit at the PCC,

α is the summation law exponent. The following exponents are recommended:

Table 2-1: Summation exponents

Harmonic Order	α
h < 5	1
5 ≤ h ≤ 10	1.4
h > 10	2

LU(h) is the planning level for voltage harmonics in the (MV or HV) system under consideration,

$T_{U(h)}$ is the transfer coefficient of voltage harmonics from the upstream system to the system under consideration; it could be determined by simulation or measurements. For an initial simplified evaluation, the transfer coefficient from the upstream system can be taken as equal to 1. In practice, however, it can often be less than 1 due to load damping, or greater than 1 due to shunt capacitor bank or filter resonances,

$L_{U(h)US}$ is the planning level for voltage harmonics in the upstream system,

S_i is the agreed apparent power of the customer installation, for example the notified maximum demand or the MVA rating of the considered installation (either load or generation),

S_t is the total supply capacity of the considered system including provision for future load growth.

The assessment of harmonic emissions from an installation for the purpose of evaluating compliance with apportioned limits is a complex exercise which has been the subject of extensive research in recent years and resulted in the publication of a plethora of papers. The two primary approaches employed in assessment are simulation using computer models of the installation and network, and analysis of harmonic voltage and current measurements taken at the POC or PCC. Assessment of harmonic emissions is discussed in more detail in section 2.9.

Non-compliance to contractual harmonic emissions may result in consequences within the contractual and regulatory frameworks applicable to the plant. In the case of renewable power plants in South Africa, the connection agreement between the generator and the utility and the relevant grid codes outline a dispute resolution process which may require reduction of the RPP's output, installation of corrective equipment within a reasonable timeframe or, ultimately, disconnection of the plant [11] [41].

2.4.2 Harmonic standards

Various national and international specifications are applied in different regions to provide guidelines and recommended practices for harmonic management and to specify harmonic limits. The standards primarily discussed in the literature are the IEC 61000-3-6 and IEEE 519 standards, while the EN 50160 standard defines quality of supply requirements for European utilities. The standard applicable to utilities and customers in South Africa is the NRS 048 specification, the development of which was guided by international (IEC and Cigré), European (CENELEC) and North American (IEEE) standards and reports, supplemented by local information [8].

2.4.2.1 IEC 61000-3-6

The International Electrotechnical Comission (IEC) has published a series of electromagnetic compatibility standards to address power quality issues including harmonic distortion. The part of this series which defines harmonic limits for medium and high voltage networks is IEC 61000-3-6 [42]. The standard applies the principle of evaluation of emissions based on voltage limits in order to ensure that harmonic currents produced within a facility do not result in excessive voltage distortion levels [36] [42] [43]. The harmonic emission from

an installation is defined as the harmonic voltage at each harmonic frequency caused by the installation at the point of evaluation; this includes harmonics generated by the plant as well as any amplification of harmonic distortion that may result from interaction of the customer installation and the supply system [43].

The standard specifies compatibility levels for LV and MV networks only and indicative planning levels for MV, HV and EHV networks. The general methodology for calculation of emission limits for large installations is based on the available system absorption capacity according to equation (2.4). Installations which are small compared to the system short circuit capacity may however use generic emissions limits. The short circuit ratio – defined as the ratio of the system short circuit current to the maximum demand current at the PCC – should be greater than 500 in order for generic limits to be applied. Emissions in excess of the standard's recommended limits may be accepted on a conditional basis by agreement between the utility its customers [42] [43]. Advanced methods are described for allocation of planning levels at HV and EHV busbars in highly meshed transmission networks.

The specification also emphasises the importance of evaluating the network harmonic impedance for the calculation of current limits based on voltage limits. Generic system harmonic impedance characteristics covering different voltage levels, types of systems, etc. may be used, but are generally applicable only for MV and LV systems. Several impedance envelopes are provided for different system voltages up to 33kV. For large installations, especially with HV or EHV connections, a best estimate of the maximum harmonic impedance over the worst operating conditions at the point of evaluation is recommended based on simulations for pre-connection assessment and based on measurement or calculation for assessment of actual emission levels [42].

2.4.2.2 IEEE 519

The IEEE 519-2014 standard applies a different approach which divides the responsibility for limiting harmonic voltage distortion between the customer and the utility [36]. The customers are responsible for limiting their harmonic current emissions whilst the utility must implement measures to decrease voltage distortion levels by modifying the supply system impedance characteristics where necessary. However, customers should not add passive equipment that affects the system impedance characteristic resulting in excessive voltage harmonic distortion [44].

To enable the implementation of this methodology, both voltage and harmonic current limits are specified. Limits for individual voltage harmonics and voltage THD are defined for system voltage ranges (LV, MV, HV and EHV systems). For each system voltage range, harmonic current limits and a total demand distortion limit are then defined according to the short circuit ratio of the installation. Incentive is provided to reduce lower order harmonic distortion by allowing increase of harmonic limits if characteristic lower order harmonics can be limited to 25 % of the normal limits.

Voltage emission assessment is based on daily 99^{th} percentile 3-second recording values being less than 1.5 times the specified limits and weekly 95^{th} percentile 10-minute recording values being less than the limits. For

current emissions to comply, daily 99th percentile 3-second harmonic currents must be less than 2.0 times the specified limits, weekly 99th percentile 10-minute values less than 1.5 times the limits and weekly 95th percentile 10-minute values less than the limits [44].

2.4.2.3 NRS 048

The NRS 048 standard is an industry standard that outlines requirements for quality of supply in South Africa. Part 2 and Part 4 contain the requirements for utilities and customers with respect to harmonic emissions [8] [41]. In terms of harmonics, the specification's approach is closely aligned with that of IEC 61000-3-6 in that only voltage emission limits are specified. The compatibility levels defined in NRS 048-2 for LV and MV are identical to the IEC values but HV compatibility levels are additionally defined for characteristic odd harmonics up to the 25th harmonic, based on Cigré TB261. Assessment methods are also defined which prescribe the reference voltage, assessment periods, retained values, exclusion of flagged or missing data and compliance criteria [8].

NRS 048-4 specifies planning levels for MV, HV and EHV networks. Guidelines for calculation of harmonic current apportionment, based on voltage limits and maximum supply impedance under any normal operating condition, are also aligned with IEC 61000-3-6 [41] [42]. However, the standard additionally recommends that a maximum harmonic impedance equal to three times the base harmonic impedance be considered in the calculation of current limits from the voltage limits:

$$|Z_h| = 3 \times |Z_0| \times h \tag{2.5}$$

where:

- $|Z_h|$ is the maximum harmonic impedance at harmonic order h to be used in the calculation of current limits, in ohms
- $|Z_0|$ is the maximum magnitude of the fundamental frequency supply impedance at the PCC for any normal system contingencies and states, in ohms
- h is the harmonic number

2.4.2.4 RPP Grid Code

The South African RPP Grid Code simply specifies that RPP's must comply with harmonic limits specified by the relevant utility. It states that the three times base harmonic network impedance characteristic should be considered in the calculation of harmonic voltage emissions based on the RPP's harmonic current emissions. The Grid Code further specifies that the plant may not connect equipment, such as shunt capacitor banks, that will cause a resonance of more than three times the base harmonic impedance at the POC [11].

2.5 Mitigation

In the case that the voltage or current harmonic disturbance in the network is determined to exceed the allocated limits or planning levels at a point in the network, mitigating actions may be required to reduce the harmonic distortion.

Three electromagnetic components interact to cause a resultant voltage harmonic distortion [38]:

- the source of the disturbance – a non-linear load such as a solar PV inverter;
- the load, or receptor, which may be affected by the voltage distortion;
- the supply network, which is the coupling between the source and the load.

Methods of reducing the magnitude of voltage harmonics and their effects may therefore be designed to influence any, or all, of these three components. Methods applicable to solar PV inverters are discussed in section 2.8.5. These include use of passive output filters, active filters and hybrid filters as well as application of different PWM control algorithms. Methods of reducing emissions from other types of harmonic sources are beyond the scope of this literature review.

The challenges associated with the supply network are typically due to high harmonic impedances caused by system resonances. The resonance phenomenon is described in section 2.7 which closes with a discussion of methods to eliminate problematic resonances (section 2.7.5).

The sensitivity of loads may be addressed by derating equipment – such as transformers, cables and motors – to withstand higher harmonic currents [38]. However, addressing load sensitivity can typically not be considered as a solution in the context of solar PV generation within the utility network where the objective is to ensure that voltage harmonic distortion at the PCC, and throughout the network, remains within acceptable limits. Therefore, harmonic mitigation by means of altering the load design is not discussed further.

2.6 Power system harmonic analysis overview

2.6.1 Fundamentals of harmonic analysis

In an ideal three-phase power system, the supply voltage at all points in the network would be a purely sinusoid with constant nominal frequency (50Hz) and balanced three-phase voltage of nominal magnitude. The electromotive force (e.m.f.) of conventional generators in a power system can be considered to be essentially sinusoidal but there are an increasing number of non-linear devices, loads, and unconventional generators connected to the network. Such equipment has a non-linear voltage/current characteristic which means that it produces non-sinusoidal currents when presented with a sinusoidal voltage at its terminals. Due to the network impedance, this non-sinusoid current produces a non-sinusoidal voltage drop which causes voltage distortion [6] [38].

French mathematician, Jean Baptiste Joseph Fourier, demonstrated in his 1822 publication that any periodic waveform can be represented as the summation of a DC component, a fundamental frequency sinusoidal component, and higher frequency sinusoidal components at frequencies which are integral multiples of the fundamental frequency [6] [38] [45]. These higher-order frequency components are called harmonics and are the primary distorting components of supply voltage and current waveforms in power systems.

Harmonic analysis is the calculation of the magnitude and phase of the fundamental and higher-order harmonics of a periodic waveform [6]. The series representing a periodic waveform in terms of its harmonic components is referred to as the Fourier series. The Fourier series of a periodic waveform with period *T* is represented mathematically by the following expression [6] [38] [46]:

$$f(t) = a_0 + \sum_{n=1}^{\infty} (a_n \cos \omega_0 nt + b_n \sin \omega_0 nt) \tag{2.6}$$

where:

$$\omega_0 = \frac{2\pi}{T} .$$

a_0 is the average value of the function $f(t)$, expressed mathematically as:

$$a_0 = \frac{1}{T} \int_{-T/2}^{T/2} f(t) dt \tag{2.7}$$

while a_n and b_n are defined as:

$$a_n = \frac{2}{T} \int_{-T/2}^{T/2} f(t) \cos(\omega_0 nt) dt \text{ for } n = 1 \rightarrow \infty \tag{2.8}$$

$$b_n = \frac{2}{T} \int_{-T/2}^{T/2} f(t) \sin(\omega_0 nt) dt \text{ for } n = 1 \rightarrow \infty \tag{2.9}$$

By application of Euler's relationship, the Fourier series is frequently represented in complex notation as:

$$f(t) = \sum_{n=-\infty}^{\infty} c_n e^{j\omega_0 nt} \tag{2.10}$$

where:

$$c_n = \frac{1}{T} \int_{-T/2}^{T/2} f(t) e^{-j\omega_0 nt} dt \tag{2.11}$$

The complex c_n coefficients in equation (2.11) are related to the a_n and b_n coefficients in equation (2.6) by means of the following relationships:

$$\begin{aligned} c_n &= \frac{1}{2}\left(a_n - jb_n\right) \\ c_n &= c_{-n}^{*} \\ c_0 &= a_0 \end{aligned} \tag{2.12}$$

The magnitude and phase of these c_n complex coefficients define the magnitude and angle of the components of the periodic waveform's harmonic spectrum. In practice, measurements for the analysis of harmonic distortion are captured as discrete samples and processed in the digital domain. The discrete Fourier transform (DFT) is a variation of the Fourier transform for harmonic analysis of sampled waveforms which are discrete in the time and frequency domains. The discrete Fourier transform and the inverse discrete Fourier transform are shown below in equations (2.13) and (2.14) respectively [46]:

$$X[k] = \sum_{n=0}^{N-1} x[n] e^{-j2\pi kn/N}, \quad k = 0,1,2,\ldots,N-1 \tag{2.13}$$

$$x[n] = \frac{1}{N} \sum_{k=0}^{N-1} X[k] e^{j2\pi kn/N}, \quad n = 0,1,2,\ldots,N-1 \tag{2.14}$$

where time- and frequency-domain spectra are both periodic with N samples per period.

The fast Fourier transform (FFT) is a collection of algorithms that are used to efficiently compute the DFT when N, the number of samples, is large [6] [46].

2.6.1.1 Sampling frequency criterion

In the process of capturing measurements for frequency-domain analysis, the sampling frequency must be chosen to be high enough to allow for unique identification of the sampled time-domain function in the frequency domain. Shannon's sampling theorem states that a function of time *f(t)*, that contains no frequency components higher than *W* Hz, is completely determined by the instantaneous values of *f(t)* at any set of points spaced *1/(2W)* seconds apart [46].

This means that the sampling frequency must theoretically be chosen to be at least twice the highest frequency contained in the original signal. The frequency that is half the sampling frequency is referred to as the Nyquist frequency and frequency components in a signal that are above the Nyquist frequency can be misrepresented in the frequency domain as lower frequencies, a phenomenon called aliasing [6]. In practice, the sampling frequency is chosen to be much higher than the twice the highest frequency in the signal to ensure that the signal is recoverable from the sampled data [46].

2.6.2 Sequence component theory

2.6.2.1 Sequence component fundamentals

Sequence component analysis – also known as symmetrical component analysis – is a powerful mathematical technique for the analysis of unbalanced three-phase power systems. Sequence components simplify the solution of complicated problems and are commonly used in the analysis of asymmetrical faults and in the study of power system harmonics [38] [47]. Problems can be solved in the sequence domain using straightforward circuit analysis and the sequence domain solutions can then be converted back into phase values.

In 1918 Fortesque developed the linear transformation that is used to convert phase domain components into sequence domain components [48]. The Fortesque transform is defined as:

$$\begin{bmatrix} V_a \\ V_b \\ V_c \end{bmatrix} = \begin{bmatrix} 1 & 1 & 1 \\ 1 & a^2 & a \\ 1 & a & a^2 \end{bmatrix} \begin{bmatrix} V_0 \\ V_1 \\ V_2 \end{bmatrix} \tag{2.15}$$

where V_a, V_b and V_c are the three phase voltages and V_0, V_1 and V_2 are the zero, positive and negative sequence voltage components respectively. a is a phasor with 1 p.u. magnitude and angle of 120°.

$$a = 1 \cdot e^{j\frac{2\pi}{3}} = -\frac{1}{2} + j\frac{\sqrt{3}}{2} \tag{2.16}$$

The matrix in equation (2.15) may denoted as **A** which allows for an abbreviated form of the equation:

$$\mathbf{V}_{abc} = \mathbf{A}\mathbf{V}_s \tag{2.17}$$

where $\mathbf{V}_s$ denotes the three-phase set of sequence components, **A** is the Fortesque transformation matrix and $\mathbf{V}_{abc}$ is the three-phase set of phase voltages.

The following properties are noted for the sequence components [47]:

1. Zero sequence components consist of three phases with equal magnitudes and zero phase displacement.
2. Positive sequence components consist of three phases with equal magnitudes, ±120° phase displacement and positive sequence – i.e. the V_{a1}, V_{b1} and V_{c1} vector phasors occur in the same order as the phase voltages V_a, V_b and V_c.
3. Negative sequence components consist of three phases with equal magnitudes, ±120° phase displacement and negative sequence – i.e. the V_{a2}, V_{b2} and V_{c2} vector phasors occur in the opposite order to the phase voltages V_a, V_b and V_c.

The inverse Fortesque transform is defined as:

$$\begin{bmatrix} V_0 \\ V_1 \\ V_2 \end{bmatrix} = \frac{1}{3}\begin{bmatrix} 1 & 1 & 1 \\ 1 & a & a^2 \\ 1 & a^2 & a \end{bmatrix}\begin{bmatrix} V_a \\ V_b \\ V_c \end{bmatrix} \tag{2.18}$$

or in compact form as:

$$\mathbf{V}_s = \mathbf{A}^{-1}\mathbf{V}_{abc} \tag{2.19}$$

The Fortesque transform and its inverse can similarly be applied for conversion of currents between the phase and sequence domains.

2.6.2.2 Sequence components and harmonic analysis

Using a complex Fourier series representation, a distorted voltage waveform can be described in complex phasor representation as [49] [50]:

$$\begin{aligned} V_a &= \sum_{n=1}^{\infty} V_{an} e^{jn(\omega t+\phi_{an})} \\ &= V_{a1}e^{j(\omega t+\phi_{a1})} + V_{a2}e^{j2(\omega t+\phi_{a2})} + V_{a3}e^{j3(\omega t+\phi_{a3})} + \\ &\quad V_{a4}e^{j4(\omega t+\phi_{a4})} + V_{a5}e^{j5(\omega t+\phi_{a5})} + V_{a6}e^{j6(\omega t+\phi_{a6})} + \ldots \end{aligned} \tag{2.20}$$

$$\begin{aligned} V_b &= \sum_{n=1}^{\infty} V_{bn} e^{jn\left(\omega t+\phi_{bn}-\frac{2\pi}{3}\right)} \\ &= V_{b1}e^{j(\omega t+\phi_{b1})-j\frac{2\pi}{3}} + V_{b2}e^{j2(\omega t+\phi_{b2})+j\frac{2\pi}{3}} + V_{b3}e^{j3(\omega t+\phi_{b3})} + \\ &\quad V_{b4}e^{j4(\omega t+\phi_{b4})-j\frac{2\pi}{3}} + V_{b5}e^{j5(\omega t+\phi_{b5})+j\frac{2\pi}{3}} + V_{b6}e^{j6(\omega t+\phi_{b6})} + \ldots \end{aligned} \tag{2.21}$$

$$\begin{aligned} V_c &= \sum_{n=1}^{\infty} V_{cn} e^{jn\left(\omega t+\phi_{cn}+\frac{2\pi}{3}\right)} \\ &= V_{c1}e^{j(\omega t+\phi_{c1})+j\frac{2\pi}{3}} + V_{c2}e^{j2(\omega t+\phi_{c2})-j\frac{2\pi}{3}} + V_{c3}e^{j3(\omega t+\phi_{c3})} + \\ &\quad V_{c4}e^{j4(\omega t+\phi_{c4})+j\frac{2\pi}{3}} + V_{c5}e^{j5(\omega t+\phi_{c5})-j\frac{2\pi}{3}} + V_{c6}e^{j6(\omega t+\phi_{c6})} + \ldots \end{aligned} \tag{2.22}$$

In the case of a balanced three-phase system, the three distorted waveforms have equal amplitudes and displaced by 120° relative to each other. V_{an}, V_{bn} and V_{cn} are equal for all n and ϕ_{an}, ϕ_{bn} and ϕ_{cn} are also equal for all n. It can then be seen by examination of equations (2.20) - (2.22) that the fundamental frequency components are positive phase sequence, as are the 4th, 7th, 10th, etc. The 2nd, 5th, 8th, etc. harmonic orders are negative sequence and the 3rd, 6th, 9th, etc. harmonics, which are commonly referred to as triplen harmonics, are zero sequence.

For a negative sequence system, similar analysis demonstrates that the fundamental, 4th, 7th, etc. harmonic orders are negative sequence, the 2nd, 5th, 8th, etc. harmonic orders are positive sequence and the triplen harmonics are zero sequence. For a zero sequence system, all three phase voltages are in phase and of equal magnitude, so all harmonic orders are zero sequence. However, only balanced three-phase systems contain purely characteristic sequence harmonics. In unbalanced three-phase systems, harmonics may be composed of positive, negative and zero sequence harmonic components. [6]

Use of the Fortesque transform for analysis of non-sinusoidal waveforms requires a redefinition of the *a* complex operator. A harmonic-dependent complex operator *a(h)* is defined as [38]:

$$a(h) = 1 \cdot e^{j\frac{2\pi h}{3}} \tag{2.23}$$

where *h*, a positive integer, is the harmonic number.

The Fortesque transform is then expressed as:

$$\mathbf{V}(h)_s = \mathbf{A}(h)\mathbf{V}(h)_{abc} \tag{2.24}$$

and the inverse Fortesque transform as:

$$\mathbf{V}(h)_{abc} = \mathbf{A}(h)^{-1}\mathbf{V}(h)_s \tag{2.25}$$

where:

V(h)s is the set of sequence voltage harmonic phasors with harmonic order h,

A*(h)* and **A***(h)*$^{-1}$ are the Fortesque and inverse Fortesque transform matrices using modified operator *a(h)*,

V*(h)*$_{abc}$ is the set of phase voltage harmonic phasors with harmonic order *h*.

2.6.3 Harmonic indices

Two common indices for quantifying the harmonic content of a waveform are the total harmonic distortion (THD) and the total demand distortion (TDD). THD can be applied to voltage and current waveforms and is the effective value of the harmonic components of a distorted waveform, i.e. the potential heating value of the harmonics relative to that of the fundamental. THD is calculated according to equation (2.26).

$$\text{THD} = \frac{\sqrt{\sum_{h=2}^{H} V_h^2}}{V_1} \times 100\% \tag{2.26}$$

where V_h is the rms value of order *h* harmonic component of the voltage (or current) and V_1 is the fundamental frequency voltage [6] [36]. According to NRS 048-2, the highest order harmonic to be considered in THD

calculations is H = 40 whilst IEC 61000-3-6 recommends that H = 40 or 50 depending on the application [8] [42]. Voltage THD is commonly referenced to the nominal voltage instead of the fundamental frequency voltage since the deviation between the two is expected to be small under normal operating conditions.

The THD may exaggerate the severity of current harmonic distortion in the case where the THD of a current waveform is high while the fundamental frequency current is low, resulting in actual harmonic currents which are small and do not pose a risk to the system. Therefore, for current harmonic distortion, TDD is often considered as an alternative metric which is defined by referencing the THD to the rated or maximum load current magnitude as described by equation (2.27).

$$\text{TDD} = \frac{\sqrt{\sum_{h=2}^{H} I_h^2}}{I_R} \times 100\% \tag{2.27}$$

where I_R is the rated current of the load or installation under consideration.

2.6.4 Harmonic propagation, cancellation and attenuation

In a balanced three-phase system, harmonics are characterised by their sequence behaviour. For example, a third harmonic appears as a zero sequence component and therefore flows in the phase and neutral / ground circuits of a grounded wye system but cannot exist in line currents of an unearthed system. Commonly used delta-wye transformers in distribution networks and PV plants therefore limit the transfer of zero sequence harmonics from one voltage level to another. Rotating machines present a low impedance to characteristic negative sequence harmonics, such as the 5th harmonic [47] [51].

The harmonic impedance of the network, particularly when it is affected by resonances caused by interaction of inductive and capacitive network elements, has a significant impact on amplification or attenuation of harmonic voltage distortion, as described in section 2.7. Another factor is harmonic cancellation which results in a reduction in global harmonic distortion due to variation in phase angles of harmonics of the same order produced by different non-linear loads. The vector sum of the harmonic currents produces a harmonic current that is smaller than the algebraic sum of the current magnitudes [52].

Lower order harmonics tend to have a limited range of phase angle variation and significant magnitudes that remain stable for long periods whilst higher order harmonics have wide variations in phase angle and magnitude. The IEC 61000-3-6 standard recommends that this be accounted for by use of a general summation law, which is applicable for both harmonic voltage and current, and is defined as [42]:

$$U_h = \sqrt[\alpha]{\sum_i U_{hi}^{\alpha}} \tag{2.28}$$

where:

Uh is the magnitude of the resulting harmonic voltage of order h

Uhi is the magnitude of the various individual harmonic emission levels

α is an exponent dependent on the degree to which individual harmonic voltages vary randomly in phase angle and magnitude and on the probability of the actual of individual harmonic distortion exceeding the calculated value.

Considering 95th percentile values for individual sources and the characteristics of typical networks, α values listed in Table 2-1 (section 2.4) are recommended.

2.7 Harmonic resonance in power systems

2.7.1 Overview

Harmonic distortion in power systems may be amplified by the presence of harmonic resonances such that sources with relatively low levels of harmonic emissions can cause significant harmonic distortion at points in the network [53]. The network impedance is frequency dependent and the interaction of inductive and capacitive network elements may result in localised system impedance resonances. Resonance is a common phenomenon in transmission and distribution networks where power factor correction capacitor banks, harmonic filters and large cable networks are present [6] [17] [54] .

Two modes of resonance exist, namely parallel resonance and series resonance. These phenomena are described below.

2.7.2 Parallel resonance

Parallel resonance results in a high impedance being presented to the harmonic source at the harmonic resonant frequency. Since harmonic sources are typically considered to be current sources, this high impedance results in high voltage harmonic distortion and high currents flowing within each leg of the parallel impedance [6]. Considering the parallel resonant L-C circuit in Figure 2-3, the impedance seen by the harmonic current source is:

$$Z_P = \frac{Z_L Z_C}{Z_L + Z_C} \tag{2.29}$$

where:

Z_P is the impedance of the parallel circuit

Z_L is the impedance of the inductor L_p ($Z_L = j\omega L_p$)

Z_C is the impedance of the capacitor C_p ($Z_C = 1/j\omega C_p$)

At the frequency where the magnitude of Z_L is equal to the magnitude of Z_C, the denominator of the fraction in equation (2.29) approaches zero and the impedance becomes large. In practice, it will not become infinite

due to the resistive components of the network impedance which are not frequency dependent. The phase angle of the impedance passes through zero at resonance [55].

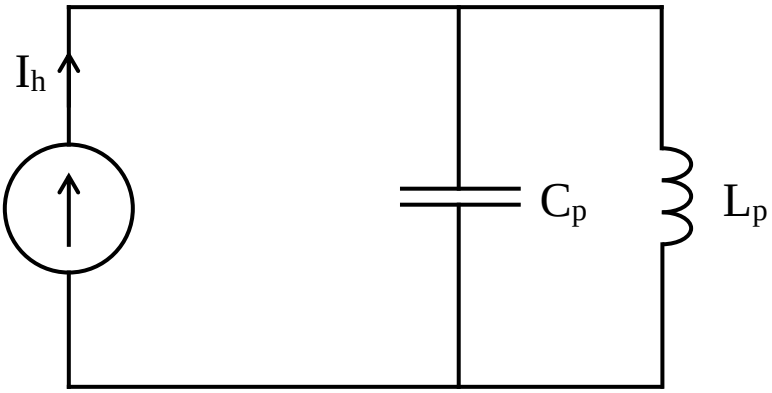

Figure 2-3: Parallel resonance circuit

The resonant frequency of a parallel resonance circuit is calculated as:

$$f_r = \frac{1}{2\pi\sqrt{LC}} \tag{2.30}$$

where f_r is the resonant frequency, L is the parallel inductance in Henries and C is the parallel capacitance in Farads. A typical frequency sweep of a parallel resonant circuit showing the magnitude of the harmonic impedance versus frequency is shown in Figure 2-4. In this example the resonant frequency is close to 500Hz.

A common cause of parallel resonance is power factor correction capacitors connected at the same point of common coupling as a harmonic source. Assuming the network impedance to be purely inductive, the resonant frequency can be calculated as [6]:

$$f_p = f\sqrt{\frac{S_S}{S_C}} \tag{2.31}$$

where:

f is the fundamental frequency [Hz],

f_p is the parallel resonant frequency [Hz],

S_s is the short-circuit rating of the network [MVA],

S_c is the capacitor rating [MVAr].

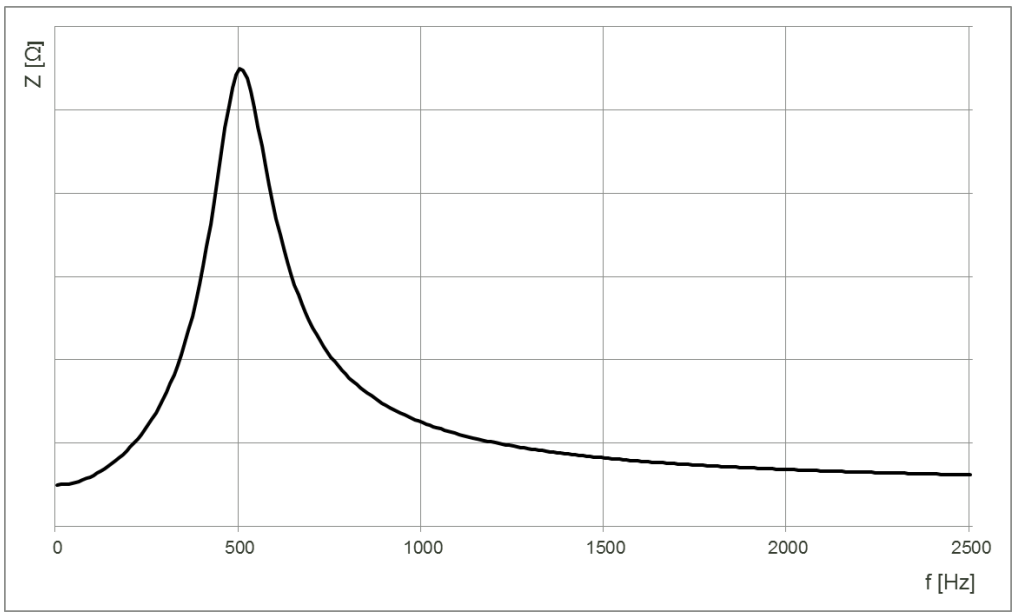

Figure 2-4: Frequency sweep of parallel resonant network

In the case of solar PV plants, the MV collector cable network has significant capacitive impedance. An inverter in a collector feeder is the source of harmonics to a parallel resonant circuit comprised of the capacitive impedance of the remaining collector feeders, together with the largely inductive park transformer and network impedance. In some cases, capacitor banks are installed to increase the reactive power capability of the plant and these may also cause parallel resonances.

2.7.3 Series resonance

Series resonance results in a low impedance being presented to the harmonic source at the harmonic resonant frequency. The network background harmonic distortion, generally considered as a voltage source, will generate large harmonic currents at frequencies close to the low impedance resonant point [6] [17]. A series resonant L-C circuit is shown in Figure 2-5.

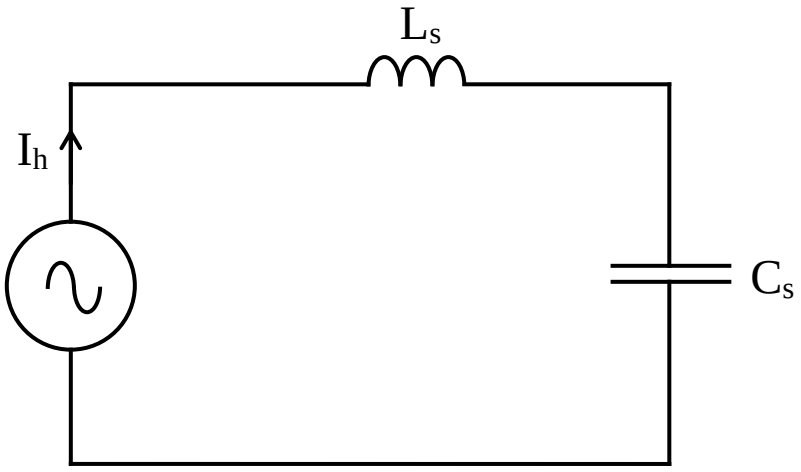

Figure 2-5: Series resonance circuit

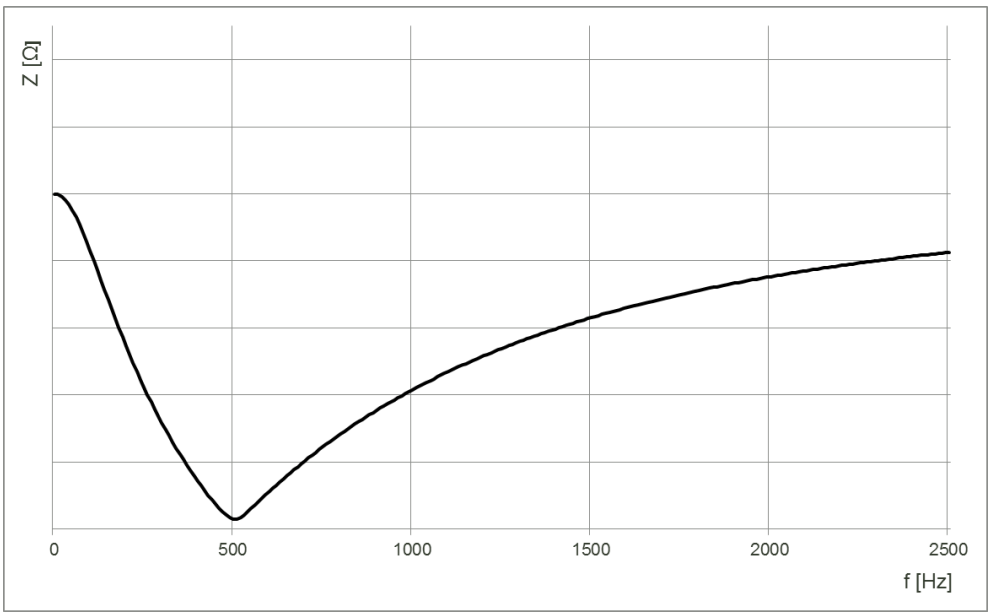

Figure 2-6: Frequency sweep of series resonant network

For series resonance, the impedance will be equal to zero when the magnitudes of Z_L, the inductive reactance, and Z_C, the capacitive reactance are equal. In practice, the resistive components of the network elements – which are not frequency dependent – ensure that the impedance magnitude at the resonant point is larger than zero. As for the parallel resonant circuit, the phase angle of the impedance passes through zero at the resonant frequency [55]. A typical frequency sweep of harmonic impedance versus frequency is shown in Figure 2-6. The resonant frequency of a series resonant circuit is also calculated according to equation (2.30) [17].

In the case of a solar farm, series resonance circuits are formed by the combination of the inductive park transformer(s) and the capacitive MV collector network and any capacitor banks which may be connected at the MV busbar. The source of voltage harmonics is the background network harmonic distortion and large currents can flow for relatively small background harmonic voltages [6].

2.7.4 Frequency dependence of impedance in power systems

In real power systems, with multiple inductive and capacitive elements, the magnitude and angle of the network impedance at any point in the network may be represented by a complex function of frequency which could contain multiple impedance peaks and troughs due to various parallel and series resonances present in the network [56] [57].

The network harmonic impedance is a key parameter in the calculation of voltage harmonic emissions based on harmonic current emissions but the assessment of harmonic impedance is a complex and difficult task [57] [58]. The network impedance at a point in the network is often determined by means of a frequency sweep analysis, as described in section 2.9.1.1, and visualised using plots of the impedance magnitude and angle. An example of the frequency sweep at a busbar in an HV network is shown in Figure 2-7.

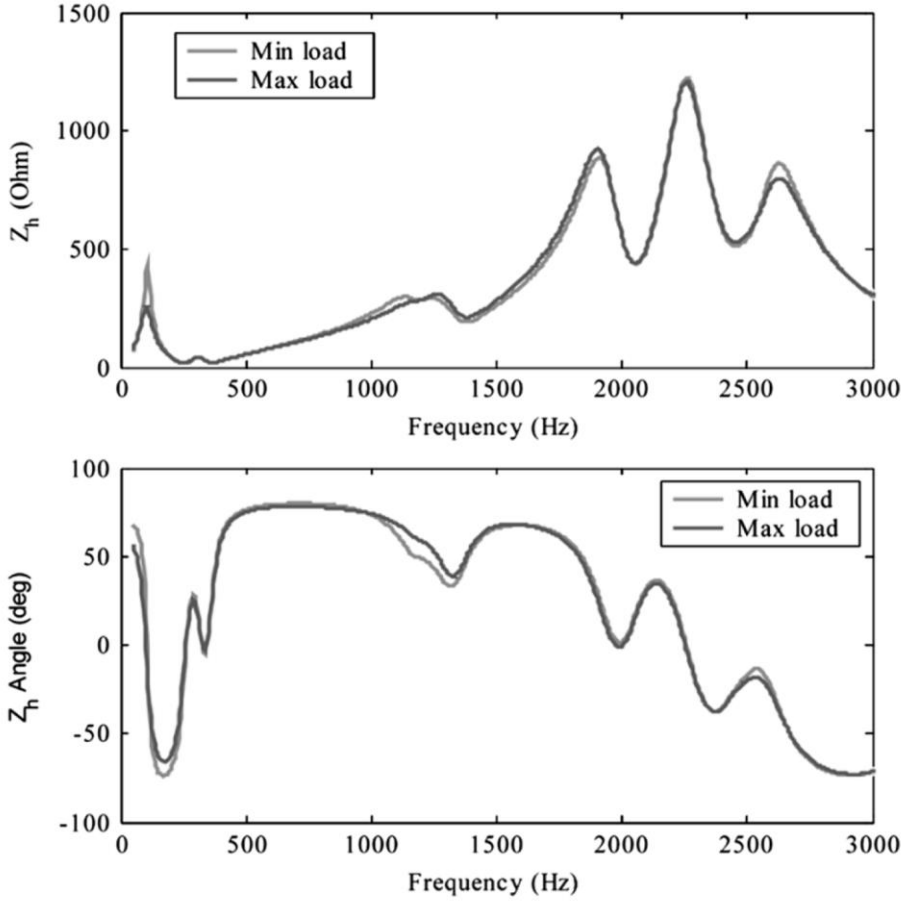

Figure 2-7: Network impedance magnitude and angle plotted versus frequency [56]

A frequency sweep may not be sufficient to identify all resonance problems in a network. Resonances which are not revealed on an impedance vs frequency plot can exist in the network. For example, a resonance could occur at a bus close to a capacitor bank which is relatively remote from the bus under study. It is therefore recommended to check the network harmonic impedance of buses close to significant harmonic sources and the transfer impedance between the harmonic source and nearby buses [55].

In some cases, worst-case impedance curves are considered based on the system fault level at the bus of interest. Calculations are made using these worst-case curves to determine whether new distorting loads can be connected with minimal risk. If calculation results indicate distortion outside of the limits, then more detailed studies may be required [57].

2.7.5 Elimination of problematic harmonic resonant peaks

Several methods can be considered to reduce or eliminate problematic system resonances:

- Add a shunt filter. A filter will absorb harmonic current at its tuning frequency and alter the system impedance characteristic. The resulting system response is often better than the original.
- Add a reactor to detune the system. A reactor may be added between a capacitor and the system source to move a problematic system resonance. This is usually done by placing the reactor in series with the

capacitor which has the added benefit of reducing capacitor inrush currents [59] or by adding a reactance to the line [36].

- Adjust capacitor sizes. Changing the size of a capacitor bank may be an economical way to move a system resonance depending on the network requirements [36] [60].
- Relocate a capacitor. Moving a capacitor to a point in the network with a different fault level or higher losses can eliminate or shift problematic resonances. This option is more likely to be feasible for utilities than for industrial customers since customer networks are frequently too small for relocation of the capacitor to make a significant difference [36] [60].
- Use an active filter or combination of active and passive filters, also referred to as a hybrid filter. An active filter is able to eliminate the resonance between a harmonic source and a passive filter. This is typically an expensive solution which is most likely to find application for low voltage, low power solutions [61] [62].
- Change the network operating configuration. Different network configurations affect the system impedance characteristic and can alter the resonance peaks caused by the combination of the installation and the network. All possible configurations must be considered in the design of installations and filters but changing the normal configuration or limiting the number of allowable configurations may assist in shifting or reducing a resonance. An example is operation of a substation in parallel bus configuration instead of split bus configuration to reduce the network impedance and increase the fault level [63].
- Eliminate a capacitor. If lower power factor, lower voltage and increased losses can be tolerated, then removal of a problematic capacitor may occasionally provide the most economical solution [36].

2.8 Solar PV plant technology

2.8.1 PV plant overview

The high-level architecture of a typical large solar PV facility is illustrated in Figure 2-8. Solar PV panels convert solar energy to direct current (DC) electricity. Panels are connected in series to form strings which produce sufficiently high DC input voltage for the inverters. String combiner boxes are used to connect multiple strings in parallel thus combining the individual string currents for input to the inverter. The inverters are distributed through the solar PV array and convert the DC voltage to three-phase low voltage AC. The inverter AC output voltage is stepped up to medium voltage by inverter transformers and the power is evacuated to a central solar park substation via MV feeder cables.

Several inverter transformers are usually located along the length of a single MV feeder. Ring main units (RMU's) are typically provided for the purpose of protecting and isolating individual inverter transformers and their associated inverters. For inverters which are not suitable for direct parallel operation but require galvanic isolation, three-winding MV/LV/LV inverter transformers are often used with one inverter connected

to each of the LV windings. For large plants, the MV power from the collector feeders is then stepped up by one or more station transformers to high voltage for connection to the distribution or transmission system.

2.8.1.1 Solar panel technology

The three most common types of PV technologies are crystalline silicon, thin film technology and concentrating PV [64]. In a utility-scale plant, panels are ground mounted on suitable mounting structures. Tracking systems may also be used to maximise efficiency by aligning the panels to receive maximum solar irradiation. Single axis tracking is the most common type of tracking system but dual axis tracking is also possible.

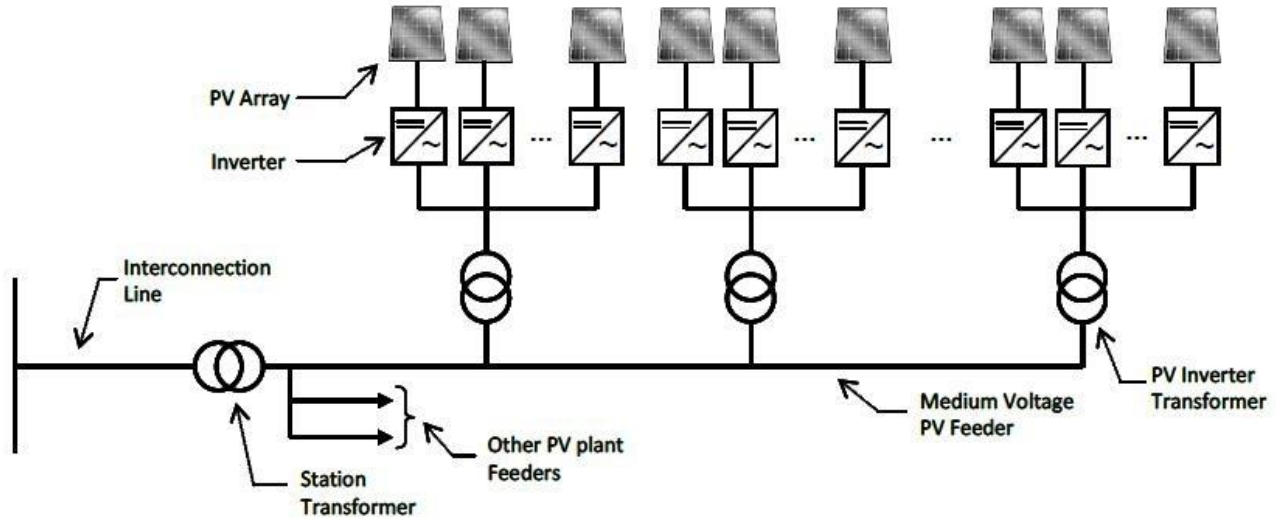

Figure 2-8: Simplified PV plant architecture [65]

2.8.1.2 Inverters

In grid-connected PV systems, inverters are required to convert the DC power supplied by the solar PV array into AC power so that the generated energy can be fed into the utility network. Assuming a high short circuit ratio, the voltage of the grid will not be substantially influenced by the inverters and the inverter AC current is proportional to DC power. The inverters therefore have the characteristic of a current source [22].

Since the early days of development of solar PV inverters, when existing uninterruptible power supply (UPS) and drive technology was modified for PV usage, more than fifty PV inverter topologies have emerged. Three types of voltage source PWM inverter topologies are commonly used: 1) transformerless topology, 2) low frequency (LF) transformer topology and high frequency (HF) transformer topology [22] [66] [67].

Transformerless inverters are commonly used for large-scale PV installations. They offer a simple, economical solution with low losses but require a high DC voltage (greater than 325 V for 230 V AC output) to produce a sinusoidal output at the required inverter output voltage (typically 220 to 690 Vac). This may be overcome by including DC-DC boost stages in the inverter but these also reduce efficiency by 1 to 2 %. In the case of a utility-scale PV plant, the DC-DC converters may be arranged in a multi-string configuration such that each string is supplied with its own DC-DC converter which performs maximum power point tracking and converts

PV string output to a controlled DC bus voltage. The DC bus is then connected to the central inverter for conversion to AC. However, most high-power commercial inverters use single stage inverter configurations with high DC string voltages and without DC-DC conversion stages [67].

2.8.2 Voltage source converter theory

Inverters are the primary sources of harmonic emissions within a solar PV plant due to the distortion of the output current as a result of the PWM switching of the inverter. Historically, three-level neutral-point-clamped inverters were developed in the 1980's due to limitations in available silicon semiconductor devices such as low breakdown voltage and high switching losses. However, modern power electronics devices operate at higher switching frequencies with high efficiency, and a simplified two level topology is feasible [68]. Currently most commercial high-power (>100 kW) PV inverters are voltage source inverters (VSI) with a two-level, single stage, three-phase full bridge topology [67]. A simplified topology of such an inverter is illustrated in Figure 2-9.

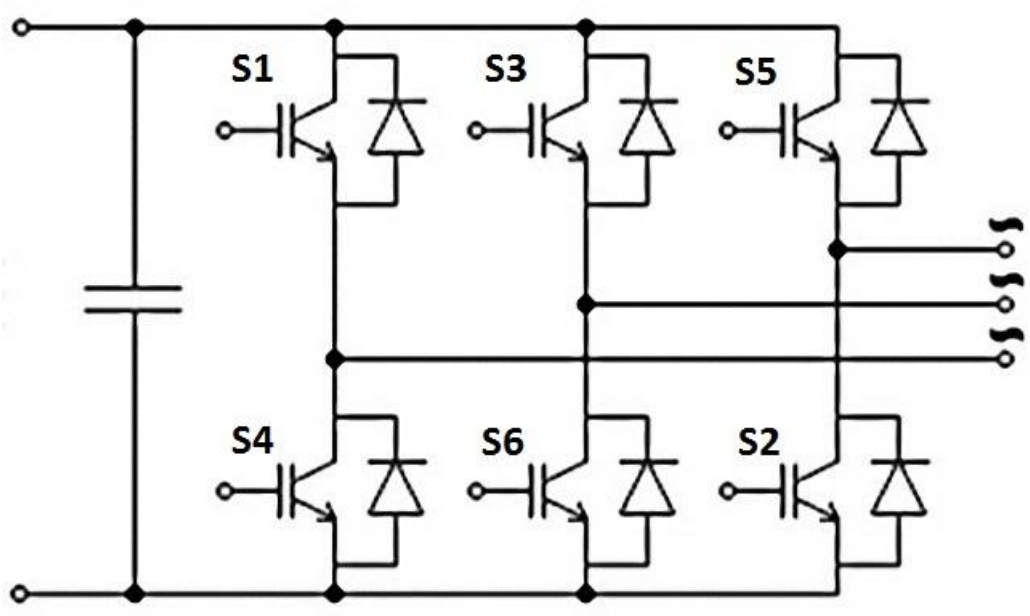

Figure 2-9: Three-phase, two-level voltage source inverter [69]

The inverter has six switches which may in practice be composed of two or more switching devices in series, depending on the DC operating voltage of the inverter. Insulated gate bipolar transistors (IGBT) are commonly used as switching devices for modern inverters and each IGBT is connected in parallel with a free-wheeling diode [70]. The purpose of the free-wheeling diode is to eliminate large voltage transients resulting from the interruption of inductive load current by providing an alternative path for the load current when the IGBT switch is opened, thus preventing damage or destruction of the IGBT's. IGBT's are rugged voltage-controlled devices which are switched on by application of a positive gate voltage and switch off when their gate voltage is zero or negative. This means that the IGBT inverter is self-commutated which enables application of PWM switching techniques for DC to AC conversion.

2.8.3 Pulse-Width Modulation (PWM)

A large number of PWM methods for power converters have been described over the past few decades and selection of a method depends on the application, the power rating and the semiconductor devices used. The PWM method is fundamental in defining the harmonic current emissions of the inverter [71]. Several common PWM methods are described below, followed by a discussion of the harmonic emissions generated by each method in section 2.8.4.

2.8.3.1 Sinusoidal PWM (SPWM)

Figure 2-10 demonstrates the principle of sinusoidal PWM. Sinusoidal three-phase modulating waves ($V_{mA,}$ $V_{mB,,}$ V_{mC}) are used with a higher-frequency, triangular carrier wave (V_{cr}). When the value of the modulating wave of a phase is greater than the value of the carrier wave, the upper switch in that phase's leg of the inverter is turned on – e.g. for $V_{ma} \geq V_{cr}$, leg A upper switch is on. When the value of the phase's modulating wave is less than the value of the carrier wave, the upper switch in the corresponding inverter leg is turned off – e.g. for $V_{ma} < V_{cr}$, leg A upper switch is off.

The switch in the lower leg always operates in the opposite state to the switch in the upper leg. Therefore, for phase A, leg A lower switch will be off when $V_{ma} \geq V_{cr}$ and on when $V_{ma} < V_{cr}$. To avoid short circuiting of the DC source during the switching of the upper and lower devices in the same leg, a blanking time is added when both switches are turned off. The line-to-line inverter voltage (V_{AB}) is calculated as the difference between the phase voltages, for example $V_{AB} = V_{AN} - V_{BN}$ as shown in Figure 2-10 [70].

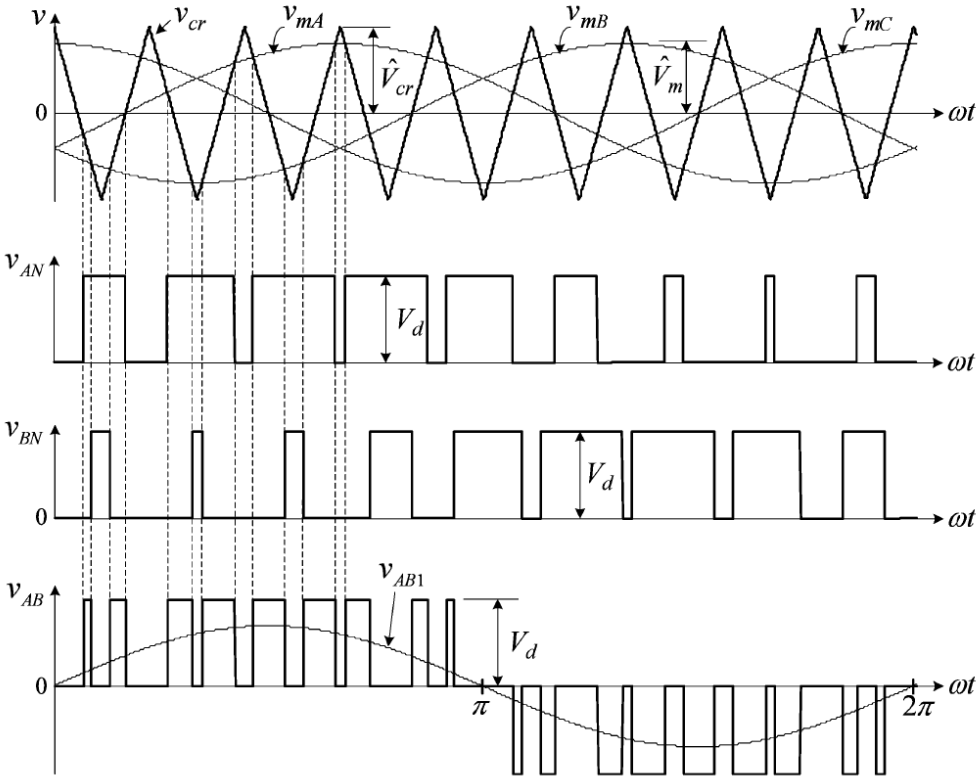

Figure 2-10: Sinusoidal pulse-width modulation (SPWM) [70]

The amplitude modulation ratio, m_a, is defined as the ratio of the modulating wave amplitude to the carrier wave amplitude. It determines the magnitude of the fundamental frequency component of the PWM waveform. The maximum value of fundamental frequency voltage achievable with SPWM is $0.612V_d$ when $m_a = 1$. Similarly, the frequency modulation index, m_f, is the ratio of carrier frequency to modulating frequency.

A variation of sinusoidal PWM uses a sinusoidal carrier wave with added triplen harmonic components resulting in a wave shape with a flattened top allowing the fundamental frequency component of the voltage to be increased to $0.707V_d$. The additional triplen harmonic components do not affect the harmonic spectrum of the inverter output [70].

2.8.3.2 Space Vector Modulation (SVM)

Space vector PWM is a commonly used digital modulation technique for control of voltage source inverters [70] [72]. SVM maximises the inverter output voltage and minimises the switching frequency [72]. The maximum fundamental frequency rms line-to-line output voltage using SVM is $0.707V_d$, which offers DC bus utilisation equivalent to third harmonic injection SPWM [70]. SVM also produces lower current harmonic distortion than SPWM [73].

2.8.3.3 Inverter control techniques

The preceding discussion of SPWM and SVM assumes an ideal inverter with constant DC link voltage. In real inverters, the DC bus voltage may vary, causing variation in the amplitude of the output waveform pulses. In the case of a solar inverter, large fluctuations in DC voltage are experienced due to varying irradiance, and phase and ground faults [74]. Open loop control may be used to compensate for low order harmonics and subharmonics in the DC link voltage. This can be achieved by adjusting the modulation according to the measured DC link voltage [72].

An alternative approach utilises feedback control whereby inverter output quantities are measured and the inverter switching adjusted according to the deviation from the desired setpoint. Several feedback control techniques exist with inverter output current usually chosen as the measured variable [75] [72]. Current control techniques can be broadly categorised as linear controllers – which operate with conventional a PWM modulator and independent controller – and non-linear controllers. Non-linear controllers include hysteresis control, pulse density modulation and neural network and fuzzy logic controllers [76]. Control performance may be improved by means of linear predictive techniques and real-time optimisation [71] [75] [76]. Robust current controller designs using H∞ and mu-synthesis are also described in the literature [74].

Various methods of controlling the active and reactive power of a PWM inverter exist. Voltage-oriented control is based on the current vector orientation with respect to the line voltage, while direct power control is based on control of instantaneous active and reactive power. Virtual-flux, direct-power control is an improvement on the aforementioned strategies since it is able to reduce harmonic distortion by producing a sinusoidal current output in the presence of non-sinusoidal line voltages [77].

2.8.4 Harmonic behaviour of solar PV inverters

Harmonic emissions from inverters can vary significantly depending on the PWM modulation scheme, control technique and switching sequence adopted. In practice, inverter emissions are quoted by the inverter manufacturer across the full range of active power output levels based on measurements taken with the inverter connected to a source with low harmonic content. The mechanisms of harmonic generation in PMW inverters and their harmonic characteristics are described in more detail in this section.

The harmonic distortion of AC currents in a PWM scheme reduces approximately linearly with increasing switching frequency. However, the switching frequency of high power converters is usually limited to a few kilohertz by the switching losses of the semiconductor devices and electromagnetic compatibility considerations [71].

Asynchronous PWM, also known as free-running PWM [73], describes a PWM implementation (SPWM or SVM) where the frequency of the carrier wave is fixed, even as the modulating frequency changes. Asynchronous SPWM can be easily implemented with analogue circuits but generates a continuous harmonic density spectrum with non-characteristic harmonics and interharmonics [70] [71]. In synchronous PWM, which is more suitable for a digital controller implementation with a low frequency modulation index, the carrier wave is synchronised with the modulating wave and m_f is an integer. The generated harmonic spectrum is discrete and only contains integer harmonics [70] [71]. It is also possible to modulate the frequency of the carrier wave using a technique called carrierless SVM, or by controlling the carrier frequency by means of a randomly varying signal. This produces in the continuous harmonic spectrum being distributed over a larger frequency range, instead of presenting as large amplitude harmonics centred around multiples of the carrier frequency [71].

In the case of synchronous SPWM, the waveform modulation is reflected in the frequency spectrum as harmonic sidebands centred around the carrier frequency, f_s, and integral multiples of the carrier frequency [70]. In order to avoid generation of non-characteristic harmonics, including even harmonics, the frequency modulation index should be chosen as an odd integer multiple of 3 (i.e. $m_f = 3.n$, $n = 1,3,5,\ldots$). For SVM, a variety of switching sequences are available which aim to minimise the number of switching operations whilst also reducing harmonic emissions – particularly at even harmonic orders for which contractual harmonic emission limits are typically low. In order to minimise generation of non-characteristic harmonics, the ratio of the output fundamental frequency, f_1, to the sampling frequency, $f_s = 1/T_s$, should be chosen as an integral multiple of 6.

The voltage and current THD of SPWM and SVM output waveforms decrease with increasing amplitude modulation index, reaching a minimum value at $m_a = 1$ [70] [71]. Examples of normalised harmonic voltage distortion versus amplitude modulation index for typical SPWM and SVM schemes are shown in Figure 2-11 and Figure 2-12 respectively. It can be seen that the rate of increase of fundamental frequency voltage exceeds

the rate of increase of harmonic voltage for all harmonic orders. Hence the percentage voltage distortion for individual harmonics also decreases at higher values of m_a.

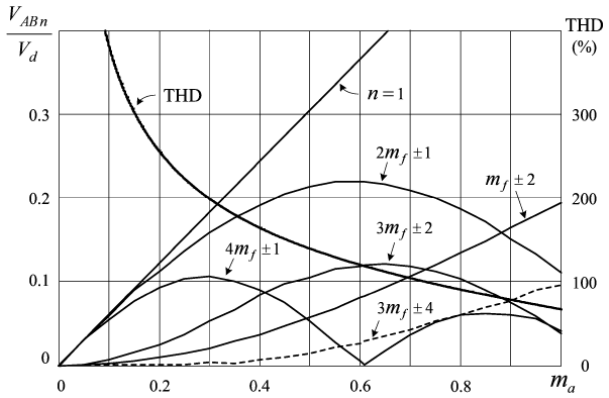

Figure 2-11: Harmonic voltage vs amplitude modulation index for a SPWM inverter [70]

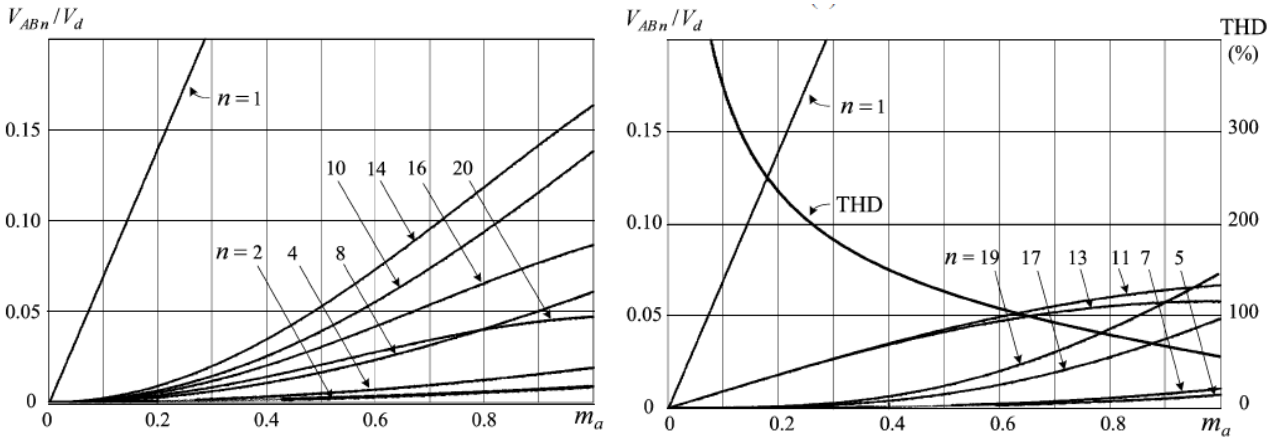

(a) Even-order harmonics ***(b) Odd-order harmonics and THD***

Figure 2-12: Harmonic voltage vs amplitude modulation index for a SVM inverter [70]

2.8.4.1 Effect of background harmonic distortion on inverter harmonic distortion

The presence of voltage distortion at the PCC may significantly impact the harmonic emissions of an inverter. Several studies have found that high background voltage harmonic distortion typically increases the harmonic emissions of an inverter [16] [78] [79]. For example, Zong, Gray and Lehn performed experimental tests on a solar inverter which showed an increase in total demand distortion (TDD) from 0.66% for an undistorted PCC voltage to more than 20% in the case of 3% voltage distortion at the PCC [78]. Hernández et al. determined from measurement of a plant containing 16 three-phase 50 kW inverters from three different manufacturers that voltage harmonics in the supply voltage strongly impacted the corresponding harmonic current emissions from the inverters. Their study also found that inverter harmonic current emissions at low harmonic orders increased background harmonic voltages at low power outputs but decreased these voltages at high power outputs [80].

2.8.4.2 Impact of solar irradiance on current harmonic distortion

Studies have shown that low solar irradiance conditions which result in low inverter power output can cause increased current THD percentage [18] [79] [81] [82] [83]. However, since the fundamental current is low at low inverter output power, the absolute harmonic currents may still be lower than harmonic currents at higher power output. Inverters operating at higher power output therefore usually have a more significant impact on the network voltage distortion [79] [83]. Factors affecting harmonic emissions at low power are deactivation of maximum power point tracking (MPPT), power factor control and harmonic control in some inverters for operation below 20% of rated power [79], and non-linear operation of inverters as a result of low DC voltages [18].

2.8.4.3 Inverter harmonic source impedance

In order to design an inverter with an unpolluted sinusoidal output current shape, even in the presence of a network voltage harmonics, the inverter output impedance must be high across a wide frequency range. In practice, output filters and damping networks at the inverter output terminals – specifically capacitive elements – may significantly reduce the output impedance and can also create a resonant circuit with the inductive network impedance [17].

2.8.5 Harmonic control and mitigation strategies for inverters

General harmonic behaviour of solar PV inverters has been discussed in section 2.8.4 and this section will discuss the current state-of-the-art of inverter harmonic emission control. Two strategies are generally adopted: passive filters and inverter control strategies, including active filtering functionality.

LC output filters employing a variety of configurations of series and parallel inductors, capacitors and damping resistors connected at the PWM inverter output terminals are applied to grid-connected single-phase inverters as described in [84] [85] and [86], and three-phase inverters as described in [54] [87] and [88], for example. The simplest configuration is to include a series inductor between the inverter and then network, but LCL filters are often preferred for high power inverters with lower switching frequencies since they offer superior harmonic attenuation performance, allowing the use of smaller, less expensive inductors and capacitors [54] [88].

Active filters are power electronic devices with the capability of dynamically adjusting to the network harmonic distortion and reactive power requirements. They are able to absorb harmonic components of the load currents such that the harmonic currents in the network are reduced and voltage quality is improved [51]. Many state-of-the-art inverters are capable of operating as active filters to improve network power quality. This capability is typically not considered in power quality standards related to renewable generation; this may lead to increased risk of interference between generation sources and the grid, or result in potential active filtering capabilities not being realised, thereby hampering further development in the use of inverters as active filters [89].

A plethora of control strategies and active filtering implementations for solar PV inverters are described in the literature. Techniques include use of robust control strategies [74], fuzzy logic controllers [90] and application of the internal model principle for current-loop control [75] [91] [92]. The authors of [93] describe a strategy for control of instantaneous real harmonic power calculated using p-q theory coupled with a DC link voltage control loop. Hybrid active filters which use a combination of passive filter elements with active filtering techniques are also frequently applied. Some examples of hybrid filter applications are described in [74] and [87].

2.9 Harmonic simulations

Two key elements are usually considered in the analysis and assessment of harmonic distortion: harmonic simulation and harmonic measurements. Network models allow for simulation studies to be performed in the planning stage to inform the design of new installations and may also be used to gain understanding of harmonic behaviour in the investigation of problems observed in the field or reported by customers [55]. Analysis of harmonic measurements, described in section 2.10, may be used as an alternative to simulation studies, to validate simulation models or to provide data required for modelling – such as background harmonic distortion levels and network harmonic impedance [6].

This section describes various simulation methods for harmonic analysis. A discussion of different software packages available for such analysis is included in section 2.13 whilst models for different network elements are described in detail in section 2.11.

The most common simulation methods for harmonic analysis are harmonic load flow calculations and frequency sweep analysis. These are frequency-domain methods used to understand periodic steady state behaviour of power system harmonics. Time-domain methods allow for more detailed analysis including the study of transient phenomena but require more detailed input information and are usually only applied in specialised applications cases where harmonic load flow methods are inadequate [6] [36] [55].

2.9.1.1 Frequency-domain methods

Direct calculation of harmonic distortion can be achieved by use of the current injection method. Harmonic sources in the network are modelled as current sources and voltage distortion is then calculated using the system admittance matrix. Although it is computationally efficient, the major shortcoming of this method is that it assumes that the network voltage is sinusoidal and is therefore only valid for low levels of harmonic distortion. The primary application of the current injection method is for frequency sweep analysis. A current injection is simulated at a busbar for a range of frequencies to calculate the voltage response, and thereby determine the magnitude and phase of the harmonic impedance characteristic of the network at the chosen bus. This assists in identification of system impedance resonances and is an important tool for filter design [6] [51] [55].

An evaluation of harmonic voltage and current distortion throughout the network can be achieved by means of an iterative harmonic load flow calculation. This is executed in a similar manner to a conventional load flow, usually by means of the Newton-Raphson method, but is calculated separately for each harmonic order for which sources are included in the network model. Harmonic loads and background harmonic distortion are represented by current or voltage sources of the relevant frequency, amplitude and phase angle and the frequency-dependent harmonic impedance characteristics of sources, loads and network elements are used to determine the network admittance matrix for each frequency. Steady-state voltage and current waveforms can be obtained by application of the inverse Fast Fourier Transform (FFT) to the calculated harmonic frequency spectrum [94] [55].

Harmonic load flow algorithms were originally developed by Xia and Heydt [95] for balanced systems while later work by several researchers developed methods for three-phase solutions suitable for unbalanced harmonic load flows [96] [97]. The three-phase fundamental frequency unbalanced power flow solution and harmonic three-phase representations of both the linear part of the power system and the harmonic sources are coupled to achieve a unified unbalanced harmonic load flow solution [6]. Balanced and unbalanced harmonic load flow methods are both available in commercial power systems analysis software packages [94].

Issues that warrant the use of unbalanced harmonic power flow solutions include the production of non-characteristic harmonics due to system unbalance, low-order resonance conditions at non-characteristic harmonic orders, substantial unbalance in transmission systems due to line geometry and the study of harmonic interactions between geographically distant harmonic sources [6].

2.9.1.2 Time-domain methods

Electromagnetic Transient (EMT) simulations are primarily designed for simulation of power system transients. They use simulation step sizes in the microsecond range to provide a time-domain solution of the voltage and current waveforms in the network. The steady-state time-domain waveforms can then be converted to the frequency domain by means of the FFT. The approach allows for detailed modelling of non-linear components including power converters and their controllers using the differential equations or state equations that define their performance. These can be defined in simulation software as programmed equations, logic blocks or a combination of the two. Calculation time for EMT simulations is frequently long due to the short step size required to achieve accurate results and highly detailed network modelling is usually required to achieve the desired results [6] [98] [94].

In certain cases, instead of using EMT simulations for a complete time-domain solution, frequency-domain analysis can be complemented by solution of local non-linear phenomena in the time domain and conversion back to the frequency domain by means of the FFT for use in a global frequency-domain solution of the entire network in an iterative manner. An early application of such an approach was demonstrated by Semlyen et al. in the modelling of transformer magnetising impedance effects [98] [99].

2.9.1.3 Other Techniques

Other methods developed for harmonic analysis include transfer function representations which are useful for representing the AC- and DC-side harmonics of power converters under different operating conditions, and harmonic domain analysis which uses a convolution technique to derive a set of non-linear equations which define the harmonic transfer through a device under steady state conditions. The harmonic domain method is well suited to evaluation of harmonic interactions between the AC system and large power converters but has the disadvantage of being very complex and requiring advanced formulations for each new component [6] [98].

2.10 Analysis of harmonic measurements

The second key component in the assessment of harmonic emissions is the analysis of harmonic data captured by means of field measurements. Methods for analysis of harmonic measurement data to quantify emissions from an installation or to estimate the harmonic impedance of the network are described in this section whilst measurement techniques and equipment are discussed in section 2.14.

2.10.1.1 Aggregation and statistical analysis of harmonic measurements

Measurement data captured according to the universally adopted IEC 61000-4-30 methodology needs to be analysed by means of a statistical approach. To extract the harmonic spectrum, the discrete Fourier transform is applied using a rectangular window whose width is 10 cycles (200 ms). The Fourier analysis assumes that the measured signal remains stationary during the measurement period. Fluctuations of the measured signal result in spectral leakage such that the energy of harmonic components is spread to adjacent spectral components and a harmonic grouping method is therefore recommended to improve the accuracy of the recovered spectrum [100] [101].

This spectral data of consecutive windows is then aggregated in the recording instrument to provide 3-second and 10-minute aggregated measurement values which are used in the harmonic analysis. The IEC recommends a minimum measurement period of one week for 10-minute values and daily assessment of 3-second measurements from seven consecutive days. Plots of the probability density function of data for individual harmonics from all measurements over a specified period can provide insight into the range of current and voltage distortion and the frequency of occurrence of a particular level of distortion [100]. The maximum, 99 % and 95 % cumulative probability (or percentile) values of daily and/or weekly voltages and currents are usually calculated for comparison with emissions limits in accordance with the requirements of the relevant standard [42] [8] [6].

Various statistical analyses are described in the literature to further characterise the harmonic behaviour of the installation. These include assessment of the impact of plant operating conditions on harmonic distortion, usually by comparing individual harmonic emissions, THD and TDD values against plant active power output [100] [102] [103] [104]. Analytical and empirical distributions can then be applied to characterise the

magnitude and phase of emissions from a distorting installation as done by Sainz et al. who used the Stacy and normal-uniform distributions to statistically characterise the current magnitudes and phase angles of a wind farm [102]. In earlier work, Cavallini et al. proposed use of Gaussian modelling to characterise distributions of harmonic vectors which they verified using measurements from a MV node [105]. Such distributions allow for further statistical studies of network harmonic distortion considering the impact of multiple similar installations, particularly with respect to analysing the harmonic cancellation effect due to the phase angle diversity of harmonic currents [102].

2.10.1.2 Waveform analysis

An alternative to the statistical analysis of aggregated recording data is the use of recorded voltage and/or current waveforms. Such recordings can be manually triggered or event triggered to capture transients due to system disturbances, for example capacitor bank switching. The recorded waveforms are seldom used for evaluation of compliance of an installation with respect to emissions limits but are commonly applied in the estimation of network harmonic impedance as described in section 2.10.3, for estimation of equipment parameters or to quantify distortion under specific operating conditions [106] [58].

2.10.2 Measurement-based methods for determination of emission contribution from an installation

Simple observation of harmonic voltage and current measurements at the point of connection of an installation is not sufficient to determine the emission levels of the individual installation. Methods of locating the source of disturbances, discriminating between network and customer contribution to the emission level and assessing the emissions from an individual installation are widely discussed in the literature [40] [58] [107] [108].

One method proposes comparison of measurements captured with the disturbing installation in and out of service. If the background distortion does not vary significantly over the measurement period, and the installation under evaluation offers a significant contribution to the disturbance at the PCC, then the magnitude of voltage emissions due to the installation (E_{hc}) can be calculated from the global emissions (U_h) and the background emissions (E_{ho}) according to the inverse general summation law as per (2.32):

$$E_{hc} = \sqrt[\alpha]{U_h^{\alpha} - E_{h0}^{\alpha}} \tag{2.32}$$

where α is the IEC 61000-3-6 general summation exponent for the relevant harmonic order according to Table 2-1. The background distortion can be measured over a period when the installation is disconnected, or extrapolated by means of a linear regression of the harmonic voltage versus installation apparent power demand to estimate the harmonic distortion when the plant apparent power is zero as shown in Figure 2-13 [58].

If possible, background measurements should be measured with the installation disconnected since the harmonic impedance of the installation can affect the overall harmonic distortion at the PCC, even if the

distorting loads are not operational. This is particularly true in the case that the installation has large capacitive loads [43]. A variation of this method is to simply take a once-off measurement before and after connection or disconnection of the plant but results must be carefully evaluated since the method lacks statistical validity [58].

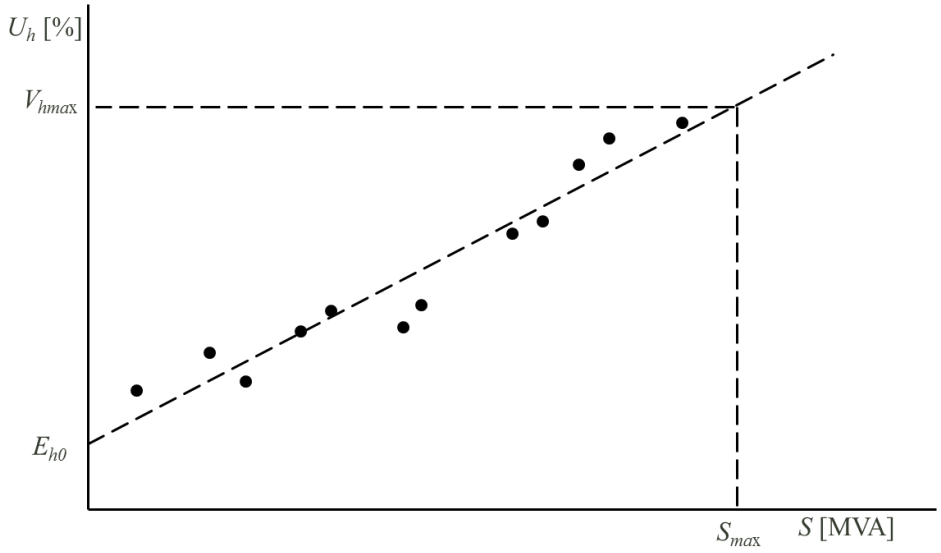

Figure 2-13: Calculation of background harmonic distortion based on linear regression of voltage harmonic distortion vs installation apparent power demand

A second approach uses long-duration simultaneous measurements of harmonic voltage and current magnitudes. The magnitude of the harmonic impedance of the network and the installation for the harmonic under consideration must be known and must remain constant; both of these conditions can be problematic in reality. The network impedance (Z_h) is typically obtained by means of simulation whilst the installation impedance (Z_{hc}) can be approximated as being equal to the impedance of the distribution transformer which connects it to the network [58].

Z_h and Z_{hc} are represented as two straight lines on a voltage vs current plot. Clustering of measurement points around the Z_h impedance line indicates the installation is the dominant source of harmonic current – i.e. harmonic currents generated by the installation are flowing into the network impedance – whilst clustering of points around the Z_{hc} line indicates that the installation is absorbing harmonics from the network. Where the points are scattered over the area delimited by the two lines, the resulting harmonic voltages are due to the combined influence of the background distortion and the installation. The three scenarios are illustrated in Figure 2-14. It is also noted that the 95th percentile voltage harmonic emission of the installation can be calculated from the 95th percentile value of the measured current harmonic emissions and the network harmonic impedance, in alignment with the IEC 61000-3-6 and NRS 048 methodologies [58].

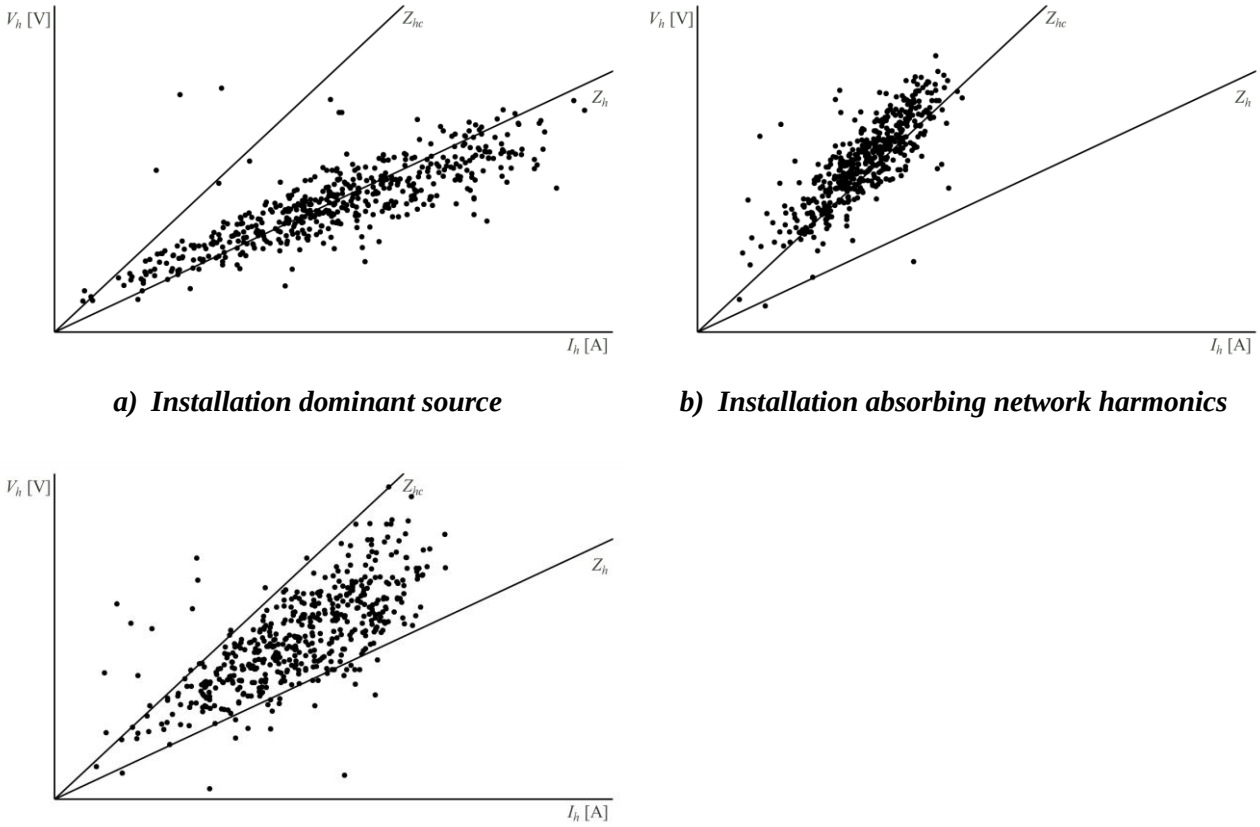

a) Installation dominant source

b) Installation absorbing network harmonics

c) Combined network and installation contributions

Figure 2-14: Method for long-duration simultaneous measurement of harmonic voltages and currents

Alternatively, if harmonic voltage phasor measurements are available, the emission voltage phasor can be calculated by the harmonic voltage phasor method according to equation (2.33).

$$\bar{E}_{hc} = \bar{U}_h - \bar{E}_{h0} \tag{2.33}$$

where $\bar{E}_{hc}$ is the harmonic emission phasor at harmonic order h, $\bar{E}_{h0}$ is the phasor of the background harmonic voltage and $\bar{U}_h$ is the harmonic voltage at the point of evaluation. The harmonic emission phasor of the installation ($\bar{V}_{pv}$) is calculated for all measurement points where the magnitude of the measured voltage exceeds the background voltage distortion, i.e. $|\bar{V}_{POC}| > |\bar{V}_{bg}|$ whilst the emission for periods when $|\bar{V}_{POC}| \leq |\bar{V}_{bg}|$, the emission is considered to be zero. The 95th percentile of the emission phasor magnitudes can then be used for assessment purposes. The phasor diagram representing equation (2.33) is illustrated in Figure 2-15 [58].

Pfajfar et al. propose a modification of the voltage phasor method called the harmonic vector method which uses reference impedances considered to improve robustness of the method and reduce the sensitivity of the calculation to changes in the utility network. They further propose the projection of the customer harmonic emission vector ($\bar{E}_{hc}$) onto the measured harmonic vector ($\bar{U}_h$) as a superior measure of the customer's contribution to the measured emission. The method can be applied to harmonic current or voltage vectors [109] [110]. Xu and Liu have proposed a similar method based on reference impedances which converts impedance changes on the customer or utility side into equivalent current source changes with the aim of separating

customer and utility contributions while isolating the effect of network impedance changes so that the customer is not held responsible for changes to the utility network impedance [111].

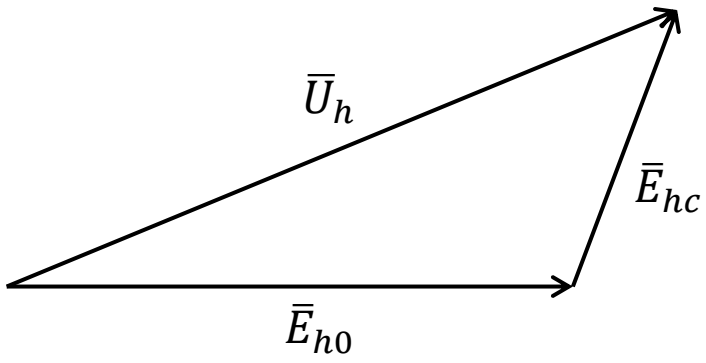

Figure 2-15: Harmonic voltage phasor method

Another suggested approach uses assessment of harmonic power to determine the source of emissions. If active power of harmonic order *h* is positive (the same direction as fundamental frequency active power), the customer is considered not responsible for the distortion but if it is negative (the opposite direction to fundamental frequency active power), customer is considered responsible. This method has the shortcoming of only attributing predominant responsibility and it can be problematic in certain scenarios due to the uncertainty with respect to the sign of harmonic power that is observed when the phase angle between voltage and current harmonics approaches 90° [108]. Several papers including work by Xu et al. and Santos et al. investigate the validity of the harmonic power method by theoretical and experimental means and demonstrate its weaknesses. Xu et al. conclude by emphatically stating that the method is not suitable for harmonic source detection [112] [113].

Further work by Li, Xu and Tayjasanant, based on harmonic reactive power measurements, also uses approximate network and customer impedances, and appears to be more accurate than the harmonic active power method in identifying the source of harmonic emissions, but cannot quantify the actual emission contribution of an installation [107] [40]. The challenge with the aforementioned reference impedance methods is the requirement for reasonable estimates of the utility network harmonic impedance, and in some cases also the customer network harmonic impedance, which are often not available. Although methods have largely been developed and tested using single-phase systems, certain methods can be extended to three-phase systems by use of symmetrical component theory [111].

Several methods are also described in the literature for assessing the relative impact of multiple installations connected to the same busbar. Zang and Yin propose a method using data selection from short-term measurements to calculate a harmonic impact index for each installation based on the bus voltage and the individual installation currents. The harmonic impact index which they define aims to quantify the influence of each installation on the overall harmonic distortion at the PCC [114]. Moustafa et al. calculate a non-linearity factor for individual installations connecting to a common bus which considers the relative distortion of the installation's measured waveform compared to the calculated waveform of an equivalent linear load

comprised of a resistor and inductor [115] [113]. Browne et al. criticise the validity of Moustafa et al.'s method by highlighting the fact that capacitance is neglected in the load model which could lead to false identification of distortion where none exists and then note that the technique lack usefulness since it does not identify any specific compliance test [40].

The preceding methods described in this section all consider harmonic voltage and current measurements captured at a single point of evaluation, usually the PCC. Methods have also been proposed which seek to locate sources or quantify emissions based on simultaneous harmonic phasor measurements at multiple buses. Some theoretical formulations, instrumentation and practical implementation recommendations for multi-point measurement schemes are described in [116], [117], [118] and [119].

2.10.3 Measurement-based methods for harmonic impedance estimation

In addition to detailed modelling and impedance loci methods described above, a significant body of work describes methods for estimating the harmonic impedance at a point in the network by means of measurements. The CIGRE-CIRED Working Group C4.109 provides a summary of some of the most promising methods which use measurement of harmonic voltages and currents in the network and can be broadly classified into two categories: non-invasive methods and invasive methods. [58]

Non-invasive methods do not require disruption of the operation of the network or harmonic loads and seek to use naturally occurring events as a source of disturbance for calculation of the impedance. One method uses a significant harmonic source in the network, such as an arc furnace or cycloconverter, to vary harmonic voltages and currents at the point of evaluation. The source must generate harmonics and/or interharmonics that greatly exceed the background levels but the variation in harmonic distortion can be achieved by changing its operating mode without requiring it to be disconnected from the network [58]. The accuracy of results is improved by use of multiple measurements of voltage and current. Linear regression or more advanced statistical methods, such as the graphical representation and statistical method proposed by Langella and Testa, can be applied to estimate the impedance based on the measurement data [57] [120].

An alternative approach relies on use of switching transients or natural variations in the power system as the source of disturbance. Switching operations of capacitor banks and transformers generate transient currents with a wide current spectrum containing many harmonic and interharmonic orders. These switching operations, particularly capacitor switching operations, are common in the normal operation of the network. However, the method has disadvantages in that currents may be unsymmetrical depending on the switching moment, transients are of short duration and the accuracy of results may be affected by pre-existing harmonic voltages or by current transformer saturation. Analysis of interharmonic frequencies may be used to avoid the influence of pre-existing dominant harmonics or alternatively, these dominant harmonics may be accounted for by means of vector subtraction of the post- and pre-switching harmonic voltages [57] [58] [106].

Natural variations in harmonic currents and voltages over a given time interval can be used to estimate the harmonic impedance of the customer installation and the external network as observed at the POC. The sign

of $\Re\left\{\frac{\Delta\bar{U}_h}{\Delta\bar{I}_h}\right\}$ is used to determine the dominant source of the change in harmonic current and voltage – the customer installation or other sources in the network. Changes caused by the customer installation can be used to estimate the network impedance whilst changes caused by other sources in the network can be used to estimate the customer installation impedance. The method appears to give fairly accurate results but requires a significant variation in harmonic levels, typically caused by some dominant disturbing loads, and needs upstream and downstream parameter variations which do not occur simultaneously [57] [58].

Xiaoquing et al. propose an improved method based on the use of statistical analysis techniques to filter customer-dominant fluctuation thereby reducing the error caused by the assumption that the utility and customer installation fluctuations do not occur simultaneously [121]. Other analysis methods have also been proposed to improve the accuracy of the impedance calculated from the measurement data, such as the use of the wavelet transform in place of the Fourier transform to allow for localisation of signals in both the time and frequency domains [122].

Invasive methods use various harmonic sources to directly inject harmonic or interharmonic currents into the power system in order to measure the harmonic impedance of the network. Proposed sources for such injection are electric railways, saturated transformers, dedicated harmonic generators and ripple control systems [58].

2.11 Review of case studies related to power system harmonics and solar PV

Several papers describe the modelling of individual PV systems to evaluate the PV system's harmonic distortion under various operating conditions. Oliva and Balda evaluated the harmonic current emissions of a 200 kW solar park within the framework of IEEE 519 emission limits using long-term measurement data recorded in 1995. They describe the variation of current and voltage THD, current TDD and selected individual current harmonics with apparent power output based on long term measurement data. Background distortion was assessed by disconnecting the installation and by repeated connection/disconnection of one PV system. They inject the measured currents into a model of the network and conclude that the contribution of the solar park to the measured voltage distortion is small [13].

Chidurala et al. study a 1.2 MW rooftop installation by modelling and harmonic measurement. They report increased current THD during periods of low solar irradiance but note that this may be due to low fundamental current magnitude. Voltage THD remains relatively constant for different levels of irradiance [12]. Similar studies for smaller LV-connected plants of 20 kW and 6 kW are described in [123] and [14] respectively.

Modelling has also been done to evaluate the impact of multiple small embedded PV systems, typically in the form of residential rooftop installations. Vasanasong and Spooner develop an experimental deterministic model of a PV inverter and then propose stochastic modelling techniques to describe the behaviour of multiple distributed inverters. The model is validated using measurement data from the Sydney Olympic Village [16].

Enslin and Heskes analysed the performance of distributed rooftop PV inverters in a Dutch suburb with a high concentration of rooftop PV systems. They use analysis, measurement and simulations to study the network and conclude that resonance effects are responsible for higher than expected current and voltage distortion [17].

One of the first studies evaluating the harmonic impact of a large utility-scale PV plant (20 MW) was published by Varma et al. in 2016 [15]. The authors develop a PSCAD/EMTDC model of the utility network in the region of the PV plant which is validated by load flow studies and SCADA measurements. Two 10 MW solar farms are modelled as aggregated harmonic current sources. The model is used to study network resonances and to analyse the harmonic impact of the plant under various network conditions. Measurement data from a period of several months were used for harmonic impact studies with different short-circuit levels and network resonance conditions. Measured harmonic currents from each solar farm POC were injected at the POC buses in the model based on the assumption that the plant acts as a pure current source.

Other papers present an analysis of the harmonic emissions of solar PV systems based purely on measurement data without modelling the system, for example [18] and [19]. Several studies have also been conducted for large wind farms. Modelling of a 10MW wind farm prior to construction of the actual plant is presented by Papathanassiou and Papadopoulos [56], while analyses of harmonic measurements from operational wind farms are presented in a number of studies [100] [102] [103]. Huan and Tayjasanant present the harmonic modelling of a 90MW wind farm with verification using actual measurement data [104]. However, their approach is limited to calculation of frequency sweeps based on the wind farm model. Validation is only presented in general terms by evaluation of harmonic voltage emissions versus active power output and by assessment of single-measurement harmonic voltage and current spectra.

2.12 Modelling techniques for harmonic simulations

2.12.1 Introduction

Accurate modelling of frequency-dependent network components is necessary to study the harmonic performance of a network. Sources of harmonic current emissions, the harmonic impedance of network elements and the network background harmonic voltage distortion must be considered [17]. Simplified representations are often required to reduce computer memory requirements and avoid excessive calculation time, but models must not be oversimplified as this may result in loss of information concerning the harmonic spectrum [124]. It is desirable to develop a model that is sufficiently accurate to allow for analysis of network harmonic behaviour up to at least the 40^{th} harmonic [125].

In this section, the modelling of network components relevant to the study of harmonic behaviour of utility-scale PV farms in the network is considered.

2.12.2 PWM solar inverters

Many harmonic models have been proposed for three-phase inverters and other power electronic devices, the most common and simplest of which is the harmonic current source model. Inverters are modelled as harmonic currents sources with current magnitudes and phase angles specified based on measured values or detailed inverter simulation models. Harmonic currents can be scaled linearly with fundamental frequency output current or a range of values specified based on tests measurements obtained across a range of output powers. Where harmonic current angle information is not available, the IEC 61000-3-6 general summation law can be applied to account for anticipated harmonic cancellation, although the validity of this approach should be tested where multiple identical inverters are used as their harmonic current phase angles may exhibit limited variation, even at higher frequencies [16] [98].

In practice, voltage source converters, such as solar inverters, do not have infinite source impedance and a may be significantly impacted by background harmonic voltage. Therefore, a Norton equivalent source may be chosen as a better representation, using data from the manufacturer to derive the equivalent impedance. Any filters, such as output choke or LCL filter, should also be represented [53]. Benhabib et al. recommend a current source in parallel with a capacitor as an adequate simplified inverter representation for harmonic modelling of distributed PV generators in a large LV network. The current source is modelled to represent the actual harmonic emissions of the inverter when the grid voltage is free from harmonic distortion, as determined from measurements taken in an experimental setup or from a detailed model of the inverter [124].

More detailed models may be necessary if voltage distortion is significant or voltages are unbalanced. The IEEE Task Force on Harmonics Modeling and Simulation identifies generic approaches to developing detailed models which include developing analytical formulae from the Fourier series as a function of terminal voltage and operating parameters, developing analytical models for harmonic source operation, and solving for the current waveform using time-domain simulations [98].

A number of papers, including [125] and [126] propose average circuit models based on the complete models of specific inverters. Detailed knowledge of the inverter topology and control strategy is required to develop such models. Vasanasong and Spooner modelled single phase inverters, based on experimental measurement data, by using linear regression to develop a series of linear equations that represents the relationship between inverter current and voltage. A stochastic model was then applied to account for the random variation of harmonic sources combined with other sources [16].

2.12.3 Overhead lines

The performance of an overhead line or cable is defined by four distributed parameters: series resistance, series inductance, shunt capacitance and shunt conductance. The parameters per unit length are calculated from line geometry and conductor data and also include the effect the earth return path [6] [127] [94]. Transmission lines are commonly modelled using a multiphase coupled nominal pi representation. For balanced harmonic analysis, the model can be simplified to a single-phase nominal pi circuit as shown in Figure 2-16 but three-

phase lines must represent coupling between phases and mutual coupling between line circuits in the case of parallel line circuits [51].

Due to the inverse relationship between frequency and wavelength, a line may appear long relative to the short wavelengths of higher harmonic orders, even if it is short compared to the fundamental frequency wavelength of 6000 km (50 Hz). Therefore long-line representations which use distributed parameter models may be required for harmonic analysis [55] [51]. Distributed parameter models which represent wave propagation parameters must be used where the line length approaches one quarter of a wavelength [47], although the IEEE task force recommends that 60Hz lines longer than 150/h miles be modelled to represent long-line effects, where *h* is the harmonic order [51]. Considering a 50 Hz system, this is equivalent to 288/*h* kilometres.

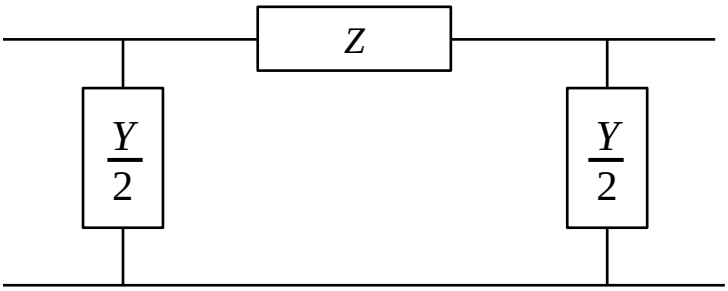

Figure 2-16: Transmission line model

The hyperbolic long-line equations are used to calculate the parameters of the distributed model representation. If, for a long line, Z' and Y' represent the series impedance and shunt admittance per unit length respectively, then the lump series impedance (Z) in Figure 2-16 is replaced by $Z_c \sinh(\gamma \cdot l)$ and each of the lump shunt admittances ($Y/2$) is replaced by $\frac{1}{Z_c}\tanh\left(\frac{\gamma \cdot l}{2}\right)$, where $Z_c = \sqrt{\frac{Z'}{Y'}}$, $\gamma = \sqrt{Z'Y'}$ and l is the line length [47].

The other key consideration is the frequency dependence of the line's series impedance which is primarily caused by two factors: the conductor skin effect and the earth return effect [51]. The skin effect is the phenomenon whereby alternating current density increases towards the outside of a conductor, resulting in the conductor's AC resistance being larger than its DC resistance. The resistance of the overhead conductors therefore increases with frequency; the exact relationship between AC and DC resistance is dependent on the conductor geometry.

Accurate skin effect calculations are based on complex Bessel function [6] [51]. Solution of the Bessel functions may be slow due to convergence problems [6], and various alternative methods and approximate formulae for different conductor types – including the ubiquitous ASCR (aluminium conductor steel reinforced) type – are proposed. Some of these are described in [6], [51], [55] and [128] which provides an approximation to include the effect of stranding of conductors.

Modern simulation packages, such as DIgSILENT PowerFactory, are able to accurately calculate the frequency-dependent impedance of conductors using numerical methods based on solution of Bessel functions

[94]. Although the series resistance is a typically a small component of the line impedance under normal conditions, resistance plays a significant role in determining system voltages and currents under system resonant and near-resonant conditions. Models which ignore the skin effect could result in large errors in voltage and current magnitudes, up to 30 - 50% in some cases [6] [55].

The effect of the earth return path should also be correctly modelled to represent its frequency dependence. The values of the earth return path resistance (R_e) and reactance (X_e) can be calculated using infinite series to solve Carson's equations, which give the self and mutual impedance of overhead conductors [6] [128]. Several simplified formulations and approximate models have been proposed which provide accurate results when compared to Carson's equations [6] [55].

2.12.4 Cables

Considerations for modelling of underground cables are similar to those for modelling of overhead lines, however long-line effects may be more significant due to the higher shunt capacitance of cables and the critical cable length above which long-line effects should be considered is 173/*h* kilometres for a 50 Hz system, where *h* is the harmonic order [51]. The cable capacitance is largely independent of frequency but must be modelled accurately for harmonic analysis since it shifts the system resonant frequency to lower orders and can result in amplification of background harmonics [53].

Nominal pi models, cascaded nominal pi models of short line sections, and distributed equivalent pi models may be applied to modelling of cables whilst advanced geometric cable modelling in the time domain provides a very accurate representation up to 1 MHz at the cost of high computational burden and difficulty in parameter estimation [53] [129]. Badrzadeh et al. therefore recommend the distributed equivalent pi model described in section 2.12.3 to provide the best trade-off between accuracy, simulation speed and ease of parameter estimation [53].

Malekian et al. further develop the distributed parameter equivalent pi model for use in sequence component calculations. They show that for single core cables installed in trefoil configuration with sheaths earthed at both ends, the positive, negative and zero sequence calculations may be performed using separate pi circuits without any coupling. Even for flat formation cables, use of separate pi circuits for phase component calculations provides a reasonable approximation with the error becoming very small at higher frequencies [130].

More detailed methods for the calculation of the cable impedance and admittance parameters are also presented in the literature. Many of these consider current flow in the coaxial loops formed by the conductor, sheath and armour and are based largely on classical formulae developed by S. A. Schelkunoff in the 1930's [6] [94] [130]. These methods have informed analytical implementations based on physical parameters in commercial modelling software packages such as DIgSILENT PowerFactory and EMTP and consider multiple facets including the earth return path, skin effect, mutual coupling effects and the influence of semiconducting tape on the admittance of MV cables [6] [94] [131].

2.12.5 Power transformers

Transformers are frequently represented by linear equivalent circuit models consisting of an ideal transformer and lumped R, L and C elements. A common T-equivalent per-phase positive sequence representation of a two winding transformer is shown in Figure 2-17 [47] [127] [94] [132]. The transformer is ideal and the other elements are defined as:

- $R_{Cu,HV}$ and $R_{Cu,LV}$ are the winding resistances which account for copper losses,
- $X_{\sigma,HV}$ and $X_{\sigma,LV}$ are the leakage inductive reactances which represent the leakage flux about the windings,
- R_{Fe} is a shunt resistance which accounts for the transformer iron losses which are comprised of eddy-current and hysteresis effects,
- X_m is a shunt inductive reactance to model the magnetising current of the transformer core.

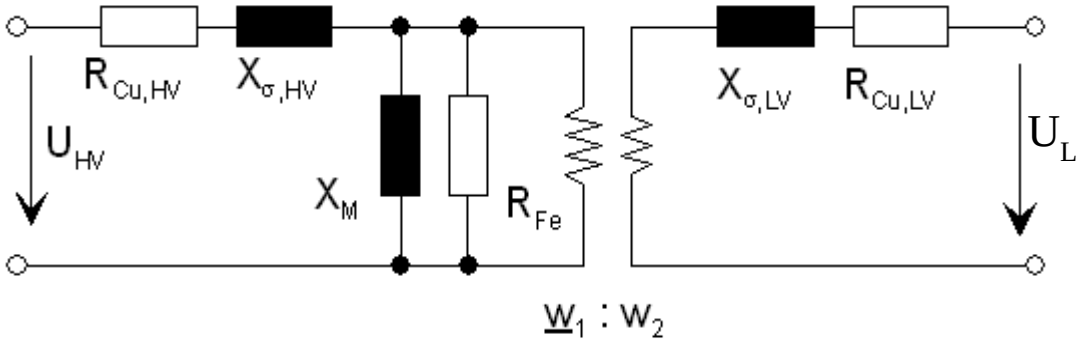

Figure 2-17: Fundamental frequency transformer model (T equivalent) [94]

The equivalent circuit parameters can be obtained from factory tests performed in accordance with IEC 60076 [133]. In the absence of more detailed information, winding resistances and leakage inductances can be modelled such they are equally shared between the HV and LV windings [132]. Tap changers can be accounted for by means of an additional ideal transformer which is modelled on the relevant side of the transformer to modify the voltage magnitude and phase according to estimated or measured transformer data. The tap dependant transformer impedance may also be included in the model. Separate zero sequence equivalent circuit models are required which are developed to represent the transformer winding arrangement (star, delta or zigzag) and neutral earthing configuration [94].

The model shown in Figure 2-17 is not adequate for harmonic simulations because it does not accurately reflect the high frequency performance of the transformer. Avila-Rosales and Avarado proposed a non-linear frequency-dependent model for the transformer core consisting of parallel branches each consisting of a series resistor and saturable inductor to account for frequency dependence of the exciting current [134]. The IEEE Task Force authors recommend that a current source be used in place of the magnetising reactance, X_M, to represent the harmonic generating effects of the magnetising branch [51]. The value of the current source may be determined from the flux-current curve and the supply voltage. Based on earlier work by Greene and Gross

[132], Dugui and Zheng [135] propose an iterative numerical algorithm using frequency- and time-domain analysis to determine the magnitude and phase of the magnetising current for each harmonic order.

Transformer saturation characteristics should also be modelled if harmonics generated by the transformer are of interest, simulations of transformer inrush are necessary, or a DC current component exists which is likely to cause core saturation. Saturation is difficult to model exactly but can be approximated using two slope or polynomial characteristics or interpolated current/flux tables [53] [51] [94].

Skin effect can also cause non-linear variation of the short circuit resistance and inductance as the frequency increases. The winding resistance increases and the inductance decreases slightly with frequency. Addition of a resistor in parallel with the HV and LV leakage reactances, $X_{\sigma,HV}$ and $X_{\sigma,LV}$, (or the R_{cu} + X_{σ} series combinations) reasonably approximates this effect [53] [51] [131]. References, such as [132] and [51] suggest that the skin effect is likely to be small in the frequency range of interest for harmonic studies.

At frequencies above 2-3 kHz the transformer winding capacitances and capacitive coupling between windings start to have a significant effect and should be included in the transformer model. At higher frequencies, inter-turn capacitances also influence the transformer's behaviour but it is not usually necessary to consider these effects for conventional harmonic studies, which are limited to consideration of frequencies below 2500 Hz [53] [51].

To account for the capacitive coupling effects, the conventional T-equivalent model may be modified to develop the second order model shown in Figure 2-18. The lumped capacitances $C_{W(HV)-E}$ and $C_{W(LV)-E}$ represent the turn-to-turn capacitance, stray lead capacitance and capacitance from the windings to the case; the values of these capacitances are highly dependent on the design of the transformer. The $C_{W(HV)-W(LV),1}$ capacitance represents the winding-to-winding capacitances and is depends on the winding geometry and separation between windings [55] [94]. Badrzadeh et al. note that ignoring the effect of transformer capacitance in a typical wind farm model has little influence on the overall network impedance since the cable capacitance of the collector cable network is dominant; capacitance of the collector cable network is in the µF range compared to transformer capacitance which is in the nF range [53]. Similar results could be anticipated for utility-scale PV plants with extensive collector cable networks.

For three-phase transformers, the phase shift caused by the transformer's vector group – usually +30° or -30° – should be represented. This is because different order harmonic voltages and currents will experience different phase shifts according to their characteristic sequence [51]. Advanced distributed models of transformers can be developed to account for the distributed nature of the actual inductances and capacitances in the transformer but this level of sophistication is considered unnecessary unless waveforms within the transformer itself are to be examined [55].

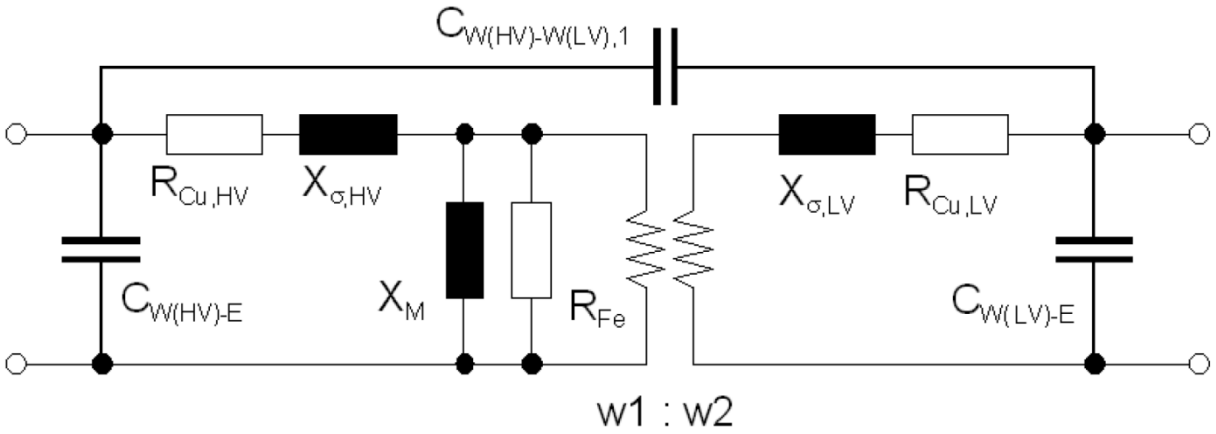

Figure 2-18: Second order transformer model [94]

2.12.6 Capacitors, reactors and filter banks

Shunt capacitors are typically modelled as a capacitive reactance between the bus and ground. A series resistor is often added to account for dielectric losses and a parallel resistor may be added to represent the discharge resistor present in real capacitors. The model is illustrated in Figure 2-19. The discharge time constant is usually of the order of 60 s, yielding a parallel resistance of more than a megohm and the discharge resistor is therefore frequently omitted from the model [55] [127].

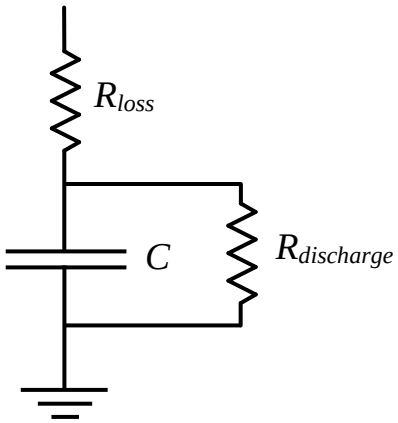

Figure 2-19: Shunt capacitor model

Filter banks are typically represented as resistors, capacitors and inductors configured in the topology of the actual filter that they represent. A small series resistor can be specified to represent the reactors' copper losses and capacitors' dielectric losses. In some simulation packages, the filter MVAr rating, tuning frequency and quality factor can be entered and the relevant R, L and C values are automatically calculated. It is also important to consider the three-phase connection of the bank (star / delta), the earthing arrangement of the star point, if present, and any stray capacitances that may exist [127] [94]. In the case that iron core reactors are used (as opposed to air core reactors), similar considerations to those described in section 2.12.5 for transformer modelling apply to account for non-linear magnetising reactance of the core.

2.12.7 Modelling of the utility network and network simplification

The wider transmission or distribution network has a frequency-dependent impedance characteristic and is a source of background harmonic distortion. Therefore, an infinite bus representation is not adequate for harmonic studies [53].

2.12.7.1 Network harmonic impedance

A simple model represents the grid impedance as an inductance and resistance defined by its fundamental frequency short circuit impedance. The magnitude of grid harmonic impedance will therefore vary linearly with frequency. Such simplified, linear grid elements(s) in the simulation model should be connected such that the network under consideration is modelled in detail up to two or three busbars distant from the point of evaluation. This is necessary to account for the influence of local reactive power compensation devices but even then, this method is generally only valid for very strong transmission connections and is should be limited to the investigation of harmonic distortion at frequencies below the first resonant frequency [53].

EMT and harmonic models of a large region of the utility network can be developed from available load flow or short circuit models using data conversion utilities [136]. In the context of renewable plant design, use of such detailed network models may require close collaboration between the plant developer and the utility due to the confidentiality and intellectual property issues which limit third-party usage of the utility's network model. As an alternative, the utility may provide frequency sweep data taken from a detailed simulation model in the form of amplitude and phase angle of the harmonic impedance up to the frequency of interest (typically the 40^{th} or 50^{th} harmonic) [53].

Watson and Arrillaga proposed the development of frequency-dependent equivalent circuit to represent the network impedance in cases where the interconnected network is linear and its configuration is known, but this appears to be a time consuming and computationally intensive method limited to use for relatively simple networks [137]. An alternative approach is the use of impedance loci, or envelopes. For a particular harmonic order, a region in the R-X plane is defined, indicating the range of impedance magnitudes and angles that can be expected under any normal or contingency network operating condition. Critical resonance conditions will always occur on the boundary of the region surrounding the possible harmonic impedance results. An example of such a locus is shown in Figure 2-20. This approach is commonly applied by some North American and European transmission system operators [136].

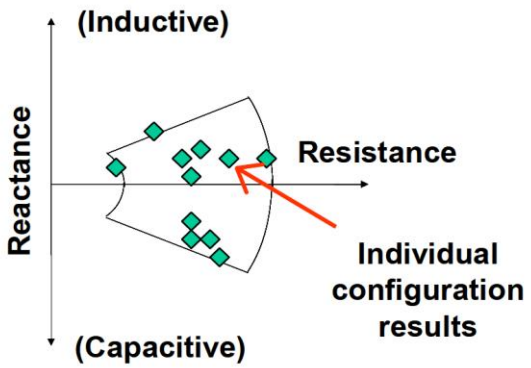

Figure 2-20: Harmonic impedance locus [136]

Caution should be exercised when considering the combined effect of background voltage harmonic distortion with the full range of network impedances determined by means of impedance loci method. The worst-case background voltage distortion may occur as a result of different network conditions from those that result in a harmonic impedance which causes a worst-case resonance. Therefore, simultaneous evaluation of the highest amplitude background harmonic distortion and a source impedance that results in worst-case impedance resonance may be excessively conservative [136].

2.12.7.2 Background harmonic distortion

The background harmonic distortion is defined by the voltage magnitude per harmonic order and tends to vary over time due to variation in operation of harmonic sources and changes in load and network configuration. To obtain accurate background harmonic distortion measurements, it may be necessary to install harmonic monitoring equipment at the point of connection over an extended period of time. Where this is impractical, typical data based on the utility's operational data can be considered or alternatively compatibility levels or planning levels from local or international standards may be applied. A statistical approach is recommended to ensure that the simulations are not overly conservative [136].

2.12.8 Load models

Passive linear loads, which do not generate harmonic emissions, have a significant impact on the network frequency response near resonant frequencies. Where reasonable estimates of network loads are available, they can be represented by an aggregated load model which should include the distribution transformer. A load model requires knowledge of the distribution transformer, static load, rotating load and load capacitance and no generally acceptable load models suitable for harmonic analysis exist [6].

However, some approximations have been proposed which model the load as a parallel R, L combination. Various formulae have been proposed for calculation of resistor and inductor values from the actual voltage, active power and reactive power; the modelled resistance and inductance may be fixed or frequency dependent [6] [51]. Some simulation packages offer equivalent load circuits that account for mixed capacitive and inductive components in the load and include the distribution transformer, or allow for a user-defined impedance characteristic to be entered [94]. The increasing percentage of non-linear load elements connected

to the network may significantly impact the harmonic performance of the network but such effects cannot be easily represented by generic models in the simulation environment.

2.13 Software simulation tools

2.13.1 Introduction

Various software tools are available for modelling, simulation and analysis of real-world power system phenomena. Tools offer a graphical interface and network representation, database of network components and parameters, a variety of analysis functions and a printout or graphical representation of results, as well as a means of exporting results data for further analysis using other software packages [6]. It is important to understand the limitations and assumptions inherent in the software implementation and in any input data and simulation parameters. In modelling any system, it is necessary to make assumptions and simplifications and the validity of these must be evaluated for each application. Where possible, results obtained from simulation packages should also be verified by suitable measurement data, comparisons or hand calculations. A summary of a few available software tools is provided in this section.

2.13.2 DIgSILENT PowerFactory

DIgSILENT PowerFactory is a commonly used power system analysis tool which is widely applied in planning and operation of power systems worldwide [94]. It has been adopted as the industry standard for utility and RPP simulations in South Africa because it is the platform used by Eskom Distribution, who own and operate the vast majority of the country's distribution networks to which the RPP's are connected.

The software provides graphical single-line diagrams and a variety of standard power system components. Users are also able to create custom dynamic models for time-domain simulations. Projects can be managed by the use of variations, operational scenarios and study cases to catalogue a variety of different network configurations and system conditions. A number of different licence options exist, of which the following are considered most relevant to harmonic analysis in power systems:

- Load flow analysis
- Short circuit analysis
- Harmonic analysis (including harmonic load flow, flicker and frequency sweep analysis)
- Stability functions (RMS and EMT dynamic simulations)

Balanced and unbalanced simulations can be executed and scripts can be developed using the DIgSILENT Programming Language (DPL) which allow for rapid execution of repetitive tasks and enable batch processing of simulations.

2.13.3 Matlab/Simulink

Matlab is a high-level programming language used by millions of engineers and scientists worldwide. It is favoured for academic studies due to its high degree of flexibility and wide range of application. Mathematical functions, including Fourier analysis functions, may be especially useful for harmonic analysis together with data processing and analysis tools and graphical data visualisation capabilities [138].

2.13.4 Electromagnetic Transient Programs

Detailed analysis of harmonic phenomena may warrant use of specialised time-domain electromagnetic transient (EMT) simulation software. Electromagnetic transient analysis in the time domain is more time consuming than frequency-domain analysis and is considered excessive for most harmonic problems [36]. Examples of EMT simulation software include EMTP-RV and PSCAD-EMTDC [139] [140].

2.13.5 Other Harmonic Analysis Programmes

A large number of different harmonic analysis software packages are available as stand-alone packages or as part of a larger power system analysis software packages. These include E-Tap, a simulation package widely used in the simulation of industrial power systems, HI_WAVE from SKM System Analysis, Ipsa 2 Power System Analysis Software, CMYE Power Engineering Software and SuperHarm.

2.14 Harmonic measurement

In order to evaluate the actual harmonic distortion in the network and assess the emissions from an installation, it is necessary to capture measurements of harmonic voltages and currents. The relevant IEC standards are the universally accepted as the definitive guide for harmonic measurement. Two of the IEC 61000 series standards are primarily applicable:

- IEC 61000-4-7 Electromagnetic compatibility (EMC): Part 4-7: Testing and measurement techniques – General guide on harmonics and interharmonics measurements and instrumentation, for power supply systems and equipment connected thereto [101].
- IEC 61000-4-30 Electromagnetic compatibility (EMC): Part 4-30: Testing and measurement techniques – Power quality measurement methods [20].

IEEE 519-2014 specifies that instruments should comply with IEC 61000-4-7 and IEC 61000-4-30 whilst NRS 048-2 specifies that instruments for comparing measured performance with standards in the case of a dispute on the accuracy of measurements shall comply with the requirements for class A meters in IEC 61000-4-30. Class A meters are therefore a minimum requirement for quality of supply monitoring of large RPP's in South Africa where the plant performance must be compared with contractual limits [44] [8]. The primary components and configuration of a measurement system for assessment of harmonic emissions in accordance with IEC requirements are described in this section.

2.14.1 Quality of supply meters

To ensure the integrity of harmonic measurements, power quality meters shall comply with the requirements of IEC 61000-4-30. The basic measurement time interval for harmonic and interharmonic magnitudes shall be 10 cycles for a 50Hz power system. The 10-cycle values are then aggregated over 150 cycle (3 s), 10 minute and 2 hour intervals using the square root of the arithmetic mean of the squared input values. Measurements are synchronised at every real-time clock 10-minute tick. Measurements are required up to the 50^{th} harmonic order. Total harmonic distortion is calculated based on harmonic orders 2 to 40 [20].

Provision is made to flag data when a dip, swell or interruption occurs to indicate the measurement algorithm for harmonics may produce an unreliable value. IEC 61000-4-30 does not list requirements regarding the use of flagged data but NRS 048-2 states that flagged data must be ignored in the assessment of power quality phenomena [20].

IEC 61000-4-7 specifies accuracy limits for harmonic current, voltage and power measurements. Class I instruments are recommended for verifying compliance with standards, resolving disputes, etc. For Class I instruments, the maximum voltage error is ±5 % for voltages above 1 % of nominal voltage, maximum current error is ±3 % for currents above 3 % of nominal current and maximum power error is ±1 % for power measurements above 150 W. Below the specified minimum thresholds, the maximum error becomes constant and is equal to the accuracy at the threshold. Maximum phase shift between individual channels should be less than 1° and an anti-aliasing low pass filter is required to attenuate frequencies outside the measuring range so that they do not affect the results. Requirements for post-processing of signals including grouping and smoothing are also described [101].

2.14.2 Transducers

For MV, HV and EHV applications, transducers are required to scale the inputs and provide isolation for the input signals. In order to ensure accurate measurements when using transducers, it is necessary to ensure that the transducers are specified correctly to use the full scale of the meter without distorting or clipping the signals and that the phase response, frequency response and burden characteristic of the transducers are suited to the application [20]. Typically, harmonic measurements are taken using permanently installed instrument transformers which have been selected primarily based on their fundamental frequency performance and it is therefore important to understand the limitations of these devices and their impact on the accuracy of measured data.

2.14.2.1 Voltage transducers

Voltage transformers (VT's) are the most commonly used transducers for voltage measurement with two types widely deployed in modern power systems: inductive voltage transformers (IVT's) – also known as electromagnetic transformers – and capacitive voltage transformers (CVT's). IVT's typically have frequency responses suitable for measurements up to 1kHz, although the range may be below this or may extend to several kilohertz [20]. Zhoa et al. performed tests and simulations to determine the frequency response of a

33 kV electromagnetic VT and found large errors in the region of a significant resonance at 4.85 kHz. The voltage ratio was found to remain within a ±5 % accuracy band for frequencies below 2 kHz [141]. A more comprehensive study considering 61 different IVT's by Klatt et al. produces similar results and suggests that medium voltage IVT's are accurate to within ±2 % up to 1 kHz, ±4 % up to 2 kHz and ±5 % up to 2.5 kHz [142].

Stiegler et al., using invasive and non-invasive measurement techniques, found the response of HV inductive VTs to be accurate up to the 19th harmonic (950 Hz) but note that general conclusions regarding VT frequency response cannot be drawn due to the differing VT designs available [143]. Similar results were also reported by Samesima et al. in their detailed analysis of an IVT considering equivalent circuit models and measurements. They demonstrate that inclusion of stray capacitances into the equivalent circuit model is necessary to reasonably approximate the frequency response up to 10 kHz and show an error of 3 % at 2 kHz for a 60 Hz, 11 kV IVT. However, they conduct a more thorough investigation into the variation of phase angle with frequency and observe a large variation in phase angle from 70° at 60 Hz to -80° at 500 Hz. The response then remains fairly stable from 500 Hz up to 5 kHz [144]. The magnitude is usually more important that the phase angle in harmonic analysis, particularly in application of the methodologies described in major harmonic standards (IEC, IEEE, NRS, etc.) [141] [142].

CVT's are essentially composed of a capacitor divider circuit and an electromagnetic transformer, and in South Africa are usually only employed for measurement of voltages above 132 kV. Simple capacitor dividers can have a frequency response that is adequate up to several hundred kilohertz but resonant circuits are frequently included which render the frequency response suitable only for fundamental frequency measurements [20]. Several researchers have investigated the transfer function of a typical complete CVT and found that the frequency response contains one bandpass and one bandstop characteristic in the harmonic band (below to 2.5 kHz) which may significantly affect the accuracy of the measured values [145] [146].

Several alternative voltage measurement solutions have been proposed to overcome the shortcomings of conventional VT's but have not achieved widespread deployment in utility or industrial harmonic measurement applications. These include use of the transconductance ratio of a CVT whereby the primary currents flowing in the capacitor divider are measured to determine the input voltage, as described by Vermeulen and Davel [146] and later adapted by Ghassemi et al. [147]. Optical or non-conventional voltage transformers have been developed which exhibit a flat frequency response up to 10 kHz but are still considered experimental and need further testing and development before they can achieve widespread practical application [141]. Dedicated resistive or capacitive dividers and capacitive taps on HV current transformers or transformer bushings are also alternatives for harmonic and transient voltage measurements [6] [20].

Correction techniques could also be considered to compensate for errors in measurement data from a specific application. Kadar et al. proposed a correction algorithm based on instrument transformer equivalent circuit models which was implemented as a digital filter to compensate for errors from voltage and current transformers in an electric arc furnace harmonic measurement installation [148].

2.14.2.2 Current transducers

Current transformers (CT's) are the most commonly used current transducer for harmonic measurements. Metering CT's are usually preferred for harmonic measurements since protection class CT's may produce large secondary currents during fault conditions that could damage measuring instruments. Current transformers are wound electromagnetic devices and their frequency response is dependent on uncertainty class, type, turns ratio, core material, cross section and connected burden. The cut-off frequency is typically between 1 kHz and a few kHz [20].

Samesima et al. found that the frequency response is equal to the fundamental frequency value and the phase angle shift between primary and secondary equal to zero up to 50 kHz for a 30/5, 15 VA, 50/60 Hz MV bar CT [144]. Chen et al. investigated the frequency response of a 33 kV multi-ratio CT and found the ratio to remain nearly constant over the frequency range from 200 Hz to 3 kHz; however, for low currents there is a significant change in ratio between 50 Hz and 200 Hz and the phase angle varies by almost 40° over the range from 50 Hz to 3 kHz. The paper concludes by stating that the CT introduces errors to the recovered signal but that the errors are predictable and can therefore be compensated by use of signal processing algorithms [149]. The 200/5 CT chosen by Erning et al. for verification of their method of on-line identification of CT frequency response exhibits a constant ratio response with a cut-off frequency of only 1 kHz [150].

Therefore, conventional current transformers provide a stable frequency response for lower harmonic orders but care should be taken to confirm the accuracy at frequencies above 1 kHz. It is also recommended that the secondary burden be minimised and its power factor maximised to reduce the CT magnetising current, thereby improving measurement accuracy. Short circuiting the CT secondary and using a precision clamp-on current transformer to measure the secondary current is also a recommended method of achieving more accurate measurement results [6].

Frequently it is not possible to interrupt the operation of an installation in order to install power quality monitoring equipment. Hence access to primary circuits is usually not possible, especially for MV and HV applications, and it is also not possible to interrupt existing CT secondary circuits due to potentially dangerous overvoltages that may result. Therefore clamp-on type current transducers are frequently connected to measure the CT secondary currents of the permanent installation. These transducers may introduce additional error into the measurement.

Rigowski coil or Hall-effect instruments are frequently used for such clamp-on field measurements. They offer a linear response and small phase error in the harmonic range and the transducer output is an AC voltage which can be directly applied to current transducer voltage inputs provided on many power quality instruments in additional to CT current inputs [151] [20] [152]. Clamp-on transducer output voltages are typically low, in the range of 50 mV to 1 V rms full scale [152] [153], and care is needed to minimise electromagnetic interference and to use the full measurement scale by selecting a transducer with the correct primary current rating for the

application (typically 1 A or 5 A for CT secondary lead measurement) [20]. The conductor position within the transducer window can also influence measurement accuracy [154].

3 Frequency response of a solar PV plant

3.1 Simplified network model

In order to evaluate the frequency response of a typical solar PV plant, a simplified network was modelled in DIgSILENT PowerFactory. For an initial evaluation to aid the understanding of the modes of resonance in a typical utility-scale PV plant, the plant was consolidated by means of aggregation, as illustrated in the single line diagram in Figure 3-1. The red numbers below each element indicate the number of elements connected in parallel in the simplified model.

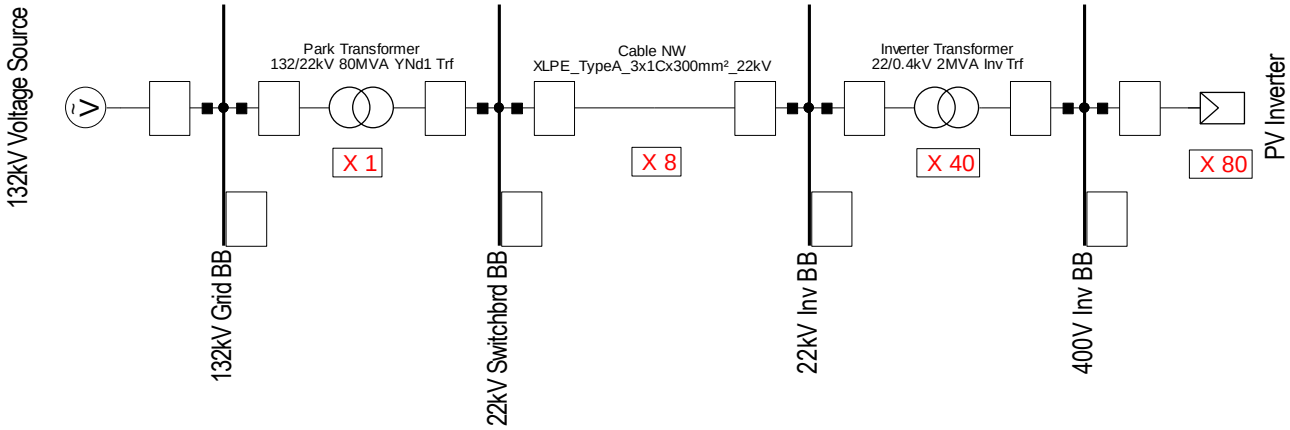

Figure 3-1: Aggregated PV plant model

The frequency response of the plant can be analysed by first considering the harmonic impedance of the electrical network components that constitute the plant. These passive network components are:

- 80 MVA 132/22 kV park transformer (1 off)
- 3 x single core, 300 mm^2 aluminium conductor, XLPE insulated cable circuit (8 in parallel)
- 2 MVA 22/0.4 kV park transformer (40 in parallel)

Thereafter, the combined harmonic impedance of the plant's collector network is considered based on an equivalent circuit developed by series connection of the individual components' equivalent circuits. In all cases, frequency sweeps are conducted over the frequency range from 10 Hz to 100 kHz. Although the harmonic band for a 50 Hz system is usually considered to be 50 - 2500 Hz, the wider frequency sweep range provides broader insight by showing higher order resonance peaks that could influence harmonic behaviour if the component parameters or network configuration were to change.

3.1.1 Cable model

Long line effects should be taken into consideration where the length of the line exceeds 173/h km for a 50 Hz system [51]. Considering a 1 km long cable, the nominal pi model shown in Figure 3-2 can be considered

accurate to h = 173 (8650 Hz) which is above the harmonic frequency range; this representation is therefore used for the DIgSILENT PowerFactory simulations. R, L and C parameters per unit length were obtained directly from the cable manufacturer's data sheet values.

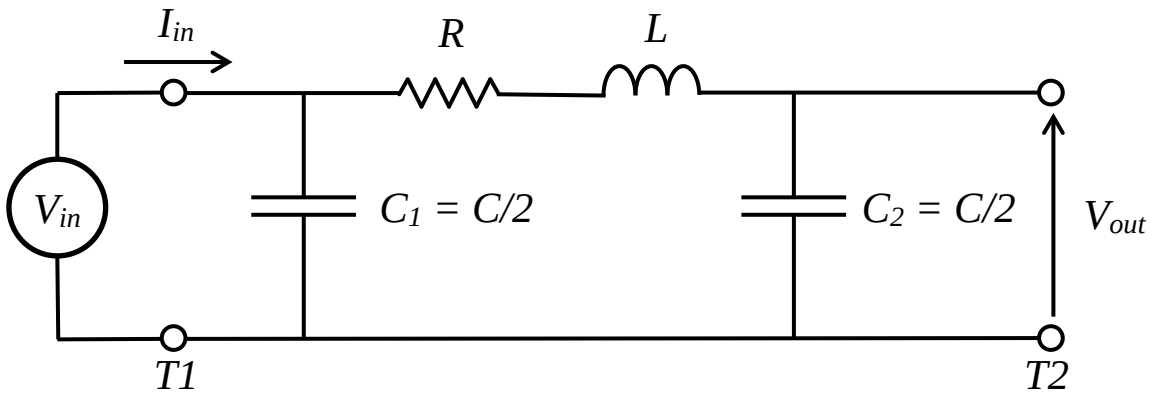

Figure 3-2: Cable circuit equivalent circuit

3.1.2 Transformer model

The park transformer and inverter transformers were modelled in DIgSILENT PowerFactory according to the second order harmonic model shown in Figure 3-3. Figure 3-3 (a) shows the transformer equivalent circuit considering an ideal transformer with the same transformation ratio as the physical transformer. In (b) the equivalent circuit parameters of the secondary circuit are referred to the primary side of the transformer to eliminate the ideal transformer, thus providing a simplified equivalent circuit.

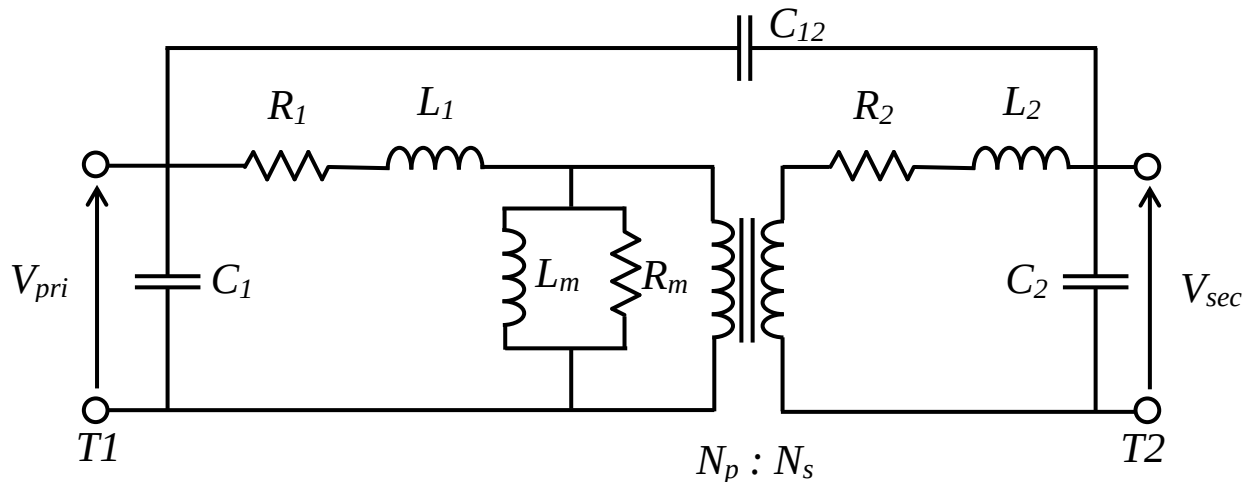

(a)

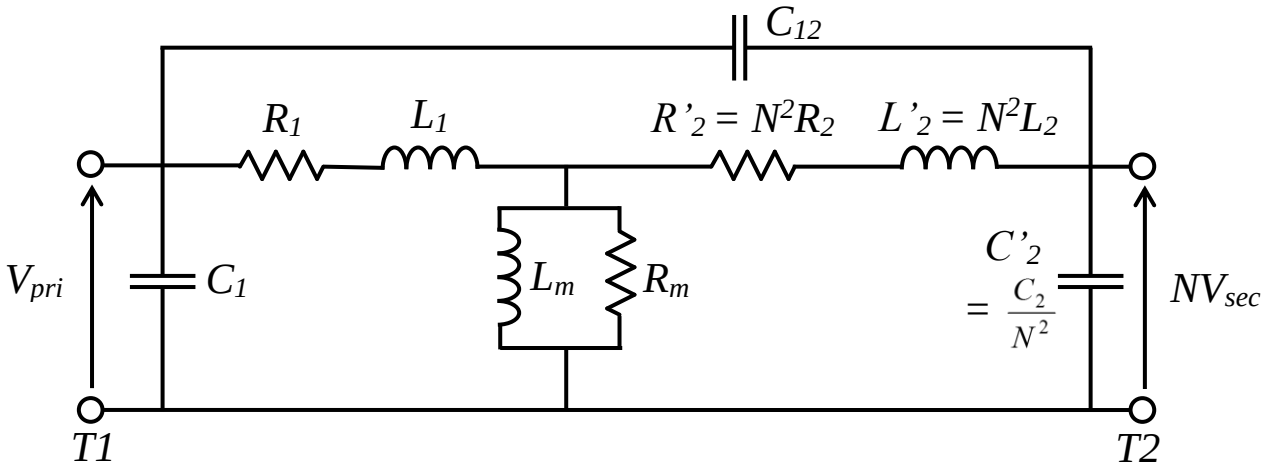

(b)

Figure 3-3: Two-winding transformer equivalent circuit (a) including ideal transformer (b) secondary quantities referred to primary side

Nameplate data for the two transformers types was based on typical data of similar transformers employed in solar PV plants in the South African network. The data are summarised in Table 3-1. The equivalent circuit parameters of Figure 3-3 (a) and (b) were derived from this nameplate data. The derivation of resistances and inductances is straightforward based on simple circuit theory and the assumption that the leakage inductance and leakage resistance are distributed evenly between the primary and secondary windings, i.e. $R_1 = R'_2$ and $L_1 = L'_2$.

Table 3-1: Park transformer and inverter transformer nameplate data

Parameter	Symbol	Unit	Park Transformer	Inverter Transformer
Rated apparent power	S	MVA	80	2
Nominal primary voltage	V_{pri}	kV	132	22
Nominal secondary voltage	V_{sec}	kV	22	0.4
Vector group			YNd1	Dyn11
Turns ratio (= V_{pri}/V_{sec})	N	-	6	55
Short circuit impedance	Z	%	11	8
Copper losses	P_{Cu}	kW	294	19
No-load current	I_{NL}	%	0.1275	0.9
No-load losses	P_{NL}	kW	34	3.5
Nominal primary current	I_{pri}	A	349.9	52.49
Nominal secondary current	I_{sec}	A	2099	2887
Nominal frequency	f_{nom}	Hz	50	50

No capacitance measurement data were available and the IEEE C37.011 methodology was applied to estimate the winding self-capacitances, C_1 and C_2, and the inter-winding capacitance, C_{12} [155]. For the park

transformer, the infinite-bus primary and secondary through-fault currents are calculated as 3.18 kA and 19.09 kA respectively. Therefore, using Figure B.2 of IEEE C37.011, the median transient recovery voltage (TRV) frequencies can be estimated as 9.2 kHz and 55 kHz for the 132 kV and 22 kV windings respectively. The transformer effective capacitance can then be calculated according to Equation (3.1) for the HV and LV windings as 3.93 nF and 3.96 nF respectively.

$$C_{eff} = \frac{1}{(2\pi f)^2 L} \tag{3.1}$$

where:

C_{eff}	is the transformer effective capacitance
f	is the transient recovery frequency
L	is the equivalent leakage inductance of the transformer

The equivalent circuit capacitances can be calculated from the effective capacitance using an estimated capacitive coupling ratio, which is typically in the range 0.1 to 0.4. Lower voltage windings have larger capacitances and the capacitive coupling ratios for lower voltage windings are assumed to be smaller than those of higher voltage windings [156]. For the park transformer, a capacitive coupling ratio of 0.3 is chosen and the equivalent circuit capacitances are calculated according to Equations (3.2), (3.3) and (3.4). The equivalent circuit capacitances of the inverter transformer are calculated according to the same methodology with a capacitive coupling ratio of 0.1. The full list of equivalent circuit parameters for each transformer is shown in Table 3-2.

$$C_{12} = \textit{Capacitive coupling ratio} \cdot C_{eff} \textit{ at the low-voltage winding} \tag{3.2}$$

$$C_2 = C_{eff} \textit{ at the low-voltage winding} - C_{12} \tag{3.3}$$

$$C_1 = C_{eff} \textit{ at the high-voltage winding} - C_{12} \tag{3.4}$$

Table 3-2: Park transformer and inverter transformer equivalent circuit parameters

Parameter	Unit	Park Transformer	Inverter Transformer
R_1	Ω	0.4002	1.1495
L_1	H	0.03811	0.0359
R'_2	Ω	0.01112	0.00038
L'_2	H	0.001059	1.011×10^{-5}
R_m	Ω	512,471	138,286
L_m	H	576.7	87.26
C_1	nF	3	0.1
C'_2	nF	0.0833	0.00595
C_{12}	nF	1	2

3.2 Cable frequency response

The harmonic impedance of a single 1 km long cable circuit consisting of three 300 mm^2 aluminium conductor, XLPE insulated, single core 22 kV cables was calculated by means of frequency sweep analyses and the results of open circuit and short circuit sweeps are shown on a log-log scale in Figure 3-4 and Figure 3-5 respectively. The impedance is the ratio of input voltage to input current. Due to the symmetrical nature of the equivalent circuit, only terminal T1 of the cable model was considered for the frequency sweep analysis.

It is clear that there are two resonances in the open circuit impedance sweep in the range 10 Hz to 100 kHz. A series resonance occurs at 22.1 kHz which is caused by the interaction of lumped capacitance C_2 with lumped inductance L. A parallel resonance is present at 31.2 kHz due to the interaction of C_1 with the series combination of L and C_2. The open-circuited cable appears capacitive except in the frequency band between the two resonance points, where it becomes inductive.

The short circuit impedance sweep exhibits a single parallel resonance at 22.1 kHz as a result of the interaction of L and C_1. This is expected because terminal T2 and capacitor C_2 are short circuited and the cable's nominal pi circuit is reduced to a simple parallel LC circuit.

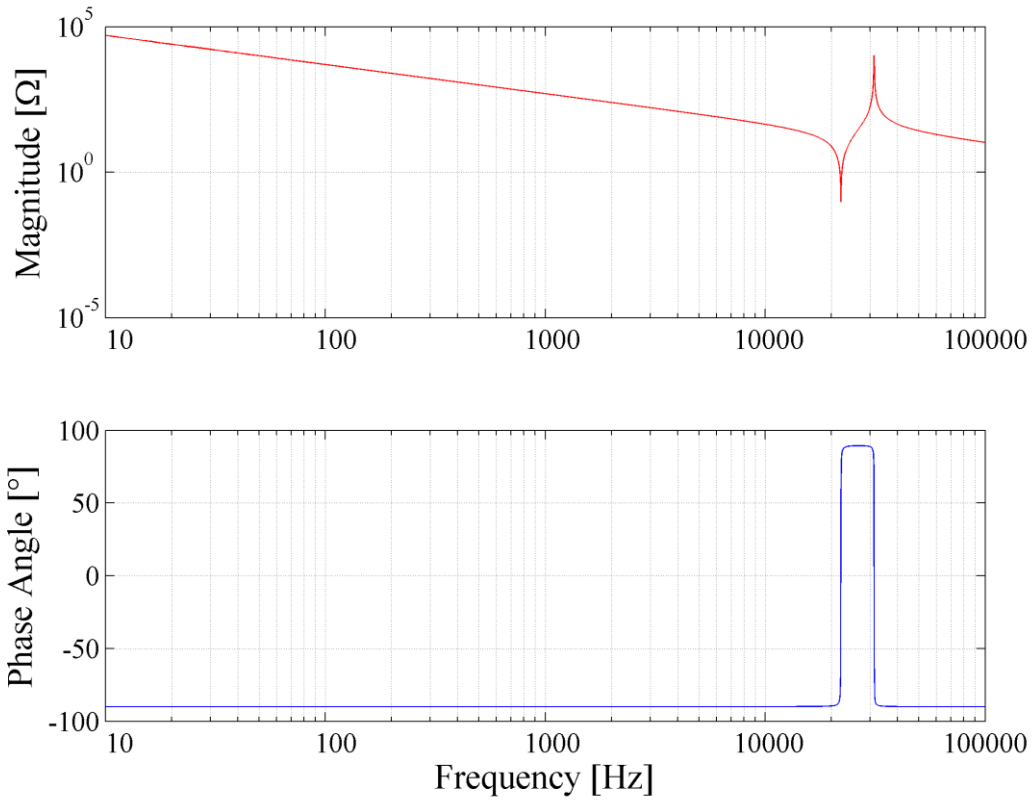

Figure 3-4: Cable circuit harmonic impedance characteristic – open circuit

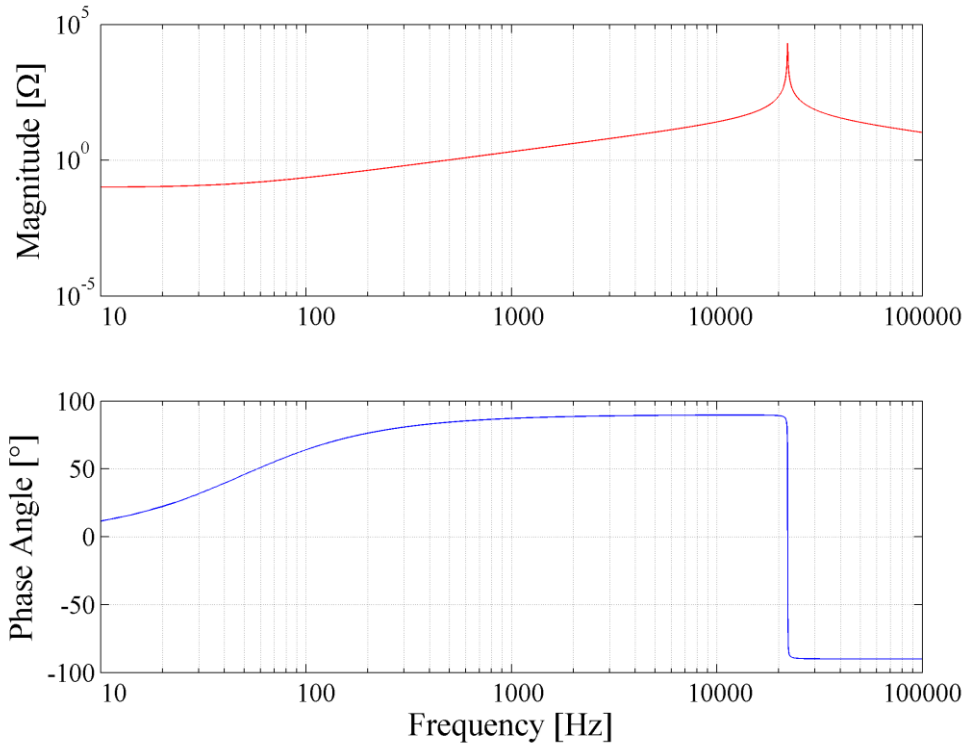

Figure 3-5: Cable circuit harmonic impedance characteristic – short circuit

3.3 Park transformer frequency response

The harmonic impedance of the two-winding transformer is calculated as the ratio of input voltage to input current for the following four test scenarios:

Table 3-3: Frequency sweep analysis scenarios for transformer harmonic analysis

Description	Primary Winding	Secondary Winding
Primary terminals, secondary open circuit	Injection point	Open circuit
Secondary terminals, primary open circuit	Open circuit	Injection point
Primary terminals, secondary short circuit	Injection point	Short circuit
Secondary terminals, primary short circuit	Short circuit	Injection point

3.3.1 Primary terminals, secondary open circuit

The harmonic impedance of the park transformer measured at the primary terminals with the secondary terminals open circuited is shown in Figure 3-6. There is a low order parallel resonance point at 107 Hz due to the combination of inductance L_m and capacitance C_1. A higher order series resonance occurs due to the series combination of L_1, L_2 and C_2. The resonant frequency for this pure series combination is 63 kHz but the inter-winding capacitance, C_{12}, in parallel with the series combination of L_1 and L_2 influences the frequency response, resulting in the series resonance observed at 54 kHz. Another parallel resonance is observed at 55 kHz due to capacitance C_1 operating in parallel with the primarily inductive branch consisting of L_1, L_2, C_{12} and C_2.

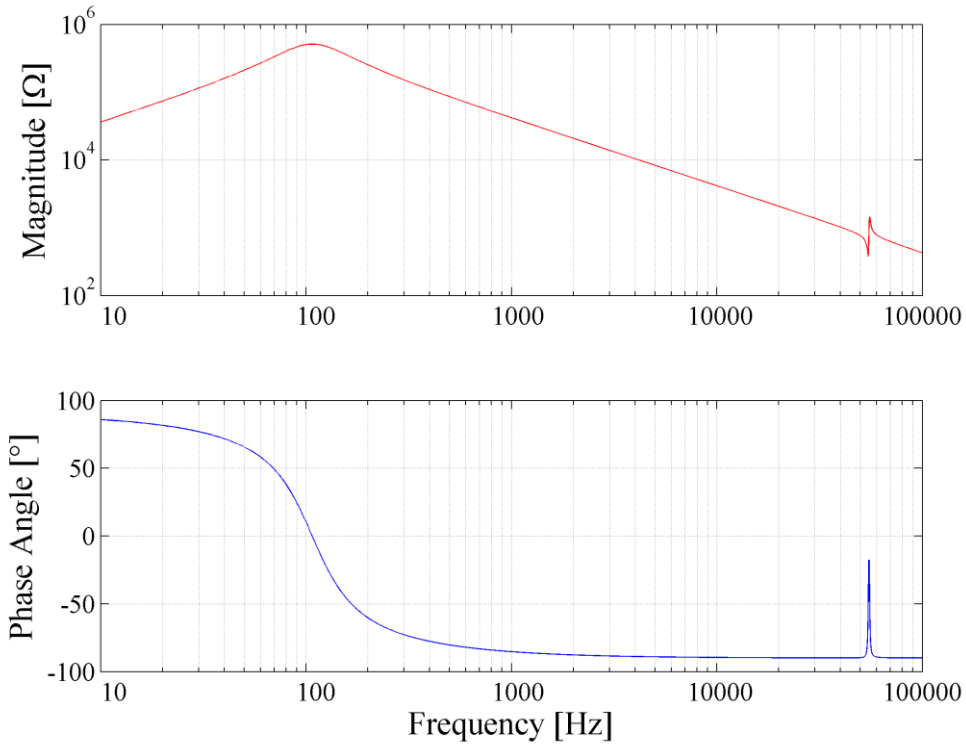

Figure 3-6: Park transformer harmonic impedance characteristic – primary terminals, secondary open circuit

3.3.2 Secondary terminals, primary open circuit

The harmonic impedance of the park transformer measured at the secondary terminals with the primary terminals open circuited is shown in Figure 3-7. There is a low order parallel resonance point at 107 Hz due to the interaction of inductance L_m with capacitance C_2. A higher order series resonance occurs due to the series combination of L_1, L_2 and C_1. The resonant frequency for this pure series combination is 10.5 kHz but the inter-winding capacitance, C_{12}, in parallel with the series combination of L_1 and L_2 influences the frequency response resulting in the series resonance observed at 9 kHz. A parallel resonance occurs at 55 kHz due to the capacitance C_2 operating in parallel with the primarily inductive branch consisting of L_2, L_1, C_{12} and C_1.

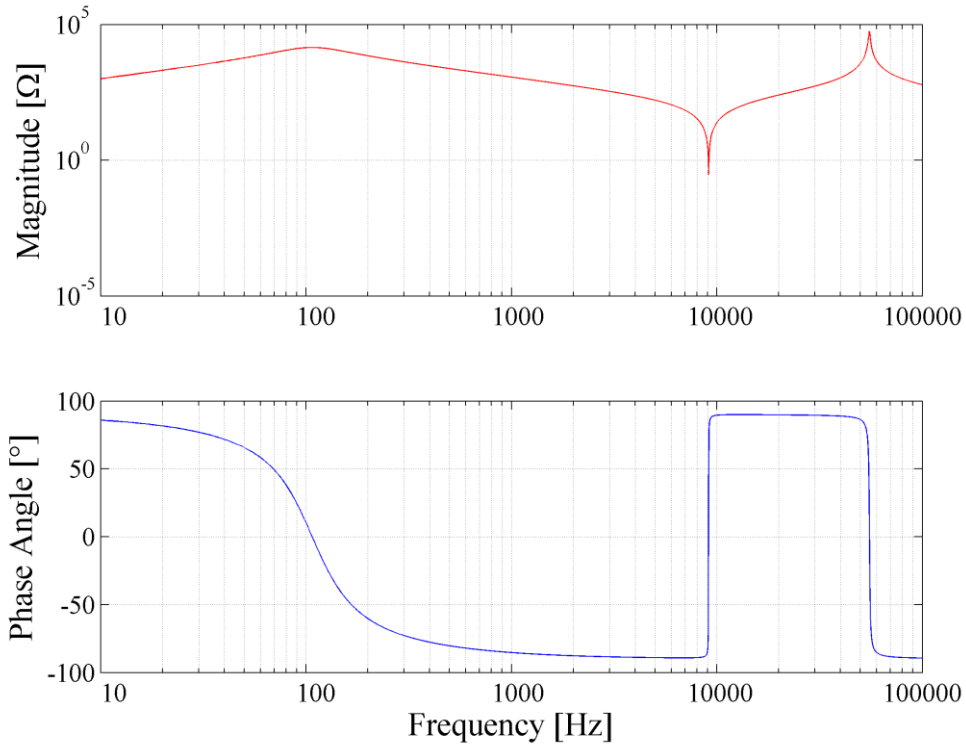

Figure 3-7: Park transformer harmonic impedance characteristic – secondary terminals, primary open circuit

3.3.3 Primary terminals, secondary short circuit

The short circuit harmonic impedance at the primary terminals is calculated as the ratio of input voltage to input current when the transformer secondary terminals are short circuited. A single parallel resonance is observed in the frequency band from 10 Hz to 100 kHz at approximately 9 kHz which is due to the three-branch parallel circuit consisting of C_1, C_{12}, and the series combination of L_1 and L_2. The frequency sweep is plotted in Figure 3-8.

3.3.4 Secondary terminals, primary short circuit

The short circuit harmonic impedance at the secondary terminals is calculated as the ratio of input voltage to input current when the transformer primary terminals are short circuited. A single parallel resonance is observed in the frequency band from 10 Hz to 100 kHz at approximately 55 kHz which is due to the three-branch parallel circuit consisting of C_2, C_{12}, and the series combination of L_2 and L_1. The frequency sweep is plot is shown in Figure 3-9.

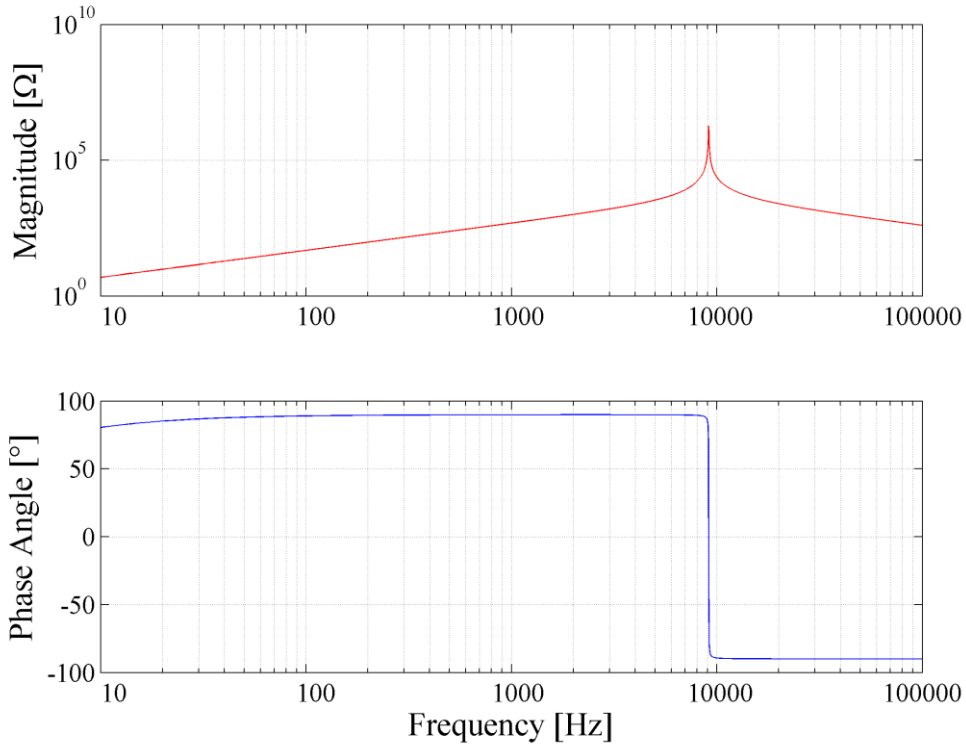

Figure 3-8: Park transformer harmonic impedance characteristic – primary terminals, secondary short circuit

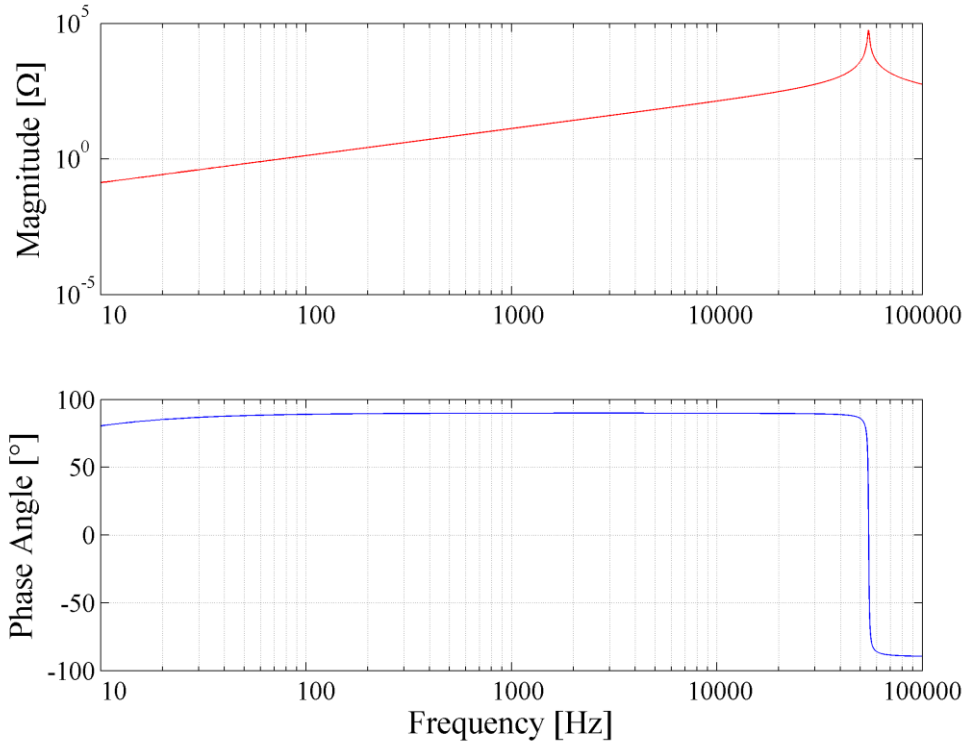

Figure 3-9: Park transformer harmonic impedance characteristic – secondary terminals, primary short circuit

3.4 Inverter transformer frequency response

The inverter transformer is also a two-winding transformer with an equivalent circuit structure that is identical to that of the park transformer; only the values of the circuit elements differ. The equivalent circuit parameters for the inverter transformer are listed in Table 3-2. The same mechanisms of harmonic resonance generation exist for the inverter transformer as for the park transformer but the frequency of the resonance points is shifted due to the different equivalent circuit parameter values. The harmonic impedance plots are presented in this section with a listing of the observed resonances. The cause of each resonance is described for the corresponding park transformer frequency sweep in section 3.3.

3.4.1 Primary terminals, secondary open circuit

The harmonic impedance of the inverter transformer measured at the primary terminals with the secondary terminals open circuited is shown in Figure 3-10. The low order parallel resonance is visible at 377 Hz but the higher order series and parallel resonances seen in the park transformer's frequency sweep plot occur in the 250 - 300 kHz range.

3.4.2 Secondary terminals, primary open circuit

The harmonic impedance of the park transformer measured at the secondary terminals with the primary terminals open circuited is shown in Figure 3-11. The low order parallel resonance point is visible at 377 Hz and a series resonance occurs at 14 kHz. In the case of the inverter transformers, the relative capacitance of the inter-winding capacitance (C_{12}) is much larger than in the case of the park transformer and this inter-winding capacitance has a significant impact on the observed resonant frequencies.

3.4.3 Primary terminals, secondary short circuit

A single parallel resonance is observed at approximately 14 kHz. The frequency sweep is plotted in Figure 3-12.

3.4.4 Secondary terminals, primary short circuit

The short circuit harmonic impedance at the inverter transformer secondary terminals does not exhibit any resonances within the frequency range of interest and the characteristic remains inductive below 100 kHz. The frequency sweep is plotted in Figure 3-13.

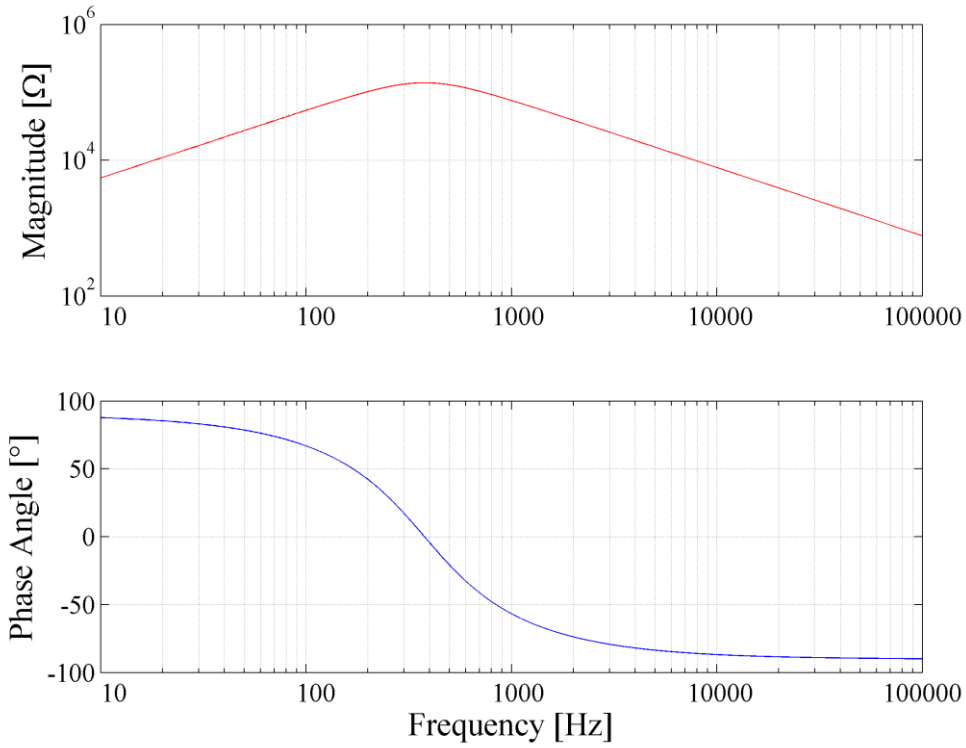

Figure 3-10: Inverter transformer harmonic impedance characteristic – primary terminals, secondary open circuit

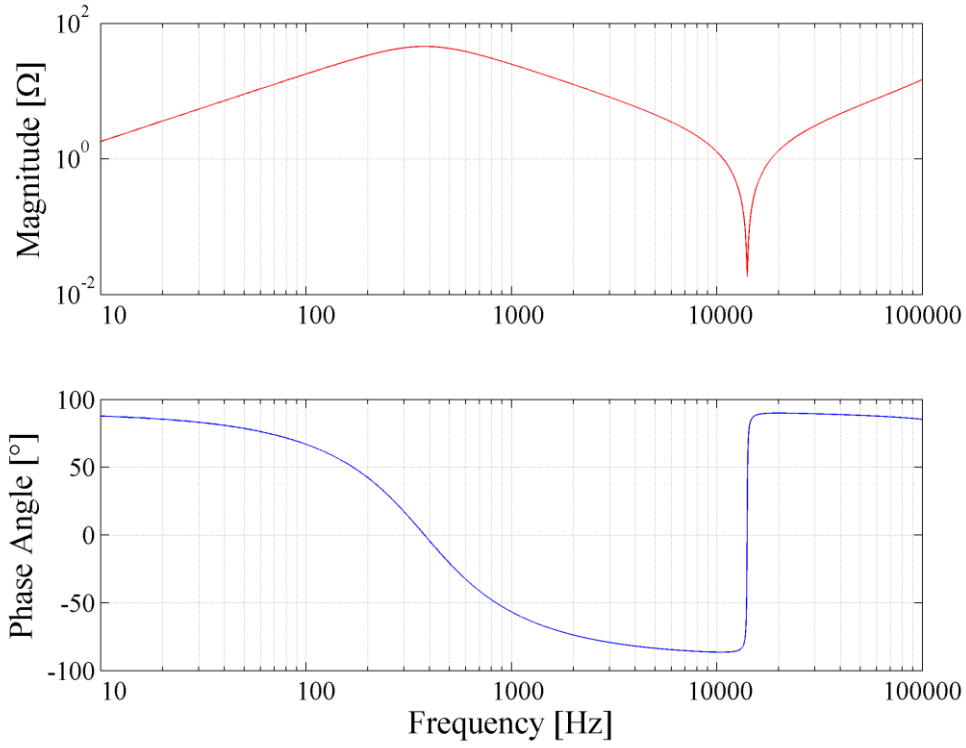

Figure 3-11: Inverter transformer harmonic impedance characteristic – secondary terminals, primary open circuit

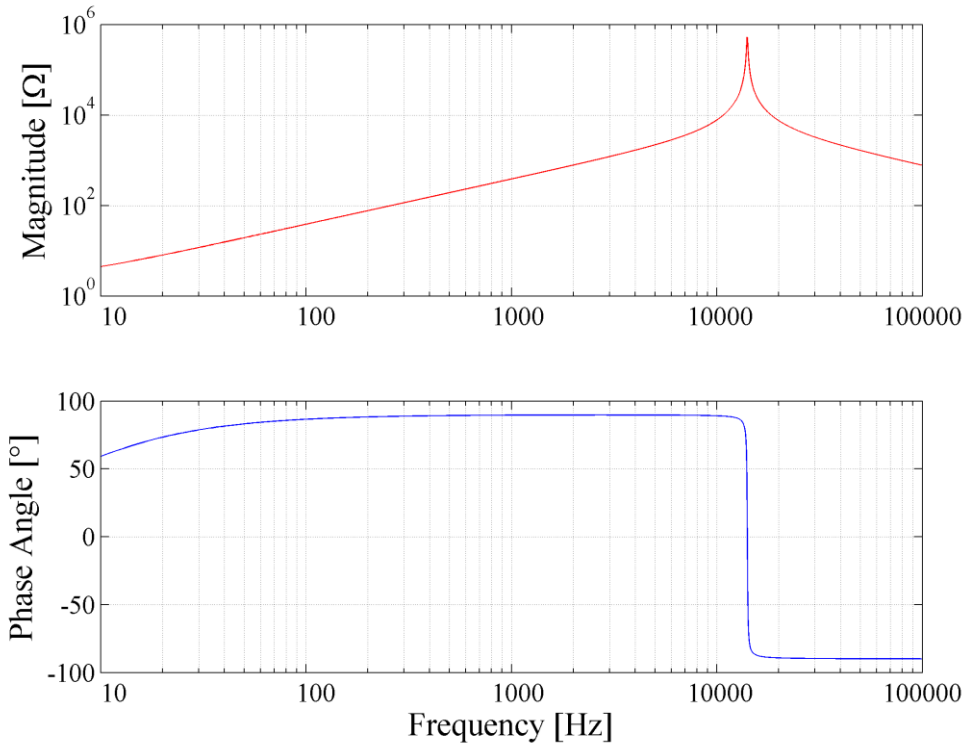

Figure 3-12: Inverter transformer harmonic impedance characteristic – primary terminals, secondary short circuit

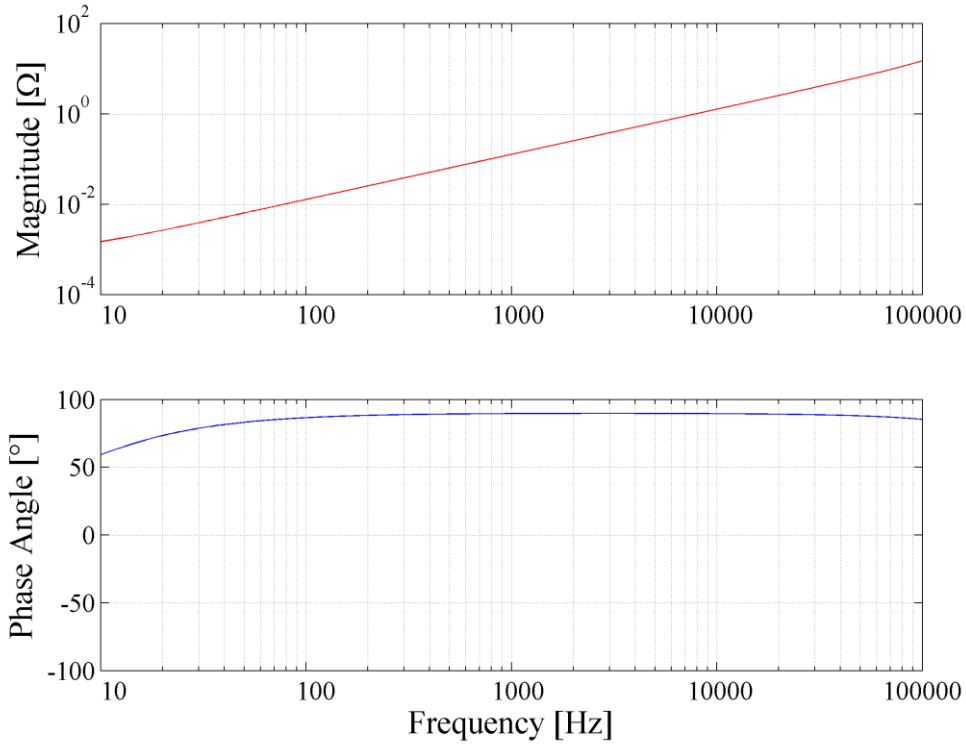

Figure 3-13: Inverter transformer harmonic impedance characteristic – secondary terminals, primary short circuit

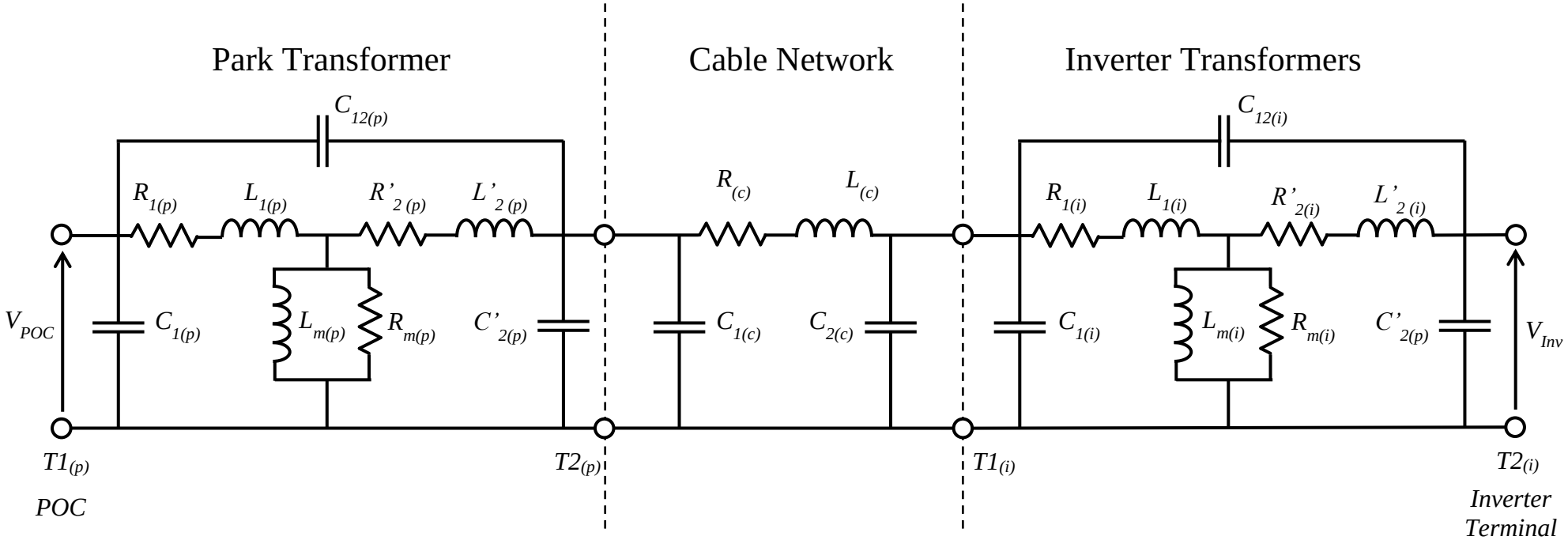

Figure 3-14: PV plant equivalent circuit

3.5 System frequency response

The harmonic impedance of the PV plant as seen from the 132 kV point of connection (POC) and from the 400 V inverter terminals was calculated by combining the individual components described above to form the equivalent circuit of the aggregated PV plant model shown in Figure 3-1 as shown in Figure 3-14. For ease of reference, the equivalent circuit parameters of the park transformer, cable and inverter transformer are suffixed with $_{(p)}$, $_{(c)}$ and $_{(i)}$ respectively in the following discussion. The impedance of the PV inverters and external network were ignored in the assessment.

It is noted that the magnitude of the equivalent cable network's capacitance ($C_{(c)}$) is 8 x 317 nF = 2,535 nF, which is much larger than the park transformer secondary winding capacitance ($C_{1(p)}$) of 3 nF and the aggregated inverter transformer primary winding capacitance ($C_{1(i)}$) of 4 nF. Ignoring the small cable inductance, these three capacitances are effectively connected in parallel and may therefore be represented by a single lumped capacitance, the 22 kV network shunt capacitance. Since it is much larger than the transformer winding capacitances, the cable capacitance is dominant in determining the frequency response of the system. Therefore, the terms 22 kV network shunt capacitance and cable capacitance are used interchangeably in the following discussion.

The harmonic impedance plots are presented in this section for the scenarios listed in Table 3-4.

Table 3-4: Frequency sweep analysis scenarios for system harmonic analysis

Description	132 kV Point of Connection	400 V Inverter Terminal
POC, inverter terminals open circuit	Injection point	Open circuit
Inverter terminals, POC open circuit	Open circuit	Injection point
POC, inverter terminals short circuit	Injection point	Short circuit
Inverter terminals, POC short circuit	Short circuit	Injection point

3.5.1 Point of connection, inverter terminals open circuit

The harmonic impedance of the PV plant internal distribution network measured at the POC with the inverter terminals open circuited is shown in Figure 3-15. A low order parallel resonance occurs at 70 Hz due to the three-branch parallel circuit formed by the park transformer magnetising impedance ($Lm_{(p)}$), the 22 kV shunt capacitance – dominated by the cable capacitance ($C_{(c)}$) – and the inverter transformer magnetising impedance ($Lm_{(i)}$).

A series resonance occurs at approximately 2.1 kHz. This resonance is generated by the park transformer leakage inductance ($L_{1(p)} + L'_{2(p)}$) and the cable capacitance ($C_{(c)}$). A higher order parallel resonance occurs at approximately 9.3 kHz due primarily to the interaction of the park transformer leakage inductance ($L_{1(p)} + L'_{2(p)}$) and the park transformer primary winding capacitance ($C_{1(p)}$). The resonant frequency is lowered slightly by the influence of the park transformer interwinding capacitance ($C_{12(p)}$) and the cable capacitance ($C_{(c)}$). It

is noted that at high frequencies, the cable network impedance is very small such that it approximates a short circuit at the park transformer secondary terminals. Hence the high frequency response of the network is dominated by the park transformer impedances and appears similar to that of the park transformer primary terminal frequency sweep when the secondary terminals are short circuited (cf. Figure 3-8).

3.5.2 Inverter terminals, point of connection open circuit

The harmonic impedance of the PV plant internal distribution network measured at the inverter terminals with the POC open circuited is shown in Figure 3-16. As for the open circuit impedance viewed from the POC, there is a low order resonance at 70 Hz due to the parallel combination of the aggregated inverter transformer magnetising inductance ($Lm_{(i)}$), the cable capacitance ($C_{(c)}$) and the park transformer magnetising inductance ($Lm_{(p)}$).

A series resonance is observed near the upper limit of the harmonic band at approximately 2.5 kHz due to the series combination of the inverter transformer leakage inductance and the cable capacitance. Three minor parallel / series resonances are observed in the 9 kHz to 100 kHz range but the impedance characteristic is dominated by the inverter transformer's leakage inductance and is therefore inductive in this region.

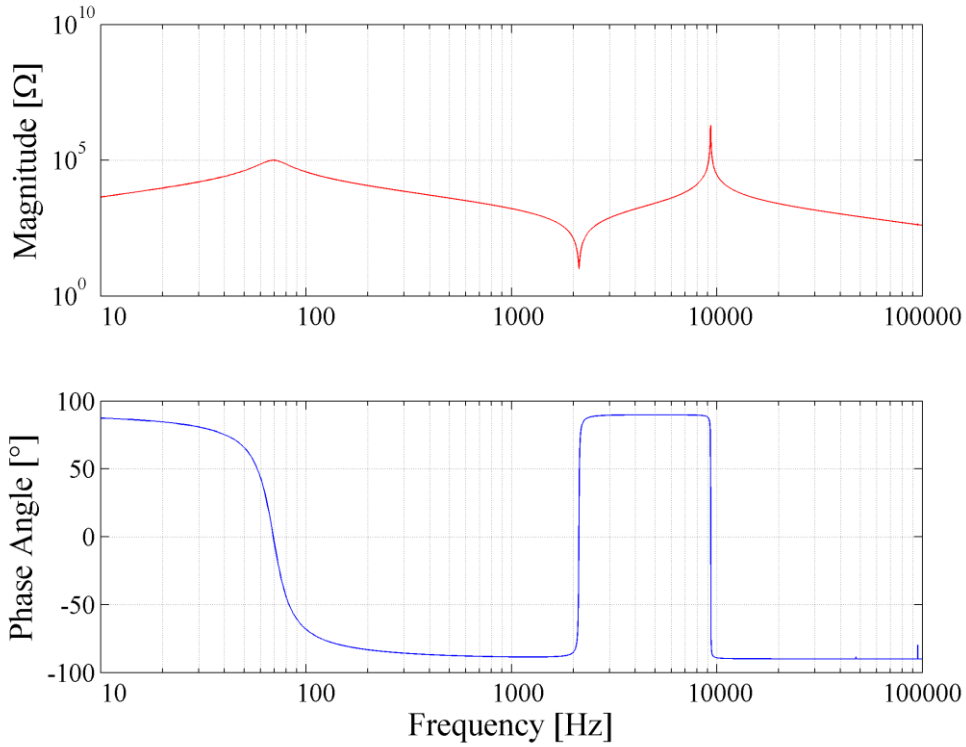

Figure 3-15: PV plant distribution network harmonic impedance characteristic – POC, inverter terminals open circuit

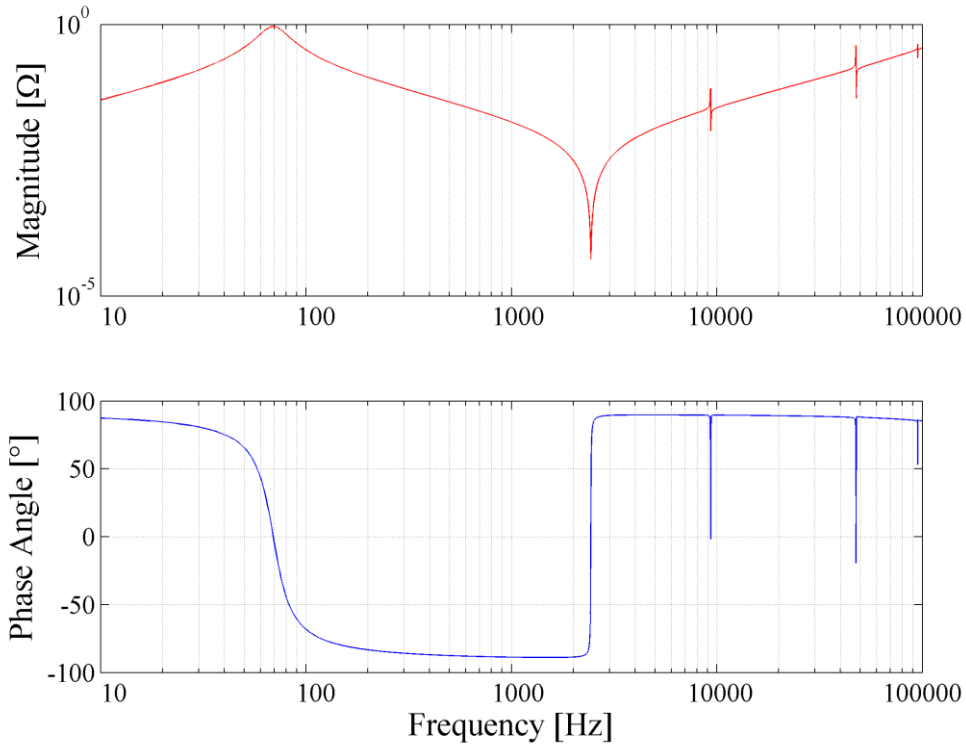

Figure 3-16: PV plant distribution network harmonic impedance characteristic – inverter terminals, POC open circuit

3.5.3 Point of connection, inverter terminals short circuit

The frequency sweep is plotted in Figure 3-17. A parallel resonance occurs at 2.4 kHz due to the 22 kV network shunt capacitance and the leakage inductance of the inverter transformers. There is a series resonance at 3.3 kHz which is due to the series combination of two parallel LC circuits. The first of these parallel circuits is formed by the park transformer leakage inductance and the park transformer inter-winding capacitance, while the second parallel circuit is formed by the inverter transformer leakage inductance and the inverter transformer inter-winding capacitance. Due to the large 22 kV network shunt capacitance, the response at higher frequencies is similar to that of the short-circuited park transformer viewed from the POC; a further parallel resonance therefore occurs at 9.3 kHz.

3.5.4 Inverter terminals, point of connection short circuit

The frequency sweep, which exhibits similar resonance mechanisms to those of the network when it is short circuited at the inverter terminals, is plotted in Figure 3-18. A parallel resonance occurs at 2.1 kHz due to the interaction of the park transformer leakage inductance and the 22 kV network shunt capacitance. The series resonance at 3.3 kHz is caused by the series connection of two parallel LC circuits. The first parallel circuit is formed by the inverter transformer leakage inductance and the inverter transformer inter-winding capacitance, while the second parallel circuit is formed by the park transformer leakage inductance and the 22 kV network shunt capacitance. The next major resonance is a parallel resonance which occurs above 100 kHz, although two smaller deviations caused by minor parallel / series resonances are visible in the 40 – 100 kHz range.

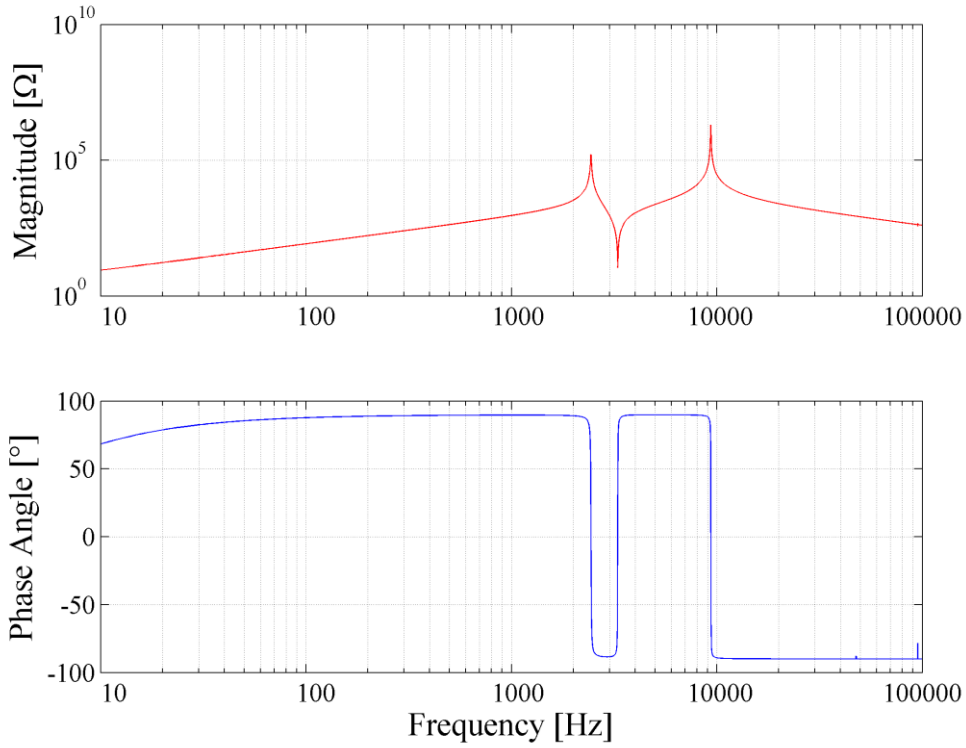

Figure 3-17 PV plant distribution network harmonic impedance characteristic – POC, inverter terminals short circuit

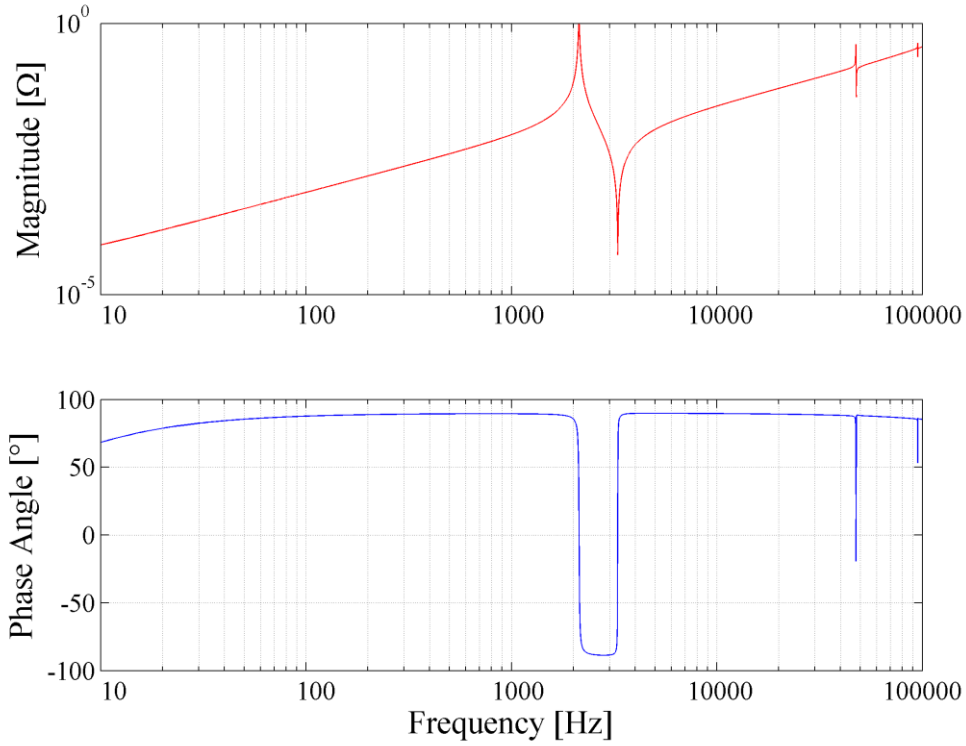

Figure 3-18: PV plant distribution network harmonic impedance characteristic – inverter terminals, POC short circuit

3.5.5 Point of connection, linear network impedance

The harmonic impedance at the POC with the PV plant connected to an external grid is considered with the inverter terminals open circuited. In the author's experience, fault levels in rural 132 kV distribution networks in South Africa typically range between 2 kA and 10 kA with X/R ratio's between 2 and 15. Frequency sweeps were simulated for external networks with an X/R ratio of 4 and fault levels of 2, 5 and 10 kA. The results are shown in Figure 3-19. The PV plant's frequency sweep without any external grid is shown for reference.

The low frequency response (< 1 kHz) at the POC is dominated by the impedance of the external grid. The general shape of the frequency sweep is equivalent to that of the PV plant alone, with a series resonance between two parallel resonances. The resonant frequency of parallel resonances increases with increasing fault level. This is because the parallel inductance at the POC is decreases and, as per equation (2.30), the resonant frequency is inversely proportional to the square root of the inductance of a resonant circuit. Due to the fixed series resonance at 2.1 kHZ, there is one parallel and one series resonance within the harmonic region of interest below 2500 kHz. The magnitude of the parallel resonance peak decreases with increase fault level.

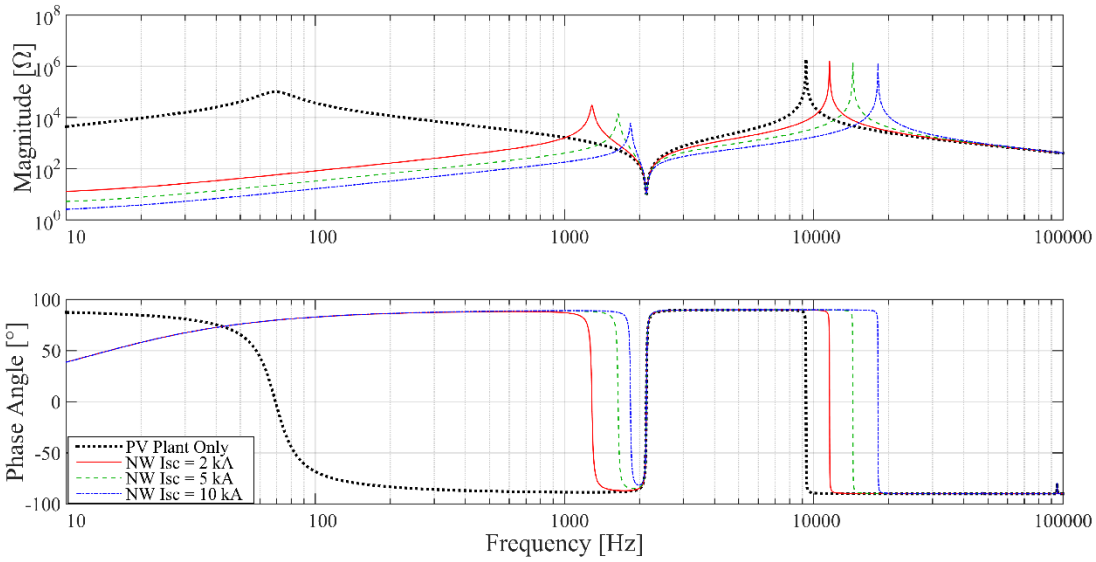

Figure 3-19: POC harmonic impedance characteristic with linear external grid impedance of varying short circuit capacity – inverter terminals open circuit

3.6 Comparison of simplified model and complete PV plant frequency response

A full model of a PV plant in the Northern Cape Province of South Africa was developed in DIgSILENT PowerFactory. The single line diagram of the PV plant is shown in Figure 3-20. The plant consists of 6 radial 33 kV cable feeders with 78 x 1 MVA, 400 V inverters and 39 x 2 MVA, 0.4 / 33 kV inverter transformers. There is a single 80 MVA 33 / 132 kV park transformer at the point of connection. The total length of 33 kV cable is 14.50 km with each feeder comprised of 400 mm^2, 240 mm^2, and 150 mm^2 cable sections. The longest cable segment is 1.07 km long and forms part of the longest cable feeder of length 2.84 km. The highest harmonic order for which the equivalent pi model is adequate is therefore 60 (173 / 2.84 = 60.9) [51]. The

nominal pi representation is therefore still valid for the full plant model for the harmonic frequency range up to the 50th order.

The transformer equivalent circuit parameters are calculated from the nameplate data according to the methodology described in section 3.1.2. The nameplate data are shown in Table 3-5 and the calculated equivalent circuit parameters are shown in Table 3-6. Where significant differences exist between the equivalent circuit parameters of the PV plant transformer and the simplified model transformer, these are primarily due to the difference in transformer ratios due to the use of a 33 kV medium voltage network compared to the 22 kV medium voltage network of the simplified model. Additionally, the actual park transformer no load current is approximately half that of the simplified model park transformer.

The calculated cable network data are shown in Table 3-7. The actual PV plant has a significantly higher cable capacitance than the simplified model. In the subsequent sections the results of a frequency analysis of the full plant are compared to the results from the simplified model presented above.

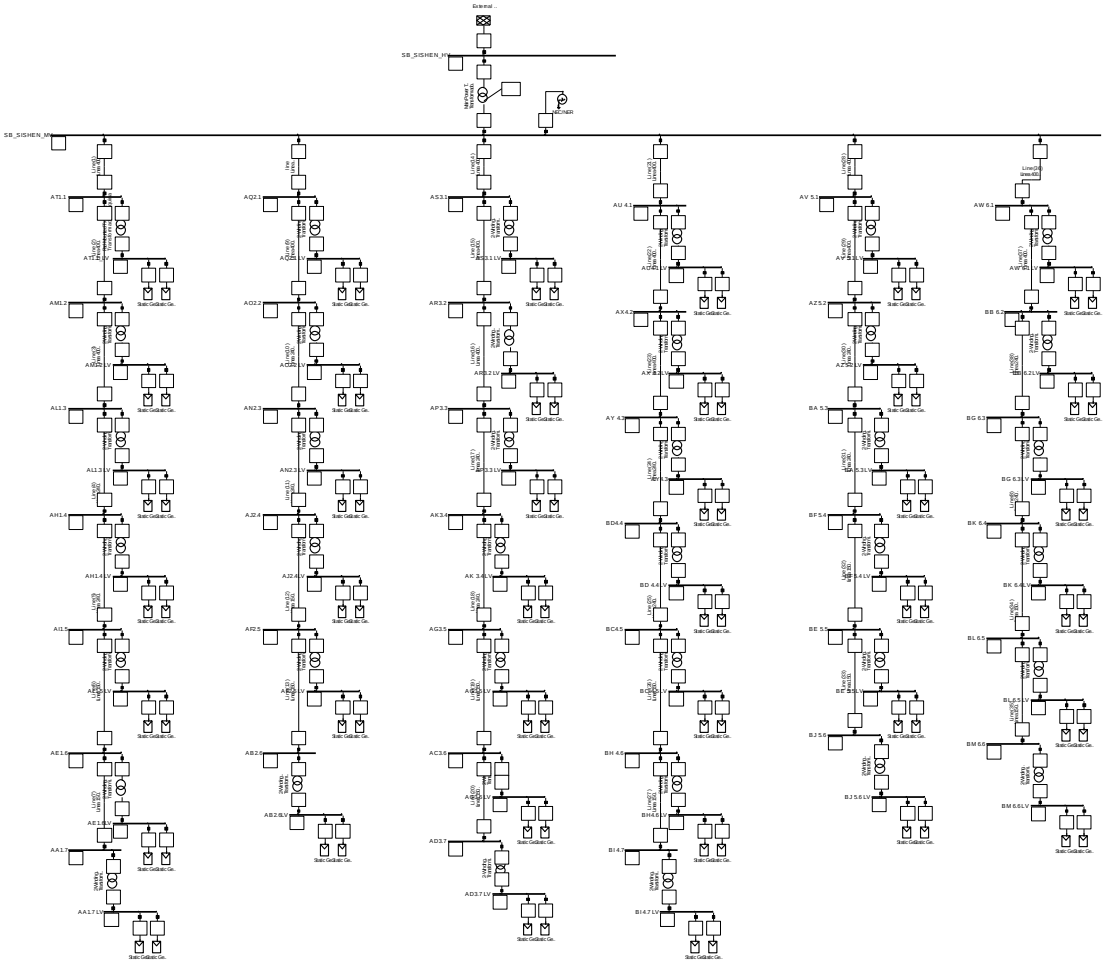

Figure 3-20: Full PV plant model of 75 MWac PV plant

Table 3-5: Park transformer and inverter transformer nameplate data

Parameter	Symbol	Unit	Park Transformer		Inverter Transformer	
			Actual Plant	Simplified Model	Actual Plant	Simplified Model
Rated apparent power	S	MVA	80	80	2	2
Nominal primary voltage	V_{pri}	kV	132	132	33	22
Nominal secondary voltage	V_{sec}	kV	33	22	0.4	0.4
Vector group			YNd1	YNd1	Dyn11	Dyn11
Turns ratio (= V_{pri}/V_{sec})	N	-	4	6	82.5	55
Short circuit impedance	Z	%	11.3	11	8	8
Copper losses	P_{Cu}	kW	334	294	19	19
No-load current	I_{NL}	%	0.06	0.1275	0.9	0.9
No-load losses	P_{NL}	kW	33	34	3.8	3.5
Nominal primary current	I_{pri}	A	349.9	349.9	34.99	52.49
Nominal secondary current	I_{sec}	A	1400	2099	2887	2887
Nominal frequency	f_{nom}	Hz	50	50	50	50

Table 3-6: Park transformer and inverter transformer equivalent circuit parameters

Parameter	Unit	Park Transformer		Inverter Transformer	
		Actual Plant	Simplified Model	Actual Plant	Simplified Model
R_1	Ω	0.4547	0.4002	2.586	1.1495
L_1	H	0.0391	0.03811	0.0688	0.0359
R'_2	Ω	0.0284	0.01112	0.00038	0.00038
L'_2	H	0.00245	0.001059	1.011×10^{-5}	1.011×10^{-5}
R_m	Ω	528,000	512,471	286,579	138,286
L_m	H	1591	576.7	197.0	87.26
C_1	nF	2.9	3	0.27	0.1
C'_2	nF	0.0144	0.0833	0.00265	0.00595
C_{12}	nF	1	1	2	2

Table 3-7: Calculated cable network parameters

Parameter	Unit	Park Transformer	
		Actual Plant	Simplified Model
R	Ω	0.068	0.0125
L	mH	0.132	0.0129
C	μF	3.38	2.54

As for the simplified network model, the harmonic impedance of the PV plant as seen from the 132 kV point of connection (POC) and from the 400 V inverter terminals was first calculated without considering the impedances of the PV inverters and external network. The harmonic impedance plots are presented for the scenarios listed in Table 3-8. The 400 V inverter terminals used for the injection are the last inverter of Feeder 1, which represents the highest cable impedance to the collector substation, and the first inverter of Feeder 6, which represents the lowest cable impedance to the collector substation.

Table 3-8: Frequency sweep analysis scenarios for system harmonic analysis

Description	132 kV Point of Connection	400 V Inverter Terminals
POC, inverter terminals open circuit	Injection point	Open circuit
Inverter terminals, POC open circuit	Open circuit	Injection point
POC, inverter terminals short circuit	Injection point	Short circuit
Inverter terminals, POC short circuit	Short circuit	Injection point

3.6.1 Point of connection, inverter terminals open circuit

The harmonic impedance of the PV plant internal distribution network measured at the POC with the inverter terminals open circuited is shown in Figure 3-21. The response is similar to that of the simplified network which is indicated by the traces with dashed lines. The difference in the resonant frequencies is primarily due to the difference in the cable capacitance of the full PV plant network and that of the simplified model which, when viewed from the POC, is further amplified by the lower ratio of the park transformer in the full plant (132/33 kV) compared to the simplified model (132/22 kV). The result is that an equivalent cable capacitance of the full PV plant, as seen from the POC, is approximately 3 times larger than that of the simplified network.

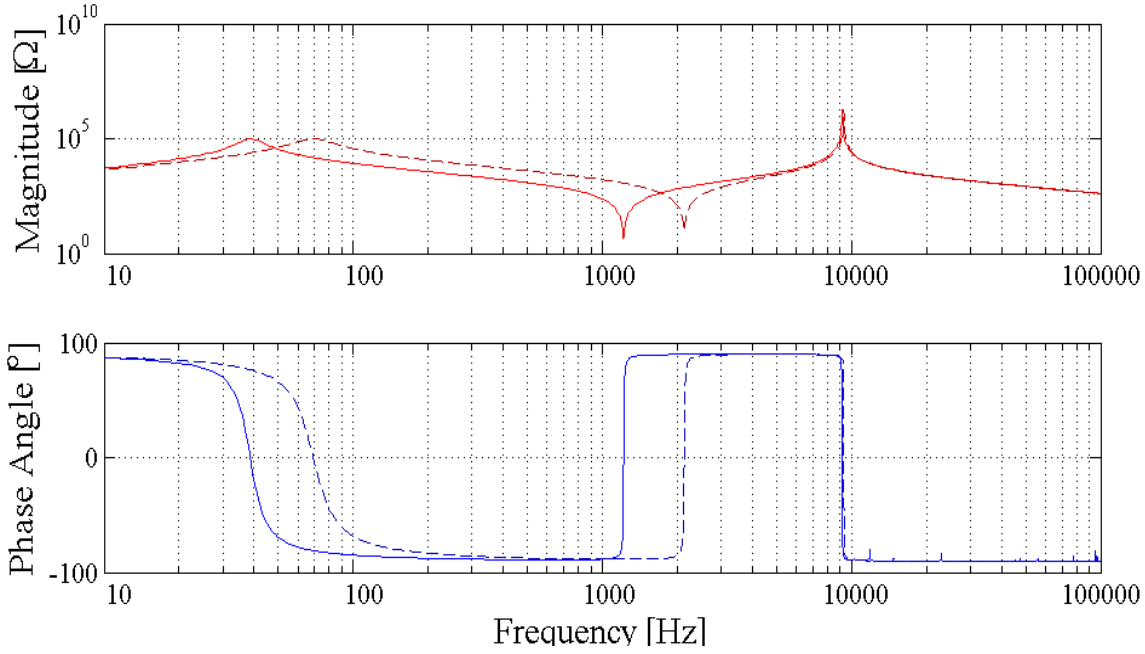

Figure 3-21: Full PV plant distribution network harmonic impedance characteristic – POC, inverter terminals open circuit (with dashed trace of the simplified model characteristic)

3.6.2 Inverter terminals, point of connection open circuit

The harmonic impedance of the PV plant internal distribution network measured at the inverter terminals with the POC open circuited is shown in Figure 3-22. The response of the furthest inverter from the POC is shown in red and the response of the nearest inverter to the POC is shown in blue. The two responses are almost identical. The response of the simplified network is indicated by the traces with black dashed lines.

The first parallel resonance is seen at a lower frequency than in the simplified model due to the larger cable capacitance described in 3.6.1. The first series resonance occurs at 230 Hz which is a much lower frequency than in the simplified model. This is partly accounted for by larger inverter transformer inductance and the larger cable network capacitance but these differences alone would result in a resonant frequency of approximately 1460 Hz. The biggest difference is that the inductive component of the series resonant circuit in the full model is formed by a single inverter transformer, whereas it is formed by the parallel combination of 40 transformers in the simplified model. This indicates a shortcoming of the simplified model in its representation of the harmonic impedance of the PV plant network as viewed from the inverter.

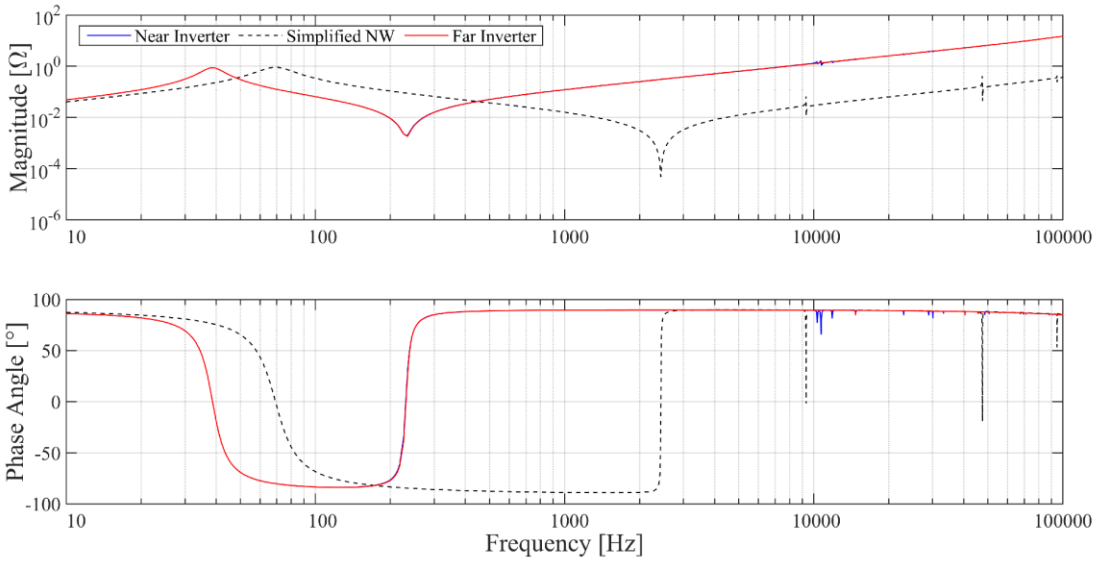

Figure 3-22: PV plant distribution network harmonic impedance characteristic – inverter terminals, POC open circuit (with dashed trace of the simplified model characteristic)

3.6.3 Point of connection, inverter terminals short circuit

The frequency sweep is plotted in Figure 3-23. The first parallel and series resonances occurs at lower frequencies than in the simplified model due to the larger cable capacitance. The higher frequency response matches the simplified model closely because it is governed by the parameters of the park transformer.

3.6.4 Inverter terminals, point of connection short circuit

The harmonic impedance of the network viewed from the inverter terminals with the POC short circuited is largely inductive due to the leakage inductance of the inverter transformer. The frequency sweep is plotted in Figure 3-24. The magnitude of the inductive impedance is significantly larger for the full network model than

the simplified model because the full model considers current injection through a single inverter transformer, whereas the simplified model considers 40 transformers in parallel. The first parallel resonance occurs at a lower frequency in the full PV plant model compared to the simplified model due to the larger capacitance of the full PV plant. The second resonance is also influenced by this capacitance but is more significantly affected by the current injection through a single inverter transformer compared to 40 parallel transformers in the simplified model. Therefore, the two resonances occur at very nearby frequencies of 1218 and 1238 Hz.

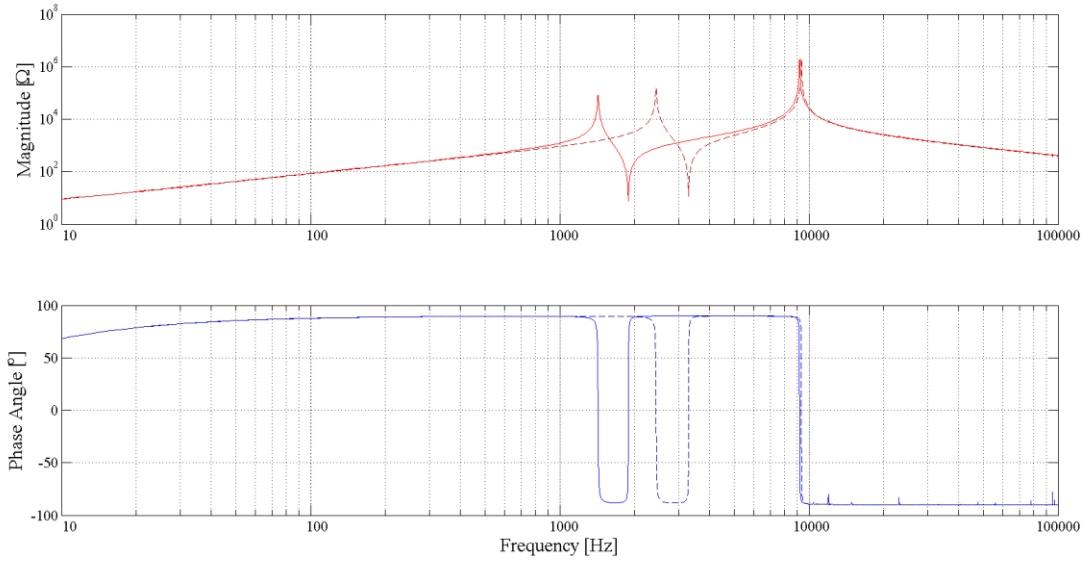

Figure 3-23: PV plant distribution network harmonic impedance characteristic – POC, inverter terminals short circuit (with dashed trace of the simplified model characteristic)

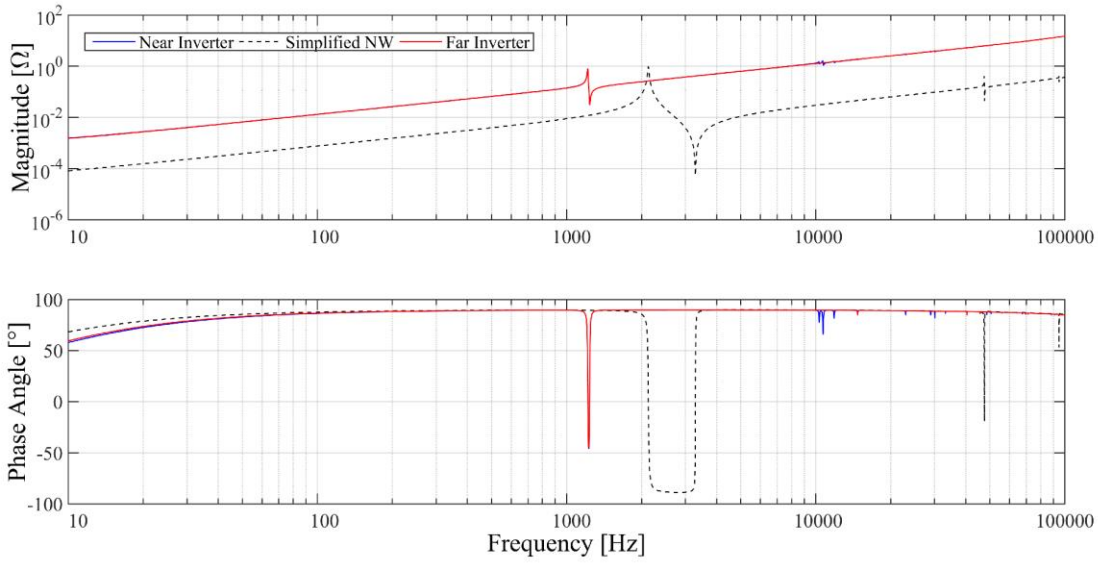

Figure 3-24: PV plant distribution network harmonic impedance characteristic – inverter terminals, POC short circuit

3.6.5 Point of connection, including external network

The harmonic impedance at the POC with the PV plant connected to an external network is considered with the inverter terminals open circuited. Three external network impedances are considered:

1) Utility frequency sweep (provided by the utility based on network model – positive sequence impedance magnitude and angle up to maximum frequency of 2500 Hz)

2) Minimum fault level sweep (Isc = 1.6 kA) with assumed X/R ratio of 4

3) Maximum fault level sweep (Isc = 3.7 kA) with assumed X/R ratio of 4

The minimum and maximum fault currents expected at the POC were provided by the utility but no corresponding X/R ratios are available. The author considers X/R = 4 to be a reasonable estimate for a rural 132 kV network in South Africa.

The results are plotted in Figure 3-25. The dotted lines represent the impedance sweeps of the three networks prior to connection of the PV plant and the corresponding colour solid lines represent the impedance at the POC after connection of the PV plant.

For all three networks, the low frequency response (< 500 Hz) at the POC is dominated by the impedance of the external network. The general shape of the frequency sweep for the two linear impedance external networks is equivalent to that of the PV plant alone. The resonant frequency of parallel resonances is higher for the network with the higher fault level.

The first parallel resonance does not present for the simulated impedance based on the utility network model. This appears to be due to a network series resonance coinciding with the PV plant parallel resonance. The series resonance due to the interaction of the park transformer leakage inductance and the cable capacitance presents at 1220 Hz. Higher order resonances cannot be evaluated since the utility sweep is only available for the range up to 2500 kHz.

3.6.6 Inverter terminals, including external network

Considering the same three external network impedances, the harmonic impedance measured at the furthest inverter terminals is shown in Figure 3-26. The characteristic is similar to that of the inverter terminals with the POC short circuited. The network harmonic impedance is predominantly inductive and is connected in series with the transformer leakage reactance. Due to the increased total impedance of this series combination, the parallel resonance caused by its interaction with the 33 kV shunt capacitance occurs at a lower frequency than for the short circuited network. Considering the utility sweep, this resonance occurs at 1,100 Hz (h = 22).

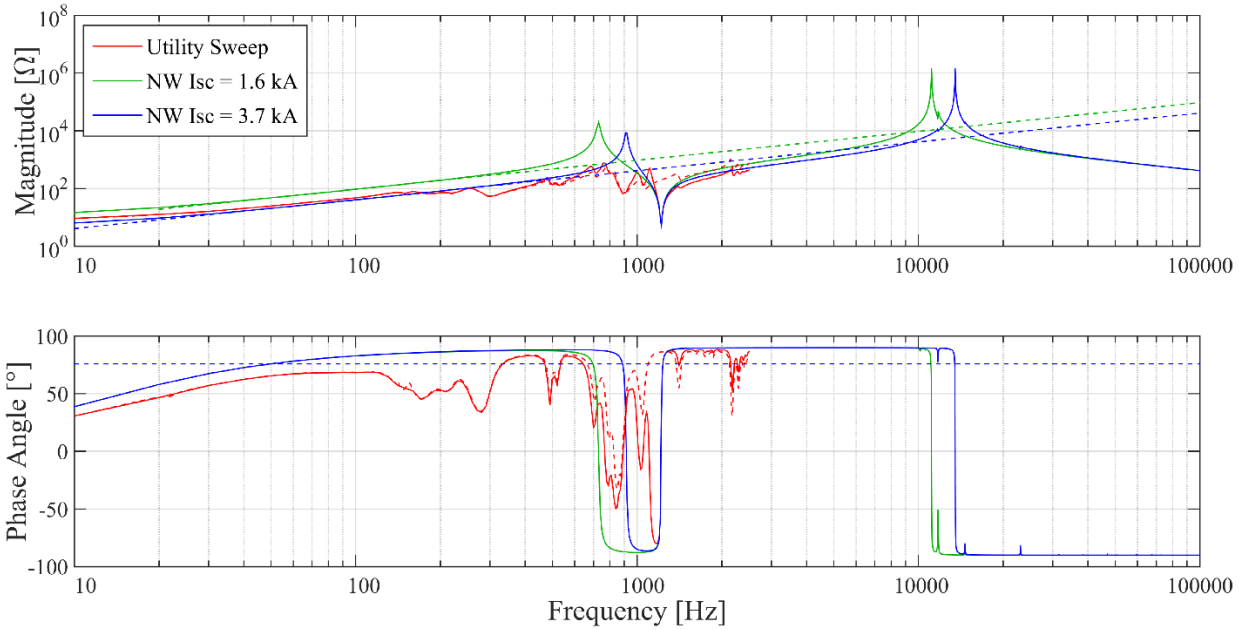

Figure 3-25: POC harmonic impedance characteristic with simulated external grid impedance (provided by the utility) and linear external grid impedances for minimum and maximum POC short circuit currents – inverter terminals open circuit. Dashed lines represent corresponding network impedances prior to connection of PV plant.

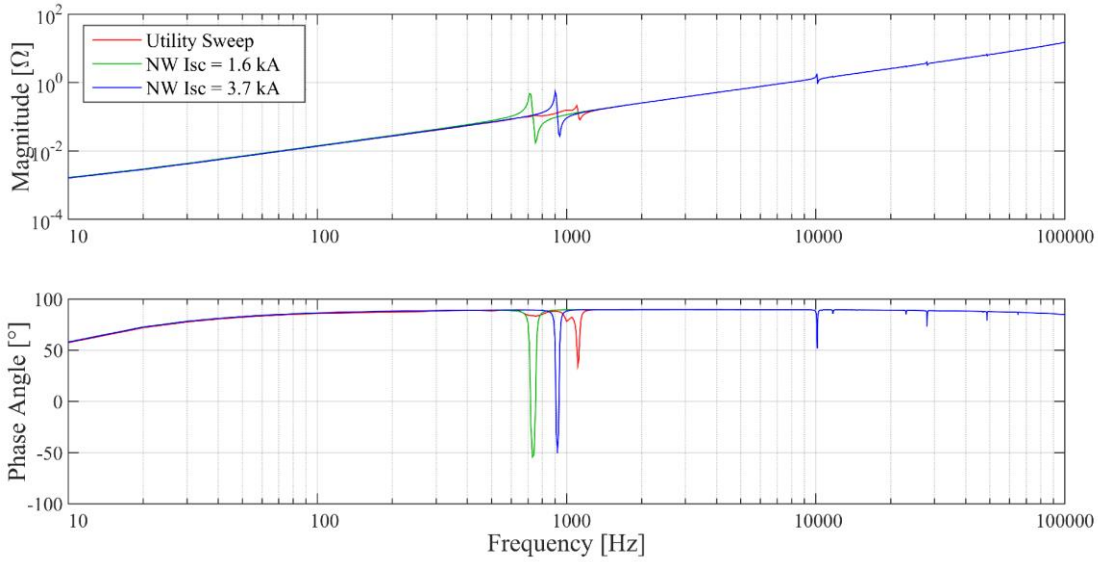

Figure 3-26: Furthest inverter terminal harmonic impedance characteristic with simulated external grid impedance (provided by the utility) and linear external grid impedances for minimum and maximum POC short circuit currents

4 Analysis of harmonic measurements

4.1 Site description

To study the harmonic performance of an actual utility-scale PV plant, measurement data were obtained from a 75 MWac single axis tracker PV plant in the Northern Cape province of South Africa. The park transformer is a single 132/33 kV, 80 MVA transformer and the plant comprises 6 cable feeders with a total of 39 two-winding 2 MVA inverter transformers and 78 x 1 MVA inverters. The topology of the plant is illustrated in the single line diagram in Figure 3-20.

The plant is connected by means of a loop-in, loop-out connection of a single circuit 132 kV traction feeder line which has a loading capacity of approximately 85 MVA. The line is only connected to the 275 kV regional transmission network at one point. The transmission substation is located 18 km from the PV plant substation and has a transformation capacity of 500 MVA.

The POC is on the primary side of the 132/33 kV, 80MVA park main transformer. According to information available from the utility, the fault level at the POC can vary between 1.6 kA (366 MVA) and 3.7 kA (846 MVA) depending on the network configuration. The network configuration and fault level during the measurement period is unknown but is expected to be closer to the higher value, as the lower value represents the fault level during contingency conditions.

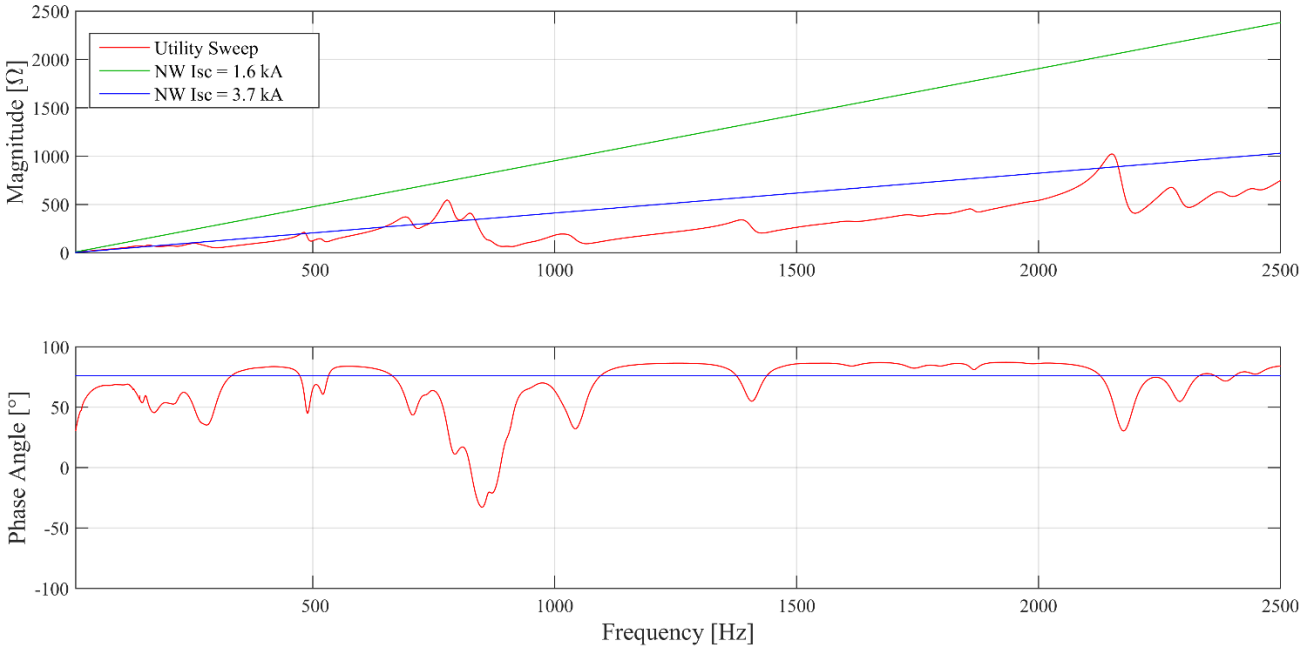

Figure 4-1: POC frequency sweep prior to connection of the PV plant compared to the linear sweeps for the minimum and maximum fault levels

The utility provided a frequency sweep for the network at the point of connection prior to the connection of the PV plant. The sweep was calculated using a simulation model of the regional distribution and transmission network. In Figure 4-1, the provided frequency sweep is compared to linear frequency sweeps at the maximum and minimum fault levels, both with an assumed X/R ratio of 4. Figure 4-1 shows that the linear frequency sweep for the maximum fault level of 3.7 kA provides a reasonable approximation of the simulated frequency sweep provided by the utility.

4.2 Measurement data

Data were measured over a period of 12 days to analyse the harmonic behaviour of the PV plant. This section starts with a description of the measurement systems and its components. Ten-minute averaged voltage and current harmonic measurement data are then analysed with the view to exploring instrument transformer accuracy and the quantization error of the meter in the context of the amplitudes of the measured harmonic components. The 10-minute averaged values are subsequently compared to 3-second averaged values with the view to determine whether the temporal fluctuations are sufficiently small that the 10-minute average values typically used in analysis and compliance monitoring provide a reasonable approximation of both the short-term and long-term behaviour of the plant. Finally, a description is provided of the methodology for processing captured waveform data to extract the harmonic spectra of the voltages and currents.

4.2.1 Site power quality measurement installation

Measurements were captured over a 12-day period, from 00h00 on 10/04/2015 to 24h00 on 21/04/2015, at the POC using an ImpedoDUO IEC-61000-4-30 Class A power quality meter installed temporarily at the site. The meter captured harmonic voltage and current measurement data, in accordance with the IEC 61000-4-7 and IEC 61000-4-30 methodologies, for harmonic orders h = 1 to 50 (50 - 2500 Hz). The single line diagram of the measurement system is shown in Figure 4-2.

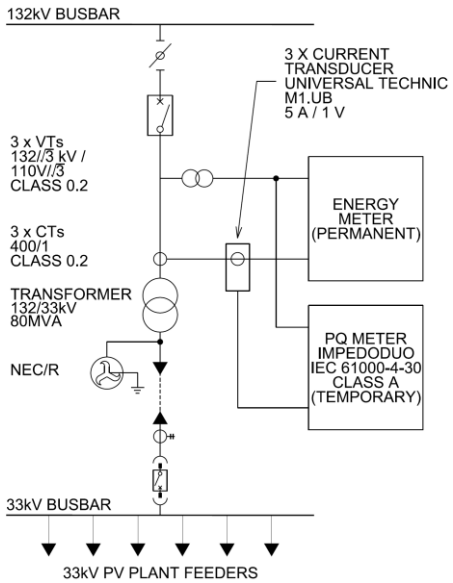

Figure 4-2: Power quality meter installation schematic diagram

The temporary metering installation made use of the 132 kV current transformers (CTs) and voltage transformers (VTs) of the permanent tariff metering installation. The instrument data for the CT's and VT's are summarized in Table 4-1.

Table 4-1: Instrument transformer data

Description	VT	CT
Type	Inductive	Inductive
Ratio	$\frac{132\ \text{kV}}{\sqrt{3}} \Big/ \frac{110\ \text{V}}{\sqrt{3}}$	400/1
Class	0.2	0.2

The meter's voltage inputs were connected directly to the VT secondary circuit bus whilst the current measurements were obtained by means of 5 A/1 V clamp-on current probes, which were clamped around the CT secondary wires such that it was not necessary to interrupt the CT secondary circuit during installation. Because the CTs on site have a secondary current of 1 A, each CT secondary lead was looped through its transducer window 5 times to improve utilization of the transducer measurement range. This corresponds to an effective CT primary current to meter voltage input ratio of 400 A / 1 V. The current probe specifications are summarized in Table 4-2.

Table 4-2: Current probe data

Description	Specification
Measurement range	0.1 A to 10 A_{RMS}
Output sensitivity	0.2 V / A
Frequency range	30 Hz to 10 kHz
Guaranteed accuracy	±2% (0.1 A to 0.5 A) ±1.5% (0.5 A to 2 A) ±1% (2 A to 5 A)

3-second and 10-minute measurements captured in accordance with the IEC 61000-4-30 methodology were available for the full recording period. Additionally, voltage and current waveforms were captured for 70 events over a 15-day period from 09/04/2015 to 23/04/2015, where these events were triggered by rms voltage changes exceeding 3%. The capture and data processing of these events is described in more detail in section 4.2.5.

The plant was shut down completely and disconnected from the network by opening of the 132 kV POC circuit breaker for a period of approximately 10 hours over the night-time period of 21/04/2015 to 22/04/2015. 132 kV harmonic voltage recordings are available for this period and are used as a comparative measure of background harmonic distortion in evaluating the harmonic emissions of the plant.

4.2.2 Measurement accuracy

It is important to consider the measurement set-up and its influence on the accuracy and reliability of the captured data prior to undertaking any analysis of the data. Detailed evaluation of the individual components of the measurement equipment, particularly the current and voltage transformers, is beyond the scope of this investigation but the following key aspects may influence the measurement accuracy:

4.2.2.1 Transducer error

As discussed in section 2.14.2, voltage and current transformers exhibit non-linear transformation ratio and phase angle characteristics with respect to frequency. Inductive VTs typically remain within an accuracy band of ±10% in the frequency range from 50 to 2500 Hz, i.e. harmonic orders h = 1 to 50 [141], [142] but harmonic phase angle error may be significant [144]. Experimental studies have shown inductive CT's to exhibit constant transformation ratios for low order harmonics up to 1 kHz and 3 kHz [149] but low accuracy has been observed at low currents [144] [149].

Given the stochastic nature of harmonic data, the frequency responses of inductive VTs and CTs are considered sufficiently flat to analyze harmonic trends and assess harmonic emissions, although non-linear frequency response for signals of very low magnitude may affect the accuracy of measurements. The instrument transformers forming part of the permanent installation at the PV plant were selected primarily for tariff metering purposes and hence are designed to measure accurately over the range of fundamental frequency voltages and currents expected during normal operation.

The manufacturer of the clamp-on current probe specifies its measurement range as 0.1 – 10 A_{RMS} over a frequency range of 30 Hz to 10 kHz. Considering the described measurement configuration with each CT lead looped 5 times through its current probe window, 0.1 A of transducer current equates to 20 mA of CT secondary current or 8 A of CT primary current, which is 2% of CT nominal current. This is much higher than the anticipated harmonic emission levels for most, if not all, harmonic orders. Values of measured current much lower than the 2% threshold are represented in the PV plant measurement data.

4.2.2.2 Harmonic amplitudes

The magnitude of harmonic voltages and currents at certain harmonic orders may be very low. This is especially true for even harmonics and higher order harmonics. The accuracy of instrument transformers and transducers at such low currents over the harmonic frequency band is usually not defined. Furthermore, secondary circuit signals of very small magnitude are susceptible to distortion by electromagnetic noise present in the substation environment.

The analogue to digital converters of the selected Class A meter have a 16-bit resolution. The single bit resolution for phase-to-neutral voltage measurement is 28.5 mV, i.e. 0.045% of VT nominal voltage. For a 132 kV VT with nominal phase-neutral secondary voltage of 63.5 V, this equates to 34.18 V on the VT primary. The single bit resolution for current measurement represents 0.324 mA current flow through the

current transducer, or 0.0648 mA CT secondary current. This is 0.00648% of the CT nominal current, which equates to 25.9 mA primary current through the 400/1 132 kV CT. At very low current and voltage values, quantization effects may introduce significant additional measurement errors.

4.2.3 Measurement trends

The fundamental frequency power trends of the power plant over the 12-day recording period are extracted by analysing the 10-minute aggregated values from the meters. The fundamental frequency active and reactive power outputs, measured at the 132 kV POC, are shown are Figure 4-3. These reflect the typical operating conditions for a tracking solar PV plant. The active power ramps rapidly in the early morning and late afternoon, while the effect of intermittent cloud cover is evident due to active power fluctuations on certain days. Active power production dips in the middle of the day due to the effect of high temperatures on PV panel production.

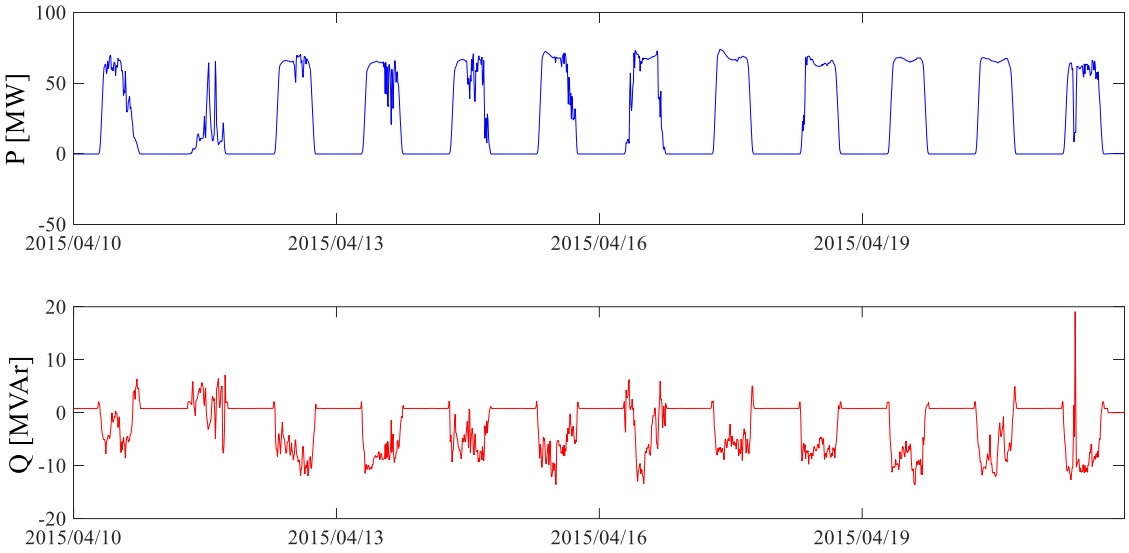

Figure 4-3: PV Plant fundamental frequency active and reactive power over the recording period

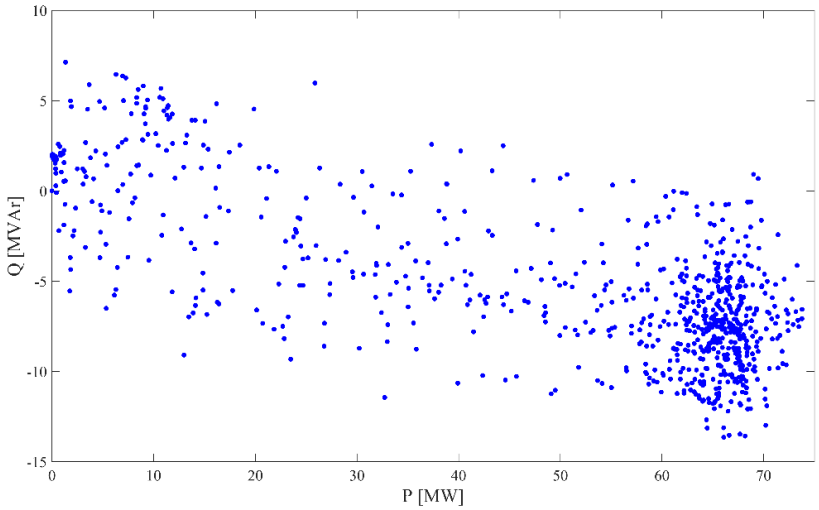

Figure 4-4: PV Plant fundamental frequency reactive power vs active power relationship

The maximum active power generated by the plant during the measurement period is 73.77 MW and the maximum power absorbed by the facility at night is 265 kW. The reactive power ranges between +19.1 MVAr (exporting) and -13.65 MVAr (importing). The plant is operated in voltage control mode and the reactive power absorbed by the facility therefore increases as the active power export increases to regulate the voltage at the POC. Figure 4-4 clearly illustrates this relationship between reactive and active power.

4.2.3.1 Overview of 10-minute averaged harmonic voltage measurement data

The measured harmonic voltages and currents are considered in terms of the magnitude of the secondary voltage and current signals to evaluate:

- the effect of quantisation in the data acquisition process,
- the likelihood that the accuracy of measurement is affected by noise,
- the likelihood that the accuracy of measurement is affected by the measurement range and accuracy of the equipment used in the measurement system.

Evaluation of the data revealed the magnitudes of signals above the 25th order to be zero, or near zero, for the full recording period. Therefore, the investigation is focused on harmonic orders 2 to 25. The mean, 95th percentile and maximum values of 10-minute aggregated red-phase harmonic voltage for harmonic orders h = 2 to 25 are shown in Figure 4-5; the other phases exhibit similar trends. The left vertical axis indicates the voltage as a percentage of VT nominal voltage while the right vertical axis indicates the VT secondary voltage as a multiple of the single bit resolution of the 16-bit A/D converter in the meter (28.49 mV).

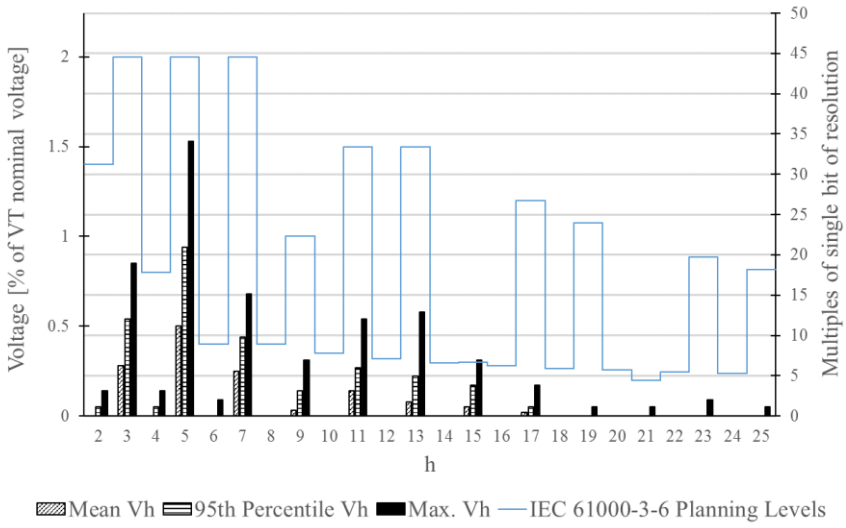

Figure 4-5: Mean, 95th percentile and maximum values of red-phase 10-minute aggregated secondary harmonic voltage (h = 1 to 25)

The 95th percentile harmonic voltage distortion is significantly below the IEC 61000-3-6 planning levels, indicated by the blue line, for all harmonic orders. [42] The voltage distortion is compared to IEC 61000-3-6 planning levels since the IEC method of compliance assessment is based on voltage distortion limits. In the following section, the harmonic current emissions are compared to the IEEE 519 current limits since the IEEE

method of assessment is based primarily on current measurements. The 3rd, 5th and 7th harmonic voltages are dominant with moderate voltage distortion for odd harmonic orders from 9 to 17. Harmonic distortion for even harmonics and higher order harmonics is very low.

The magnitudes of the measured 10-minute aggregated secondary voltages for harmonic orders 1 to 9 of the red phase 132 kV VT at the POC are shown in Figure 4-6. The fundamental frequency voltage is predictably close to the nominal secondary voltage of 63.5 V, averaging 65.2 V (102.7%). Quantisation effects, where the signal takes on discrete values which are a multiple of a single bit of resolution of the meter's A/D converter are clearly visible for non-dominant harmonic orders including 2, 4 and 9. The manufacturer has stated that the meter may experience input fluctuations of one bit due to noise at the input, even in the absence of any input signal.

The levels below which a signal's accuracy is inadequate for it to be useful for analysis purposes are rather subjective. However, in cases where the 95th percentile value is less than 5 times a single bit of resolution, the quantization errors become large and the reliability of the measurement data is in doubt. This is true for even voltage harmonics and for all voltage harmonics with harmonic order greater than 15.

A signal amplitude of 5 times a single bit resolution corresponds to a secondary voltage of 142 mV, i.e. 0.22% of the VT nominal voltage. Apart from quantization effects, the measurement equipment is considered adequate to measure this level of secondary voltage since the Class A measuring instrument is required to operate with an accuracy of 0.2% of full scale measurement for the fundamental frequency. However, the exact measurement accuracy of such low voltages is uncertain.

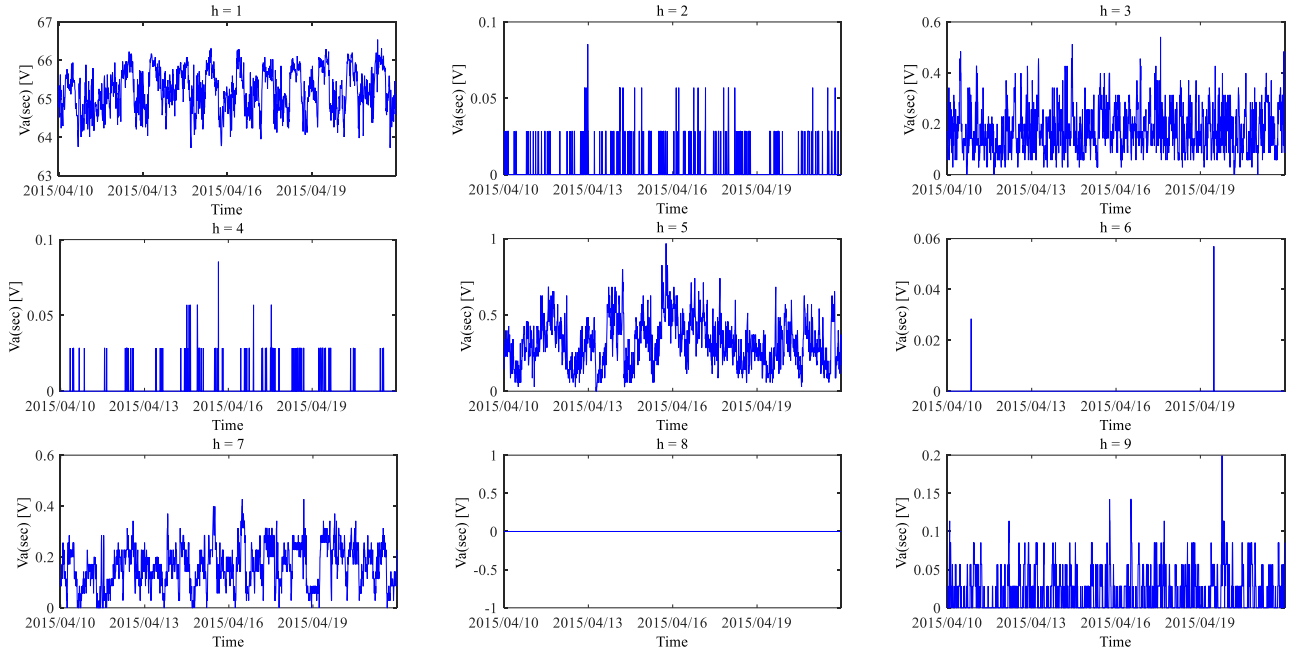

Figure 4-6: Red phase 132 kV VT secondary harmonic 10-minute aggregated voltages (h = 1 - 9)

4.2.3.2 Overview of 10-minute averaged harmonic current measurement data

The average, 95th percentile and maximum values of 10-minute aggregated red-phase harmonic current for h = 2 to 25 are shown in Figure 4-7; the other phases exhibit similar trends. The left vertical axis indicates the current as a percentage of CT nominal current while the right vertical axis indicates the CT secondary current as a multiple of a single bit of resolution of the 16-bit A/D converter in the meter. The blue line in Figure 4-7 indicates the IEEE 519-2014 current distortion limits applicable to a 132 kV generation plant considering the maximum demand current to be 345.3 A, which is the current output of the plant when it operates at rated power output (75 MW), rated power factor (0.95 lead/lag) and nominal voltage. The 95th percentile current emission remains below the IEEE limits for all harmonic orders. Only the 5th and 7th order harmonic currents are dominant.

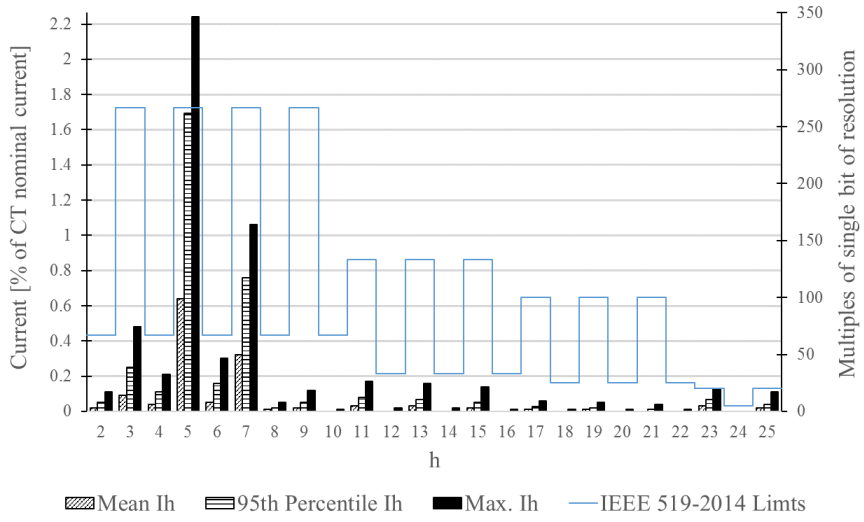

Figure 4-7: Mean, 95th percentile and maximum values of red-phase 10-minute aggregated secondary harmonic current (h = 1 – 25)

The magnitudes of the measured 10-minute aggregated secondary currents for harmonic orders 1 to 9 of the red phase 132 kV CT at the point of connection are shown in Figure 4-8. The fundamental frequency current peaks at 777.8 mA (311.1 A primary) which would equate to a plant output power of approximately 73 MVA, considering the average 132 kV voltage of 102.7%.

All even harmonics above the 10th harmonic order and all harmonics with harmonic order greater than 25 have a 95th percentile value less than 5 multiples of a single bit of resolution and are therefore likely to be significantly affected by quantisation error. The manufacturer has stated that the meter may experience input fluctuations of one bit, even in the absence of any input signal. Quantisation effects are noticeable in, for example, the 8th and 9th harmonic current plots but for all of the lower order harmonics in Figure 4-8, the harmonic current trend between daytime periods (when the plant is operating) and the night-time periods (when it is not operating) is clear.

In the case of the harmonic current measurements, even 0.1% of the nominal CT rating is equal to 15 times a single bit of resolution. Therefore, the errors introduced by the CTs and current probes and by meter input

noise are expected to dominate over the quantization error of the 16-bit A/D. The 95th percentile harmonic current is less than 0.05% of the CT nominal current for even harmonics of order greater than 6 and odd harmonics of order greater than 15, apart from the 23rd harmonic. The 95th percentile current only exceeds 0.1% of CT nominal current for h = 3 to 7.

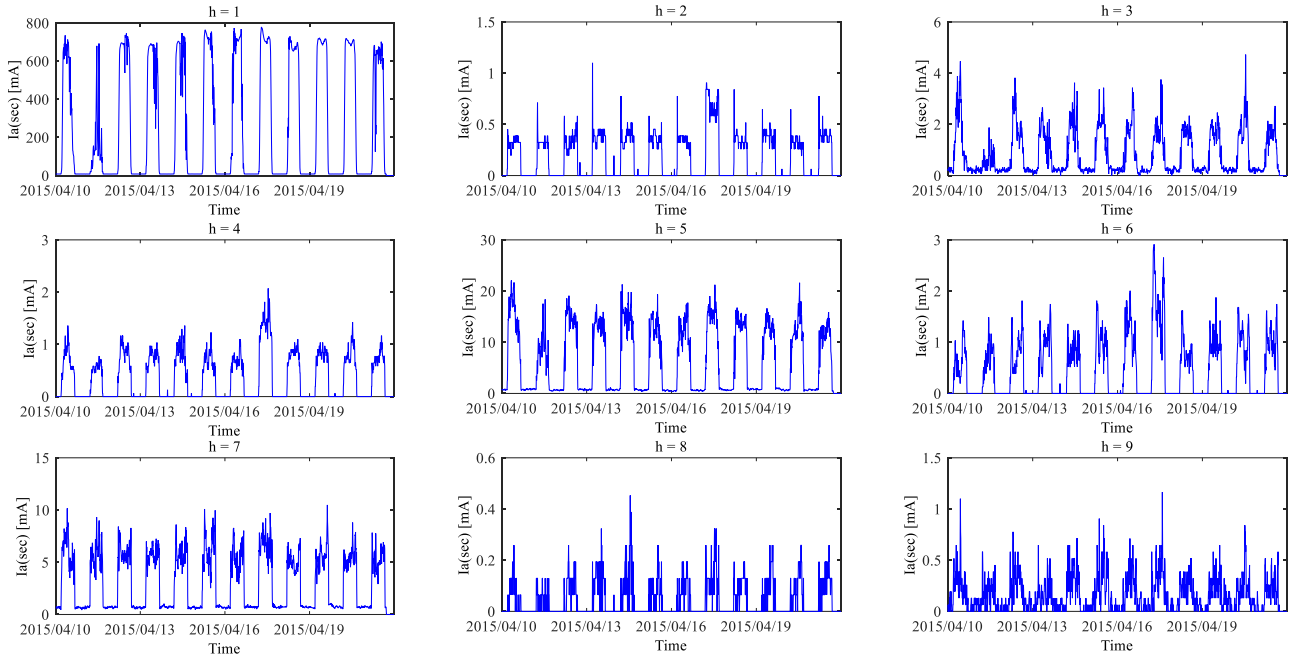

Figure 4-8: Red phase 132 kV CT secondary 10-minute aggregated harmonic currents (h = 1 - 9)

4.2.4 Comparison of the 3-second aggregated values and the 10-minute aggregated values

To evaluate the usefulness of 10-minute aggregated values for harmonic analysis, it is necessary to understand whether the 10-minute averages are representative of the harmonic measurements for shorter time periods. Large fluctuations in the 3-second aggregated values compared to the 10-minute aggregated values indicate that the 10-minute average is not a good representation of the short-term harmonic behaviour of the plant and that caution should be exercised in use and interpretation of the 10-minute aggregated values. The standard deviation of the 3-second harmonic measurement values within each 10-minute period defines the dispersion of the 3-second data and is therefore useful as a measure of the degree of fluctuation of the measured harmonic quantities during each 10-minute period.

4.2.4.1 Fundamental frequency voltage and current fluctuation

The 3-second values (red) of red phase fundamental current and voltage are plotted over the 10-minute values (blue) for two typical days in Figure 4-9 and Figure 4-10 respectively. Day 2 (11/04/2015) is a cloudy day with significant fluctuations in the plant output throughout the day and Day 10 (19/04/2015) is a clear day with little fluctuation in the power output of the plant.

On a clear day, fundamental frequency current increases rapidly from approximately 07h00 to 08h30 as the sun rises and decreases rapidly from approximately 16h30 to 18h00. Although the current ramps smoothly during these period, the rate of change of current results in a large deviation between the 3 s values at the

beginning and end of the period and the 10-minute average. Rapid fluctuations of the output current with significant magnitude are visible during the initial start-up period of the plant in the early morning and, to a lesser extent, at the shutdown of the plant in the evening. Both of these times represent conditions of low irradiance and the 10-minute aggregated fundamental frequency measurements from the plant are clearly not representative of the short-term behaviour visible in the 3-second data during these short time periods.

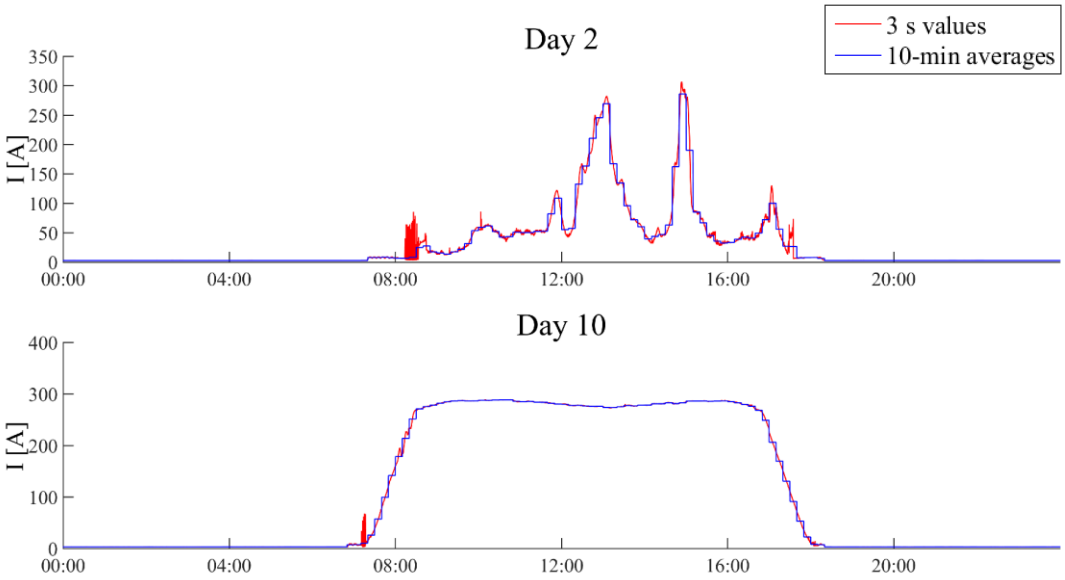

Figure 4-9: Red phase 132 kV fundamental frequency current (Ia) – 3 s values and 10-min averages

Figure 4-10 shows that the fundamental frequency voltage fluctuates rapidly and apparently randomly within each 10 minute-period. This is due to fluctuating loads within the local network and the voltage control action of the PV plant which was operating in voltage control mode for the duration of the recording period.

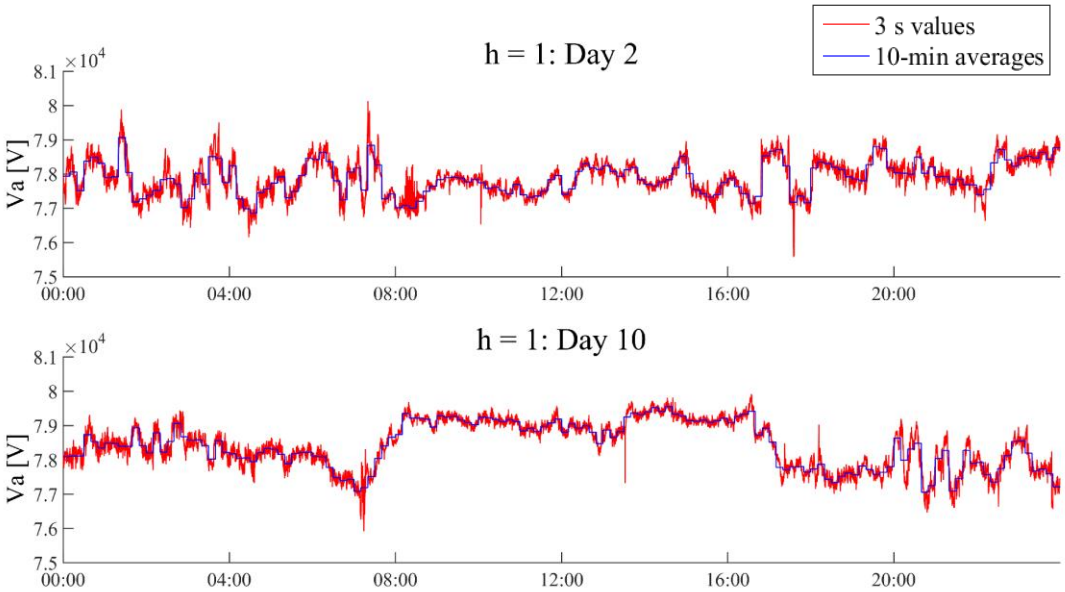

Figure 4-10: Red phase 132 kV fundamental frequency voltage (Va) – 3 s values and 10-min averages

4.2.4.2 Harmonic voltage fluctuation

Figure 4-11 shows a plot of the 3-second standard deviations vs 10-minute averages for the 3rd harmonic voltage while Figure 4-12 shows a comparison of the 3-second and 10-minute 3rd harmonic voltages on 19/04/2015, a typical day. The grid spacing in Figure 4-11 is one bit of voltage resolution. The spread of voltage standard deviations across the range of 10-minute voltages is relatively uniform with the increased maximum standard deviations for 10-minute values between 0.2 and 0.5 V attributable to the increased number of sample points in this range and because large fluctuations are not possible for very small average voltage magnitudes.

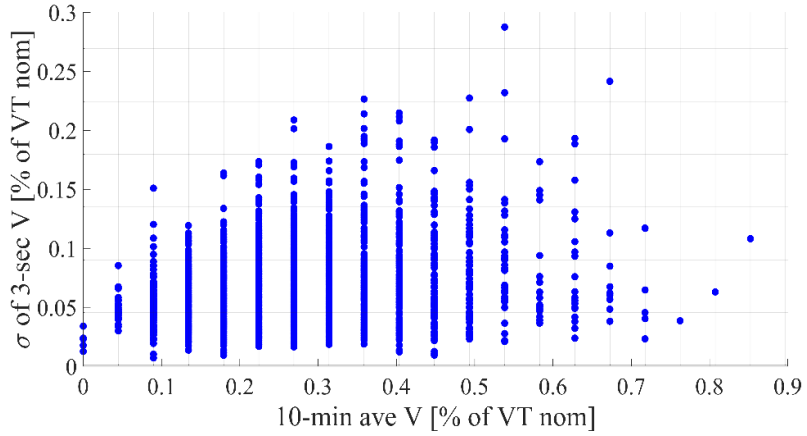

Figure 4-11: Standard deviation of 3-second aggregated 3rd harmonic voltages per 10-minute period plotted against the corresponding 10-minute aggregated values.

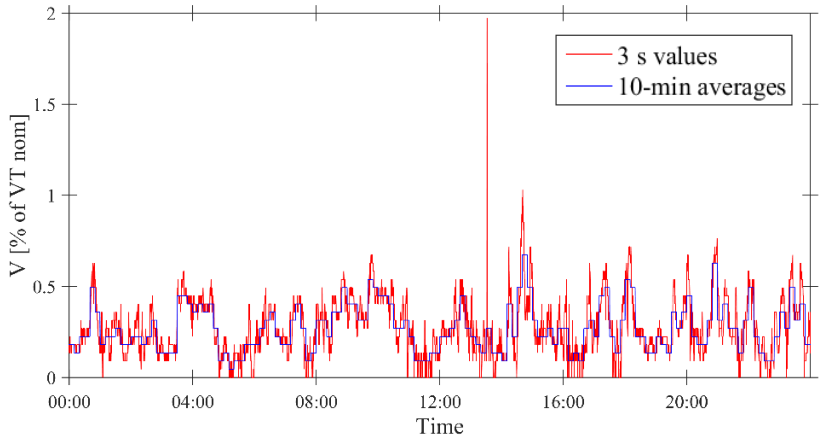

Figure 4-12: 3rd harmonic voltage on 19/04/2015. 3-second aggregated values vs 10-minute aggregated values.

Figure 4-13 shows the 95th percentile standard deviations vs the 95th percentile 10-minute voltages for harmonic orders up to 25. The fluctuation for harmonic voltages with a P95 standard deviation of less than one bit of resolution is strongly influenced by measurement error. Only odd harmonics below h = 15 exceed this level (indicated by the red dashed line in Figure 4-13). The P95 standard deviation for the third harmonic voltage is 26% of the P95 10-minute average. Considering the voltage plot of Figure 4-12, many periods are influenced by quantisation error, but there are also more significant deviations from the 10-minute averages

during certain periods. Overall, the fluctuations are sufficiently small that the trend of 10-minute voltages appears representative of the 3-second measurement signal.

For odd harmonics up to the 15th, the P95 standard deviation is less than 33% of the P95 10-minute voltage. For these harmonics, the mean of the standard deviations is only 25 – 50% of their P95 value and the fluctuations are moderate to small.

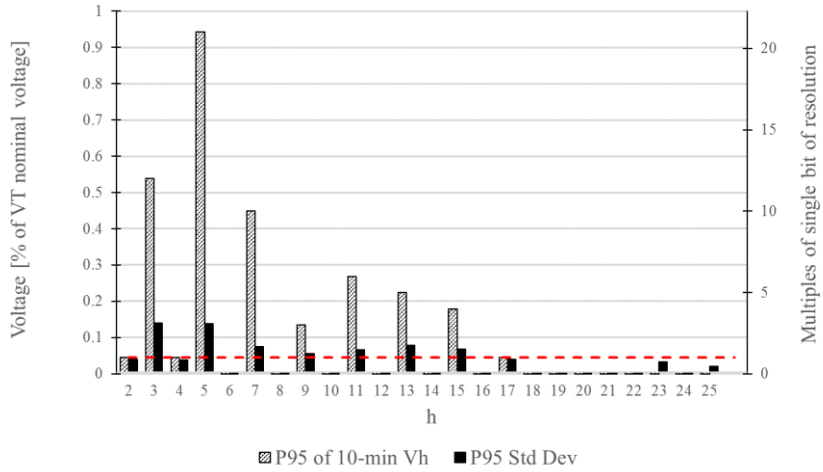

Figure 4-13: 95th percentile of 3-second harmonic voltage standard deviation per 10-minute period vs 95th percentile of 10-minute harmonic voltages.

4.2.4.3 Harmonic current fluctuation

Figure 4-14 shows a plot of the 3-second standard deviations vs 10-minute averages for the 3rd harmonic current while Figure 4-15 shows a comparison of the 3-second and 10-minute 3rd harmonic currents on 19/04/2015. The grid spacing in Figure 4-14 is one bit of current resolution. The current standard deviations are noticeably higher when the plant is operating – represented primarily by currents above 0.03% of the CT ratio in the case of the 3rd harmonic current. This trend is noted for all dominant harmonic orders.

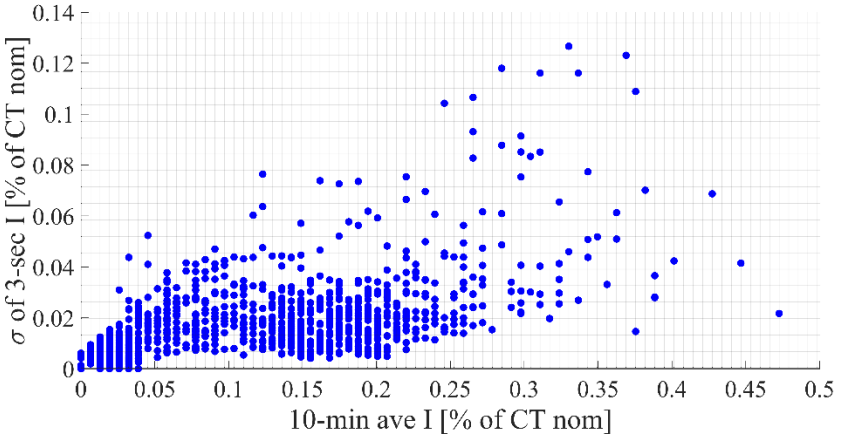

Figure 4-14: Standard deviation of 3-second aggregated 3rd harmonic currents per 10-minute period plotted against the corresponding 10-minute aggregated values.

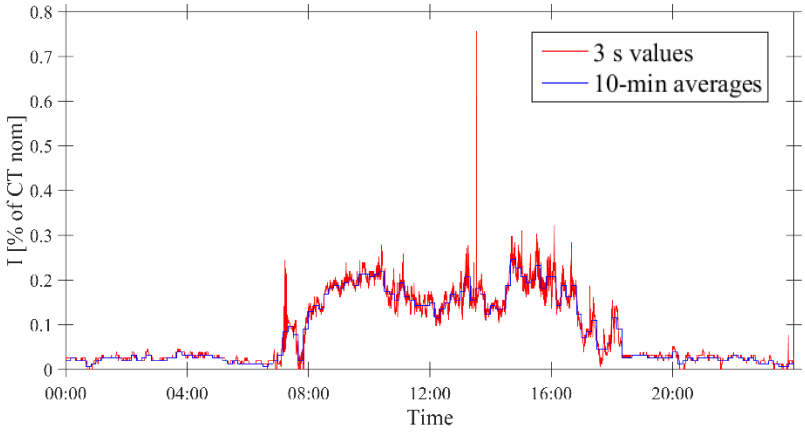

Figure 4-15: 3rd harmonic current on 19/04/2015. 3-second aggregated values vs 10-minute aggregated values.

Short periods with large fluctuations of harmonic current – reflected in the 3-second data but not the 10-minute data – do occur, usually during the start-up of the plant, as seen before 08h00 in Figure 4-15. These fluctuations coincide with fluctuations noted in the fundamental frequency current, as described in 4.2.4.1 above. Considering the standard deviation for harmonic orders from 2 to 10 plotted in Figure 4-16, the trend of large fluctuations in harmonic current output – evidenced by high standard deviation of the measured 3 second values within a 10-minute period –during plant start-up (near 07h30) and shutdown (near 18h00) is clear for most lower order harmonics.

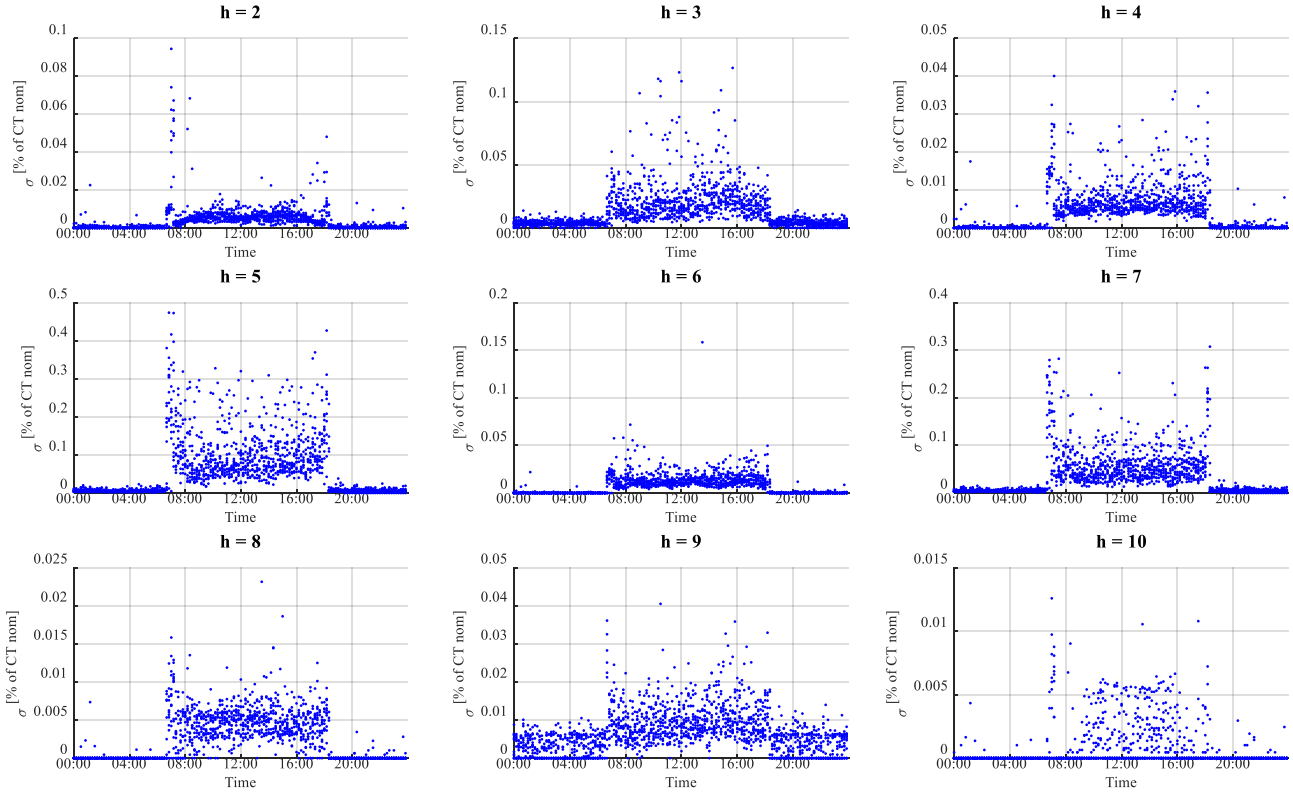

Figure 4-16: Standard deviation of 3-second aggregated harmonic currents per 10-minute period plotted against time of day (h = 2 – 10).

Figure 4-17 shows the 95th percentile standard deviations vs the 95th percentile 10-minute currents. The vertical axis is plotted with a logarithmic scale. All harmonics, excepting the 3rd, 5th and 7th, exhibit a P95 standard deviation less than 0.025% of CT nominal current (indicated by red dashed line). It is likely that the fluctuations for these harmonics are strongly influenced by measurement uncertainty.

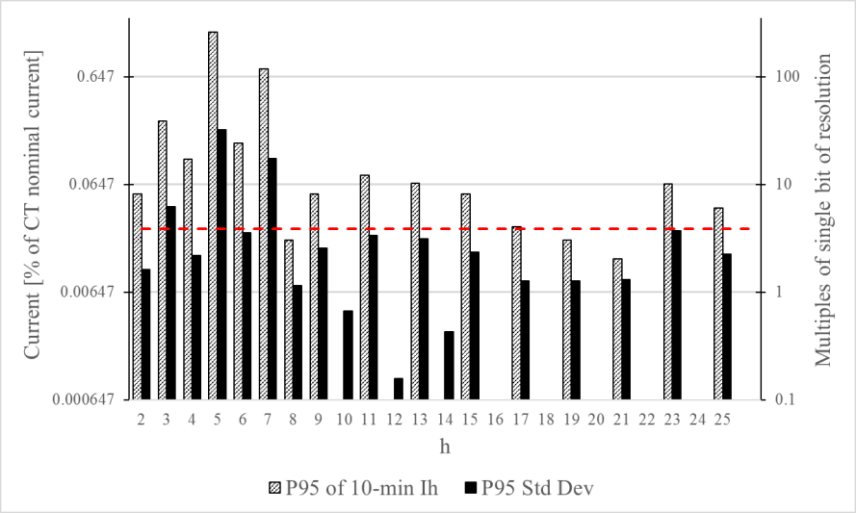

Figure 4-17: 95th percentile of 3-second harmonic current standard deviation per 10-minute period vs 95th percentile of 10-minute harmonic currents.

The P95 standard deviation for the third harmonic current is 16% of the P95 10-minute average. Considering the current plot of Figure 4-15, this represents a trend where the 10-minute currents reasonably approximate the 3-second measurement signal. For all harmonics up to the 7th, the P95 standard deviation is less than 20% of the P95 10-minute current. For harmonic orders up to the 15th, the mean standard deviation of harmonic currents does not exceed 25 – 50% of the P95 value of the standard deviations.

Based on this analysis, it appears that fluctuation of all harmonic currents when the plant is not operating and fluctuation of non-dominant harmonic currents during operation are within the range of measurement uncertainty. The dominant 3rd, 5th and 7th harmonic orders exhibit small to moderate fluctuations within each 10-minute period which is probably due to fluctuating harmonic current emissions from the solar inverters.

4.2.5 Extraction of harmonic components from event triggered waveform recordings

70 event-triggered waveform recordings were captured over a 15-day period commencing one day prior to the 12-day recording period used for the 10-minute and 3-second data. Signals were acquired with a sampling rate of 500 kHz and digitally downsampled to 50 kHz. Events were triggered by a significant rms voltage change of 3% where the rms voltage was monitored by means of a 1/6 cycle sliding window principle. The temporal distribution of the captured events is illustrated in the timeline in Figure 4-18.

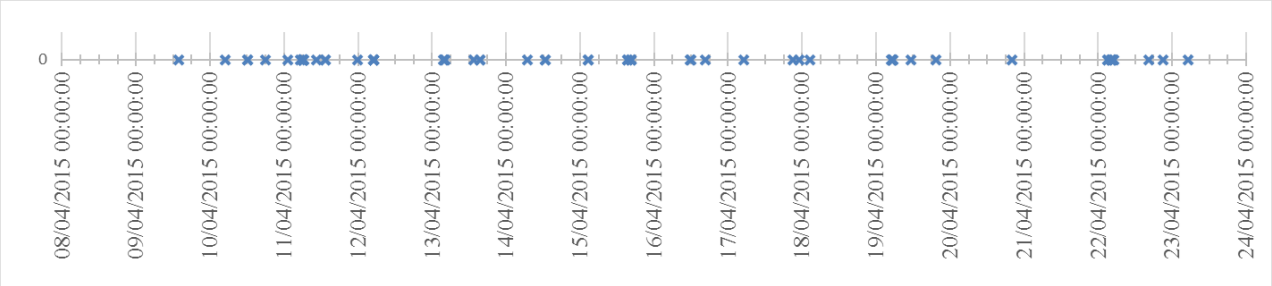

Figure 4-18: Temporal distribution of event-triggered event recordings.

Small rapid voltage changes may be caused by switching operations including motor starting, capacitor bank switching, load switching and transformer energisation. They may also result from transformer tap changer operations and sudden changes in load or generation from variable sources such as wind or solar generation [157]. Therefore, the operation of the plant itself may cause rapid voltage changes. Another likely cause of rapid voltage changes is intermittent traction load connected at the PCC. Furthermore, larger voltage changes may be caused by voltage dips or surges as a result of faults in the local distribution or transmission network.

For each event, voltage and current waveforms were captured for a period commencing 5 cycles prior to the start of the event and ending 5 cycles after the end of the event with a maximum recording duration of 2 seconds. The study of harmonic emissions is by definition concerned with steady-state period behaviour of the voltage and current waveforms. Therefore, the transients inherent in the waveform data available for this research due of the event-triggered recorder setup needed to be removed prior to commencement of harmonic analysis.

Time invariant waveform segments were extracted according to the following methodology:

1. A 15-cycle segment of all six waveforms (3-phase voltages and currents) is extracted using a rectangular window commencing at the first voltage zero crossing of the red-phase voltage waveform. Use of zero-crossing detection instead of a fixed-length window accommodates variations in system frequency to allow for better FFT results with lower risk of aliasing error. The voltage THD of the waveforms is considered to be sufficiently small that deviation of the zero-crossing position from the fundamental frequency zero crossing will be negligible.
2. The centre 5-cycle segment of the 15-cycle segment is then extracted by zero crossing detection.
3. The 5-cycle segment is cross correlated with the 15-cycle segment for each of the 6 waveforms and normalised by dividing by the peak value of the correlation result [46].
4. Each cross correlation results in a 25 cycles long signal. The peak values of centre 15 cycles, where full overlap of the 5-cycle and 15-cycle waveforms occurs are extracted.
5. The 5-cycle segment is retained if the average value of the voltage peaks exceeds 0.99 and the average value of the current peaks exceeds 0.95.
6. The method is repeated for the next 15-cycle segment commencing 5 cycles after the first segment.

7. Contiguous retained 5-cycle blocks are used for harmonic analysis. 72 waveforms were extracted according to this methodology with durations varying between 20 cycles and 100 cycles. These events are considered to be time invariant and suitable for FFT analysis to extract their harmonic components.

Next the two-sided complex frequency spectrum for each of the 72 time-invariant waveform segments was calculated using the Matlab fft() function. The single-sided complex rms frequency spectrum is then calculated according to Equation (4.1) [138].

$$F(n) = \frac{2}{\sqrt{2}N} \text{fft}(\text{VIData}) \tag{4.1}$$

where: VIData is a 6 column matrix whose the columns contain the three phase voltages and three phase currents of the time-invariant waveform segment,

N is the number of samples in the waveform segment.

The first N/2+1 samples are considered, corresponding to the frequencies 0 to fs/2 in steps of fs/N, where the sampling frequency, fs, is 50000. The frequency spectrum values corresponding to integer harmonics of the waveform fundamental frequency are extracted to yield the harmonic spectrum of the waveform. Sequence components of the harmonic spectrum are calculated from the phase components by means of the inverse Fortesque transform. The average active, reactive and apparent powers for the segment are calculated from the fundamental frequency voltages and currents. The fundamental frequency active and reactive power of the 72 time-invariant waveform segments is shown in Figure 4-19.

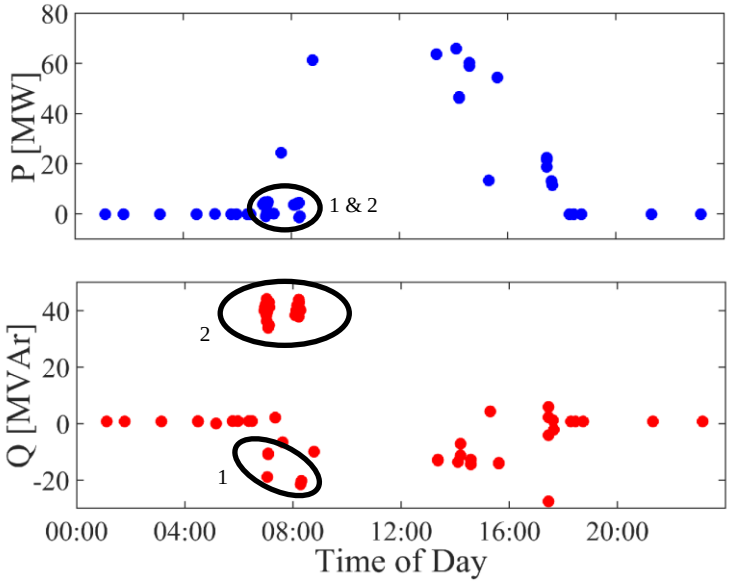

Figure 4-19: Fundamental frequency active and reactive power of processed time-invariant events.

Of the 72 time-invariant events, 27 occur at times when the plant active output power is less than 0 MW meaning that the plant is not operating – i.e. at night. However, 4 of these events are associated with high absorption of reactive power, in excess of 10 MVAr. These events are in the regions indicated as "1" in Figure 4-19. This reactive power absorption can only be as a result of the inverter action indicating that the plant is

operating although it is not exporting active power. It is also noted that these events occur between 06h30 and 08h30 and are therefore associated with the start-up of the plant. Therefore, 23 of the 27 events are categorised as occurring at night or when the plant is not operating and the remaining 4 as start-up events.

Inverters have been observed to produce high current THD at low levels of irradiance [79] [81] [82] and it therefore worthwhile considering start-up events as a separate category from normal operation events. The plant also has motor drives for the single-axis tracking mechanisms of the PV mounting structures. During the initial start-up of the plant, all of these drives operate simultaneously to tilt the PV array towards the rising sun. These drive loads may also influence the total harmonic emissions at the POC during the startup period differently than they do at other times.

Of the remaining 49 events, 25 are associated with high magnitudes of reactive power export (|Q| > 10 MVAr) and low values of active power output (P < 5 MW). All of these events occur between 06h30 and 08h30 and they are also categorised as start-up events. These events are in the regions indicated as “2” in Figure 4-19. There are, therefore, a total of 29 start-up events. Start-up data points with large reactive power magnitudes can be seen on certain days in the 3-second aggregated reactive power measurements as shown in Figure 4-20. Several short positive and negative reactive power spikes with a duration of a single 3-second period occur over a period of several minutes during the plant start-up phase. The duration of these spikes is probably less than 3 seconds with a reduction in the peak height due to averaging over 3 second periods. The start-up phenomena are barely noticeable in the 10-minute reactive power plot shown in Figure 4-3.

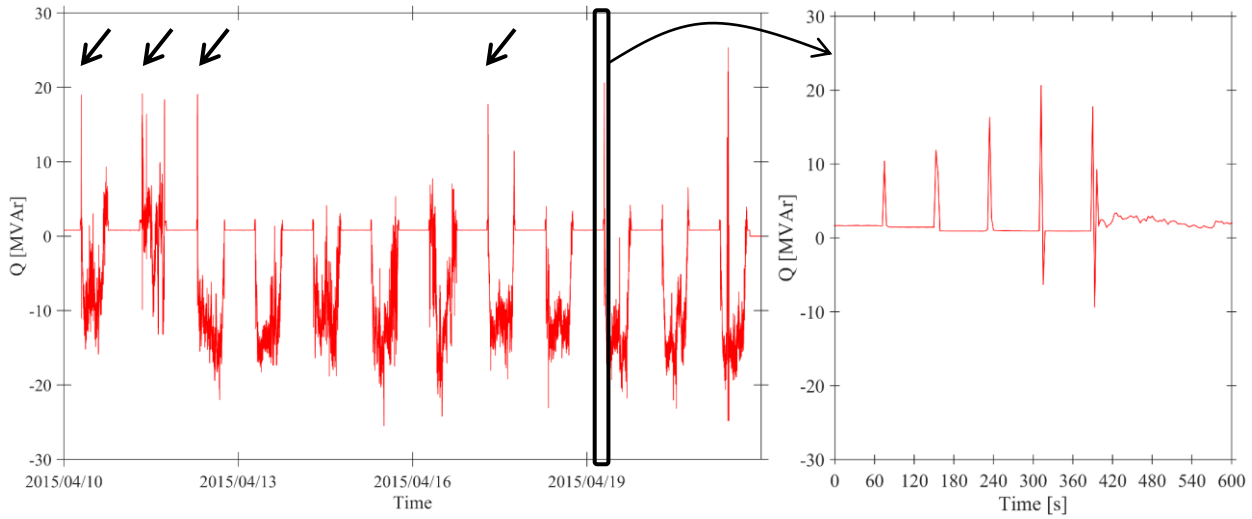

(a) ***(b)***

Figure 4-20: (a) 3-second aggregated reactive power measurements over full measurement period. Arrows indicate high reactive power output associated with plant start-up. (b) 3-second aggregated reactive power measurements for a 10-minute period during the plant start-up on 19 April 2015.

The remaining 20 events are categorised as normal operation events and comprise all events with active power output greater than 0 MW but exclude events categorised as start-up events according to the criteria listed above.

4.2.6 Conclusions from quality assessment of harmonic measurement data

Analysis of 10-minute data shows that measurement accuracy may significantly impact the reliability of harmonic voltage and current measurements for even harmonics above the 6th order and odd harmonics above the 15th order due to the small magnitude of the measured signals. Quantisation effects introduced by the meter's A/D converter are the dominant source of inaccuracy in voltage measurements while transducer error is likely to impact the accuracy of current measurements. The focus of this investigation will therefore be on the lower order harmonics but the data is considered suitable for identification of trends based on statistical analysis for harmonics up to the 25th order. The suitability of measurement data above the 15th harmonic order for compliance assessment would be questionable in cases where measured signal magnitudes are not found to be zero, or at least significantly below the prescribed limits.

Comparative analysis of the 3-second and 10-minute harmonic measurements reveals that the 10-minute aggregated measurements provide a reasonable representation of the short-term and long-term behaviour of the plant, with the possible exception of plant start-up and shutdown periods when some short-term fluctuations of the harmonic quantities are observed. The investigation will focus on analysis of the 10-minute aggregated values in alignment with the NRS and IEC methodologies, excepting where specific investigation warrants the additional analysis of the 3-second data.

A small sample of waveform data is available for normal operation, plant start-up and non-operation periods. This data is useful in understanding plant harmonic behaviours and for testing emissions assessment methods by means of calculated harmonic phasors. The data lacks statistical robustness due to the small sample size and due to the event-triggered nature of the waveform capture but it is considered valuable to provide an alternative insight into the plant's instantaneous harmonic behaviour.

4.3 Evaluation of plant harmonic behaviour

In this section, general trends in harmonic behaviour are noted for the 10-minute aggregated data, the 3-second aggregated data and the event data. First the relationship between harmonic distortion and active and reactive power is considered. Thereafter, the harmonic emissions vs time of day are considered. Scatter plots of the 10-minute voltage and current emissions vs active and reactive power for all harmonic orders up to h = 25 are included in Appendix A. Scatter plots of the 10-minute and 3-second voltage and current emissions vs time of day for all harmonic orders up to h = 25 are included in Appendix B.

4.3.1 Variation of harmonic emissions with plant active power output

The three-phase 10-minute aggregated harmonic voltages over the 12-day recording period are plotted against fundamental frequency plant active power output in Figure 4-21 for harmonic orders 2 to 10. The trends between 10-minute and 3-second values are similar and only the 10-minute values are considered in the following discussion.

To provide a simple overview of the trends in harmonic voltage emissions for all harmonics up to h = 25 in a single figure, the 10-minute voltage data were sorted into 5 bins, a bin for periods when P < 0 MW (i.e. plant not operating) and four equal bins of 25% of nominal plant power covering the active power output range of 0 to 75 MW. The mean of the harmonic voltage magnitudes of all three phases was calculated per harmonic per bin. The results for harmonics h = 2 – 25 and the voltage THD as a percentage of nominal voltage are shown in the bar chart of Figure 4-22. The THD is calculated considering voltages up to the 50th harmonic.

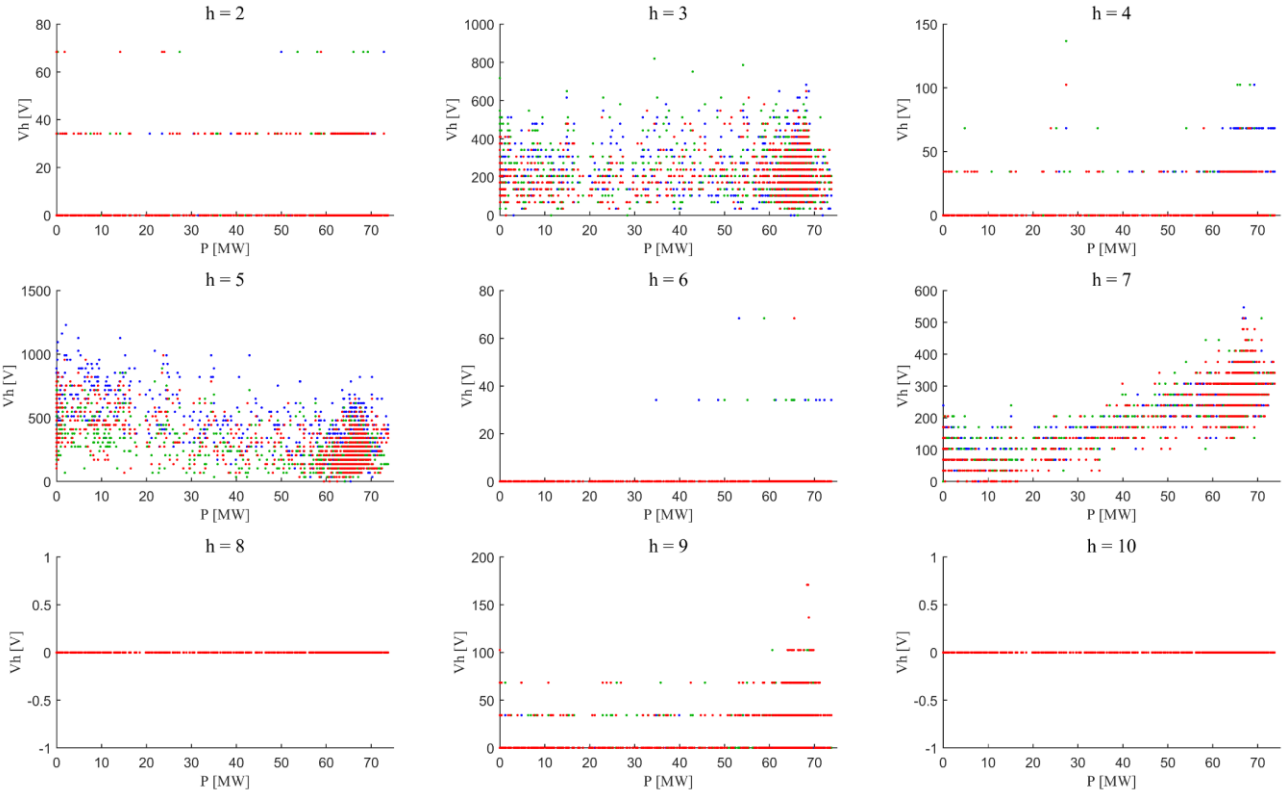

Figure 4-21: 10-minute harmonic voltage emissions vs plant active power generation (h = 2 – 10) Red, white and blue phases represented by red, green and blue dots respectively.

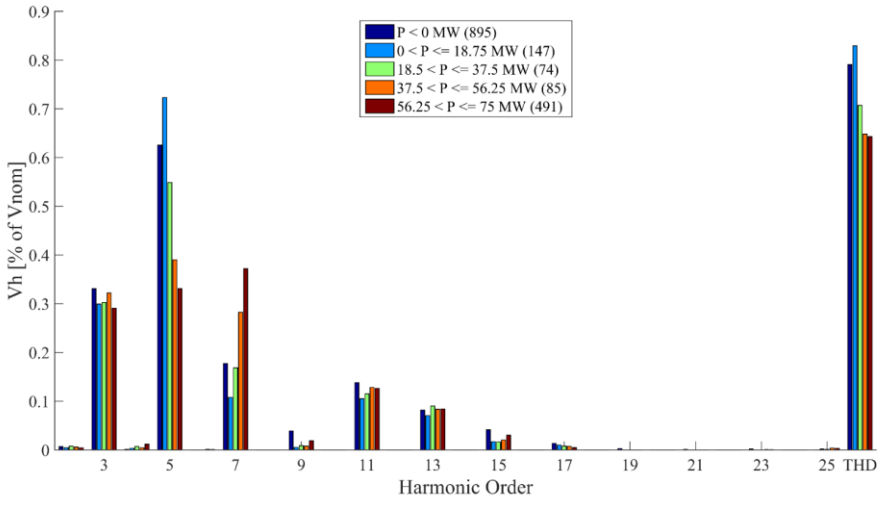

Figure 4-22: 10-minute harmonic voltage emissions vs plant active power generation trends based on active power bins of 25% of nominal power. Numbers in brackets in the legend indicate the number of 10-minute values within each power bin.

From Figure 4-22, the voltage harmonic distortion increases with increasing active power generation for harmonic orders 7, 9, 11 and 15. The voltage distortion decreases with increasing active power for harmonic orders 5 and 17. These trends are also clearly visible for the dominant 5th and 7th harmonics in the scatter plots in Figure 4-21. The THD also decreases with increasing active power as it is dominated by the 5th harmonic voltage contribution.

The harmonic current emissions are similarly plotted against active power in Figure 4-23 and Figure 4-24. The nominal current to calculate percentage values of harmonic current emissions in Figure 4-24 is 328 A, which considers plant operation at 75 MW, unit power factor and nominal POC voltage of 132 kV. Current harmonic distortion increases or remains approximately constant with increasing harmonic current for all harmonic orders. Of the dominant harmonic orders, it is evident from both Figure 4-23 and Figure 4-24 that the 5th harmonic current increases significantly and approximately linearly with increasing plant active power while the 7th harmonic current remains almost constant across the active power range.

Another observation from the scatter plots in Figure 4-23 is that the harmonic currents of the three phases appears to be significantly unbalanced for the even harmonics 2, 4 and 6. Noting that the plotting order of the phases is blue, white, red from back to front, the blue phase current appears largest for all three of these harmonics whilst the white phase appears to be the smallest for at least the 4th and 6th orders. The harmonic current magnitudes of these even orders are small – of the order of 0.2 to 0.5 A – and the author believes the most likely source of the unbalance is current transformer mismatch which introduces systematic errors between the phases for very small harmonic currents.

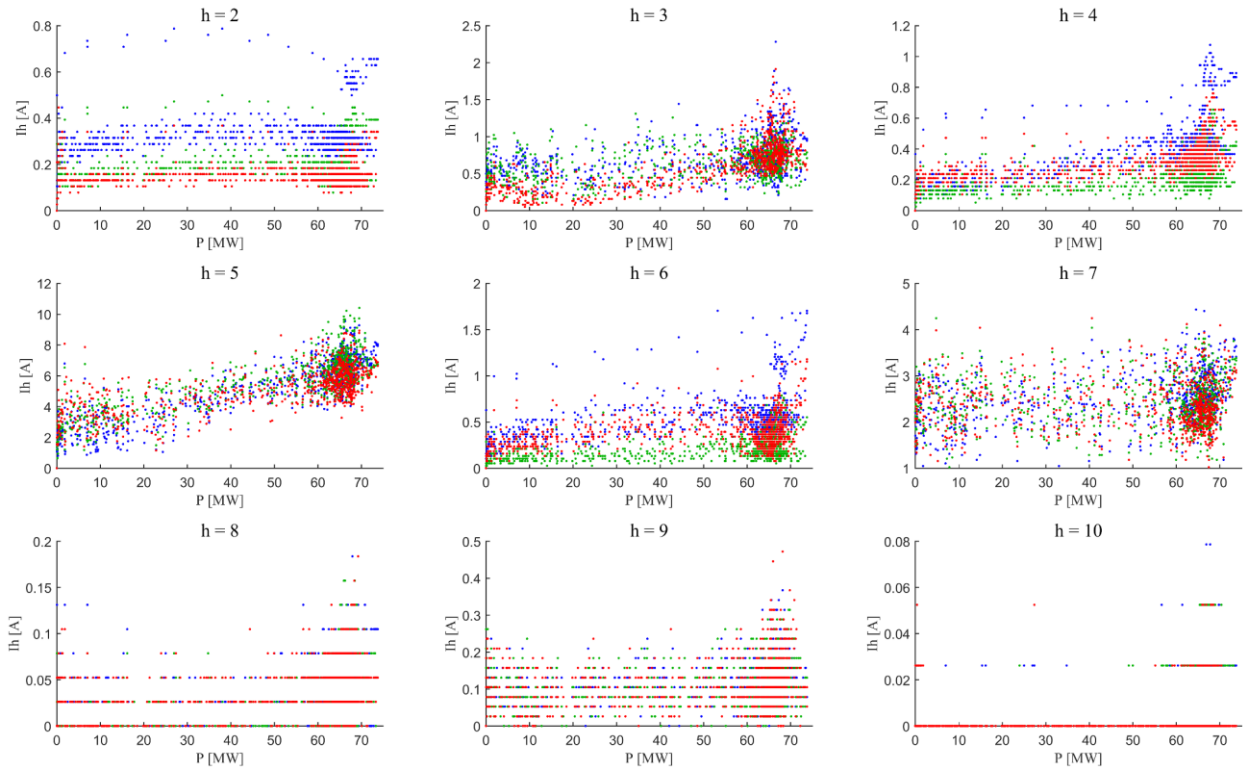

Figure 4-23: 10-minute harmonic current emissions vs plant active power generation (h = 2 – 10) Red, white and blue phases represented by red, green and blue dots respectively.

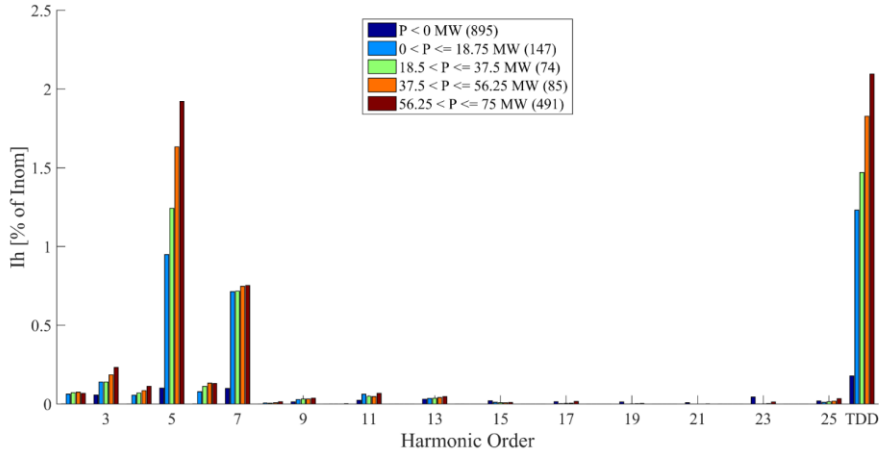

Figure 4-24: 10-minute harmonic current emissions vs plant active power generation trends based on active power bins of 25% of nominal power. Numbers in brackets in the legend indicate the number of 10-minute values within each power bin.

4.3.2 Variation of harmonic emissions with plant reactive power output

A similar analysis was performed to evaluate the relationship between harmonic quantities and plant reactive power output. For the bar plots, 10-minute measurements were divided into 5 bins of 5 MVAr each, covering the range from -15 MVAr to 10 MVAr. Considering the scatter plots of Vh vs Q in Figure 4-25, it is difficult to discern a clear relationship. Grouping the data into bins and averaging (Figure 4-26) shows that the 5th and 17th harmonic voltages and the voltage THD increase with increasing reactive power whilst the 7th harmonic voltage decreases. This is opposite to the relationship of these harmonics with active power.

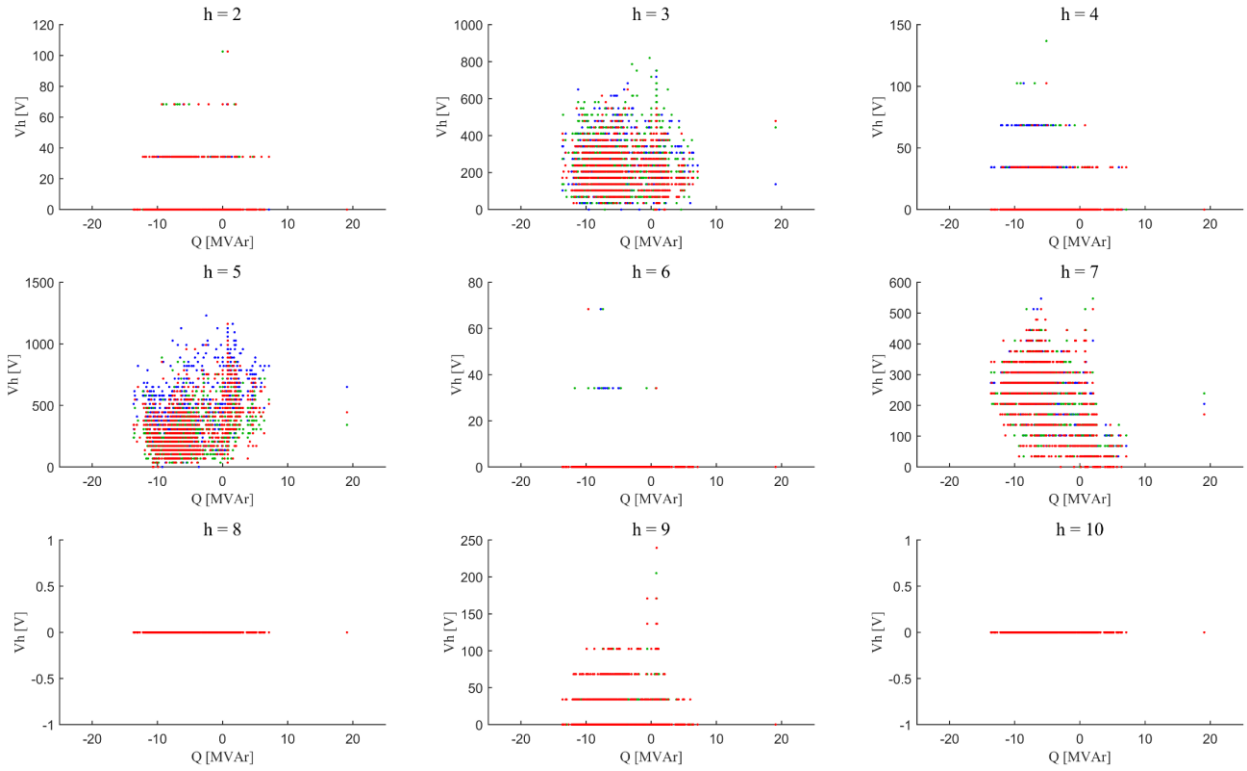

Figure 4-25: 10-minute harmonic voltage emissions vs plant reactive power output (h = 2 – 10) Red, white and blue phases represented by red, green and blue dots respectively.

The plant was operating in voltage control mode during the full recording period, resulting in a linear correlation between active and reactive power such that reactive power decreases as active power increases, as shown in Figure 4-4. Without independent variation of active and reactive power, the relative influence of each on the harmonic distortion at the POC cannot be verified.

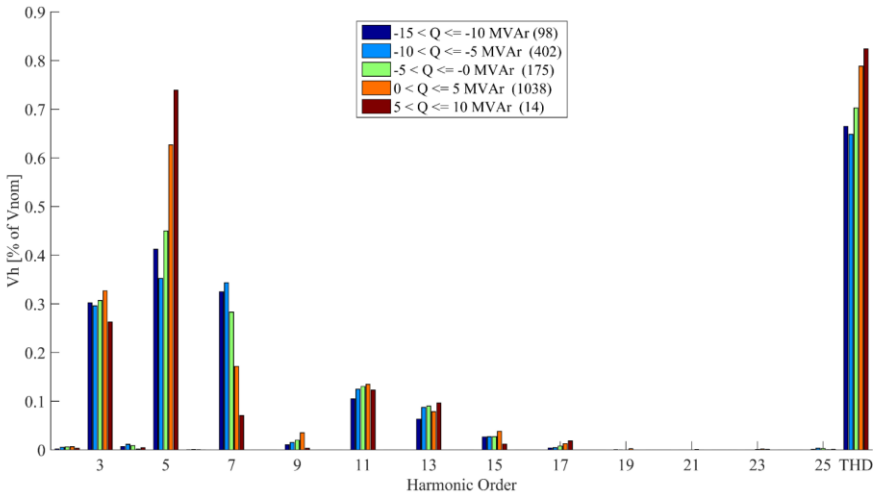

Figure 4-26: 10-minute harmonic voltage emissions vs plant reactive power output trends based on 5 MVAr reactive power bins. Numbers in brackets in the legend indicate the number of 10-minute values within each reactive power bin.

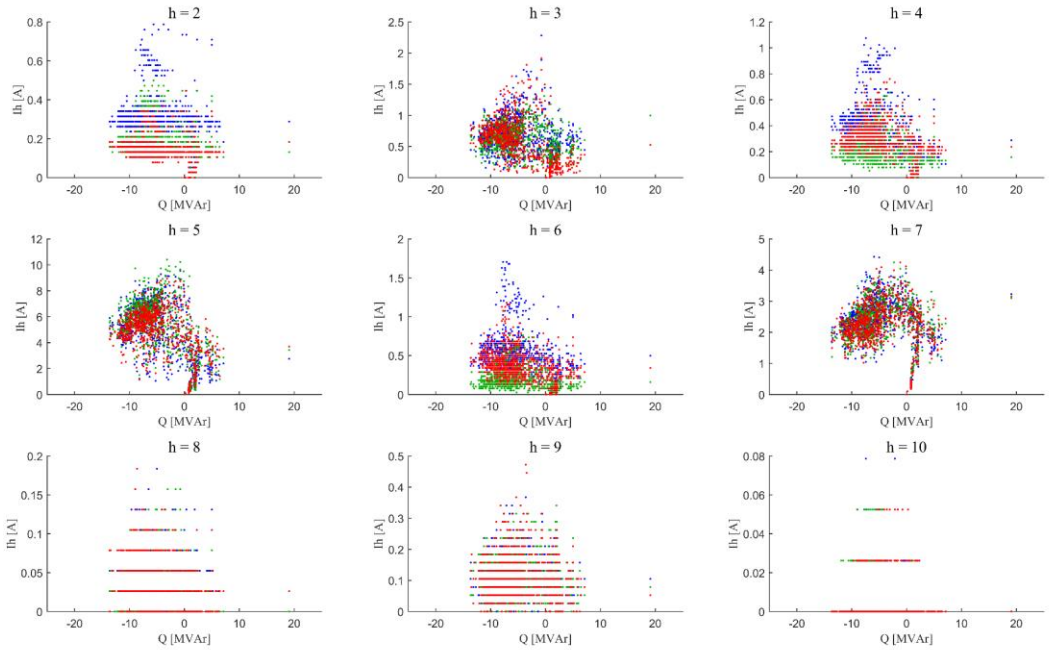

Figure 4-27: 10-minute harmonic current emissions vs plant reactive power generation (h = 2 – 10) Red, white and blue phases represented by red, green and blue dots respectively.

The relationship between harmonic current emissions and plant reactive power output is illustrated in Figure 4-27 and Figure 4-28. In Figure 4-28, the 0 to 5 MVAr bin contains most of the 10-minute periods when the plant is not operating and is therefore expected to exhibit low mean harmonic currents across most harmonic orders. There are only 14 data points in the 5 to 10 MVAr range and its mean values are not statistically robust.

Considering only the remaining three bins and the scatter plots in Figure 4-27, no strong correlations between harmonic currents and reactive power output are evident.

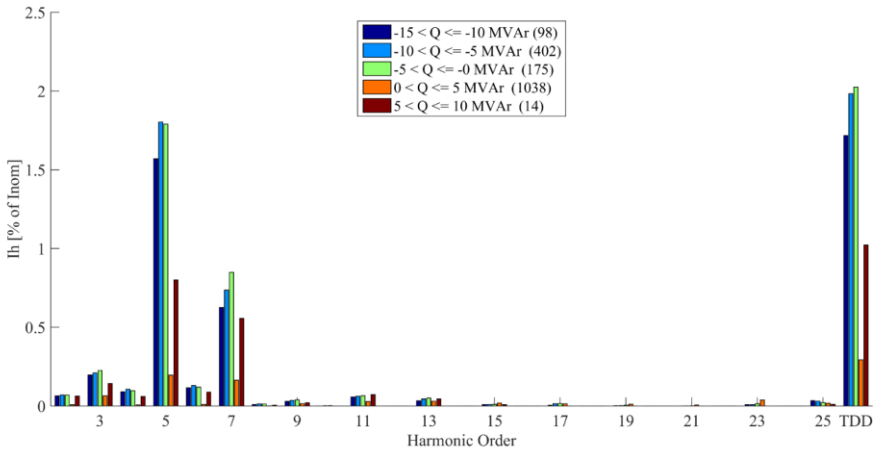

Figure 4-28: 10-minute harmonic current emissions vs plant reactive power output trends based on 5 MVAr reactive power bins. Numbers in brackets in the legend indicate the number of 10-minute values within each reactive power bin.

4.3.3 Variation of harmonic emissions with time of day

3-second aggregated values of harmonic voltage and current are useful to study the relationship between harmonic emissions and time of day since they provide superior temporal resolution compared to 10-minute values. However, the additional averaging in the 10-minute data reduces the number of data points and the spread of the data, thus emphasising differences between periods of high and low emissions. All 10-minute and 3-second values plotted as points against time of day are included in Appendix B.

Examination of the scatter plots show a reduction of 5^{th} harmonic voltage and corresponding increase in 5^{th} harmonic current between 08h00 and 17h00 when the plant is operating. The 7^{th} harmonic voltage and current both increase during the plant's operating hours. This aligns with the active and reactive power relationships described above. It appears that the plant is acting as a 5^{th} harmonic filter during operation by injecting 5^{th} harmonic current with a phase angle that causes a reduction in the 5^{th} harmonic voltage at the point of connection. At the 7^{th} harmonic order, the plant causes an increase in both voltage and current and is clearly a source of 7^{th} harmonic distortion.

All current harmonic orders up to the 18^{th}, with the exception of the 15^{th}, show a clear increase in harmonic current over the period that the plant operates (approximately 07h00 and 18h00). It is further evident, especially from the 3-second data, that peak levels of harmonic current distortion occur during the start-up and shutdown periods of the plant around 07h30 and 18h00 for several harmonic orders including 2, 10, 11, 13 and 15.

For harmonic orders between 19 and 23, the harmonic current is higher at night than during the day. It is difficult to evaluate the change in harmonic voltage between daytime and night-time periods in this harmonic range due to the low voltage magnitudes and significant quantisation error in the measurements. However, the voltage distortion for these harmonics also appears to be higher at the night, so it is likely that lower damping

due to reduced load results in increased background voltage harmonic distortion at night and the increased harmonic current is a consequence of the increased background harmonic voltage. The inverter manufacturer's datasheet shows very low harmonic current emissions in this range, suggesting that the network is the dominant source of the measured voltage and current distortion.

5 Comparative analysis of harmonic emission assessment calculation methods

Various methods have been proposed to assess the harmonic emission contribution of an installation, including those discussed in section 2.10.2. In this section, the methods listed in Table 5-1 will be applied to the PV plant using the event and 10-minute recording data captured at the site. Due to the nature of the methods, certain methods can only be applied to either the event data, or the 10-minute data. The data to which each method is applied are also listed in Table 5-1.

Studies were carried out comparing the 3-second and 10-minute data and, due to the averaging inherent in the methods, the results were found to be substantially similar. Therefore, the analysis of 3-second data is excluded from the presented results. A detailed description of the methods and results is presented considering the mean emissions values. This is followed by the presentation of results of assessment using the 75th and 90th percentile values.

Table 5-1: Methods for assessment of the harmonic contribution of the PV plant

No.	Method Description	Event	10-min
1	Reverse application of the general summation law	Yes	Yes
2	Harmonic voltage phasor method	Yes	No
3	IEC 61000-3-6 long-duration simultaneous measurement of harmonic voltages and currents	No	Yes
4	Harmonic vector method	Yes	No
5	Network simulation based on manufacturer's quoted harmonic current emissions	N/A	N/A

5.1.1 Background harmonic emission calculation methodology

To assess the contribution of the plant according to methods 1 and 2, a level to be used as the background harmonic voltage distortion must first be established. It is recommended that background harmonic distortion be measured over a period when the PV plant is disconnected from the network due to the impact of the connected PV plant distribution network on the system harmonic impedance, even when the plant is not operating [43]. Background harmonic voltage distortion is assessed as the mean of 10-minute voltage harmonic data from a 10-hour period over the night of 21/04/2015 to 22/04/2015 when the entire plant, including the main park transformer, was disconnected from the network by opening of the POC circuit breaker. Unfortunately, these data are not strictly representative since measurements were captured at night whereas the plant can only operate during the day. Furthermore, due to the limited duration of the measurement period on a single night, the statistical robustness of the measured data as a representation of typical night-time, much less daytime, background distortion is in doubt.

In certain assessments, it may be difficult to obtain any measurements with the plant disconnected, even at night, due to the operational constraints of the plant. Therefore, for comparative purposes, background harmonic voltages are also assessed as the mean of periods when the plant active power was less than 0 MW. The number of such 10-minute values over the full 12-day period is much higher than those captured during the 10-hour period of plant disconnection. These data are also almost exclusively captured at night-time when the plant is not operating.

In addition, background harmonic phasors can be calculated as the mean of the 23 night-time harmonic events. The magnitude of the background harmonic voltage is the mean of the individual harmonic voltage phasor magnitudes, whilst the prevailing angle, $\varphi_{\text{agg},h}$, is calculated as the prevailing angle according to the phasor sum method [158], according to (5.1) where $V_{ev,h,i}$ is the harmonic voltage phasor of order h of the ith event.

$$\varphi_{\text{agg},h} = \arg\left(\sum_{i=1}^{27} \overline{V}_{ev,h,i}\right) \tag{5.1}$$

Phase angle information is only meaningful in cases where there is a limited variation in phase angles across the measured events. The prevailing ratio, $PR_{\text{agg},h}$, quantifies the level of variation and is defined as:

$$PR_{\text{agg},h} = \frac{\left|\sum_{i=1}^{27} \overline{V}_{ev,h,i}\right|}{\sum_{i=1}^{27} \left|\overline{V}_{ev,h,i}\right|} \tag{5.2}$$

Meyer et al. define four levels of prevalence according the prevailing ratio [158]:

1. HP: High prevalence ($PR_{\text{agg},h} \geq 0.95$)

   The individual harmonic phasors have high similarity and the aggregated harmonic phase angle has very low uncertainty.

2. MP: Medium prevalence ($0.89 \leq PR_{\text{agg},h} < 0.95$)

   The individual harmonic phasors have good similarity and the aggregated harmonic phase angle has low uncertainty.

3. LP: Low prevalence ($0.8 \leq PR_{\text{agg},h} < 0.89$)

   The individual harmonic phasors are more dispersed, but a general tendency can still be identified. The aggregated harmonic phase angle has an acceptable uncertainty.

4. NP: No prevalence ($PR_{\text{agg},h} < 0.8$)

   The individual harmonic phasors are widely dispersed and no prevalence can be identified. An aggregated harmonic phase angle does not have any meaning and should not be reported.

In the averaging of background harmonic voltage phasors, and in the calculation of all other harmonic phasor quantities, aggregated phase angles are only therefore considered valid in cases where $PR_{agg,h} \geq 0.8$.

In the case where the background voltage measurements are obtained with the plant connected to the network, an improved estimate of the actual background harmonic voltage can be calculated using the impedances of the network and the PV plant. Considering the equivalent circuit in Figure 5-1, in the case where the plant is not operating and the inverter terminals are open circuit, $I_{PV} = 0$ and the background harmonic voltage, V_{bg}, is calculated from the POC voltage, V_{POC}, the network harmonic impedance, Z_{NW}, and the PV plant harmonic impedance, Z_{PV}, according to Equation (5.3) where Z_{pv} and Z_{nw} are complex impedances. For 10-minute aggregated data, the magnitude of V_{bg} can be calculated according to Equation (5.4).

$$\bar{V}_{bg} = \bar{V}_{POC} \frac{\bar{Z}_{pv} + \bar{Z}_{nw}}{\bar{Z}_{pv}} \tag{5.3}$$

$$\left|\bar{V}_{bg}\right| = \left|\bar{V}_{POC}\right| \times \left|\frac{\bar{Z}_{pv} + \bar{Z}_{nw}}{\bar{Z}_{pv}}\right| \tag{5.4}$$

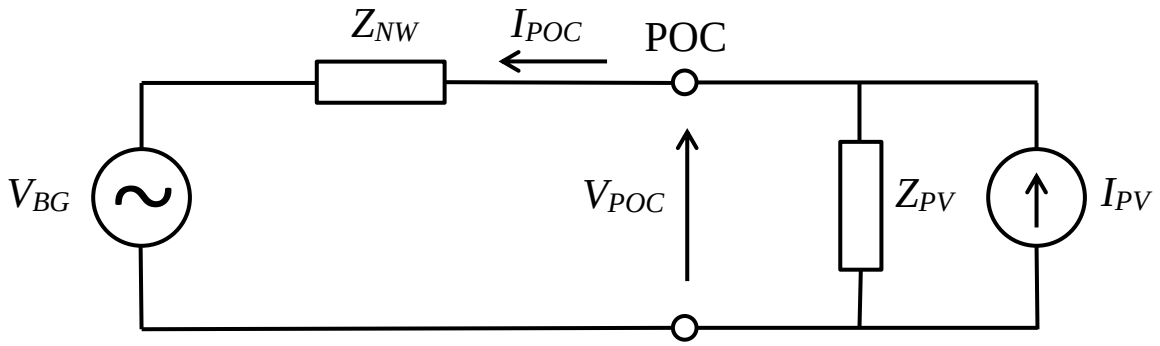

Figure 5-1: Equivalent circuit for evaluation of individual harmonic emissions [58]

The CIGRE-CIRED joint working group on harmonics also proposes a method which applies linear regression of the harmonic voltage versus installation apparent power demand to estimate the harmonic distortion when the plant apparent power is zero [58]. The method appears to be aimed primarily at load customers but is included for comparative purposes.

For the above methods, background harmonic voltages are calculated separately for all three phases. For the event measurement data, sequence components are calculated for each event with P < 0 MW and the aggregated background sequence components are then calculated according to the same methodology as that applied for the phase components. In the calculation of background sequence harmonic voltage according to equation (5.3), the sequence impedances must be used. Only positive sequence impedance data was available for the utility network impedance and the positive sequence network and PV plant impedances are therefore used in the calculation of positive and negative sequence background harmonic voltages according to (5.3).

It is reasonable to assume that the positive and negative sequence impedances of the network are similar but the zero sequence impedance may differ substantially from the positive sequence impedance. Due to the lack of zero sequence impedance data and because there are delta winding transformers between the POC and the inverters which act to substantially filter zero sequence harmonics generated by the plant, zero sequence harmonics are excluded from the analysis.

In summary, the following methods of calculation are considered in the calculation of the background harmonic voltage.

Table 5-2: Methods for assessment of the background harmonic voltage

No.	Method Description	*Short Description	Event (Phase & Sequence)	10-min
1	Mean of measured values during plant shutdown (10-hour period)	Plant off	No	Yes
2	Mean of measured values when plant active power output is less than zero	P < 0 MW	Yes	Yes
3	Mean of measured values when plant active power output is less than zero multiplied by $(Z_{pv} + Z_{nw}) / Z_{pv}$	Vbg Calc	Yes	Yes
4	Linear regression of harmonic voltage vs apparent power output	LR	Yes	Yes

* Used for legend in graphs in following sections

5.2 Background harmonic emission calculation results

5.2.1 Linear regression of harmonic voltage versus installation apparent power demand

Linear regression was considered based on the daytime (i.e. P > 0) 10-minute aggregated measurements and the daytime event measurements to estimate the background harmonic voltage. Separate linear regressions were calculated for each phase. The coefficient of determination, R^2, was calculated for each linear regression according to (5.5) as in indication of the goodness of fit. Values of R^2 can vary between 0 and 1 with higher values indicating a better fit of the line to the data points.

$$R^2 = 1 - \frac{\sum_{i=1}^{n} \left(V_i - \hat{V}_i\right)^2}{\sum_{i=1}^{n} \left(V_i - \bar{V}\right)^2} \tag{5.5}$$

where:

R^2 is the coefficient of determination

V_i is the ith measurement harmonic voltage

$\widehat{V}_i$ is the *i*th calculated harmonic voltage based on the apparent power output and the linear approximation

$\bar{V}$ is the average harmonic voltage

The R^2 values for linear regression of 10-minute and event data are shown in Table 5-3 for harmonic orders 2 to 15. For both 10-minute data and event data, only the 5th and 7th harmonic exhibit an R^2 value greater than 0.1 for all three phases. The poor fit for other harmonic orders is largely due to quantisation errors or weak correlation between the measured harmonic voltage and the plant apparent power. Results shown as "N/A" indicate that all measurement datum points were equal to zero.

Table 5-3: R² values for Vh vs S linear regression

	10-minute daytime voltages			Event daytime voltages		
h	**R**	**W**	**B**	**R**	**W**	**B**
2	0.001	0.007	0.000	0.046	0.016	0.041
3	0.019	0.005	0.01	0.001	0.196	0.141
4	0.005	0.000	0.115	0.04	0.047	0.081
5	0.331	0.284	0.416	0.253	0.622	0.45
6	0.001	0.003	0.004	0.106	0.059	0.085
7	0.727	0.647	0.684	0.515	0.54	0.665
8	N/A	N/A	N/A	0.107	0.081	0.022
9	0.102	0.019	0.008	0.246	0.083	0.045
10	N/A	N/A	N/A	0.007	0.014	0.005
11	0.063	0.037	0.002	0.013	0.19	0.275
12	N/A	N/A	N/A	0.091	0.053	0.044
13	0.024	0.000	0.002	0.007	0.01	0.179
14	N/A	N/A	N/A	0.006	0.011	0.06
15	0.026	0.038	0.001	0.322	0.112	0.102

The linear regressions of the 7th harmonic order 10-minute voltages – which represents the best fitting data – are shown in Figure 5-2 (a). Red, white and blue phases are indicated by red, green and blue traces respectively and the black line indicates the linear regression of all three phases considered collectively. The lines reasonably approximate the data but small changes in fit may have a significant impact on the calculated background harmonic data, which is the y-intercept point of the line. The variation of intercept between phases is significant.

Figure 5-2 (b) shows the linear regression of the 3rd harmonic 10-minute voltages. There is no strong correlation between the harmonic voltage and the apparent power; harmonic voltage remains relatively constant across the range of apparent power outputs. Therefore, although the intercept appears to reasonably approximate the background voltage, the R^2 values are low. Again, small variations in the slope of the lines between phases significantly impacts the estimated background voltage.

Figure 5-2 (c) shows the effect of quantisation error on the linear regression of the 9th harmonic order. Similar quantisation effects are visible for all even and higher-order odd harmonics and the linear regression results in such cases are considered to be unreliable.

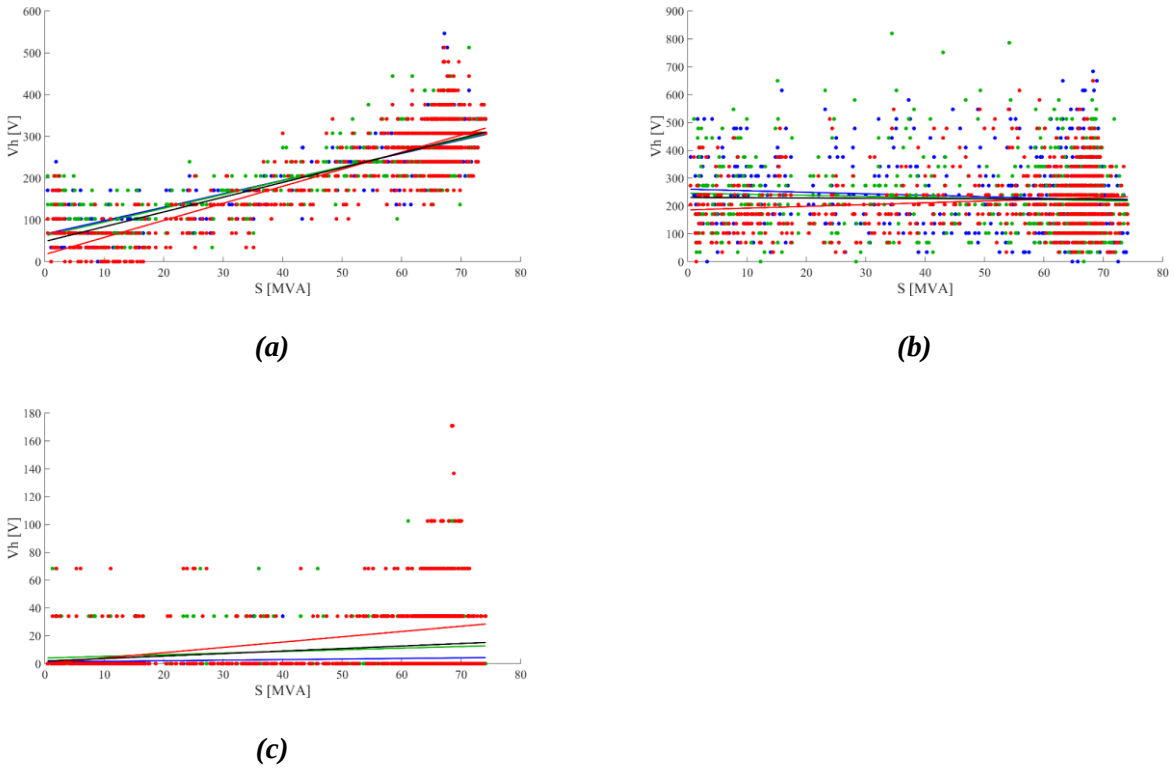

Figure 5-2: Linear regression of 10-minute voltages vs apparent power for (a) 7th, (b) 3rd and (c) 9th harmonic orders

Based on this analysis, the estimation of background voltage emissions by means of linear regression of harmonic voltage versus output apparent power is considered to be unreliable and calculation of background harmonic voltages using this method is excluded from the assessment of emissions.

5.2.2 Background harmonic voltage assessment

5.2.2.1 Phase components

The results of background harmonic voltage assessment considering methods 1 to 3 of Table 5-2 are shown in Figure 5-3 for the red phase. The white and blue phases exhibit similar trends and the plots for all phases are included in Appendix C. From all methods of assessment, the 3rd 5th, 7th and 11th harmonic voltages appear to be dominant in the network. Considering the 10-minute values, the mean of the measured harmonic voltage at the POC is generally lower for periods when the plant is disconnected (red bars) than it is for periods when the plant is connected but not operating (green bars). This may in part be due to the short duration of the 10-hour recording period when the plant was not connected resulting in mean harmonic voltages which are not statistically representative compared to the 12-day recording period available for periods when plant active power was less than 0 MW.

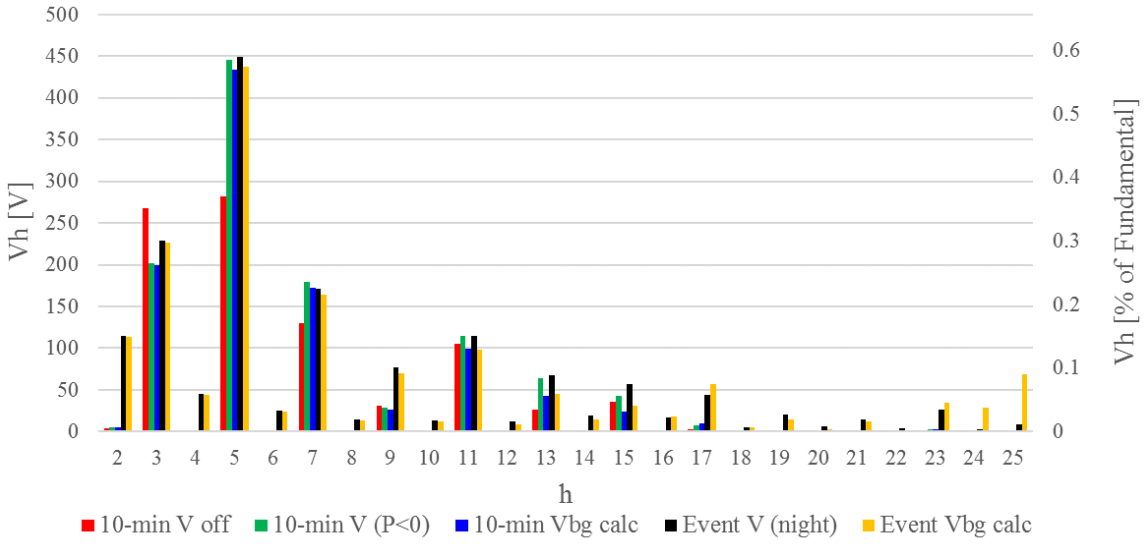

Figure 5-3: Background harmonic voltage assessment results (Red Phase)

However, it is also noted that the simulated utility harmonic impedance is inductive over the frequency range from 50 to 2500 Hz (h = 1 to 50), except between 825 and 887 Hz (h = 16.5 to 17.7), while the simulated PV plant harmonic impedance is capacitive over the frequency range from 50 to 1217 Hz (h = 1 to 24.3) and inductive over the rest of the harmonic range up to 2500 Hz. At lower harmonic orders, the PV plant impedance is much greater than the network harmonic impedance. Therefore, the magnitudes of the measured night-time voltages and the background voltages calculated according to (5.4) are similar up to the 12th harmonic. The calculated background harmonic voltage is slightly smaller than the measured voltage because $|Z_{nw} + Z_{pv}|$, the numerator of the multiplier term in (5.4), is smaller than $|Z_{pv}|$, the denominator, as illustrated in Figure 5-4 (a).

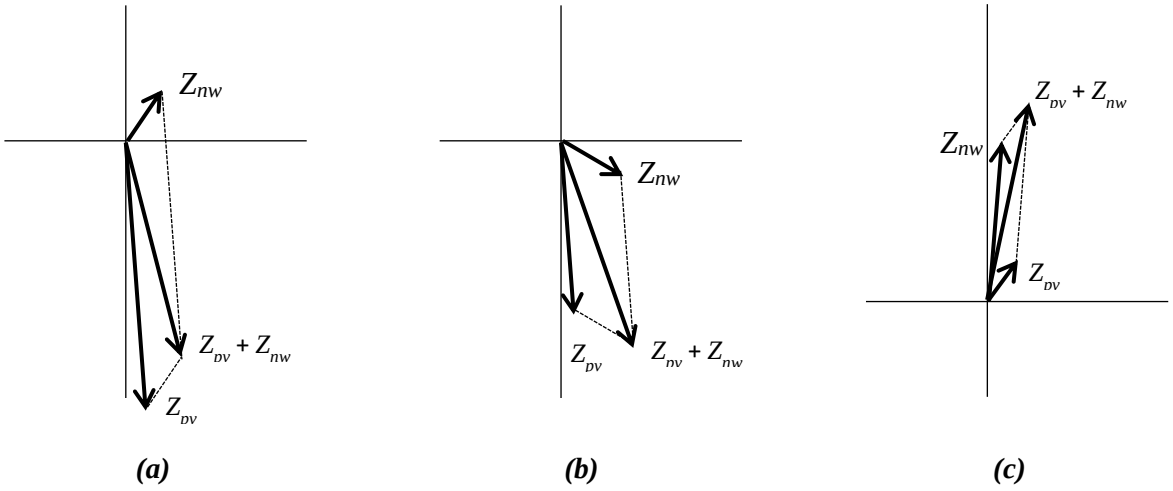

Figure 5-4: Effect of network and PV plant harmonic impedances in calculation of background harmonic impedance from harmonic measurements taken at night

Considering the capacitive region of the network impedance around the 17th harmonic order, as illustrated in Figure 5-4 (b), $|Z_{nw} + Z_{pv}|$ is greater than $|Z_{pv}|$ and the calculated background harmonic voltage is greater than the measured voltage. As described in section 3.6.1, the PV plant harmonic impedance characteristic exhibits a series resonance near the 24th harmonic (1217 Hz) due to the interaction of the park transformer leakage

inductance and the collector network cable capacitance. Near this resonance point, the PV plant impedance becomes much smaller than the network impedance, as shown in Figure 5-4 (c), resulting in a calculated background voltage much larger than the measured voltage.

A final observation related to the assessment of mean background harmonic voltage measurements is that the mean of the event voltages is significantly higher for non-dominant harmonic orders, especially for even harmonics and higher order harmonics. This could be accounted for by the averaging effects of the long-term measurements compared to a limited number of short-duration waveform measurements. But the waveform recordings are triggered by rapid voltage changes which may result from events network events which generate transient non-characteristic harmonics. In particular, the 2nd harmonic distortion is very high for event recordings compared to the negligible mean value from 10-minute aggregated recordings. This is likely due to transformer core saturation which produces high 2nd harmonic currents (in addition to smaller harmonic components including 3rd, 4th and 5th orders) by two primary mechanisms [159] [160]:

- transformer energisation with associated high second harmonic currents which cause second harmonic voltage distortion due to voltage drop over the system impedance, and
- rapid voltage changes caused by other types of network events – such as large load fluctuations or faults – inducing saturation of transformers in the network, including the PV plant park transformer, due to the change in voltage at the transformer terminals. Such voltage changes cause a transient flux resulting in transformer saturation until the average flux over a cycle has decayed to nearly zero and a new steady state condition is reached.

The $PR_{agg,h} \geq 0.8$ prevailing angle assessment criterion is applied to the background harmonic emissions calculated from the waveform data and only the 5th, 7th (red phase only), 11th and 13th harmonics have aggregated harmonic phase angles with acceptable uncertainty, as shown in Figure 5-5. Only these components are considered reliable for phasor calculations.

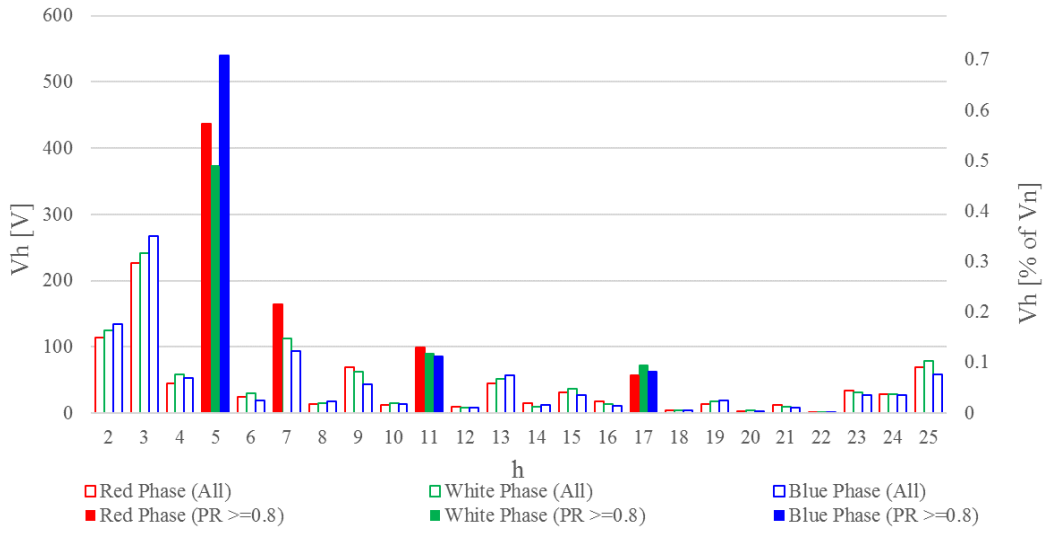

Figure 5-5: Application of $PR_{agg,h} \geq 0.8$ criterion to phase components of calculated event background harmonic emissions

Considering the background harmonic voltage assessment described above, the calculated harmonic voltages – based on non-operational period measurements and the network and PV plant impedances – are considered as the basis for emission calculations. This is because of doubts regarding the statistical validity of the measurements taken over a short 10-hour period with the plant disconnected. The calculated background voltages are similar to non-operational measured data from which they are calculated for low order harmonics but the calculated background voltages are considered to be more reliable in accounting for the effect of the series resonance identified by simulation of the PV plant harmonic impedance.

5.2.2.2 Sequence components

The calculation of sequence component mean background harmonic distortion is performed on the sequence components of the 23 night-time event measurements. The background sequence event harmonic voltages are calculated from the mean of the measured voltages according to equation (5.3) using the positive sequence harmonic impedances for the network and PV plant. The results are shown in Figure 5-6. Solid bars indicate harmonic sequence components which pass the $PR_{\mathrm{agg},h} \geq 0.8$ criterion indicating that the level of uncertainty in the aggregated sequence phasor angle is acceptable and that the phasors can be used in phasor calculations. As mentioned previously, zero sequence components are considered unreliable due to the lack of zero sequence impedance data for the utility network and due to the small magnitude of the zero sequence components.

In a balanced system, each harmonic order exhibits one characteristic sequence component but significant positive, negative and zero sequence components are apparent for most harmonic orders indicating that measured harmonics are unbalanced. For example, the third harmonic component is dominated by negative sequence, rather than a zero sequence component. The voltage magnitude unbalance is evident from the mean phase values in Figure 5-5 but the degree of unbalance is masked by averaging of the event magnitudes and examination of the individual event phasors also shows that the voltage phasors are not equally spaced with separation of 120°. The unbalance is likely due to a combination of factors including measurement inaccuracies, unbalanced loading in the network – including traction loading – and slow transient phenomena present due to the event-triggered nature of the available recordings. However, the positive phase sequence component is dominant for the 7^{th}, 13^{th} and 25^{th} harmonic orders and the negative phase sequence component is dominant for the 5^{th}, 11^{th} 17^{th} and 23^{rd} harmonic orders which aligns with expected results for a balanced 3-phase system.

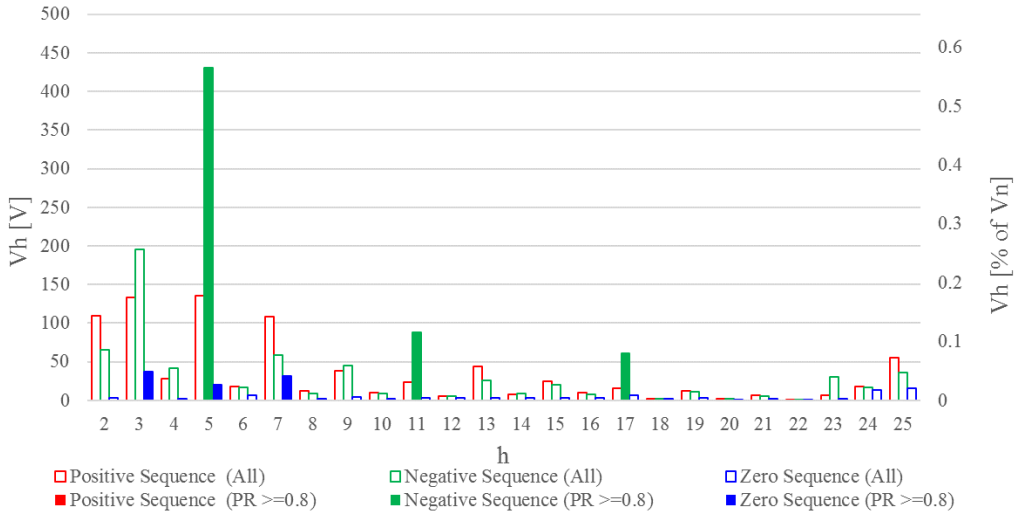

Figure 5-6: Calculated sequence components of background harmonic emissions showing application of $PR_{agg,h} \geq 0.8$ criterion

5.3 Current harmonic emissions for non-operational periods

The red phase mean harmonic currents measured at the POC for 10-minute periods and events when the plant is not operating are shown in Figure 5-7. Despite the very small magnitude of the average current when the plant is not operating, there is close alignment between the mean values from the 10-minute aggregated data and the event data. The 3rd, 5th and 7th harmonics from event measurements exhibit high prevalence ($PR_{agg,h}$ > 0.95) for all three phases while selected phases exhibit low prevalence ($PR_{agg,h}$ > 0.8) for odd harmonics of higher orders. The 5th and 7th harmonic currents are dominant. The magnitudes of the mean 23rd and 25th harmonic currents are very large considering the negligible mean background voltage harmonic distortion component (cf. Figure 5-3).

This observed behaviour correlates with the series resonance in the PV plant's harmonic impedance characteristic near the 24th harmonic order identified by frequency sweep simulations. The PV plant presents a low impedance at the 23rd and 25th harmonic orders and allows large harmonic currents to flow even for small background harmonic voltage magnitudes. The high magnitude of the measured 23rd and 25th harmonic currents therefore validate the frequency response of the PV plant model developed in chapter 3.

The sequence components of the harmonic currents measured for events when the plant is not operating are shown in Figure 5-8. The characteristic sequence components of the harmonics are generally dominant except for the triplen harmonic orders which are characterized by high positive and negative components but low zero sequence components. Considering the phase and sequence component phasor diagrams of the 3rd harmonic current in Figure 5-9, the individual phasors of each event – indicated by the dots – are closely grouped, giving a high prevalence ratio. The average phasors, indicated by the arrows are therefore a good representation of the measured data but they do not have similar phase angles as expected for zero sequence current components. The reason for this is not clear but if the measured events were triggered by intermittent traction load injecting

3rd harmonic into two phases only, this could explain the larger white and blue phase emissions with these phasors being almost 180° out of phase.

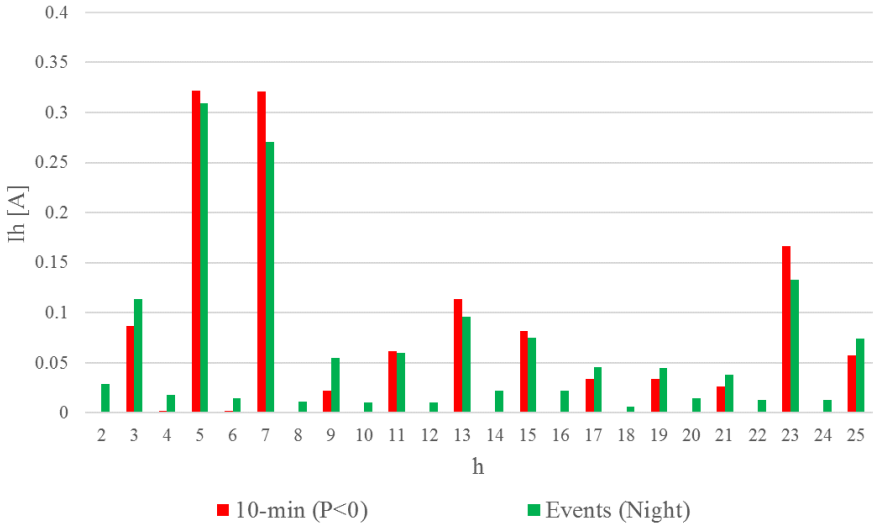

Figure 5-7: Mean red phase harmonic currents measured at the POC when the plant is not operating

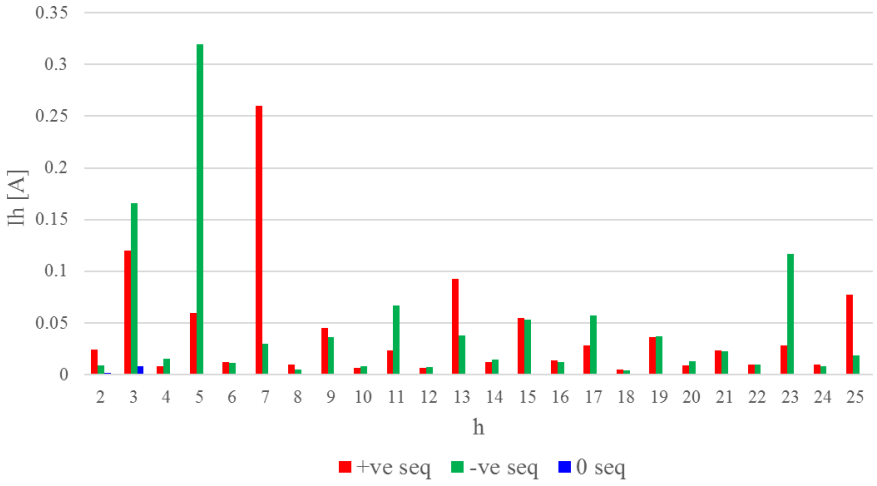

Figure 5-8: Mean harmonic sequence currents measured at the POC when the plant is not operating

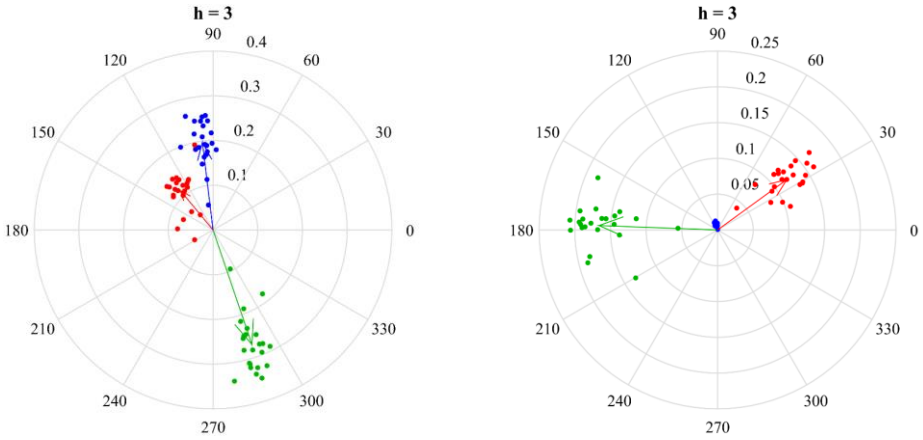

(a) ***(b)***

Figure 5-9: (a) Phase and (b) sequence component phasor diagrams of the third harmonic current in amperes

5.4 Harmonic voltage emissions during plant operation

5.4.1 Phase components

The mean red phase harmonic voltages from plant operational periods are shown in Figure 5-10. The 10-minute mean considers all periods when the PV plant is exporting active power into the network (P > 0). Normal events are events captured during the normal operation of the plant and start-up events are events which are observed during the morning start-up period of the plant and are associated with high reactive power output as described in section 4.2.5. Markers indicate the calculated 10-minute and event background voltages as per Figure 5-3. The dominant voltage harmonics are the 3rd, 5th, 7th, 11th and 13th.

It is immediately clear that the mean voltage distortion of the 5th, 7th, 11th, 13th, 17th and 23rd harmonics of start-up events significantly exceeds the event background voltage distortion. The plots for all phases are included in Appendix C. In general, considering the 10-minute aggregated and normal event harmonic voltages for dominant harmonics:

- the mean 7th and 13th harmonics exceed the respective background harmonic emissions,
- the mean 2nd, 5th, 9th and 17th harmonic voltages are lower than the background values,
- the mean 11th harmonic voltages are approximately equal to the background values.

The 10-minute and start-up event 3rd harmonics are similar in magnitude to their respective background values but the normal event 3rd harmonic voltage is significantly higher than the background level.

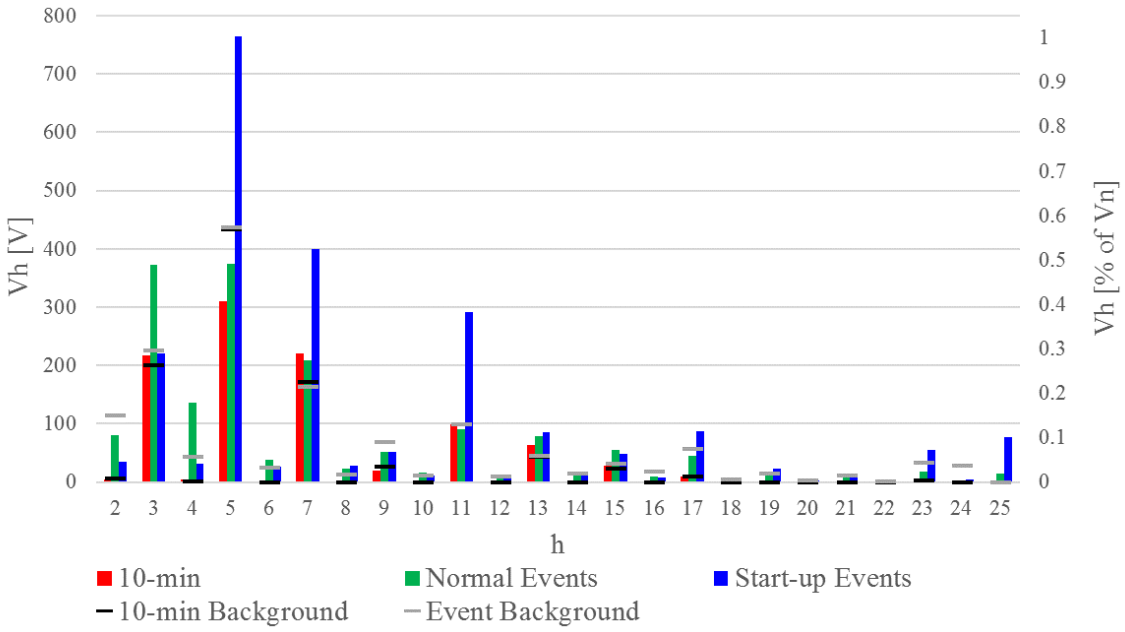

Figure 5-10: Mean red phase harmonic voltages from periods with P > 0

The prevailing ratios for phase component phasors for normal and start-up events are shown in Table 5-4. Only phasors with a $PR_{agg,h}$ greater than 0.8 are considered reliable for use in phasor calculations.

Table 5-4: Prevailing ratio, $PR_{agg,h}$, values for normal and start-up events

	Normal Events			Start-up Events		
h	**R**	**W**	**B**	**R**	**W**	**B**
2	0.14	0.43	0.37	0.39	0.92	0.79
3	0.73	0.58	0.25	0.75	0.92	0.92
4	0.26	0.12	0.36	0.82	0.78	0.87
5	0.69	0.83	0.87	0.94	0.96	0.98
6	0.34	0.65	0.28	0.65	0.52	0.76
7	0.82	0.90	0.85	0.98	0.99	0.99
8	0.68	0.34	0.74	0.88	0.75	0.88
9	0.83	0.72	0.31	0.79	0.41	0.87
10	0.60	0.24	0.49	0.75	0.90	0.80
11	0.95	0.93	0.94	0.99	0.99	1.00
12	0.80	0.27	0.76	0.70	0.66	0.50
13	0.63	0.68	0.69	0.41	0.80	0.50
14	0.39	0.39	0.32	0.33	0.53	0.70
15	0.25	0.42	0.36	0.50	0.16	0.63
16	0.66	0.57	0.35	0.63	0.59	0.57
17	0.89	0.87	0.87	0.98	0.98	0.98
18	0.46	0.06	0.73	0.53	0.39	0.64
19	0.17	0.68	0.47	0.69	0.47	0.29
20	0.71	0.21	0.58	0.72	0.42	0.40
21	0.79	0.58	0.35	0.57	0.61	0.84
22	0.14	0.13	0.58	0.63	0.80	0.79
23	0.50	0.12	0.61	0.74	0.82	0.77
24	0.39	0.31	0.55	0.76	0.67	0.42
25	0.37	0.16	0.26	0.95	0.89	0.93

$PRagg,h \geq 0.95$
$0.89 \leq PRagg,h < 0.95$
$0.8 \leq PRagg,h < 0.89$
$0.7 \leq PRagg,h < 0.8$
$PRagg,h < 0.7$

5.4.2 Sequence Components

The mean positive and negative sequence harmonic voltages from normal and start-up events are shown in Figure 5-11 and Figure 5-12 respectively. Markers indicate the sequence components of event background voltages shown in Figure 5-6. Solid bars represent harmonic components with reliable angle aggregation based on the $PR_{agg,h} \geq 0.8$ criterion.

For normal events:

- of the characteristic positive sequence harmonics, the mean positive sequence components of the 7th and 13th harmonic voltages significantly exceed their respective background harmonic emissions, the 25th is significantly less than the background level, and the 19th harmonic is approximately equal to the background level,
- of the characteristic negative sequence harmonics, the negative sequence components of the 5th, 17th and 23rd harmonics are less than the background harmonic levels, whilst the 11th is similar to the background level,
- the positive sequence component of the 3rd and 4th harmonic voltages significantly exceeds the background harmonic voltage level,
- the positive and negative sequence components of the 2nd harmonic voltage are both lower than the background level,

- positive and negative sequence components of most other harmonic orders are similar in magnitude to those of the background harmonic voltage sequence components.

For start-up events:

- of the characteristic positive sequence harmonics, the mean positive sequence components of the 7th, 13th and 19th harmonic voltages significantly exceed their respective background harmonic emissions,
- of the characteristic negative sequence harmonics, the mean negative sequence components of the 5th, 11th, 17th and 23rd harmonic voltages significantly exceed their respective background harmonic emissions,
- the positive and negative sequence components of the 2nd harmonic voltage are both lower than the background level,
- positive and negative sequence components of most other harmonic orders are similar in magnitude to those of the background harmonic voltage sequence components.

The values of zero sequence harmonic voltages are small but it appears that all zero sequence harmonics for normal and start-up events are less than the background levels.

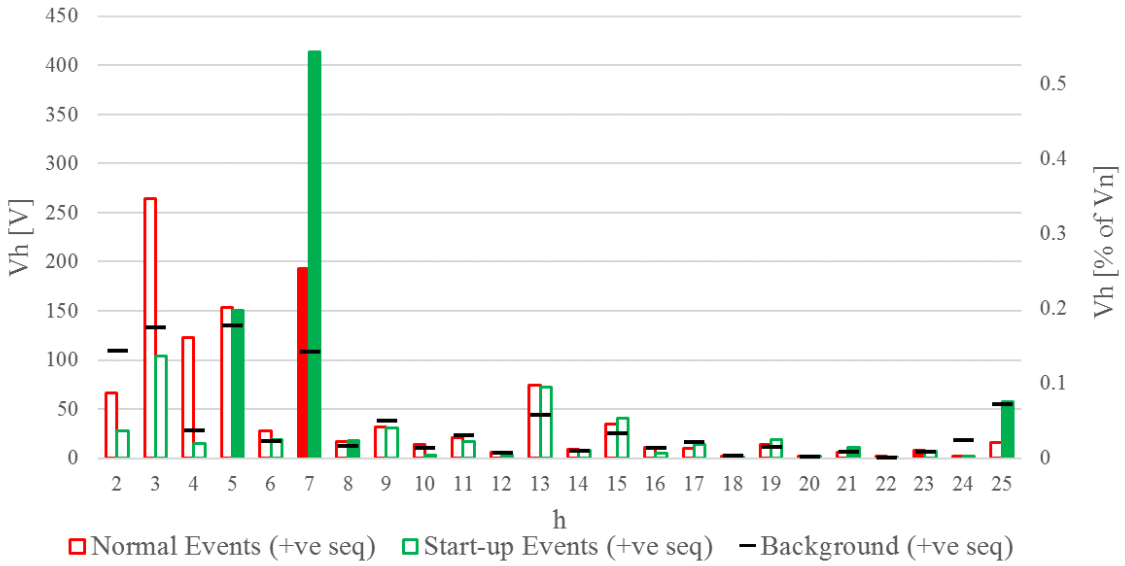

Figure 5-11: Mean positive sequence harmonic voltages from measurements during plant operation

From the above comparison of operational and night-time measurements, it appears that the 7th and 13th harmonic voltages increase and the 2nd and 5th harmonic voltages decrease during normal operation by comparison to the background harmonic distortion. The event recordings captured during normal operation also show an increase in 3rd and 4th harmonic distortion during operation but this behaviour is not visible in the 10-minute data. The PV plant is a dominant source of harmonic distortion during the start-up period with significant increases in mean values of several dominant harmonic orders compared to the background harmonic voltages. Increases are noted for the 5th, 7th, 11th, 13th, 17th and 23rd harmonic orders.

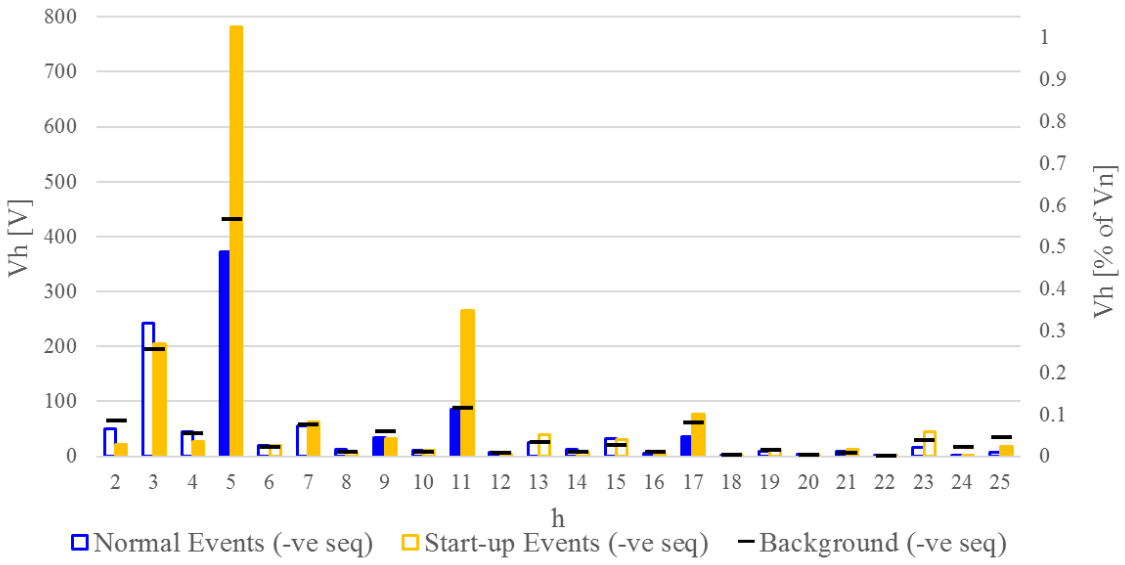

Figure 5-12: Mean negative sequence harmonic voltages from measurements during plant operation

However, a simple comparison of the operating and background harmonic magnitudes is not sufficient to evaluate the emission contribution of the PV plant at the POC. Several methods are proposed for such an evaluation. A comparative assessment of different methods proposed in the literature and applied in industry is presented in section 5.6.

5.5 Harmonic current emissions during plant operation

5.5.1 Phase components

The mean red phase harmonic currents during operation based on 10-minute and event measurements are compared to the mean background currents in Figure 5-13. The other two phases exhibit similar trends.

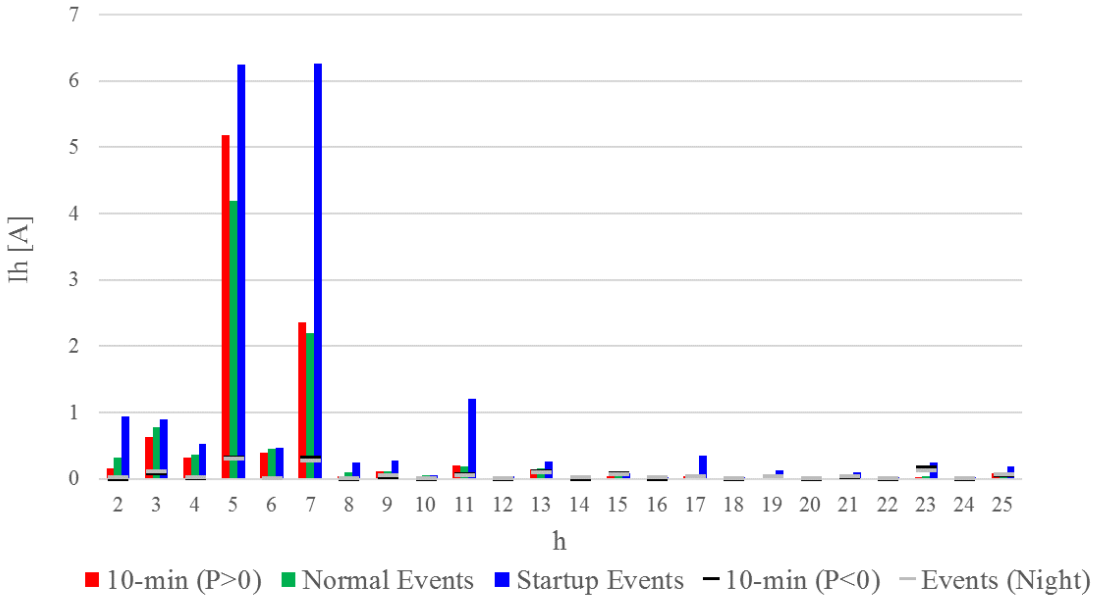

Figure 5-13: Mean red phase harmonic current from measurements during plant operation

The 5th and 7th harmonic currents are dominant with all harmonic currents up to the 9th order significantly exceeding the levels for periods when the plant is not operating. Small contributions of other characteristic harmonic currents are visible (h = 11, 13, 17, 19, 23 and 25). The highest mean harmonic current is consistently that of the start-up events across all harmonic orders. Although the average current magnitudes are very small, the 23rd harmonic is the only current harmonic which shows a decrease in mean value during operation (10-minute averages and normal-events). This could be due to lower 23rd order background harmonic distortion during the day or due to the impact of the inverter impedance on the PV plant harmonic impedance during operation.

The prevailing ratios for phase component phasors for normal and start-up event currents are shown in Table 5-5. Only phasors with a $PR_{agg,h}$ greater than 0.8 are considered reliable for use in phasor calculations. Start-up events generally exhibit low to high prevalence across a wide range of harmonics but normal events only exhibit low to medium prevalence in one or more phases for harmonic orders 3, 5, 6 and 7 with no prevalence for the remaining orders.

Table 5-5: Prevailing ratio, $PR_{agg,h}$, values for normal and start-up events

	Normal Events			Start-up Events		
h	**R**	**W**	**B**	**R**	**W**	**B**
2	0.27	0.37	0.45	0.75	0.84	0.88
3	0.80	0.89	0.62	0.82	0.72	0.42
4	0.47	0.11	0.46	0.85	0.88	0.90
5	0.89	0.94	0.88	0.79	0.82	0.86
6	0.57	0.47	0.83	0.89	0.78	0.87
7	0.81	0.73	0.83	0.99	0.98	0.99
8	0.35	0.33	0.17	0.91	0.75	0.91
9	0.15	0.22	0.34	0.86	0.87	0.92
10	0.41	0.38	0.32	0.63	0.86	0.81
11	0.35	0.30	0.10	0.97	0.98	0.97
12	0.29	0.07	0.46	0.72	0.76	0.48
13	0.76	0.75	0.76	0.79	0.88	0.89
14	0.24	0.22	0.25	0.74	0.65	0.78
15	0.11	0.33	0.31	0.64	0.76	0.84
16	0.42	0.50	0.17	0.42	0.78	0.68
17	0.67	0.80	0.78	0.92	0.95	0.95
18	0.32	0.10	0.54	0.78	0.70	0.68
19	0.32	0.39	0.25	0.57	0.41	0.62
20	0.24	0.26	0.60	0.54	0.76	0.66
21	0.38	0.28	0.18	0.88	0.44	0.82
22	0.23	0.10	0.21	0.53	0.71	0.75
23	0.20	0.27	0.17	0.81	0.85	0.82
24	0.30	0.20	0.47	0.79	0.85	0.52
25	0.51	0.57	0.58	0.95	0.93	0.97

$PRagg,h \geq 0.95$
$0.89 \leq PRagg,h < 0.95$
$0.8 \leq PRagg,h < 0.89$
$0.7 \leq PRagg,h < 0.8$
$PRagg,h < 0.7$

5.5.2 Sequence components

The mean positive and negative sequence harmonic currents from normal and start-up events are shown in Figure 5-14 and Figure 5-15 respectively. Markers indicate the sequence components of event currents during periods when the plant is not operating. Solid bars represent harmonic components with reliable angle aggregation based on the $PR_{agg,h} \geq 0.8$ criterion.

The presentation of harmonic currents according to their characteristic sequence components is much clearer than it is for the voltage measurements, although the triplen harmonics present as positive and negative components with a small zero sequence component. For normal events, the 5th (negative sequence) and 7th (positive sequence) harmonic currents are dominant. For start-up events, the 5th and 7th are again dominant but there is a significant 11th (negative sequence) component. Higher-order mean harmonic currents are smaller but 13th, 17th, 19th, 23rd and 25th harmonics are visible for start-up events and present according to their characteristic sequence. Current emissions at the 3rd, 4th, 6th, 8th and 9th present with both positive and negative sequence components; a possible source of these components is transformer saturation as a result of rapid voltage changes in the network.

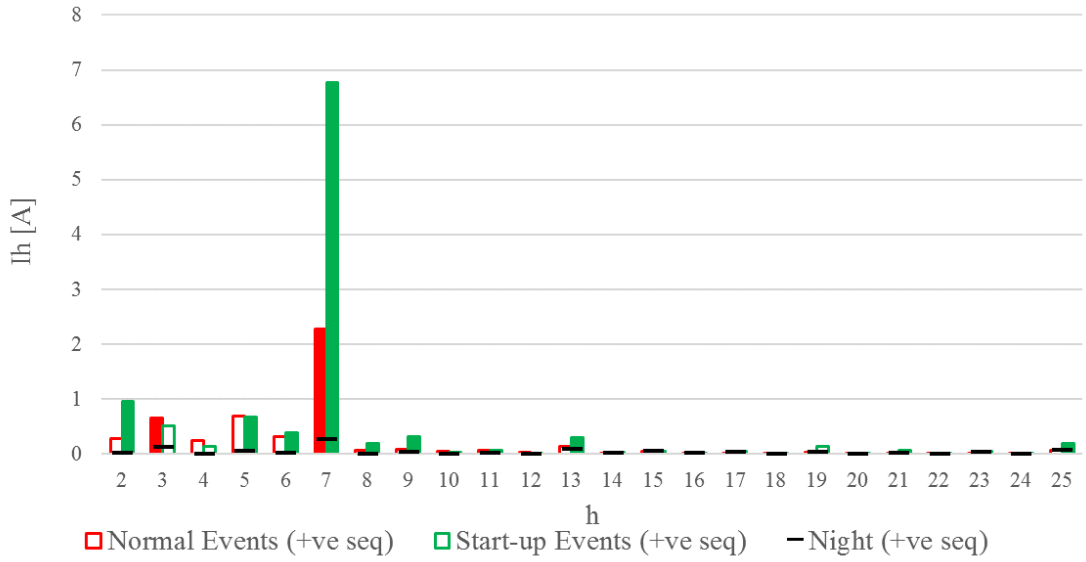

Figure 5-14: Mean positive sequence harmonic currents from measurements during plant operation

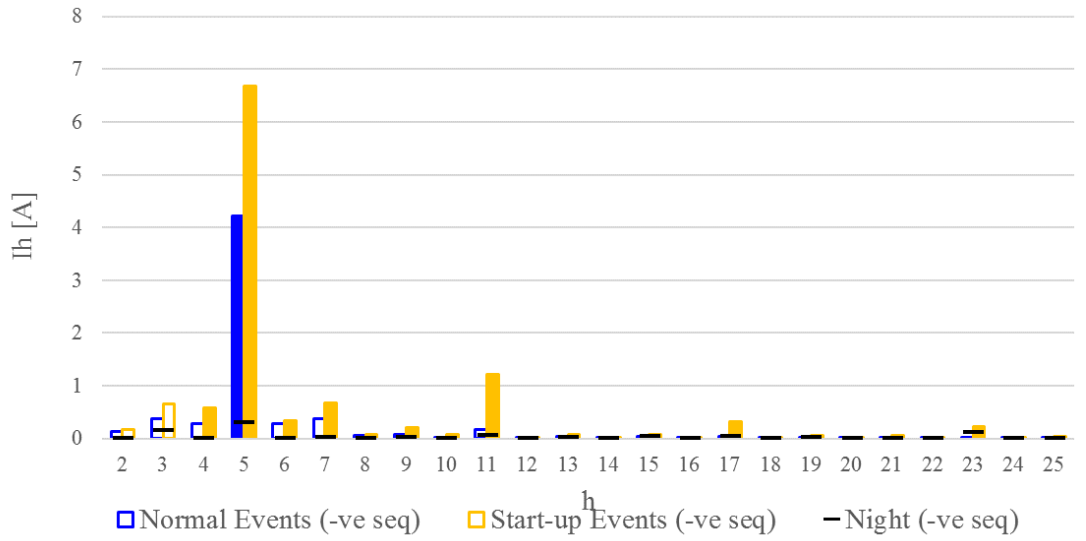

Figure 5-15: Mean negative sequence harmonic currents from measurements during plant operation

5.6 Comparative assessment of harmonic emissions calculation methods

Using the measured harmonic voltages and currents, the mean background harmonic voltages calculated in section 5.2 and the mean harmonic voltage and current emissions during the plant operation calculated in sections 5.4 and 5.5, the five methods listed in Table 5-1 are used to calculate the harmonic contribution of the plant. In the following sections, the calculation methodology and results of the various methods are presented followed by a comparative analysis of the results. Finally, the results of calculations for the dominant 5th and 7th harmonics using the 75th and 90th percentile harmonic emissions values are presented and discussed.

5.6.1 Calculation method 1: Reverse application of the general summation law

As described in section 2.10.2, the mean PV plant harmonic voltage emissions (V_{pv}) are calculated from the mean voltage emissions during operation (V_{POC}) and the mean background voltage harmonic emissions (V_{bg}), according to [58]:

$$V_{pv} = \sqrt[\alpha]{V_{POC}^{\alpha} - V_{bg}^{\alpha}} \tag{5.6}$$

where α is the summation law exponent as shown the following table:

Table 5-6: Summation exponents

Harmonic Order	α
h < 5	1
5 ≤ h ≤ 10	1.4
h > 10	2

If the magnitude of V_{POC} is less than that V_{bg}, the emission is considered to be equal to zero.

The results of the mean emissions calculation for the red phase using Method 1 are shown in Figure 5-16 for the following cases:

Table 5-7: Method 1 calculation data summary

Case	Measured Emission Voltage (V_{POC})	Background Voltage (V_{bg})
1A	10-minute periods with P > 0	10-minute periods with plant disconnected
1B	10-minute periods with P > 0	Calculated 10-minute background voltage
1C	Normal events	Calculated event background voltage
1D	Start-up events	Calculated event background voltage

The other phases exhibit a similar trend to that of the red phase and the results are included in Appendix D. Based on 10-minute and event data for normal operation (Calculations 1A, 1B and 1C), the only significant voltage harmonic emissions during normal operation of the plant are the 7th and 13th orders. Considering the

10-minute mean voltage with the plant disconnected as the background voltage (Calculation 1A), the plant also generates a 5th harmonic emission. Considering normal events (Calculation 1C), there are significant 3rd and 4th harmonic emissions as well as a smaller 15th harmonic emissions.

The harmonic emissions during start-up are much greater than those during operation. Significant contributions are observed at the 5th, 7th, 11th, 13th, 15th, 17th and 23rd harmonic orders. The 5th and 7th harmonic emissions of the white and blue phases are observed to be approximately 50% larger than the red phase emissions for start-up events.

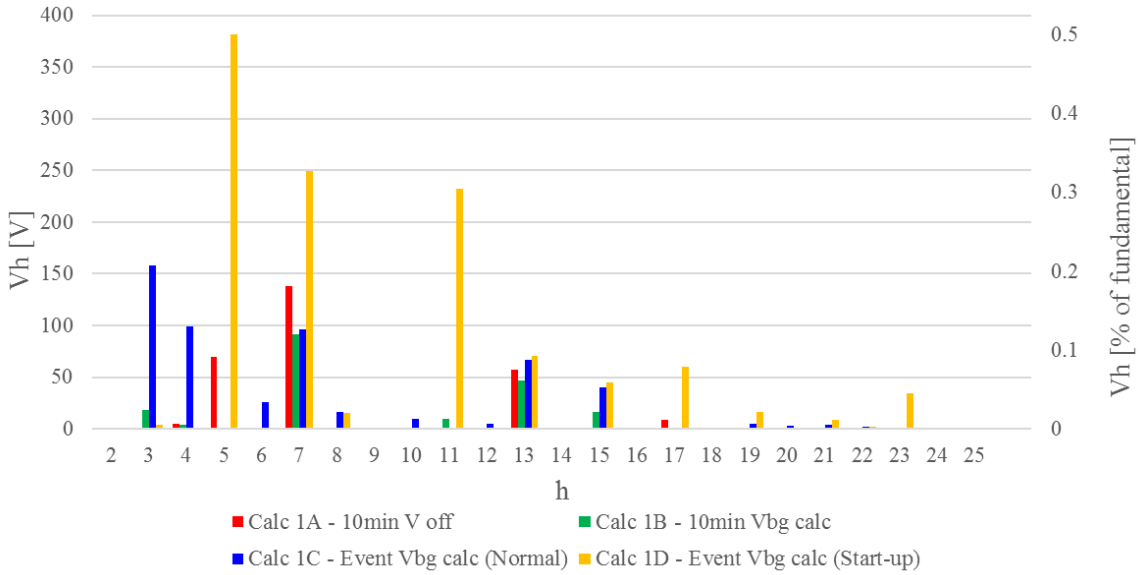

Figure 5-16: Mean harmonic emissions (red phase) – Calculation 1: Reverse application of the general summation law

5.6.2 Calculation method 2: Harmonic voltage phasor method

The emission voltage phasor can be calculated according to equation (5.7):

$$\bar{V}_{pv} = \bar{V}_{POC} - \bar{V}_{bg} \tag{5.7}$$

The harmonic emission phasor of the installation ($\bar{V}_{pv}$) is calculated for all measurement points where the magnitude of the measured voltage exceeds the background voltage distortion, i.e. $|\bar{V}_{POC}| > |\bar{V}_{bg}|$ whilst for periods when $|\bar{V}_{POC}| \leq |\bar{V}_{bg}|$, the emission is considered to be zero [58]. The mean of the emission phasor magnitudes, including the zero value emissions, is then calculated as the mean harmonic emission of the plant. The method is defined as Method 2A.

This method will always produce a mean voltage if at least one measured value exceeds the background voltage level. Thus, especially in the case of a small sample size, as available for this study, this method may indicate emissions at voltages where they are not present. As an alternative, the emission is also calculated as the vector subtraction of the mean background harmonic voltage phasor from the mean operating harmonic voltage

phasor (normal and start-up events). This adaptation of the harmonic voltage phasor method is defined as Method 2B.

The results of mean emission calculations for the red phase using Method 2A and Method 2B are shown in Figure 5-17. Results for the other phases are included in Appendix D. The two methods are substantially similar but Method 2A shows emissions for normal events at the 2nd, 5th, 11th and 17th harmonic orders where Method 2B shows zero emissions. Method 2B aligns more closely with the results of Method 1. The trends in emissions using Method 2A and Method 2B are similar to the results using Method 1 but the magnitudes vary significantly at certain orders. For normal events Method 2A / 2B calculate much higher emissions at the 3rd and 7th orders than Method 1. For start-up events, Method 2A / 2B calculate much higher emissions at the 7th order than Method 1.

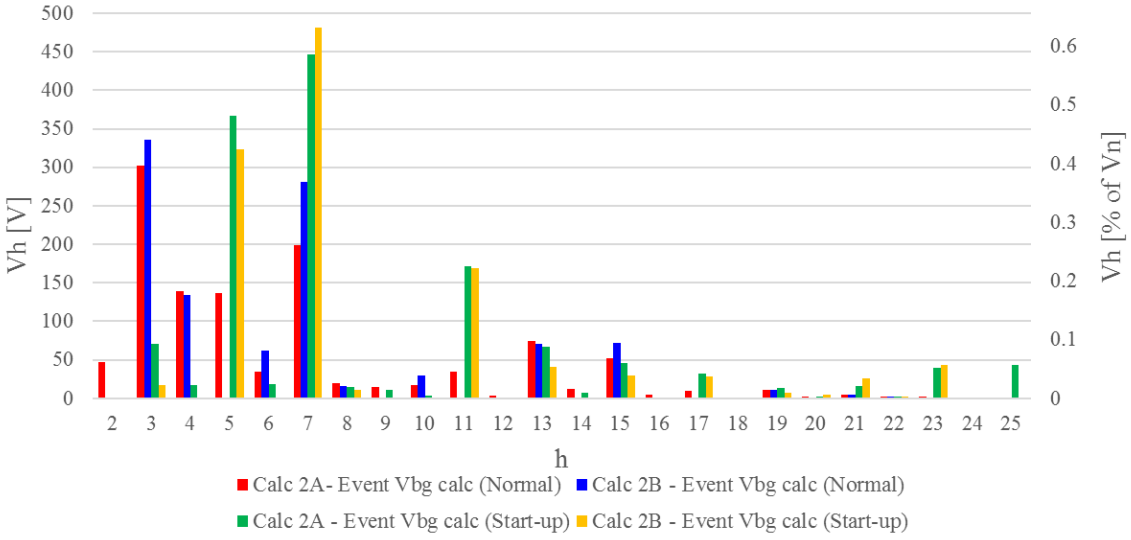

Figure 5-17: Mean harmonic emissions (red phase) – Calculation 2A: Harmonic voltage phasor method, Calculation 2B: Adapted harmonic voltage phasor method

These differences can be explained by consideration of the phasor diagrams shown in Figure 5-18. In all three cases, there is a significant phase angle difference between the mean background voltages and mean voltages measured during plant operation. In the case of the red-phase 7th harmonic for normal events (Figure 5-18 (a)), the phase angle difference is 94°. In the case of the red-phase 7th harmonic for start-up events (Figure 5-18 (b)), the phase angle difference is 141°. Due to these phase angle differences, the vector difference between emissions during operation and the background emissions is greater than the algebraic difference of their magnitudes, i.e. $\left|\overline{V}_{POC} - \overline{V}_{bg}\right| > \left|\overline{V}_{POC}\right| - \left|\overline{V}_{bg}\right|$.

For the red phase 7th harmonic, background measurements have a medium prevalence ($PR_{agg,h}$ = 0.92), the normal events have low prevalence ($PR_{agg,h}$ = 0.82) and start-up events have high prevalence ($PR_{agg,h}$ = 0.98). Therefore, the results of the phasors calculations are considered reliable. The white phase and blue phase background harmonics exhibit no prevalence, with $PR_{agg,h}$ values of 0.46 and 0.58 respectively. Hence, although the calculated emissions for these phases are similar to the red phase, the accuracy of the harmonic voltage phasor methods for these phases is uncertain.

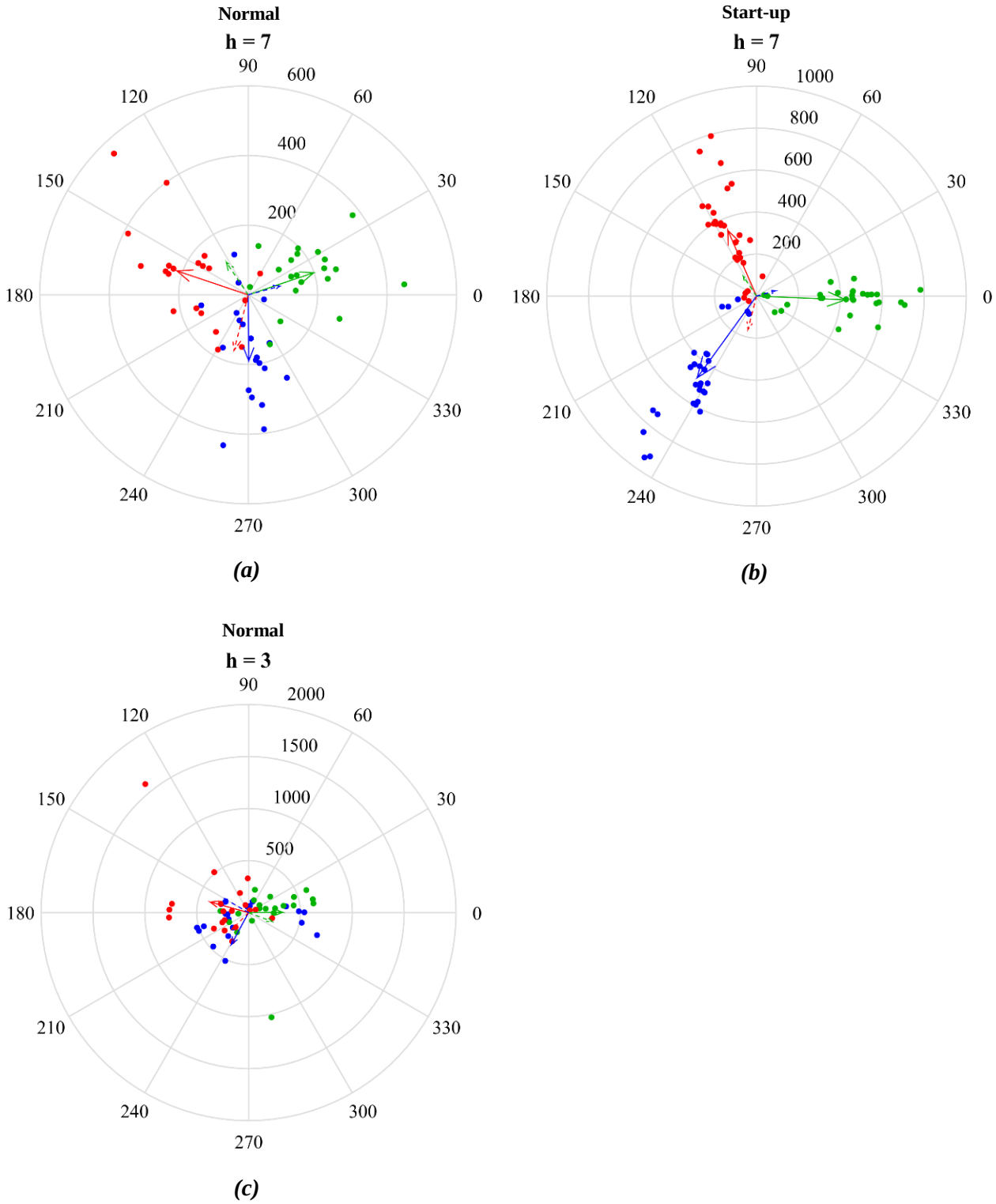

Figure 5-18: Phasor diagrams showing individual events as dots, mean V_{poc} phasors as solid arrows and mean V_{bg} phasors as dashed arrows. (a) Normal events 7th harmonic, (b) Start-up events 7th harmonic, (c) Normal events 3rd harmonic

The phase angle difference between normal events and background emissions also explains the increased 3rd harmonic emission compared to Method 1. However, there is no prevalence for any of the mean background phase emissions or the mean normal event phase emissions (i.e. $PR_{agg,h} < 0.8$ for all cases). Therefore, large

differences exist between the calculated emissions for different phases and the results of the harmonic voltage phasor calculation are meaningless.

Phasor calculations relying on averaging of multiple event phasors are only meaningful where there is reasonably low level of variation of phase angles between events represented by $PR_{agg,h} \geq 0.8$. For Method 2A, the background voltages must have adequate angle prevalence, while for Method 2B, both the background voltage and the measured POC voltages during operation (normal or start-up) must have adequate angle prevalence.

For Method 2A, it is also useful to know what percentage of voltage measurements exceed the background voltage level and contribute to the average calculation. The accuracy of mean emissions calculated using Method 2A may be low if the harmonic measurements exhibit low prevalence ratios or if only a small number of outlying events exceeds the background voltage level. The heatmap in Table 5-8 illustrates these values with the left half of each cell indicating the fraction of measurements with magnitude greater than the background level and the right half indicating the minimum prevalence ratio of the background voltage.

Harmonic vector calculations by Method 2A are only valid for the 5th, 7th (red phase), 11th and 17th harmonics which have reliable angle aggregation for the background harmonics. Of these harmonics, for normal events, only the red phase 7th harmonic has more than 50% of measurement points exceeding the background voltage level. The majority of measured events for all of these harmonics exceed the background voltage level for start-up events.

Table 5-8: Calculation Method 2A Reliability Heatmap

	Normal Events						Start-up Events					
	R		W		B		R		W		B	
2	0.15	0.45	0.30	0.41	0.20	0.73	0.00	0.45	0.00	0.41	0.00	0.73
3	0.70	0.31	0.55	0.33	0.60	0.59	0.52	0.31	0.41	0.33	0.38	0.59
4	0.55	0.36	0.35	0.47	0.50	0.66	0.21	0.36	0.10	0.47	0.21	0.66
5	0.35	0.80	0.40	0.84	0.50	0.88	0.83	0.80	0.86	0.84	0.83	0.88
6	0.30	0.24	0.35	0.48	0.40	0.38	0.38	0.24	0.14	0.48	0.69	0.38
7	0.60	0.92	0.95	0.46	0.75	0.58	0.83	0.92	0.93	0.46	0.90	0.58
8	0.50	0.69	0.25	0.17	0.35	0.35	0.72	0.69	0.41	0.17	0.55	0.35
9	0.20	0.34	0.30	0.26	0.30	0.18	0.21	0.34	0.03	0.26	0.59	0.18
10	0.40	0.39	0.40	0.56	0.45	0.42	0.31	0.39	0.38	0.56	0.28	0.42
11	0.40	0.92	0.40	0.91	0.35	0.92	0.83	0.92	0.86	0.91	0.86	0.92
12	0.30	0.62	0.35	0.36	0.35	0.40	0.21	0.62	0.24	0.36	0.14	0.40
13	0.90	0.17	0.85	0.45	0.60	0.45	0.69	0.17	0.66	0.45	0.59	0.45
14	0.35	0.44	0.45	0.30	0.50	0.05	0.34	0.44	0.45	0.30	0.28	0.05
15	0.60	0.39	0.55	0.61	0.60	0.52	0.59	0.39	0.48	0.61	0.83	0.52
16	0.15	0.35	0.30	0.32	0.40	0.26	0.03	0.35	0.00	0.32	0.28	0.26
17	0.20	0.88	0.00	0.89	0.00	0.88	0.90	0.88	0.76	0.89	0.59	0.88
18	0.25	0.41	0.45	0.18	0.30	0.23	0.00	0.41	0.03	0.18	0.00	0.23
19	0.50	0.49	0.40	0.78	0.45	0.41	0.62	0.49	0.41	0.78	0.76	0.41
20	0.45	0.31	0.65	0.21	0.45	0.17	0.34	0.31	0.14	0.21	0.24	0.17
21	0.45	0.55	0.55	0.71	0.50	0.04	0.62	0.55	0.86	0.71	0.83	0.04
22	0.80	0.16	0.90	0.46	0.75	0.51	0.90	0.16	0.69	0.46	0.72	0.51
23	0.05	0.50	0.00	0.54	0.25	0.39	0.76	0.50	0.83	0.54	0.72	0.39
24	0.00	0.66	0.00	0.26	0.00	0.54	0.00	0.66	0.00	0.26	0.00	0.54
25	0.00	0.53	0.00	0.57	0.10	0.39	0.52	0.53	0.14	0.57	0.66	0.39

Fraction of $V_{POC} > V_{bg}$ (Left half of cell)
- <0.25
- 0.25 to 0.5
- 0.5 to 0.75
- >0.75

$PR_{agg,h}$ of V_{bg} (Right half of cell)
- < 0.7
- 0.7 to 0.8
- 0.8 to 0.89
- 0.89 to 0.95
- *>0.95*

A similar heatmap for Method 2B is shown in Table 5-9 but in this case the first half of each cell is binary indicating 0 where the mean voltage during operation is less than the mean background voltage and 1 otherwise. Since background and operating phasors are aggregated, the prevalence ratio indicated for each

harmonic is the minimum of the background and operational (normal / start-up) prevalence ratios. For normal events, the 5th, 11th and 17th harmonic have high prevalence but the mean value is less than the mean background voltage and they are therefore considered as zero emissions. However, for start-up events, these same harmonics exhibit high prevalence and have a mean value greater than the background voltage. The red-phase 7th harmonic angle has $PR_{agg,h} > 0.8$ and constitutes an emission for both normal and start-up events.

A shortcoming of Method 2B is the case where the mean magnitudes of V_{bg} and V_{POC} are similar but there is a significant difference in the phase angle between these two phasors. Then, if the magnitude of the phasor mean of measured voltage ($\overline{V_{POC}}$) is marginally less than magnitude of the phasor mean of the background voltage ($\overline{V_{bg}}$) the emission will be zero. But, if the magnitude of $\overline{V_{POC}}$ increases to be marginally greater than the magnitude of $\overline{V_{bg}}$, the emission could be significant. This is illustrated in Figure 5-19 (a). This problem persists in the case that the method is applied to the 95th percentile phasors instead of the mean phasors.

Table 5-9: Calculation Method 2B Reliability Heatmap

	Normal Events						Start-up Events					
	R		W		B		R		W		B	
2	0	0.14	0	0.41	0	0.37	0	0.39	0	0.41	0	0.73
3	1	0.31	1	0.33	1	0.25	1	0.31	0	0.33	0	0.59
4	1	0.26	1	0.12	1	0.36	0	0.36	0	0.47	0	0.66
5	0	0.69	0	0.83	0	0.87	1	0.80	1	0.84	1	0.88
6	1	0.24	1	0.48	1	0.28	0	0.24	0	0.48	1	0.38
7	1	0.82	1	0.46	1	0.58	1	0.92	1	0.46	1	0.58
8	1	0.68	1	0.17	1	0.35	1	0.69	1	0.17	1	0.35
9	0	0.34	0	0.26	0	0.18	0	0.34	0	0.26	1	0.18
10	1	0.39	1	0.24	1	0.42	0	0.39	0	0.56	0	0.42
11	0	0.92	1	0.91	0	0.92	1	0.92	1	0.91	1	0.92
12	1	0.62	1	0.27	1	0.40	0	0.62	0	0.36	0	0.40
13	1	0.17	1	0.45	1	0.45	1	0.17	1	0.45	1	0.45
14	0	0.39	1	0.30	1	0.05	0	0.33	1	0.30	0	0.05
15	1	0.25	1	0.42	1	0.36	1	0.39	1	0.16	1	0.52
16	0	0.35	1	0.32	1	0.26	0	0.35	0	0.32	0	0.26
17	0	0.88	0	0.87	0	0.87	1	0.88	1	0.89	1	0.88
18	0	0.41	1	0.06	0	0.23	0	0.41	0	0.18	0	0.23
19	1	0.17	1	0.67	1	0.41	1	0.49	1	0.47	1	0.29
20	1	0.31	1	0.21	1	0.17	1	0.31	0	0.21	0	0.17
21	1	0.55	1	0.58	1	0.04	1	0.55	1	0.61	1	0.04
22	1	0.14	1	0.13	1	0.51	1	0.16	1	0.46	1	0.51
23	0	0.50	0	0.12	0	0.39	1	0.50	1	0.54	1	0.39
24	0	0.39	0	0.26	0	0.54	0	0.66	0	0.26	0	0.42
25	0	0.37	0	0.16	0	0.26	0	0.53	0	0.57	1	0.39

$V_{POC} > V_{bg}$
(Left half of cell)
0
1

Minimum PR agg,*h* of V_{bg} and V_{POC}
(Right half of cell)
< 0.7
0.7 to 0.8
0.8 to 0.89
0.89 to 0.95
>0.95

In application of Method 2A for calculation of the 95th percentile emission, outliers are excluded from the 95th percentile calculation. Therefore, in a representative sample, if less than 5% of measurements exceed the P95 background level, the calculated 95th percentile value will be zero. However, a similar binary threshold exists between zero emissions and potentially significant emissions if 5% plus one measurements exceed the threshold. It is proposed that in the application of Method 2A and Method 2B for mean and 95th percentile evaluations, the magnitudes of mean (or P95) background and mean (or P95) measured values be compared to determine whether calculated values of emission are representative for cases where these magnitudes are similar.

The harmonic voltage phasor method reveals the complexity of assessing an emission contribution. Referring to Figure 5-19 (b), if the emission phasor ($\bar{V}_{pv}$) remains constant under different levels of background distortion, then the ratio of the magnitudes of measured and background voltages varies significantly

depending on the background voltage level. This applies per measurement point for Method 2A and for the phasor averages in Method 2B. For background voltage 1 ($\bar{V}_{bg1}$), the measured voltage ($\bar{V}_{POC1}$), is marginally smaller than the background voltage and the emission is considered to be zero. If the background voltage increases to ($\bar{V}_{bg3}$), the measured voltage is significantly smaller than the background voltage and the emission remains zero. However, if the background voltage magnitude decreases to ($\bar{V}_{bg2}$), the measured voltage becomes much larger than the background voltage and the emission voltage is considered to be equal to $\bar{V}_{pv}$.

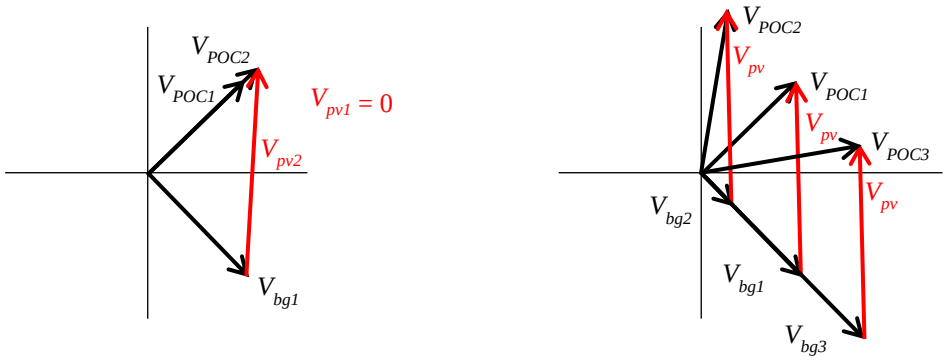

(a) ***(b)***

Figure 5-19: (a) Effect of small changes in mean of measured voltage magnitude on calculated emission for Method 2B. (b) Effect of changing background voltage level with constant harmonic emission.

5.6.3 Calculation method 3: IEC 61000-3-6 long-duration simultaneous measurement of harmonic voltages and currents

For this method, the long-duration simultaneous measurements of harmonic voltage and current magnitudes are used to generate scatter plots of voltage versus current per harmonic. The network impedance, Z_{nw}, (from the utility frequency sweep) and the PV plant impedance, Z_{hc}, (obtained by simulation as described in chapter 3), are plotted as straight lines on the voltage vs current plot. From these plots, it may be possible to infer the dominant source of harmonics. Clustering of measurement points around the Z_{nw} impedance line indicates that the PV plant is the dominant source of harmonic current – i.e. harmonic currents generated by the installation are flowing into the network impedance – whilst clustering of points around the Z_{pv} line indicates that the installation is absorbing harmonics from the network and the network is the dominant source. Where the points are scattered over the area delimited by the two lines, the resulting harmonic voltages are due to the combined influence of the background distortion and the installation [58].

Furthermore, the voltage harmonic emission of the installation can be calculated as the current harmonic emission multiplied by the network harmonic impedance, in alignment with the IEC 61000-3-6 and NRS 048 methodologies [58]. The mean harmonic voltage emission based on 10-minute measurements over the 12-day recording period is calculated from the mean current emission for two scenarios:

- all measurements (Method 3A),
- measurements for periods when the plant is operating – defined for this assessment as periods when active power export is greater than zero at the POC (Method 3B).

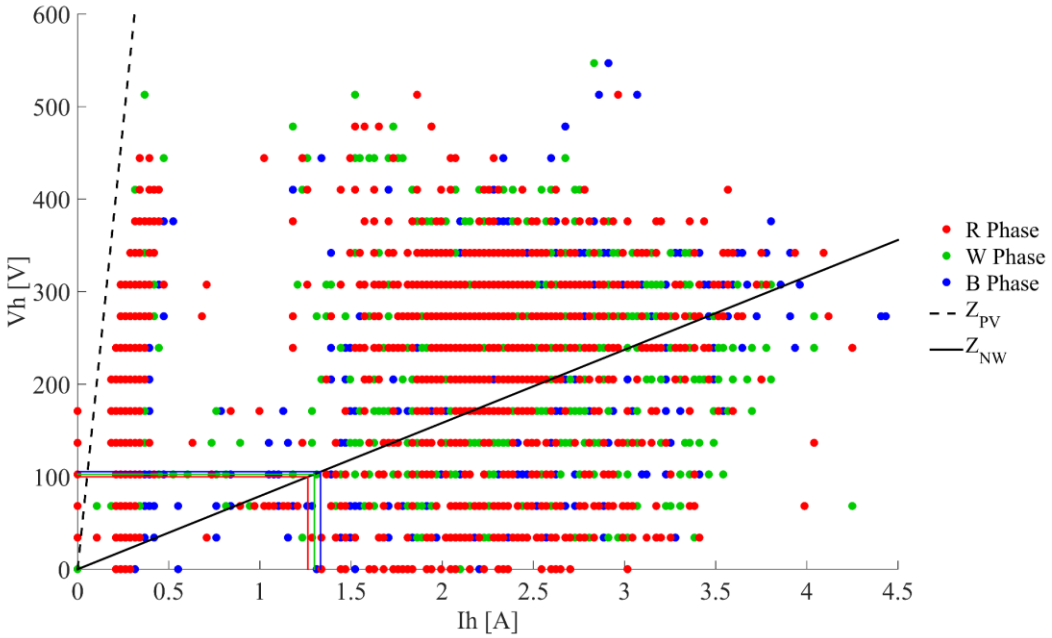

Figure 5-20: Scatter plot of 7th harmonic 10-minute voltage vs current measurements with network and PV plant harmonic impedances. Red, green and blue lines indicate mean of all red, white and blue harmonic current measurement periods and corresponding mean voltage emissions calculated as $V_{pv} = I*Z_{nw}$.

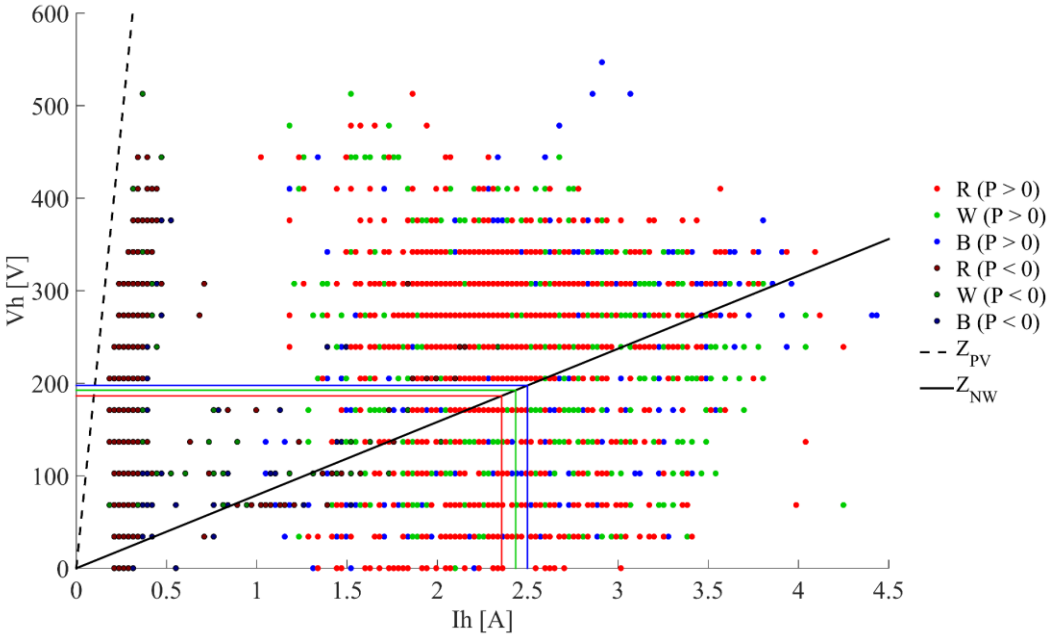

Figure 5-21: Scatter plot of 7th harmonic 10-minute voltage vs current measurements with network and PV plant harmonic impedances. Red, green and blue lines indicate mean of operational red, white and blue phase harmonic current measurement periods (i.e. periods with P > 0) and corresponding mean voltage emissions calculated as $V_{pv} = I*Z_{nw}$.

Figure 5-20 illustrates the application of the method for the 7th harmonic. The mean harmonic current is approximately 1.3 A for the 12-day period. Applying Ohms law with the network impedance magnitude at the 7th harmonic order, the corresponding voltage emission is approximately 100 V. In Figure 5-21, the measurement periods when the plant is not operating (P < 0) are indicated by darker colour points. There are two clear clusters of point. The darker points are clustered near to the Z_{pv} line indicating that the PV plant is absorbing harmonic current generated by external sources in the network when it is not operating. The lighter

points are spread over a wide area but are more closely aligned with the Z_{nw} line indicating that currents generated by the PV plant are being absorbed by the network, or at least that there are contributions from the plant and the network when the plant is operating. The mean harmonic current of periods with $P > 0$ is approximately 2.4 A and the corresponding voltage emission approximately 190 V.

There is a significant difference between the mean values of all measurements and of the measurements during operation only since the harmonic currents are much lower at night, when the plant is not operating, and these non-operational periods comprise more than 50% of the measurement duration. Therefore, the mean value of all measurements may underestimate the emission contribution whist the mean of non-operational periods may overestimate it.

The scatter plot method is commonly applied using 95th percentile currents to determine the 95th percentile voltage for comparison to emission limits. The 95th percentiles of the full period and the operational period are likely to be more similar than the mean values of these periods. Therefore, for the 95th percentile assessment, utilization of all measurements from the full period is may prove simpler and more robust, as it can also account for cases where the distortion is higher when the plant is not operating.

The scatter plots of several other dominant harmonic orders are shown in Figure 5-22. The 2nd and 4th orders exhibit significant quantisation effects, especially in the voltage measurements, making it difficult to identify any clustering of points or useful trends. This is the case for all even harmonics and higher order harmonics as noted in the quality assessment of the measurement data in section 4.2.2. A significant unbalance in the mean current values for these harmonic is noted which the author attributes primarily to CT mismatch, other measurement error or natural statistical variation between phases although some current unbalance may exist in the network.

The third harmonic shows a wide scattering of points between the two impedance lines indicating that both the plant and the network contribute to the emissions. The 5th harmonic shows a tight clustering of non-operational values around the PV plant impedance line indicating that the PV plant is absorbing these at night. During plant operation, the points are scattered over a wide range but there is a trend of decreasing voltage with increasing current. This suggests that the inverters operate as active filters injecting 5th harmonic currents which tend to cancel the 5th harmonic voltage distortion at the POC and that the operation of the inverters is beneficial in reducing 5th harmonic voltage distortion in the network. This reinforces the result of methods 1B, 1C and 2B which yield a zero voltage emission for the 5th harmonic. The 11th and 13th harmonics again seem to exhibit a trend of night-time values aligning with the PV plant harmonic impedance and operational period values spread over a wide range between the two impedance lines indicating contribution from the plant and the network.

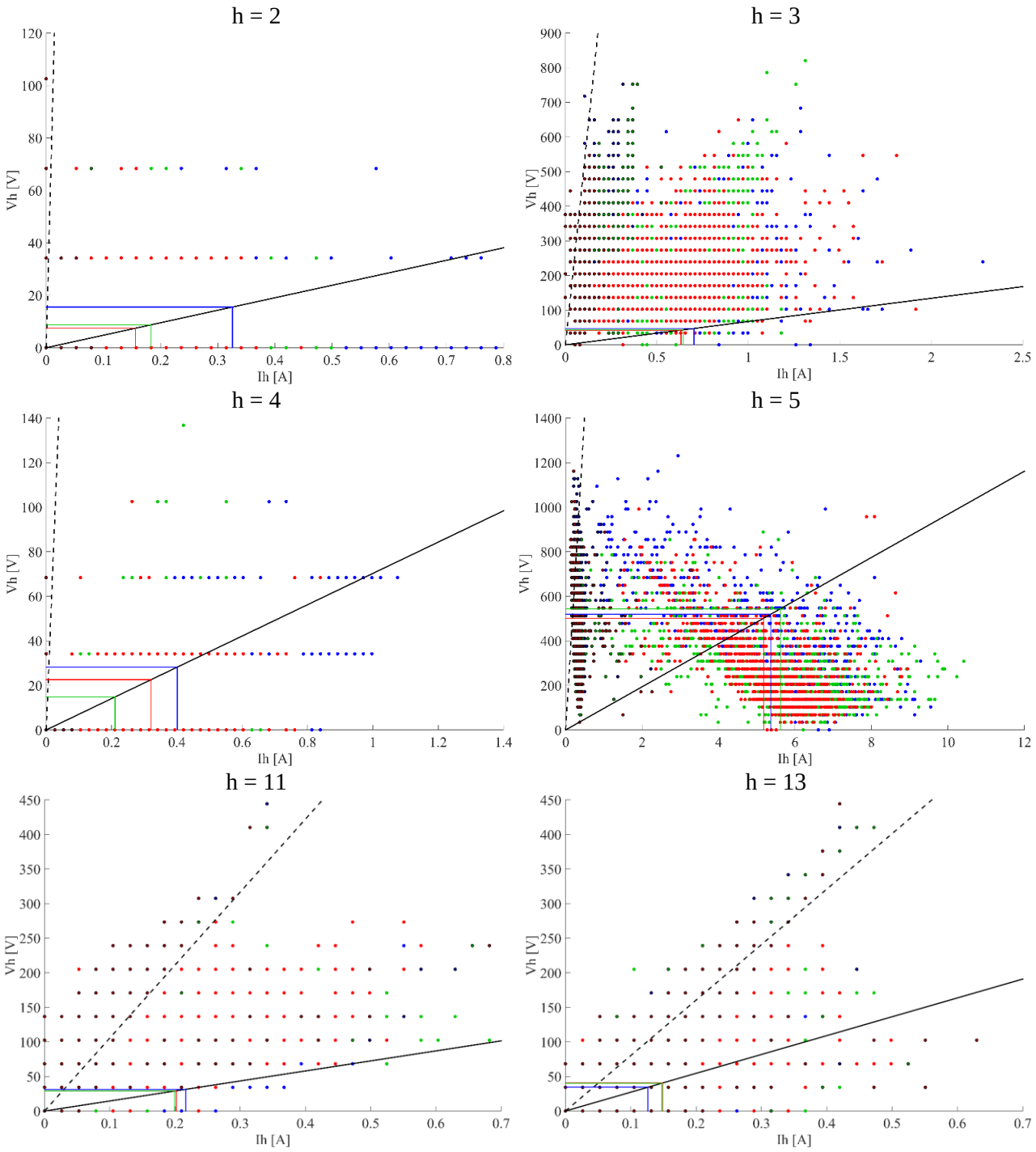

Figure 5-22: Voltage vs current scatter plot of selected dominant harmonic orders

The calculation results of Method 3A and 3B for mean red phase voltage emissions for harmonic orders 2 to 25 are shown in Figure 5-23. The trend is similar to Methods 1 and 2 with dominant 5^{th} and 7^{th} harmonics, although the 5^{th} harmonic voltage emission can be considered to be zero due to the positive effect of the plant in reducing 5^{th} harmonic voltage distortion at the POC during operation. However, unlike the Methods 1 and 2, Methods 3A and 3B do not consider the background harmonic emission in the calculation of the PV plant contribution. This is advantageous because of the difficulty of determining a representative background level to be used in a comparative assessment but is problematic since it apportions all responsibility for the measured current emission onto the PV plant. PV plant voltage emissions are only considered to be zero if clear evidence from the scatter plots, or other methods, indicates that the utility network is the dominant source of the

emission. In the case of the PV plant under study, this is only true for the 5th harmonic order. The other key advantage of this method is that the assessment does not require phasor angle information.

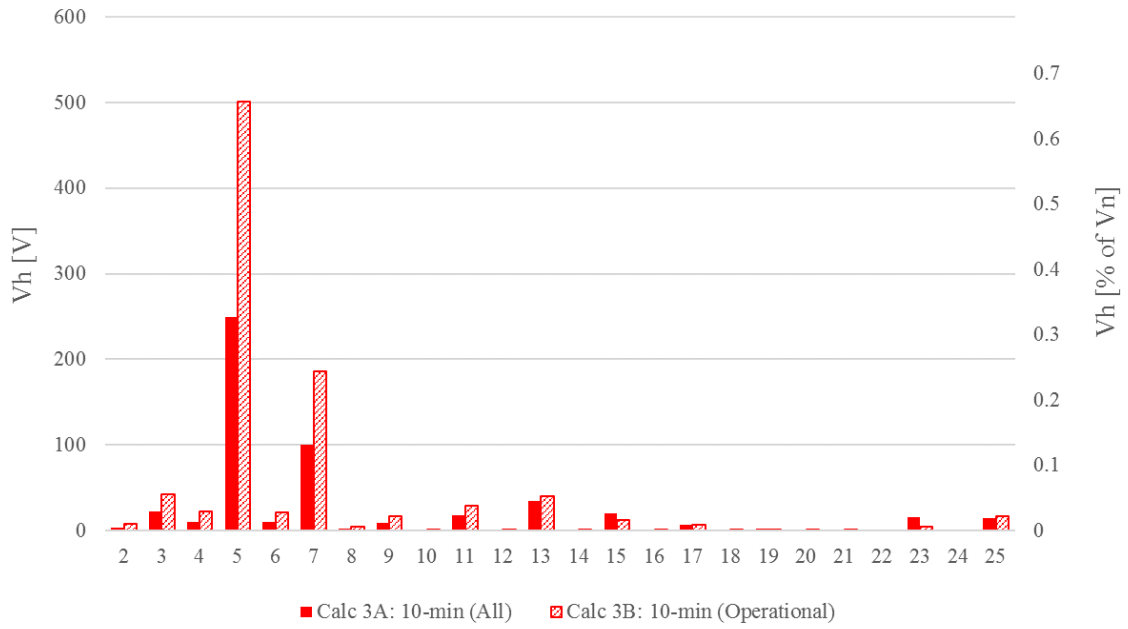

Figure 5-23: Red-phase PV plant mean voltage emissions calculated according to Method 3A and 3B

5.6.4 Calculation method 4: Harmonic vector method

The circuit shown in Figure 5-24 is equivalent to that of Figure 5-1 but with both the utility and the PV plant represented by Thevenin equivalent circuits. Based on this representation, the PV plant Thevenin equivalent source ($V_{pv\text{-}Thev}$) can be calculated as [110]:

$$\overline{V}_{pv\_Thev} = \overline{V}_{POC} + \overline{I}_{POC}\overline{Z}_{pv} \tag{5.8}$$

and the contribution of the PV plant at the POC then evaluated as:

$$\overline{V}_{pv} = \overline{V}_{pv\_Thev}\frac{\overline{Z}_{nw}}{\overline{Z}_{nw} + \overline{Z}_{pv}} \tag{5.9}$$

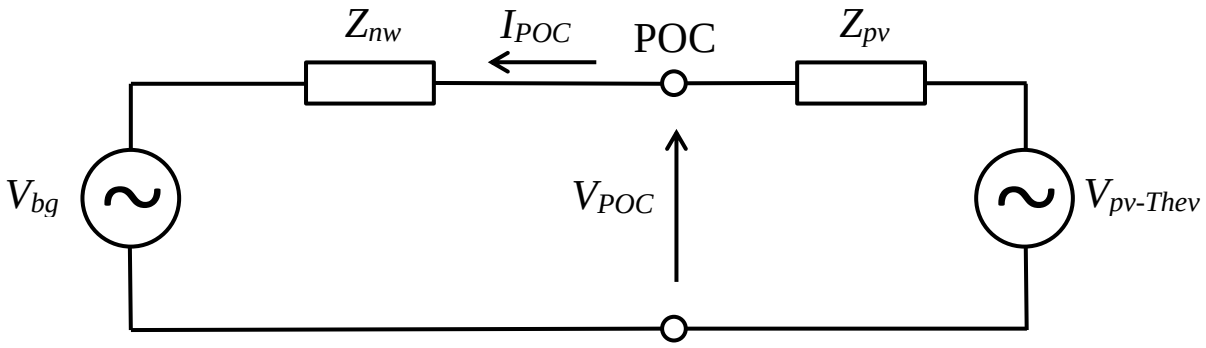

Figure 5-24: Thevenin equivalent circuit for evaluation of individual harmonic emissions [110]

This method is a formulation of the harmonic vector method and it does not require knowledge of the background harmonic voltage. The plant is only considered to be a source of emissions in instances where $|V_{POC}| > |V_{bg}|$. This can be determined by evaluating the sign of the scalar quantity V_{pvs}, which is the projection of the PV plant contribution onto the measured POC voltage [110]. V_{pvs} can be calculated using Equation (5.10) where δ_{pv} is the angle of the PV emission phasor $\bar{V}_{pv}$, and δ_{POC} is the angle of the POC voltage $\bar{V}_{POC}$.

$$\bar{V}_{pvs} = \left|\bar{V}_{pv}\right| \cos\left(\delta_{pv} - \delta_{POC}\right) \tag{5.10}$$

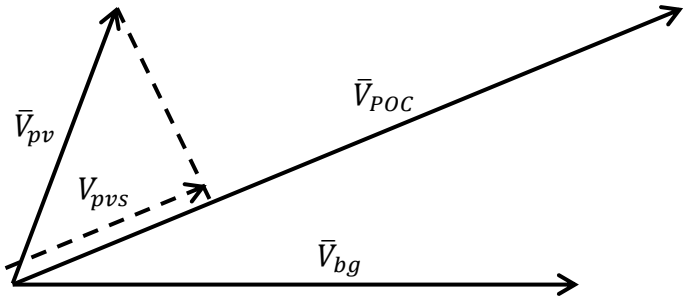

Figure 5-25: Harmonic vector method [110]

For measurements where V_{pvs} is negative, the PV plant is considered to improve the harmonic performance and the emission counted as zero [58]. The mean of the emission phasor magnitudes is then calculated as the mean harmonic emission of the plant. The calculated mean red phase emissions are shown in Figure 5-26. The yellow bars indicate all measurements excluding the start-up events since these present high distortion and are overrepresented in the measurement data and will therefore skew the mean calculations.

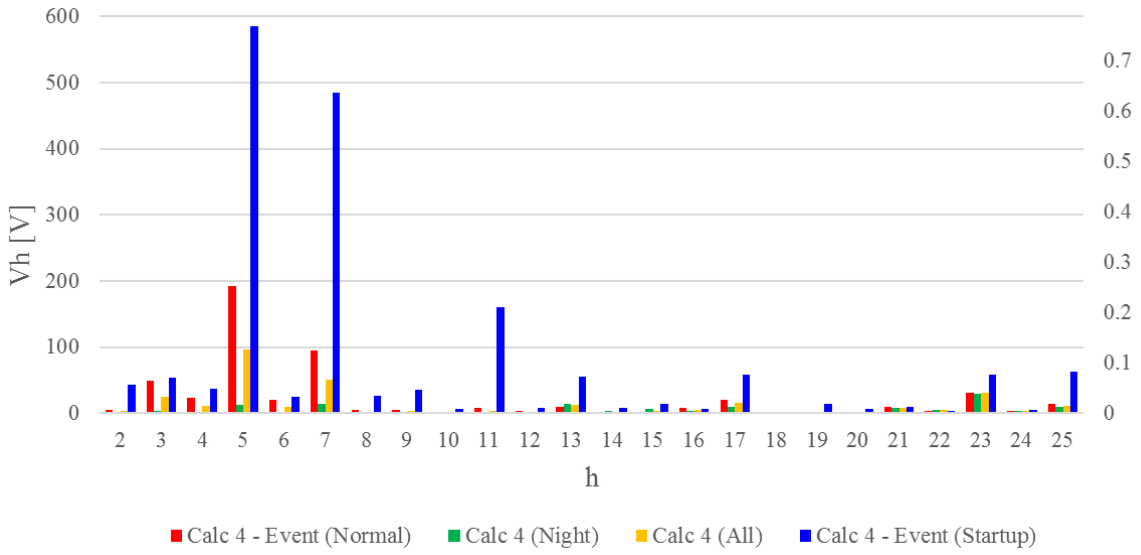

Figure 5-26: Mean harmonic emissions (red phase) – Calculation 4: Harmonic vector method

The trends are similar to the previous methods with dominant 5th and 7th harmonic emissions but some differences are noted in respect of the emissions calculated from the normal events. The 5th harmonic emission is larger than the 7th as opposed to Methods 1 and 2 which calculate the 7th to be larger than the 5th.

The large 3rd and 4th harmonic voltage emissions are not present as for Methods 1 and 2. For the 3rd and 4th orders, the mean value of voltage emissions, especially for the red phase, is affected by a few measurement samples with very high harmonic voltages. The harmonic vector method, which includes the current measurement, discriminates between the PV plant and network contributions. In the case of these points, the network is determined to be the dominant contributor to the emission and the plant emission is calculated to be much smaller than it is by use of methods considering only voltage measurements. This is illustrated in Figure 5-27. The emission by the voltage phasor method (Method 2A), indicated in red, is very large because the measured voltage is much larger than the background harmonic voltage. The harmonic vector method (Method 4) determines the network to be the dominant contributor to this measurement sample and the emission vector, shown in blue, is much smaller than that from Method 2A.

The harmonic vector method shows the 23rd order harmonic emission to have similar magnitude for events during normal operation and at night. This is due to the series resonance present near the 24th harmonic order which establishes the PV plant as having a negative impact on 23rd harmonic distortion at the POC even at times when the inverters are not operating.

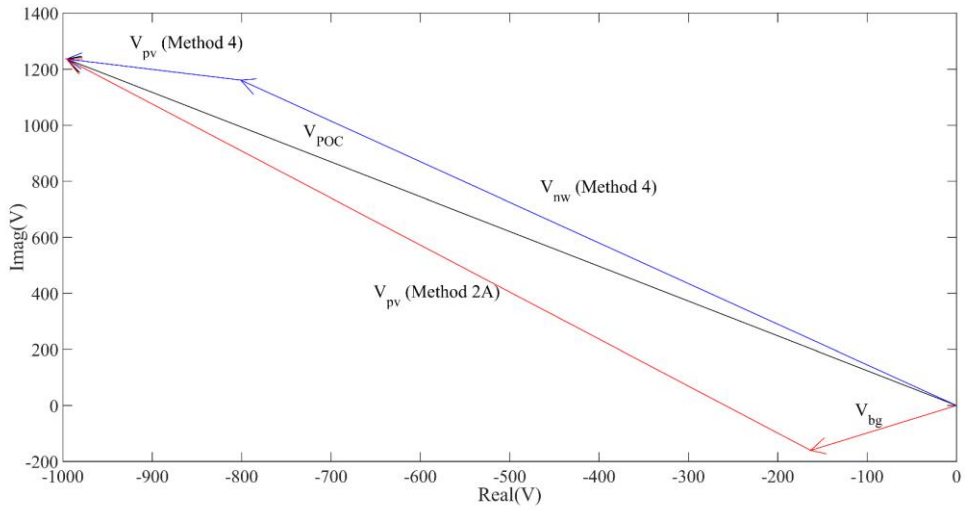

Figure 5-27: 3rd harmonic emission calculation for Event 20 – Comparison of voltage phasor method (Method 2) and harmonic vector method (Method 4)

The fraction of measurement points with V_{pvs} greater than zero shows how often the plant increases the measured emission and how often it has a positive impact in reducing distortion at the POC. The harmonic vector method applies independent calculation for each measurement period and therefore does not require reliable aggregation of phasor angles as required to achieve meaningful results as for the harmonic voltage phasor method. Nevertheless, it is worth investigating the prevalence ratio of the calculated emissions to determine whether phase angle of the emissions vary widely or remain constant over the recording period. These two metrics are presented as a heat map in Table 5-10. For normal events, the PV plant is seen to add to the distortion at the POC for more than 50% of measurement periods at the following harmonic orders: 3, 4, 6, 7, 16, 17 and 21-25. The 3rd, 5th, 7th and 17th harmonic orders show reasonable prevalence in the angle of the calculated emissions. For start-up events, the plant adds to the measured harmonic distortion at almost all harmonic orders.

Table 5-10: Calculation Method 4 Reliability Heatmap

	Normal Events						Start-up Events					
	R		W		B		R		W		B	
2	0.50	0.26	0.15	0.38	0.30	0.45	0.83	0.75	0.93	0.84	0.59	0.88
3	1.00	0.79	0.80	0.90	0.75	0.62	0.93	0.82	0.72	0.74	0.69	0.40
4	0.80	0.47	0.95	0.12	0.85	0.49	1.00	0.85	0.90	0.88	0.93	0.89
5	0.35	0.90	0.30	0.94	0.20	0.89	0.86	0.78	0.86	0.81	0.83	0.85
6	0.80	0.57	0.60	0.46	0.65	0.84	0.93	0.89	0.76	0.78	0.97	0.87
7	0.65	0.80	0.90	0.71	0.95	0.83	0.93	0.99	1.00	0.98	1.00	0.99
8	0.55	0.42	0.50	0.37	0.35	0.25	0.93	0.91	0.69	0.74	0.93	0.91
9	0.35	0.26	0.15	0.33	0.35	0.26	0.76	0.86	0.59	0.86	0.79	0.90
10	0.10	0.48	0.05	0.37	0.25	0.42	0.79	0.60	0.86	0.85	0.83	0.80
11	0.15	0.51	0.20	0.40	0.20	0.39	0.83	0.95	0.90	0.96	0.83	0.94
12	0.30	0.46	0.05	0.14	0.20	0.60	0.72	0.66	0.76	0.71	0.66	0.37
13	0.05	0.73	0.05	0.73	0.15	0.72	0.52	0.80	0.14	0.94	0.28	0.95
14	0.05	0.28	0.05	0.31	0.00	0.30	0.55	0.54	0.45	0.34	0.52	0.51
15	0.00	0.11	0.10	0.29	0.05	0.32	0.28	0.06	0.45	0.42	0.52	0.47
16	0.65	0.55	0.80	0.58	0.90	0.32	0.79	0.22	0.86	0.63	0.86	0.63
17	1.00	0.87	1.00	0.87	0.95	0.90	1.00	0.93	1.00	0.94	1.00	0.96
18	0.45	0.38	0.15	0.08	0.45	0.76	0.76	0.80	0.69	0.80	0.86	0.62
19	0.00	0.19	0.25	0.80	0.05	0.53	0.72	0.42	0.66	0.69	0.76	0.68
20	0.25	0.56	0.35	0.28	0.15	0.65	0.86	0.47	0.72	0.72	0.48	0.47
21	0.85	0.78	0.70	0.60	0.70	0.29	0.90	0.72	0.90	0.59	0.93	0.74
22	0.55	0.11	0.25	0.13	0.60	0.53	0.66	0.17	0.83	0.81	0.83	0.74
23	1.00	0.51	1.00	0.12	1.00	0.64	1.00	0.68	1.00	0.78	1.00	0.70
24	1.00	0.38	1.00	0.30	1.00	0.53	1.00	0.76	1.00	0.66	0.97	0.41
25	1.00	0.31	1.00	0.18	1.00	0.30	1.00	0.95	1.00	0.90	1.00	0.94

Fraction of $V_{pvs} > 0$
(Left half of cell)
- <0.25
- 0.25 to 0.5
- 0.5 to 0.75
- >0.75

$PR_{agg,h}$ of V_{bg}
(Right half of cell)
- < 0.7
- 0.7 to 0.8
- 0.8 to 0.89
- 0.89 to 0.95
- *>0.95*

5.6.5 Calculation method 5: Harmonic load flow simulation

As a comparative assessment, the results of a harmonic load flow simulation using the DIgSILENT PowerFactory PV plant model are presented. The development and parameterisation of the model is described in Chapter 3. The inverters were modelled as harmonic current sources based on the manufacturer's quoted harmonic current emissions which are shown in Figure 5-28 for operation at rated inverter power. The external network was modelled as a frequency-dependent impedance according to the frequency sweep data provided by the utility.

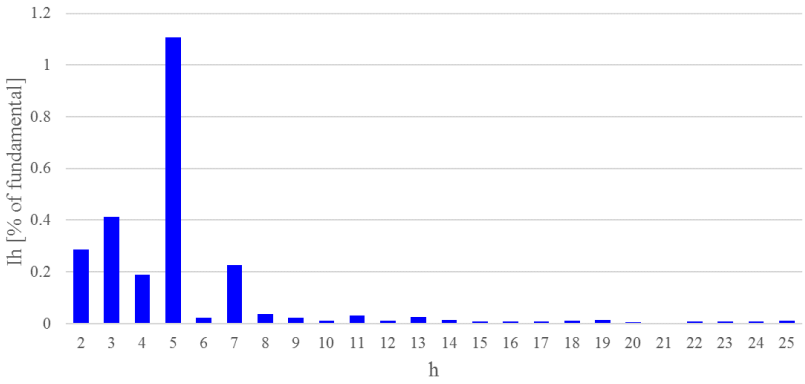

Figure 5-28: Inverter harmonic current emissions

The harmonic emissions at the POC were calculated by harmonic load flow simulation according to two methods:

- IEC 61000-3-6 method with application of the general summation law
- Phase correct method

Since the phase angle of the harmonic currents is unknown, the angle is set to zero for all harmonic sources. Since all inverters and inverter transformers are identical, this results in an approximately direct summation of

the currents from the individual inverters and represents a worst-case emission. The balanced phase-correct simulation results in perfect cancellation of triplen harmonics by transformer delta windings resulting in zero triplen voltage harmonic emissions at the POC. The results of the simulation are shown in Figure 5-29.

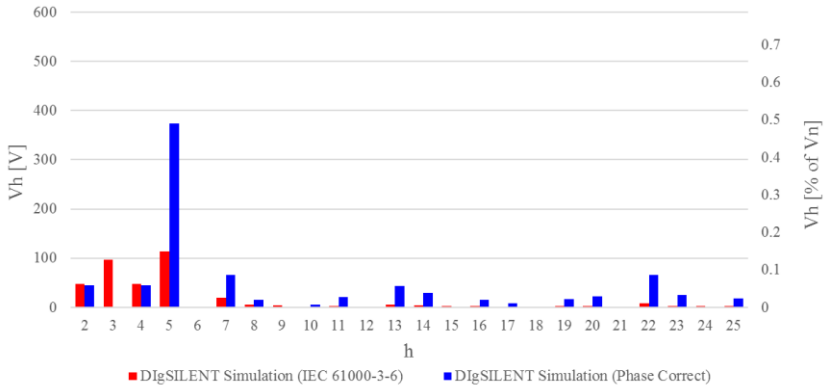

Figure 5-29: Simulated PV plant harmonic voltage emissions at the POC

For harmonics orders 2 to 4, the results of the two methods are similar since the summation exponent of 1 equates to direct summation for the IEC 61000-3-6 method. The dominant 2nd, 3rd, 4th, 5th and 7th harmonics are represented in the output voltage whilst there appears to be some amplification around the 13th and 22nd harmonics. As described in section 3.6.6, the frequency sweep at the inverter terminals presents a parallel resonance at the 22nd harmonic order which explains the amplification around the 22nd harmonic order.

5.6.6 Comparison of calculation results for dominant harmonic orders

The results of various calculation methods described in the literature have been presented in the preceding sections. The 5th and 7th harmonic orders are consistently seen to be dominant orders with significant emission magnitudes and reasonable prevalence of phase angles across a range of event-triggered measurement samples. The magnitudes of the calculated red-phase 5th harmonic voltage emissions for normal plant operation are compared in Figure 5-30. There is a wide variation in the calculated values. As discussed, the plant appears to reduce the 5th harmonic voltage distortion at the POC by active filtering effects. Methods 1B, 1C and 2B consider the mean performance of the plant and evaluate the plant's 5th harmonic emission contribution as zero.

Although emissions for Method 3A and 3B are shown, evaluation of the scatterplot trends show that the plant has an active filtering effect and these can also be taken as zero. For Method 2A and Method 4, emissions for individual measurements are set to zero for periods where the plant is not contributing to the emission. However, there are still periods where the plant is found to contribute to the measured distortion. Therefore, although there are many zero emission points, the remaining points still give some plant contribution when the values are averaged. Given the limited number of event data points for evaluation, it is possible that the emission contribution is exaggerated and that a larger, more representative measurement set would yield a lower emission. The simulation software does not represent the interaction of the network voltage and the inverter control and the emissions calculated by means of harmonic load flow methods are not representative of the actual performance.

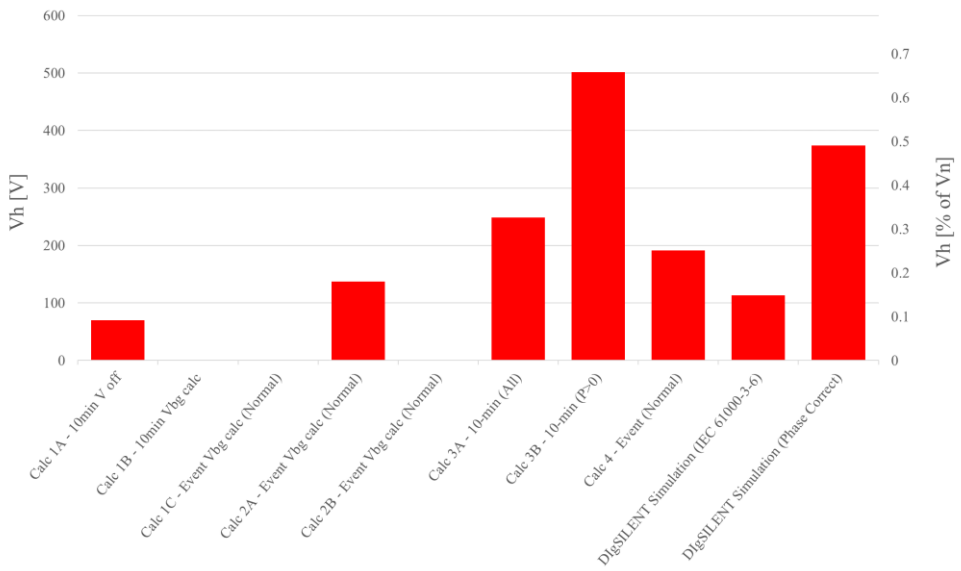

Figure 5-30: Comparison of calculation methods for normal operation (h = 5, Red phase)

For start-up events, by comparison, the plant is clearly a source of 5th harmonic voltage distortion. The red phase emissions calculated by the presented methods have similar magnitudes, although the harmonic vector method shows a higher contribution than the other methods. The results are shown in Figure 5-31.

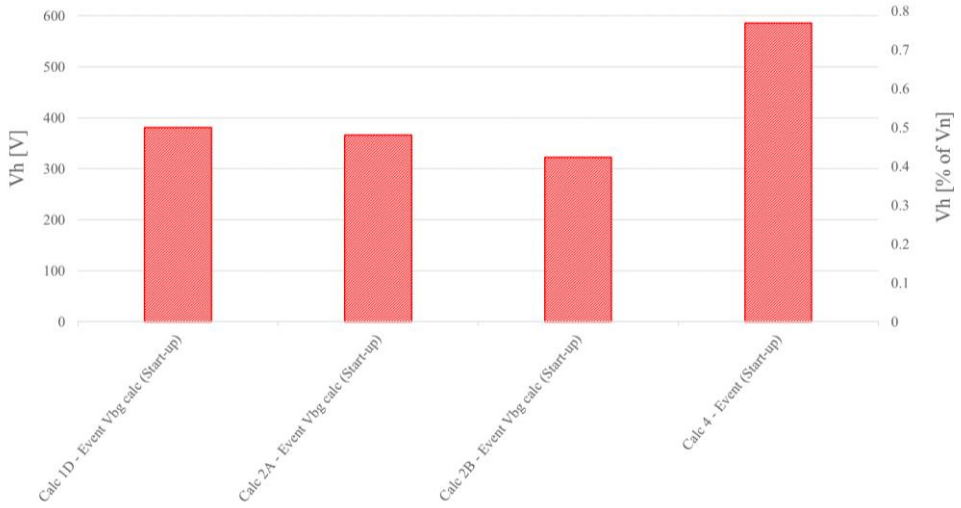

Figure 5-31: Comparison of calculation methods for start-up operation (h = 5, Red phase)

The results for the red-phase 7th harmonic emission contribution are compared in Figure 5-32. All methods show that the plant is a dominant contributor to the measured distortion although the calculated measurement magnitude does show significant variation. The harmonic load flow simulation according to IEC 61000-3-6 significantly underestimates the plant contribution and it appears that there is insufficient phase angle diversity between inverters to justify use of an alpha summation exponent of 1.4. Event the phase-correct method seems to underestimate the distortion as the simulation represents maximum emission whilst the calculation methods represent the mean emission.

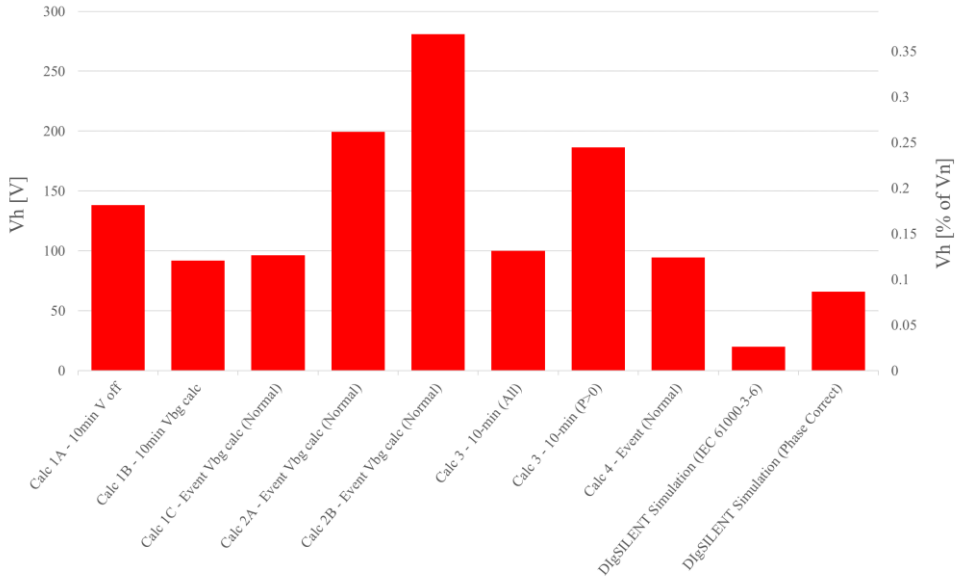

Figure 5-32: Comparison of calculation methods for normal operation (h = 7, Red phase)

A larger contribution is calculated for start-up events than for normal operation. Figure 5-33 shows that the voltage phasor calculation and harmonic vector calculation methods yield similar results for start-up events.

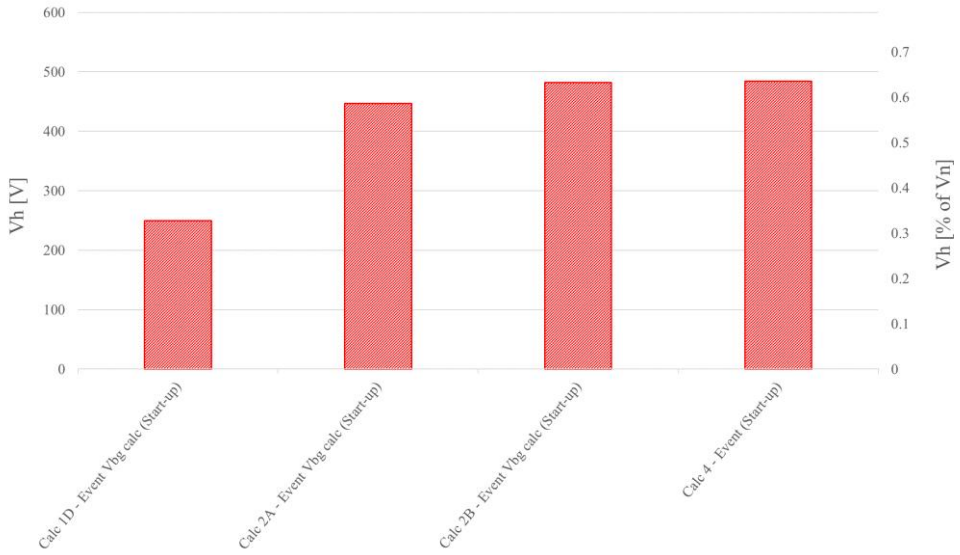

Figure 5-33: Comparison of calculation methods for start-up operation (h = 7, Red phase)

Comparison of the calculation results for the white and blue phases of the 5th and 7th harmonic orders are included in Appendix D.5 in plots which show comparison of mean, 75th percentile and 90th percentile emissions.

5.6.7 Comparison of mean, 75th percentile and 95th percentile emissions

In the comparative assessment described above, the mean values of emissions have been considered for all analyses. It is common in evaluation of harmonic distortion, particularly in the assessment of compliance to prescribed limits, to assess the 95th percentile, 99th percentile or other percentile values rather than the mean value; this provides a measure of maximum distortion which excludes periods with high harmonic distortion

at the edge of the normal probability distribution. Given the small sample size of waveform data (20 to 30 samples per group), it is not appropriate to consider the 95th percentile in this study as it does not exclude outliers in the data as intended. Therefore the 75th percentile and 90th percentile harmonic emissions are considered.

The mean, P75 and P90 harmonic voltage emissions for the red phase 5th and 7th harmonics are compared in this section, since these harmonics are dominant and demonstrate reasonable angle prevalence ($PR_{agg,h} \geq 0.8$). Results for all three phases of the 5th and 7th harmonics are included in Appendix D.5. In cases where the background harmonic emission is calculated (Methods 1 and 2), the same criterion is applied in calculating the background emission and the final emission, e.g. 75th percentile emission is assessed using the 75th percentile background harmonic voltage and 75th percentile operating voltage.

Figure 5-34 compares the mean, P75 and P90 5th harmonic voltage emissions. The harmonic voltage phasor method (Method 2A) and harmonic vector methods (Method 4), consider emissions to be zero for periods when the plant has a positive impact on harmonic distortion at the POC. Due to the plant's action in reducing the 5th harmonic voltage during operation, many emission points are assessed as zero and the 75th percentile value is less than the mean. The 90th percentile is very large because it is affected by a few outlying points. In a more representative dataset of long-term phasor measurements there may be a lower percentage of outliers, in which case the voltage distortion calculated as a 90th or 95th percentile assessment would be low, or even zero. Considering the IEC 61000-3-6 scatter plot method (Method 3), the assessed emission increases from the mean to the 75th to the 90th percentile. The positive impact of the plant is not evident from the calculation and would need to be motivated by evaluation of the relationship between harmonic voltages and currents.

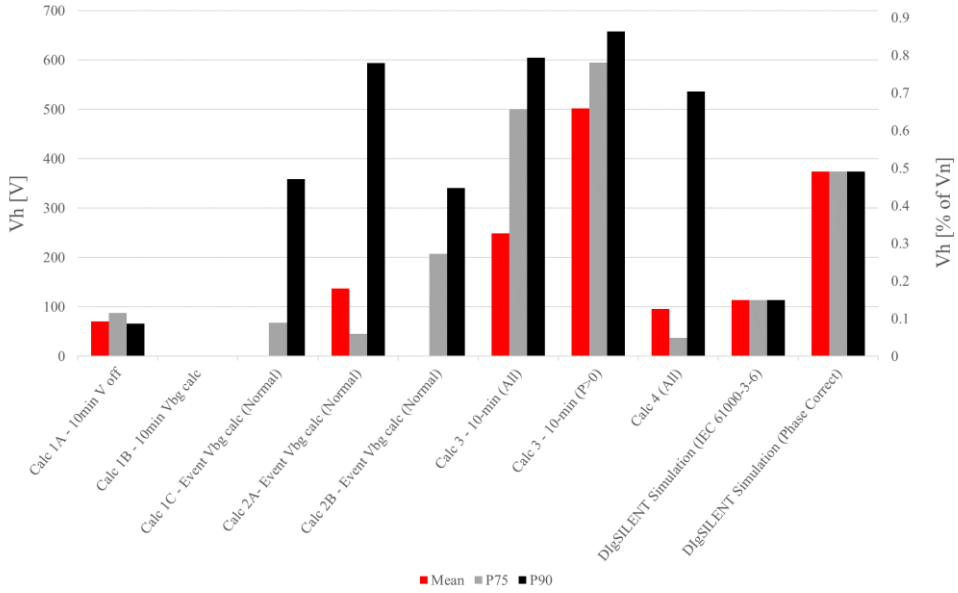

Figure 5-34: Comparison of mean, P75 and P90 emissions calculations for normal operation (h =5, Red phase)

By comparison, as shown in Figure 5-35, the voltage distortion increases for Methods 2A and 4 from the mean to the 75th to the 90th percentile for start-up events since the plant is a dominant source of 5th harmonic distortion during start-up.

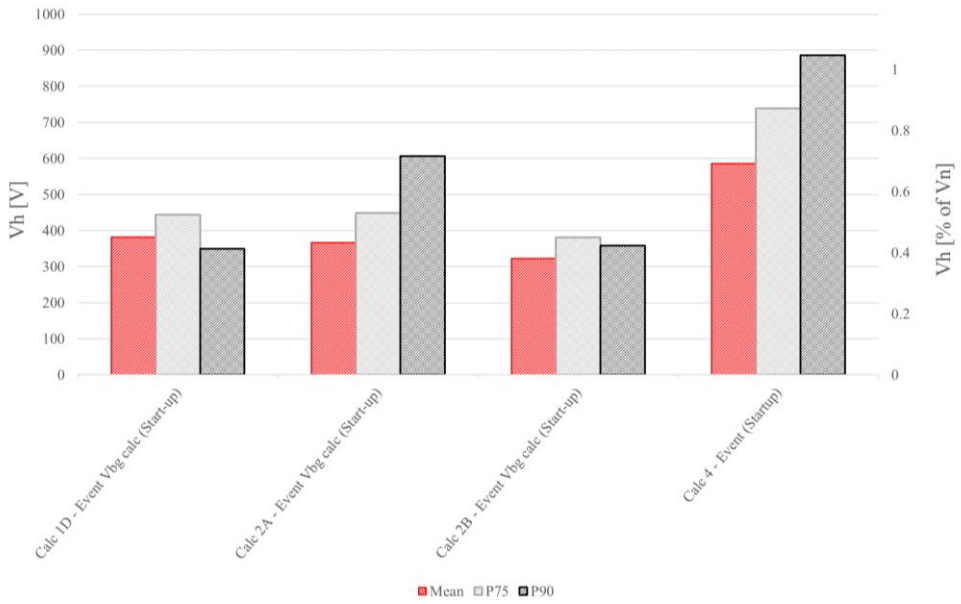

Figure 5-35: Comparison of mean, P75 and P90 emissions calculations for start-up operation (h =5, Red phase)

Considering the 7th harmonic results, shown in Figure 5-36 and Figure 5-37 for normal and start-up operation respectively, the emissions increase for almost all assessed methods from mean to P75 to P90. For normal operation, the 90th percentile voltages have a similar magnitude of approximately 200 V for all methods except the harmonic voltage phasor methods (Method 2A and 2B). As mentioned in section 5.6.2, the assessed emission using Method 2 is large because of the phase angle difference between the background voltage phasor and the emission phasors during operation. Harmonic load flow simulations underestimate the voltage emissions contribution. This may be due to higher current emissions from the inverters than those established in type tests due to the distorted network voltage [16] [78] [79]; current measurements at the inverter terminals should be captured to confirm this hypothesis.

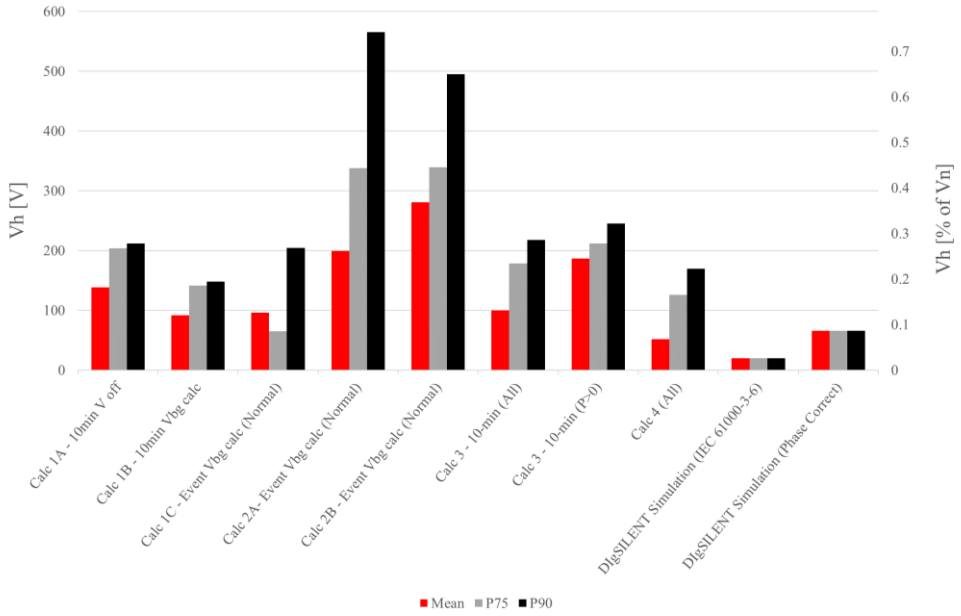

Figure 5-36: Comparison of mean, P75 and P90 emissions calculations for normal operation (h =7, Red phase)

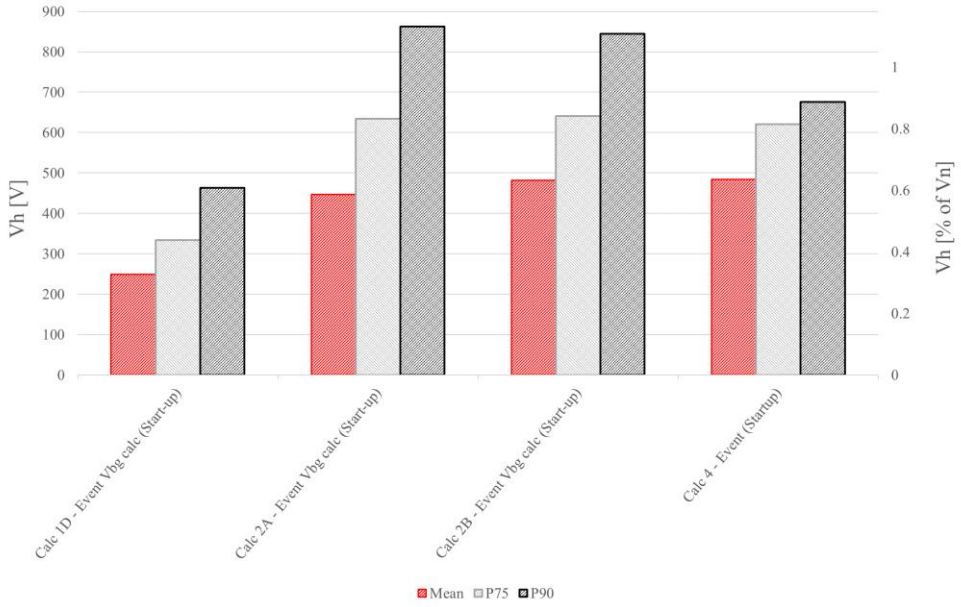

Figure 5-37: Comparison of mean, P75 and P90 emissions calculations for normal operation (h =7, Red phase)

For start-up periods, all methods of assessment show increasing emissions magnitudes from mean to P75 to P90. The magnitudes of emissions calculated by the harmonic voltage phasor and harmonic vector methods (Methods 2A, 2B and 4) are similar for mean and 75th percentile values with the 90th percentile of the Method 4 slightly lower than Methods 2A and 2B.

The results for the 7th harmonic show that different methods offer reasonable alignment in their calculated results based on a percentile evaluation in cases where the plant is the dominant source of the harmonic emission. The results for the 5th harmonic show the difficulty in assessing an emission where the PV plant is not the dominant source. In this instance, the harmonic vector method appears to provide the most reliable assessment.

6 Conclusions and recommendations

6.1 Introduction

In this chapter, conclusions are drawn with reference to the research objectives listed in section 1.3.1. Each objective is discussed considering the relevant results and research outputs from the previous chapters. The conclusions are followed by recommendations for further research.

6.2 Conclusions

6.2.1 Overview

The research set out to investigate the harmonic behaviour of a utility-scale PV plant based on network modelling and statistical analysis of harmonic voltage and current measurements captured at the plant's POC. The research was motivated by the increasing number of large PV plants – both globally and in South Africa – and the difficulties experienced in evaluating the harmonic emission contribution of such plants to determine their harmonic impact and to assess their compliance with prescribed emission limits.

The remainder of this section discusses conclusions drawn with reference to the original research objectives.

6.2.2 Development of a harmonic simulation model of a solar PV plant and evaluation of the frequency response of the plant using the model

A literature review was conducted to establish the recommended methods for harmonic modelling of the network elements from which the PV plant is constructed. Based on the recommendations of the IEEE Task Force on Harmonics Modelling and Simulation, the nominal pi representation was found to be adequate to model cables for simulations in the harmonic frequency range of 50 to 2500 Hz for both the simplified model and the full plant model [51]. Transformers are modelled as T-equivalent circuits with HV and LV winding capacitances and winding-to-winding capacitances included due to their impact on high frequency response [53] [51]. Since the capacitance values for the transformer were not available, a parameter estimation method was applied to determine their approximate values [156]. Core magnetising and saturation effects were ignored since harmonic generation by the transformer is not of primary interest in the investigation.

The simplified model illustrated in Figure 3-1 was considered to aid in understanding of harmonic mechanisms in a typical PV plant. The model is a two-terminal circuit, with the HV POC terminal and LV inverter terminal considered as injection points for evaluation of the harmonic impedance. A full network model of the PV plant was developed considering the as-built configuration of the plant and the manufacturer's data for the installed equipment. The utility network was represented as a complex positive sequence impedance based on an impedance sweep provided by the utility and, alternatively, as a linear inductive network with impedances based on the minimum and maximum fault levels provided by the utility for the POC busbar.

It was not possible to develop a detailed model to represent the solar inverters due to the lack of available inverter data. Therefore, a simple current source model with infinite impedance was considered [98]. Other methods proposed in the literature considering Norton representations or more complex equivalent circuit models [53], analytical models [98], average circuit models [125] [126] and linear equation models [16] all require varying degrees of information related to the inverter topology and / or control strategy which were not available from the inverter manufacturer and could not be determined experimentally from the available measurement data.

The harmonic impedance of the simplified, aggregated plant was evaluated from the POC and the inverter with the opposite terminal alternatively open and short circuited. From both ends, the open-circuit frequency sweeps exhibit a minor parallel resonance at 70 Hz and a series resonance in the 2 - 3 kHz range. The short-circuit sweeps exhibit a single parallel resonance at the upper end of the harmonic frequency range and higher-frequency series and parallel resonances.

The same methodology was applied to the evaluation of the frequency response of the full network model of the PV plant. Similar mechanisms of resonance were observed for the full model, although the resonant frequencies were significantly different in some instances. In all cases, the key resonance points shifted to lower frequencies than those observed in the simplified, aggregated model, with a series resonance presenting at 1.22 kHz (h = 24.4) for all frequency sweeps at the plant POC with or without the equivalent utility network. The short-circuit frequency sweeps of the full model present one parallel and one series resonance in the harmonic frequency band. The harmonic impedance at the inverter terminals with the equivalent utility network connected is largely linear and inductive but exhibits a minor parallel resonance at 2.2 kHz followed immediately by a minor series resonance.

Differences between the response of the full model and the simplified aggregated model could be explained primarily by three differences:

- Aggregation of the inverter transformers in the simplified model results in current injection from the inverter terminal through 40 parallel transformers instead of a single transformer for each inverter in the full model.
- The cable capacitance of the cable network in the full model is larger than that of the aggregated model, resulting in a higher shunt capacitance.
- The MV collector network voltage in the aggregated model is 22 kV and in the full model it is 33 kV which impacts on the magnitude of impedances when they are referred from the primary to the secondary side of the transformers or vice versa.

6.2.3 Quality assessment of harmonic measurement data captured at a utility-scale PV plant

Data measurements were captured over a 12-day period at the POC of a 75 MW single-axis tracking PV plant in the Northern Cape province of South Africa according to the IEC 61000-4-7 and IEC 61000-4-30

methodologies. 10-minute aggregated measurements and 3-second aggregated measurements of 3-phase harmonic voltage and current up to the 50th harmonic order were available for the full period, representing operational and non-operational (night-time) measurement periods. 10-minute and 3-second voltage harmonic measurements with the plant disconnected were also available from a 10-hour night-time shutdown of the facility when the plant was disconnected from the network by opening of the POC circuit breaker. Additionally, voltage and current waveforms were captured for 70 events over a 15-day period from 09/04/2015 to 23/04/2015, where these events were triggered by rms voltage changes exceeding 3%.

Evaluation of the data revealed the magnitudes of signals above the 25th order to be zero, or near zero, for the full recording period. Therefore, the author decided to focus the data quality assessment on harmonic orders 2 to 25. Analysis of the 10-minute data revealed that, due to the small magnitude of the measured signals, the accuracy of measurements is likely to have been significantly affected by the measurement instruments. This is especially true for even harmonics above the 6th order and all harmonics above the 15th order. The primary source of error in harmonic voltage measurements is quantisation error due to the resolution of the 16-bit A/D converter of the selected power quality meter despite its IEC 61000-4-30 certification; transducer error may also have an effect on voltage measurement accuracy. Quantisation effects were less significant in the current measurement data but it is likely that transducer error introduced by the HV current transformers and clamp-on current transducers used in the temporary metering installation affected the accuracy of current measurements.

Comparison of 3-second aggregated data to 10-minute aggregated data revealed limited fluctuation within a typical 10-minute period such that the 10-minute data is considered to be representative of both the short-term and long-term behaviour of the plant. One exception to this is that significant fluctuation at certain harmonic orders was observed in the early morning and late afternoon during the periods when the plant was starting-up or shutting down.

Waveform data was processed using cross correlation methods to extract 72 time-invariant waveform segments of durations varying between 20 cycles and 100 cycles. These waveforms were processed using FFT analysis to extract the harmonic phasor components. Based on assessment of fundamental frequency active and reactive power, the events were classified as occurring during normal operation, start-up operation or non-operational periods. Start-up period recordings all occurred between 06h30 and 08h30 and are characterised by high reactive power and low active power magnitudes.

Based on the data quality assessment, the data were found to be suitable for analysis of low order harmonic phenomena for odd harmonics up to the 15th harmonic order and for even harmonics up to the 6th order. The data were also considered suitable to identify harmonic trends for higher order harmonic behaviour for all even and odd harmonics up to the 25th harmonic order. 10-minute data were considered adequate for statistical analysis of harmonic phenomena except in cases where specific phenomena warranted investigation using the 3-second data.

6.2.4 Investigation of the harmonic behaviour of the PV plant based on trends in the recorded harmonic voltages and currents under different operating conditions of the plant

Scatter plots and data binning techniques were used to determine the relationship between the harmonic voltage and current emissions of the plant and the plant active and reactive power outputs at the POC. Harmonic voltage distortion was found to increase with increasing active power generation for the 7^{th}, 9^{th}, 11^{th} and 15^{th} harmonic orders and to decrease with increasing active power for the 5^{th} and 17^{th} harmonic orders. The harmonic current distortion was found to increase or remain constant with increasing active power for all harmonic orders. The 5^{th} and 7^{th} harmonic currents are dominant when the plant is operating with the 5^{th} harmonic current increasing linearly and the 7^{th} harmonic current remaining almost constant across the range of active power outputs. Since the 5^{th} harmonic voltage decreases with increasing 5^{th} harmonic current, it appears that the inverters have an active filtering effect for 5^{th} harmonic distortion.

The relationship between harmonic voltage and current distortion and plant reactive power was less clear. It was noted that the 5^{th} and 17^{th} harmonic voltage distortion increase with increasing reactive power while the 7^{th} harmonic voltage distortion decreases. This is opposite to the variation of these harmonic voltages with active power but, since the plant operates in voltage control mode, there is an approximately linear decrease in reactive power output with increasing active power. It is therefore not possible to evaluate the relative influence of active reactive power on the POC harmonic distortion due to their interdependency. No clear relationship between harmonic current emissions and reactive power output was evident.

Variation of harmonic emissions with time of day was investigated using both 3-second values for their superior temporal resolution and 10-minute values for their averaging effects, which reduce the number of data points and spread of the data thus emphasising periods of high and low emissions. Of the dominant harmonic orders, the 5^{th} harmonic voltage decreases during operation accompanied by an increase in 5^{th} harmonic current. The 7^{th} harmonic voltage and current both increase during operation. Considering the 3-second data, several harmonic orders show peak harmonic currents during start-up and shutdown periods of the plant. Authors of several papers, including [12], describe changes in inverter behaviour during periods of low irradiance. Considering, also the large reactive power outputs observed from waveform recordings during start-up periods, inverter behaviour is surmised to be primarily responsible for this behaviour. However, it is also possible that the operation of the motor drives which operate the plant's tracker system generate additional harmonics as they operate to position all of the PV panels to face towards the sun in the morning and return them to a flat position in the evening.

6.2.5 Comparative analysis of different methods of assessing the harmonic emissions contribution of the PV plant

The mean harmonic contribution from the PV plant was assessed using the harmonic measurement data according to the following four methods:

1. Reverse application of the general summation law

2. Harmonic voltage phasor method
3. IEC 61000-3-6 long-duration simultaneous measurement of harmonic voltages and currents
4. Harmonic vector method

The emissions were also simulated using the DIgSILENT PowerFactory PV plant model.

The first two methods required a background harmonic voltage to be defined to enable the calculation of the emission contribution based on the difference between operational and background periods. Different methods were considered in the calculation of the background voltage distortion. Linear regression of harmonic voltage versus PV plant apparent power [58] was tested but found to be unreliable due to significant dispersion of the data resulting in poor fit of the linear approximation as assessed by the coefficient of determination and visual inspection of the results.

Background voltage is therefore assessed from 10-minute values as

1. mean harmonic voltage for the 10-hour period when the plant was disconnected,
2. mean harmonic voltage for periods when the plant was not operating (i.e. $P < 0$) and
3. calculated background voltage based on the mean harmonic voltage for periods when the plant was not operating but considering the effect of the voltage divider circuit formed by the harmonic impedances of the network and PV plant in the equivalent circuit representation of Figure 5-1.

The latter two assessments were also applied to voltage phasors from events recorded during non-operational periods.

The trend from all methods of background voltage assessment was similar with the 3^{rd}, 5^{th}, 7^{th} and 11^{th} harmonic voltages dominant in the network. The measurements with the plant disconnected are generally lower than those with the plant connected which may be partly due to the larger sample size of data with the plant connected but not operational. It also aligns with the expected voltage divider effect of the predominantly inductive utility network and the capacitive PV plant causing an amplification of the background voltage at the POC when the plant is connected.

The calculated background harmonic voltage was selected as the base case for the emission contribution assessment as it considers the impact of the network and PV plant harmonic impedances and is based on a more statistically reliable sample of measurements. Furthermore, a background level for event data could be calculated using the same methodology allowing for consistency in the analysis of 10-minute data and event data. Background voltages assessed using event data were similar to those from the 10-minute data for most characteristic harmonics but the magnitude of even and higher order harmonic voltages were greater for event data; this may be attributed to the smaller sample of events, the averaging effects in the 10-minute periods and the event-triggered nature of the waveform recordings.

The mean harmonic current during non-operational periods was evaluated and exhibits dominant 5th and 7th components as expected from the background voltage levels. However, it also exhibits large 23rd and 25th harmonic components compared to very small corresponding background voltages. This is consistent with the plant presenting a low impedance around the 24th harmonic order as predicted by the series resonance in the simulation frequency sweeps.

Reverse application of the general summation law identifies the plant as contributing to the 7th and 13th harmonic voltage distortion during normal operation and having a significant contribution at many orders, including the characteristic 5th, 7th, 11th and 13th orders, during plant start-up.

Two variations of the harmonic voltage phasor method were applied to phasors calculated from the waveform data. Normal and start-up events were considered separately. In the first instance, Method 2A, emissions were calculated using phasor subtraction of the background voltage from each measured event voltage with the results averaged to determine the mean emission contribution. Method 2B averaged the measured voltages to produce a single phasor representing the mean POC harmonic voltage during operation (normal or start-up). The emission is calculated by vector subtraction of the background voltage phasor from this mean phasor. Method 2B aligns more closely with the trends from Method 1 in evaluating zero emissions contribution for the 5th, 11th and 17th whereas Method 2A assigns some contribution to the plant at these orders.

Shortcomings of the Method 2A and 2B and their application to the available data were noted. Method 2A can only be considered valid where the background harmonic voltage angles exhibit sufficient prevalence that the aggregated background harmonic phase angle has acceptable uncertainty as evaluated by means of the prevailing ratio [158]. Method 2B additionally requires sufficient angle prevalence of phasors from normal and start-up operation. Considering the available event data, only the 5th, 7th (red phase), 11th and 17th order phasors exhibit a sufficiently high prevalence ratio. A further shortcoming of this method is that, in the case that the measured and background voltages have similar magnitudes but significantly different phase angles, the emission could be evaluated as zero if the magnitude of the measured voltage is marginally smaller than that of the background voltage but be evaluated as a large voltage contribution if the magnitude of the measured voltage is increases to be marginally larger than the background voltage.

Scatter plots of 10-minute harmonic voltage vs current were evaluated in Method 3 to determine whether clustering of measurement data around lines representing the harmonic impedance of the network or PV plant could be used to determine the dominant source of the harmonic emission. None of the plots exhibited definitive clustering around a single impedance line. In separating the operational and non-operational periods, the network appears to be the dominant source of 7th harmonic distortion at night and the PV plant dominant during the day. Mean distortion was assessed using Ohm's law based on the mean harmonic current and the network impedance. The accuracy of the calculated results is therefore dependent on the accuracy of the frequency sweep provided by the utility.

Mean currents were calculated based on all current measurements and on current measurements during periods of operation only. In general, the emission contribution is much higher considering only operational periods but the 15th and 23rd harmonics are exceptions to this rule. The results show that this method is more suitable for evaluation of 95th percentile emissions to properly account for behaviour during both operational and non-operational periods. The method has the advantage of not requiring any background voltage measurement but it assumes that the PV plant is fully responsible for the harmonic current measured at the POC unless it can be proven otherwise by evaluation of scatter plots or other methods.

Next the emission contribution was assessed from voltage and current phasors using the harmonic vector method (Method 4). The method relies on accurate estimates of the utility and PV plant network impedances. The method uses harmonic voltage and current measurements taken at the POC and does not require knowledge of the background harmonic. The method also does not require angle prevalence as the contribution is calculated per measurement phasor and the mean emission contribution assessed as the mean of the resulting phasor magnitudes.

Assessment was carried out for normal events, start-up events and night-time events. The 5th and 7th harmonic contributions are dominant. Significant emission contributions observed for the 2nd and 3rd harmonics from evaluation of normal events are attributed to the network, whereas these are attributed to the plant by Methods 1 and 2. Also, the 23rd order voltage emission caused by the plant's series resonance is attributed to the plant for both daytime and night-time periods. This is correct since the plant is responsible for altering the harmonic impedance and thereby amplifying the voltage distortion at the POC.

Finally, results of DIgSILENT PowerFactory harmonic load flow simulations considering the inverters as the only source of harmonic distortion were presented. Simulation according to the IEC 61000-3-6 general summation law appears to underestimate the distortion caused by the plant, especially at the 7th harmonic order. This is probably because of limited phase angle diversity in the harmonics generated by identical inverters throughout the plant. Even the phase-correct simulations appear to underestimate 7th harmonic contribution, possibly because of increased inverter emissions in the presence of network voltage distortion. The simulations also show a significant 22nd harmonic voltage distortion which aligns with the parallel resonance observed in the frequency sweep at the inverter terminals with the utility network sweep connected at the POC. In reality, 22nd harmonic distortion appears to be negligible.

Comparative analysis of the different methods for determining the emissions contribution of the plant show similar trends in respect of identifying dominant harmonics and general behaviour. However, the magnitudes of the calculated emissions do differ between the methods, quite significantly in some instances. Comparison of the mean, 75th percentile and 95th percentile emissions assessments demonstrate the effectiveness of percentile assessment in eliminating outlying high distortion periods from the assessed results.

The harmonic impedance representation of the PV plant appears to be representative considering that the only series resonance present in the simulation sweep in the assessed range below 1250 Hz could be identified by

the increased 23rd and 25th harmonic currents measured at the POC. If similar confidence can be placed in the impedance sweep provided by the utility, based on their detailed network model, then the harmonic vector method appears to be a simple and robust method for the assessment of harmonic emissions where harmonic phasor data are available. The method is able to discriminate between utility and PV plant contributions better than the other evaluated methods.

Where no phasor data are available, the IEC 61000-3-6 long-duration simultaneous measurement of harmonic voltages and currents is the simplest method to apply. The first two methods assessed are problematic in their need to establish a level of background distortion against which the plant emissions can be assessed. Harmonic emission assessment by simple harmonic load flow simulation is not recommended due to the difficulty of representing the complexities of active sources and harmonic interactions which occur within the real power system.

6.3 Recommendations

The research gives rise to several recommendations for further work, including the following:

- The quality assessment of the measurement data highlighted concerns related to measurement accuracy in the captured harmonic voltage and current data due to the small magnitude of the measured signals. Further work is required to quantify the error introduced by transducers and to consider methods of improving the metering methodology to reduce the level of error.
- Waveform data was captured using event-triggered waveform recordings. The author is concerned that the power system events which triggered the recordings may have introduced long duration transient harmonics which are not representative of the PV plant normal operation. Furthermore, only a relatively small number of waveform recordings were available to perform any analyses which required harmonic phasor quantities. It is recommended that waveform recordings be captured at set time intervals over a period of several days to obtain a more representative sample. Alternatively, short aggregated measurements, for example 1-second measurements, should be captured with prevailing phase angles. This will provide a statistically representative dataset for more rigorous testing of the harmonic voltage phasor and harmonic vector methods.
- Harmonic measurements should be captured while the active and reactive power output of the plant are varied independently to determine the relative impact of each of these parameters on the harmonic performance of the plant.
- The plant start-up phenomena should be investigated in more detail. Rapid changes in reactive power were observed in the 3-second plots. Hence, harmonic phasor data with temporal resolution higher than 3 seconds over one or more complete start-up periods is recommended for the analysis. Further data regarding the inverter topology and control philosophy as well as the PV plant operating philosophy in respect of control of the PV panel tracking mechanisms is required to provide insight into the mechanisms behind the high harmonic distortion observed during plant start-up. Detailed data on the inverter control

and operation would also enable further work into developing a more accurate inverter model and hence a PV plant model which better approximates the harmonic emissions of the plant under different operating conditions.

- The research assumes that the frequency sweep data provided by the utility for the POC is accurate since very little data pertaining to the utility network in the region of the POC was available. Verification of the frequency sweep and a sensitivity analysis to determine whether it is likely to change during different network loading or operating conditions would be beneficial to confirming the validity of the study results.
- The analysis should be extended to other utility-scale PV plants. The analysis of measurement data was limited to the data from a single PV plant. Similar analysis should be applied to data from other PV plants to tests the generic applicability of the observed behaviour.

7 References

[1] International Energy Agency, “Technology Roadmap – Solar Photovoltaic Energy,” International Energy Agency, 2014.

[2] S. Gonzalez, M. Ropp, A. Fresquez and M. Montoya, “Multi-PV Inverter Utility Interconnection Evaluations,” in *37th IEEE Photovoltaic Specialists Conference*, Seattle, 2011.

[3] A. Eberhard, J. Kolker and J. Leigland, “South Africa’s Renewable Energy IPP Procurement Program: Success Factors and Lessons,” Public-Private Infrastructure Advisory Facility (PPIAF), 2014.

[4] J. Enslin, “Network Impacts of High Penetration of Photovoltaic Solar Power Systems,” in *Power and Energy Society General Meeting*, Minneapolis, 2010.

[5] J. R. Oliva, J. C. Balda, D. W. McNabb and R. D. Richardson, “Power-quality monitoring of a PV generator,” *IEEE Transactions on Energy Conversion*, vol. 13, no. 2, pp. 188-193, 1998.

[6] J. Arrillaga and N. R. Watson, Power System Harmonics, 2nd ed., New York: Wiley, 2003.

[7] D. Patel, R. K. Varma, R. Seethapathy and M. Dang, “Impact of wind turbine generators on network resonance and harmonic distortion,” in *23rd Canadian Conference on Electrical and Computer Engineering*, Calgary, 2010.

[8] NRS 048-2:2007, “Electricity Supply – Quality of Supply. Part 2: Voltage characteristics, compatibility levels, limits and assessment methods”.

[9] D. Lowe, R. Waddell and M. McGranaghan, “Utility Perspective on Applying Harmonic Limits for Customers,” in *IEEE Transmission and Distribution Conference and Exhibition*, Dallas, 2006.

[10] S. M. Halpin, “Harmonic limit compliance: issues associated with harmonics modeling and simulation,” in *IEEE Power Engineering Society Summer Meeting*, Seattle, 2000.

[11] “Grid Connection Code for Renewable Power Plants (RPPs) Connected to the Electricity Transmission System (TS) or the Distribution System (DS) in South Africa. Version 2.8”.

[12] A. Chidurala, T. K. Saha, N. Mithulananthan and R. C. Bansal, "Harmonic Emissions in Grid Connected PV Systems: A Case Study on a Large Scale Rooftop PV Site," in *IEEE PES General Meeting*, National Harbor, 2014.

[13] A. R. Oliva and J. C. Balda, "A PV Dispersed Generator: A Power Quality Analysis Within the IEEE 519," *IEEE Transactions on Power Delivery*, vol. 18, no. 2, pp. 525-530, 2003.

[14] M. Ayub, C. K. Gan, A. Fazliana and A. Kadir, "The Impact of Grid-Connected PV Systems on Harmonic Distortion," in *IEEE Innovative Smart Grid Technologies - Asia*, Kuala Lumpur, 2014.

[15] R. K. Varma, S. A. Rahman and M. D. Dang, "Harmonic Impact of a 20-MW PV Solar Farm on a Utility Distribution Network," *IEEE Power and Energy Technology Systems Journal*, vol. 3, no. 3, pp. 89-98, 2016.

[16] E. Vasanasong and E. D. Spooner, "The Effect of Net Harmonic Currents Produced by Numbers of the Sydney Olympic Village's PV Systems on Power Quality of Local Electrical Network," in *International Conference on Power System Technology*, Perth, 2000.

[17] J. H. Enslin and P. J. Heskes, "Harmonic Interaction Between a Large Number of Distributed Power Inverters and the Distribution Network," *IEEE Transactions on Power Electronics*, vol. 19, no. 6, pp. 1586-1593, 2004.

[18] D. Chenvidhya, J. Thongpron, U. Sangpanich, N. Wongyao, K. Kirtikara and C. Jivacate, "A Thai National Demonstration Project on PV Grid Interactive Systems: Power Quality Observation," in *3rd World Conference on Photovoltaic Energv Conversion*, Osaka, 2003.

[19] S. Rönnberg, M. Bollen and A. Larsson, "Grid Impact From PV-Installations In Northern Scandinavia," in *22nd International Conference and Exhibition on Electricity Distribution*, Stockholm, 2013.

[20] IEC 61000-4-30 2008 Edition 2, "Electromagnetic compatibility (EMC) Part 4-30: Testing and measurement techniques - Power quality measurement methods.".

[21] R. E. Sims, "Renewable Energy: A Response to Climate Change," *Solar Energy*, vol. 76, no. 1-3, pp. 9-17, 2004.

[22] A. Luque and S. Hegedus, Handbook of Photovoltaic Science and Engineering, 2nd ed., Hoboken, NJ, USA: John Wiley & Sons, 2010.

[23] O. Edenhofer, R. Pichs-Madruga, Y. Sokona, K. Seyboth, P. Matschoss, S. Kadner, T. Zwickel, P. Eickemeier, G. Hansen, S. Schlömer and C. von Stechow, "IPCC, 2011: Summary for Policymakers," in *IPCC Special Report on Renewable Energy Sources and Climate Change Mitigation*, Cambridge and New York, Cambridge University Press, 2011.

[24] International Energy Agency, "Energy Technology Perspectives 2012," International Energy Agency, 2012.

[25] G. Masson, S. Orlandi and M. Rekinger, "European Photovoltaic Industry Association Global Market Outlook For Photovoltaics: 2014-2018".

[26] M. Schmela, G. Masson and N. Mai, "Global Market Outlook for Solar Power / 2016 - 2020," SolarPower Europe, 2016.

[27] A. Pegels, "Renewable energy in South Africa: Potentials, barriers and options for support," *Energy Policy*, no. 38, pp. 4945-4954, 2010.

[28] R. Inglesi, "Aggregate electricity demand in South Africa: Conditional forecasts to 2030," *Applied Energy*, no. 87, pp. 197-204, 2010.

[29] Department of Minerals and Energy, "Interventions to address electricity shortages," January 2008. [Online]. Available: http://www.polity.org.za/article/national-response-to-south-africas-electricity-shortage-january-2008-2008-01-30. [Accessed 14 April 2015].

[30] Department of Energy, " Integrated Resource Plan for Electricity 2010-2030, Revision 2, Final Report," 25 March 2011. [Online]. Available: http://www.doe-irp.co.za/content/IRP2010_promulgated.pdf. [Accessed 16 April 2015].

[31] Minister Tina Joemat-Pettersson, "Briefing on expansion and acceleration of the Independent Power Producer Procurement Programme," 16 April 2015. [Online]. Available: http://www.gov.za/speeches/minister-tina-joemat-pettersson-briefing-expansion-and-acceleration-independent-power. [Accessed 16 April 2015].

[32] Department of Energy, "List of REIPP Preferred Bidders for Bid Window 1 - 4," [Online]. Available: https://ipp-projects.co.za/PressCentre/GetPressRelease?fileid=287d28e7-3d94-e511-9437-2c59e59ac9cd&fileName=REIPP%20-%20Bid%20Window%201-4%20Preferred%20Bidder%20List.pdf. [Accessed 22 07 2017].

[33] "List of Power Stations in South Africa," [Online]. Available: https://en.wikipedia.org/wiki/List_of_power_stations_in_South_Africa. [Accessed 31 May 2015].

[34] L. Luo and Y. Yang, "Pollution of Renewable Energies to the Grid: Measured Data and Statistical Analysis via Largescale Urban Power Quality Monitoring System," in *IEEE Global High Tech Congress on Electronics*, Shenzhen, 2013.

[35] T. V. Dao, H. T. Nguyen, S. Chaitusaney and R. Chatthaworn, "Local Reactive Power Control of PV Plants for Voltage Fluctuation Mitigation," in *11th International Conference on Electrical Engineering/Electronics, Computer, Telecommunications and Information Technology*, Nakhon Ratchasima, 2014.

[36] R. Dugan, M. McGranaghan, S. Santoso and H. Beaty, Electrical Power Systems Quality, 2nd ed., McGraw-Hill, 2003.

[37] V. E. Wagner, J. C. Balda, D. C. Griffith, A. McEachern, A. Barnes, T. M. Hartmann, D. P. Phileggi, A. E. Emannuel, W. F. Horton, W. E. Reid, R. J. Ferraro and W. T. Jewell, "Effects of Harmonics on Equipment," *IEEE Transactions on Power Delivery*, vol. 8, no. 2, pp. 672-680, 1993.

[38] A. Baggini, Handbook of Power Quality, John Wiley & Sons, 2008.

[39] A. Medina and M. Martinez-Cardenas, "Analysis of the Harmonic Distortion on the Operation of Digital Protection Systems," in *IEEE Power Engineering Society General Meeting*, 2005.

[40] T. J. Browne, V. J. Gosbell and S. Perera, "Conditions for the Assessment of the Harmonic Compliance of an Installation," in *13th International Conference on Harmonics and Quality of Power*, Wollongong, 2008.

[41] NRS 048-4:2009, "Electricity Supply – Quality of Supply. Part 4: Application Practices for Licensees".

[42] IEC 61000-3-6 2008 Edition 2.0, "Electromagnetic compatibility (EMC) - Part 3-6: Limits - Assessment of emission limits for the connection of distorting installations to MV, HV and EHV power systems".

[43] M. McGranaghan and G. Beaulieu, "Update on IEC 61000-3-6: Harmonic Emission Limits for Customers Connectted to MV, HV and EHV," in *IEEE PES Transmission and Distribution Conference and Exhibition*, Dallas, 2006.

[44] IEEE 519-2014, "IEEE Recommended Practice and Requirements for Harmonic Control in Electric Power Systems".

[45] J. Fourier, The Analytical Theory of Heat, Cambridge University Press, 1978.

[46] C. Phillips, J. M. Parr and E. A. Riskin, Signals, Systems and Transforms, 4th ed., Upper Saddle River: Pearson Prentice Hall, 2003.

[47] J. D. Glover, M. S. Sarma and T. J. Overbye, Power System Analysis and Design, Stamford: Cengage Learning, 2012.

[48] C. L. Fortesque, "Method of Symmetrical Co-Ordinates Applied to the Solution of Polyphase Networks," *Transactions of the AIEE,* vol. 37, no. 2, pp. 1027-1140, 1918.

[49] G. Atkinson-Hope, "Relationship between Harmonics and Symmetrical Components," *International Journal of Electrical Engineering Education*, vol. 41, no. 2, pp. 93-104, 2004.

[50] K. L. Shum, "Analysis of Symmetrical Components of Harmonics for Three Phase Power Systems," MSc. Dissertation, Electrical and Electronic Engineering. University of Cape Town, South Africa, 1986.

[51] Task Force on Harmonics Modeling and Simulation, "Modeling and simulation of the propagation of harmonics in electric power networks – Part I: Concepts, models and simulation techniques," *IEEE Transactions on Power Delivery*, vol. 11, no. 1, pp. 452-465, 1996.

[52] S. Z. Djokic and A. J. Collin, "Cancellation and Attenuation of Harmonics in Low Voltage Networks," in *IEEE 16th International Conference on Harmonics and Power Quality*, Bucharest, 2014.

[53] B. Badrzadeh, M. Gupta, N. Singh, A. Petersson, L. Max and M. Høgdahl, "Power System Harmonic Analysis in Wind Power Plants – Part I: Study Methodology and Techniques," in *IEEE Industry Applications Society Annual Meeting*, Las Vegas, 2012.

[54] A. Reznik, M. G. Simões, A. Al-Durra and S. M. Muyeen, "LCL Filter Design and Performance Analysis for Grid-Interconnected Systems," *IEEE Transactions on Industry Electronics*, vol. 50, no. 2, pp. 1225-1232, 2014.

[55] G. Heyd, Electric Power Quality, Stars in a Circle Publications, 1991.

[56] S. A. Papathanassiou and M. P. Papadopoulos, “Harmonic Analysis in a Power System with Wind Generation,” *IEEE Transactions on Power Delivery,* vol. 21, no. 4, pp. 2006-2016, 2006.

[57] A. Robert and T. Deflandre, “Guide for Assessing the Network Harmonic Impedance,” *CIGRE Electra,* no. 167, pp. 96-131, 1996.

[58] E. De Jaeger, “Review of Emission Assessment Techniques,” CIGRE-CIRED joint working group C4.109, 2011.

[59] G. Lemieux, “Power System Harmonic Resonance – A Documented Case,” *IEEE Transactions on Industry Applications,* vol. 26, no. 3, pp. 486-488, 1990.

[60] J. C. Das, “Passive Filters – Potentialities and Limitations,” in *Conference Record of the 2003 Annual Pulp and Paper Industry Technical Conference,* Charleston, 2003.

[61] F. Z. Peng and D. J. Adams, “Harmonic Sources and Filtering Approaches - Series/Parallel, Active/Passive, and their Combined Power Filters,” in *IEEE Industry Applications Conference,* Phoenix, 1999.

[62] D. Detjen, J. Jacobs, R. W. De Doncker and H.-G. Mall, “A New Hybrid Filter to Dampen Resonances and Compensate Harmonic Currents in Industrial Power Systems With Power Factor Correction Equipment,” *IEEE Transactions on Power Electronics,* vol. 16, no. 6, pp. 821-827, 2001.

[63] D. A. González and J. C. McCall, “Design of Filters to Reduce Harmonic Distortion in Industrial Power Systems,” *IEEE Transactions on Industry Applications,* Vols. IA-23, no. 3, pp. 504-511, 1987.

[64] A. Ellis, B. Karlson and J. Williams, “Utility-Scale Photovoltaic Procedures and Interconnection Requirements,” February 2012. [Online]. Available: http://energy.sandia.gov/energy/renewable-energy/solar-energy/photovoltaics/. [Accessed 8 May 2015].

[65] A. Ellis, B. Karlson and J. Williams, “Utility-Scale Photovoltaic Procedures and Interconnection Requirements,” [Online]. Available: http://wiki-cleantech.com/solar-photovoltaics/utility-scale-photovoltaic-procedures-and-interconnection-requirements. [Accessed 30 July 2015].

[66] F. Schimpf and L. E. Norum, “Grid connected Converters for Photovoltaic, State of the Art, Ideas for Improvement of Transformerless Inverters,” in *Proceedings of the Nordic Workshop on Power and Industrial Electronics,* Espoo, 2008.

[67] J. V. Núñez, "Multilevel Topologies: Can New Inverters Improve Solar Farm Output," *Solar Industry Magazine*, vol. 5, no. 12, January 2013.

[68] C. N. M. Ho, "Challenges and Design Considerations of PV Inverters in the Future Smart Grids," in *9th IET International Conference on Advances in Power System Control, Operation and Management*, Hong Kong, 2012.

[69] "Semikron," [Online]. Available: http://www.semikron.com/products/product-lines/semikube.html. [Accessed 17 May 2015].

[70] B. Wu, High Power Converters and AC Drives, Piscataway: IEEE Press, 2006.

[71] J. Holtz, "Pulsewidth Modulation – A Survey," *IEEE Transactions on Industrial Electronics*, vol. 39, no. 5, pp. 410-420, 1992.

[72] M. H. Rashid, Power Electronics Handbook, Burlington: Butterworth-Heinemann, 2011.

[73] H. W. van der Broeck, H.-C. Skudelny and G. V. Stanke, "Analyis and Realization of a Pulsewidth Modulator Based on Voltage Space Vectors," *IEEE Transactions on Industry Applications*, vol. 24, no. 1, pp. 142-150, 1988.

[74] M. Chhabra and F. Barnes, "Robust Current Controller Design Using Mu-Synthesis for Grid Connected Three Phase Inverter," in *IEEE 40th Photovoltaic Specialist Conference*, Denver, 2014.

[75] T. Hornik and Q.-C. Zhong, "A Current-Control Strategy for Voltage-Source Inverters in Microgrids Based on H∞ and Repetitive Control," *IEEE Transactions on Power Electronics*, vol. 26, no. 3, pp. 943-952, 2011.

[76] M. P. Kazmierkowski and L. Malesani, "Current Control Techniques for Three-Phase Voltage-Source PWM Converters: A Survey," *IEEE Transactions on Industrial Electronics*, vol. 45, no. 5, pp. 691-703, 1998.

[77] M. Malinowski, M. Jasiński and M. P. Kazmierkowski, "Simple Direct Power Control of Three-Phase PWM Rectifier Using Space-Vector Modulation (DPC-SVM)," *IEEE Transactions on Industrial Electronics*, vol. 51, no. 2, pp. 447-454, 2004.

[78] X. Zong, P. A. Gray and P. W. Lehn, "New Metric Recommended of IEEE Std. 1547 to Limit Harmonics Injected into Distorted Grids," *IEEE Transactions on Power Delivery*, vol. PP, no. 99, 2015.

[79] G. Chicco, J. Schlabbach and F. Spertino, "Experimental Assessment of the Waveform Distortion in Grid-Connected Photovoltaic Installations," *Solar Energy*, vol. 83, pp. 1026-1039, 2009.

[80] J. C. Hernández, M. J. Ortega and A. Medina, "Statistical Characterisation of Harmonic Current Emission for Large Photovoltaic Plants," *International Transactions on Electrical Energy Systems*, vol. 24, no. 8, pp. 1134-1150, 2014.

[81] G. Chicco, R. Napoli and F. Spertino, "Experimental Evaluation of the Performance of Grid Connected Photovoltaic Systems," in *Proceedings of the 12th IEEE Mediterranean Electrotechnical Conference*, Dubrovnik, 2004.

[82] J. Schlabbach and J. Kammer, "Prediction of Harmonic Currents of PV-Inverters Using Measured Solar Radiation Data," in *IEEE Mediterranean Electrotechnical Conference*, Benalmádena, 2006.

[83] M. Patsalides, A. Stavrou, A. Efthymiou and G. E. Georghiou, "Towards the Establishment of Maximum PV Generation Limits Due to Power Quality Constraints," *Electrical Power and Energy Systems*, vol. 42, no. 1, pp. 285-298, 2012.

[84] M. Prodanović and T. C. Green, "Control and Filter Design of Three-Phase Inverters for High Power Quality Grid Connection," *IEEE Transactions on Power Electronics*, vol. 18, no. 1, pp. 373-380, 2003.

[85] J. Bian, H. Li and T. Q. Zheng, "Stability Analysis of Grid-Connected Inverters with LCL-Filter Based on Harmonic Balance and Floquet Theory," in *2014 International Power Electronics Conference*, Hiroshima, 2014.

[86] W. Wu, Y. Sun, M. Huang, X. Wang, F. Blaabjerg, M. Liserre and H. S. Chung, "A Robust Passive Damping Method for LLCL-Filter-Based Grid-Tied Inverters to Minimize the Effect of Grid Harmonic Voltages," *IEEE Transactions on Power Electronics*, vol. 29, no. 7, pp. 3279-3289, 2014.

[87] B. Mariappan, B. G. Fernandes and M. Ramomoorty, "A Novel Single-Stage Solar Inverter Using Hybrid Active Filter with Power Quality Improvement," in *40th Annual Conference of the IEEE Industrial Electronics Society*, Dallas, 2014.

[88] R. G. Ramteke and U. V. Patil, "Design of Third Order L-C-L Filter for Diode-Clamped Multi-Level Inverter," in *International Conference on Circuit, Power and Computing Technologies*, Nagercoil, 2014.

[89] C. Mayr, R. Brundlinger and B. Bletterie, “Photovoltaic-Inverters as Active Filters to Improve Power Quality in the Grid. What Can State-of-the-art Equipment Achieve?,” in *9th International Conference on Electrical Power Quality and Utilisation*, Barcelona, 2007.

[90] R. Sunny and R. Anto, “Harmonics Control and Performance Analysis of a Grid Connected Photovoltaic System,” in *International Conference on Advanced Computing and Communication Systems*, Coimbatore, 2013.

[91] Y. Yang, K. Zhou, H. Wang, F. Blabjerg, D. Wang and B. Zhang, “Frequency Adaptive Selective Harmonic Control for Grid-Connected Inverters,” *IEEE Transactions on Power Electronics*, vol. 30, no. 7, pp. 3912-3924, 2014.

[92] K. Zhou, Z. Qiu, N. R. Watson and Y. Liu, “Mechanism and elimination of harmonic current injection from single-phase grid-connected PWM converters,” *IET Power Electronics*, vol. 6, no. 1, pp. 88-95, 2013.

[93] W. L. Neves, D. Gonçalves, J. G. Pinto, R. Alves and J. L. Afonso, “Single-Phase Shunt Active Filter Interfacing Renewable Energy Sources with the Power Grid,” in *35th Annual Conference of IEEE Industrial Electronics*, Porto, 2009.

[94] DIgSILENT GmbH, DIgSILENT PowerFactory Version 15 User Manual, 2014.

[95] D. Xia and G. T. Heydt, “Harmonic Power Flow Studies,Part I - Formulation and Solution, Part II - Implementation and Practical Application,” *IEEE Transactions on Power Apparatus and Systems*, Vols. PAS-101, pp. 1257-1270, 1982.

[96] W. Xu, J. R. Marti and H. W. Dommel, “A Multiphase Harmonic Load Flow Solution Technique,” *IEEE Transactions on Power Systems*, vol. 6, no. 1, pp. 174-182, 1991.

[97] M. Valcarel and J. G. Mayordomo, “Harmonic Power Flow for Unbalanced Systems,” *IEEE Transactions on Power Delivery*, vol. 8, no. 4, pp. 2052-2059, 1993.

[98] Task Force on Harmonic Modeling and Simulation, IEEE PES Harmonic Working Group, “Characteristics and Modeling of Harmonic Sources – Power Electronic Devices,” *IEEE Transactions on Power Delivery*, vol. 16, no. 4, pp. 791-800, 2001.

[99] A. Semlyen, E. Acha and J. Arrillaga, “Harmonic Norton equivalent for the magnetizing branch of a transformer,” *Proceedings of the IEE*, vol. 134C, no. 2, pp. 162-169, 1987.

[100] S. Liang, Q. Hu and W.-J. Lee, "A Survey of Harmonic Emissions of a Commercially Operated Wind Farm," *IEEE Transactions on Industry Applications,* vol. 48, no. 3, pp. 1115-1123, 2012.

[101] IEC 61000-4-7 2009 Edition 2.1, "Electromagnetic compatibility (EMC) Part 4-7: Testing and measurement techniques - General guide on harmonics and interharmonics measurements and instrumentation, for power supply systems and equipment connected thereto".

[102] L. Sainz, J. J. Mesas, R. Teodorescu and P. Rodriguez, "Deterministic and Stochastic Study of Wind Farm Harmonic Currents," *IEEE Transactions on Power Delivery,* vol. 21, no. 4, pp. 2006-2016, 2006.

[103] W.-K. Wu, G. W. Chang and L. Wang, "Power Quality Measurements and Analysis for Zhong-Tun Wind Farm in Penghu," in *CACS International Automatic Control Conference,* Nantou, 2013.

[104] C. X. Huan and T. Tayjasanant, "Modeling Wind Power Plants in Harmonic Resonance Study - A Case Study in Thailand," in *2013,* Yogyakarta, International Conference on Information Technology and Electrical Engineering.

[105] A. Cavallini, R. Langella, A. Testa and F. Ruggiero, "Gaussian Modeling of Harmonic Vectors in Power Systems," in *8th International Conference on Harmonics and Quality of Power Proceedings,* Athens, 1998.

[106] W. Xu, E. E. Ahmed, X. Zhang and X. Liu, "Measurement of Network Harmonic Impedances: Practical Implementation Issues and Their Solutions," *IEEE Transactions on Power Delivery,* vol. 17, no. 1, pp. 210-216, 2002.

[107] C. Li, W. Xu and T. Tayjasanant, "A "Critical Impedance"-Based method for Identifying Harmonic Sources," *IEEE Transactions on Power Delivery,* vol. 19, no. 2, pp. 671-678, 2004.

[108] M. G. Ippolito, G. Morana and F. Russo, "A Contribution to Solve the Problem of Attributing Harmonic Distortion Responsibility," in *18th International Conference and Exhibition on Electricity Distribution,* Turin, 2005.

[109] T. Pfajfar, B. Blažič and I. Papič, "Harmonic Contributions Evaluation With the Harmonic Current Vector Method," *IEEE Transactions on Power Delivery,* vol. 23, no. 1, pp. 425-433, 2008.

[110] T. Pfajfar, B. Blažič and I. Papič, "Methods for estimating customer voltage harmonic emission levels," in *13th International Conference on Harmonics and Power Quality,* Wollongong, 2008.

[111] W. Xu and Y. Liu, "A Method for Determining Customer and Utility Harmonic Contributions at the Point of Common Coupling," *IEEE Transactions on Power Delivery,* vol. 15, no. 2, pp. 804-811, 2000.

[112] W. Xu, X. Liu and Y. Liu, "An Investigation on the Validity of Power-Direction," *IEEE Transactions on Power Delivery,* vol. 18, no. 1, pp. 214-219, 2003.

[113] I. N. Santos, J. C. Oliveira and S. F. Paula Silva, "Critical Evaluation of the Performance of the," *IEEE Latin America Transactions,* vol. 9, no. 5, pp. 740-746, 2011.

[114] H. Zang and Z. Yin, "Responsibility Identification Method for the Power System Harmonic Problems," in *2011 International Conference on Electrical and Control Engineering*, Yichang, 2011.

[115] A. A. Moustafa, A. M. Moussa and M. A. El-Gammal, "Separation of Customer and Supply Harmonics in Electrical Power Distribution Systems," in *Ninth International Conference on Harmonics and Power Quality*, Orlando, 2000.

[116] E. J. Davis, A. E. Emanuel and D. J. Pileggi, "Harmonic Pollution Metering: Theoretical Considerations," *IEEE Transactions on Power Delivery,* vol. 15, no. 1, pp. 19-23, 2000.

[117] D. Saxena, B. Sayak and S. N. Singh, "Identification of Multiple Harmonic Sources in Power System Using Optimally Placed Voltage Measurement Devices," *IEEE Transactions on Industrial Electronics,* vol. 61, no. 5, pp. 2483-2492, 2014.

[118] K. Morimoto, K. Konishi, T. Miki, N. Nagaoka and A. Ametani, "Harmonic Source Identification by Simultaneous-Multipoint Harmonic Measurements," in *42nd International Universities Power Engineering Conference*, Brighton, 2007.

[119] A. Carta, N. Locci and C. Muscas, "A PMU for the Measurement of Synchronized Harmonic Phasors in Three-Phase Distribution Networks," *IEEE Transactions on Instrumentation and Measurement,* vol. 58, no. 10, pp. 3723-2730, 2009.

[120] R. Langella and A. Testa, "A New Method for Statistical Assessment of the System Harmonic Impedance and of the Background Voltage Distortion," in *International Conference on Probabilistic Methods Applied to Power Systems*, Stockholm, 2006.

[121] H. Xiaoqing, N. Peng and G. Hualin, "A New Assessment Method of Customer Harmonic Emission Level," in *Asia-Pacific Power and Engineering Conference*, Chengdu, 2010.

[122] X. Y. Xiao and H. G. Yang, "Assessing Harmonic Impedance by Synchronously Layered Distortion Waves Based on Wavelet," in *IEEE International Conference on Electric Utility Deregulation, Restructuring and Power Technologies*, Hong Kong, 2004.

[123] I. T. Papaioannou, A. S. Bouhouras, A. G. Marinopoulos, M. C. Alexiadis, C. S. Demoulias and D. P. Labridis, "Harmonic Impact of Small Photovoltaic Systems Connected to the LV Distribution Network," in *5th International Conference on European Electricity Market*, Lisbon, 2008.

[124] M. C. Benhabib, P. R. Wilczek, J. M. Myrzik and J. L. Duarte, "Harmonic Interactions and Resonance Problems in Large Scale LV Networks," in *Proceedings of the 16th Power Systems Computation Conference*, Glasgow, 2008.

[125] F. Wang, J. L. Duarte, M. A. Hendrix and P. F. Ribeiro, "Modelling and Analysis of Grid Harmonic Distortion Impact of Aggregated DG Inverters," *IEEE Transactions on Power Electronics,* vol. 26, no. 3, pp. 786-797, 2011.

[126] D. Maksimovic, A. M. Stankovic, V. J. Thsottuvelil and G. C. Verghese, "Modeling and Simulation of Power Electronic Converters," *Proceedings of the IEEE,* vol. 89, no. 6, pp. 898-912, 2001.

[127] IEEE 399-1997, "IEEE Recommended Practice for Industrial and Commercial Power Systems Analysis".

[128] R. H. Galloway, W. B. Shorrocks and L. M. Wedepohl, "Calculation of Electrical Parameters for Short and Long Polyphase Transmission Lines," *Proceedings of the Institution of Electrical Engineers,* vol. 111, no. 12, pp. 2051-2059, 1964.

[129] R. Langella, L. Nunges, F. Pilo, G. Pisano, G. Petretto, S. Scalari and A. Testa, "Preliminary Analysis of MV Cable Line Models for High Frequency Harmonic Penetration Studies," in *Power and Energy Society General Meeting*, San Diego, 2011.

[130] K. Malekian, U. Schmidt, A. Hoshmeh and A. Shirvani, "A. Frequency Dependant Model of Underground Cables for Harmonic Calculations in the Frequency Domain," in *6th International Conference on Information Technology and Electrical Engineering*, Yogyakarta, 2014.

[131] H. W. Dommel, EMTP Theory Book, 1996: Microtan Power System Analysis Corporation.

[132] J. D. Greene and C. A. Gross, "Nonlinear Modelling of Transformers," *IEEE Transactions on Industry Applications,* vol. 24, no. 3, pp. 434-438, 1988.

[133] IEC 60076-1 2011 Edition 3, “Power Transformers Part 1: General”.

[134] J. Avila-Rosales and F. L. Alvarado, “Nonlinear Frequency Dependent Transformer Model for Electromagnetic Transient Studies in Power Systems,” *IEEE Transactions on Power Apparatus and Systems,* no. 11, pp. 4281-4288, 1982.

[135] W. Dugui and X. Zheng, “Harmonic model of power transformer,” in *International Conference on Power System Technology,* Beijing, 1998.

[136] M. Bradt, B. Badrzadeh, E. Camm and D. Meuller, “Harmonics and Resonance Issues in Wind Power Plants,” in *IEEE Power and Energy Society General Meeting,* San Diego, 2011.

[137] N. R. Watson and J. Arrillaga, “Frequency-Dependent AC System Equivalents for Harmonic Studies and Transient Converter Simulation,” *IEEE Transactions on Power Delivery,* vol. 3, no. 3, pp. 1196-1203, 1988.

[138] “Mathworks,” [Online]. Available: http://www.mathworks.com. [Accessed 25 July 2015].

[139] “EMTP-RV,” [Online]. Available: http://emtp.com. [Accessed 25 July 2015].

[140] Manitoba HVDC Research Centre Inc, “Applications of PSCAD / EMTDC,” 2007.

[141] S. Zhoa, H. Y. Li, P. Crossley and F. Ghassemi, “Testing and Modelling of Voltage Transformer for High Order Harmonic Measurement,” in *4th International Conference on Electric Utility Deregulation and Restructuring and Power Technologies,* Weihai, 2011.

[142] M. Klatt, J. Meyer, M. Elst and P. Schegner, “Frequency Responses of MV Voltage Transformers in the Range of 50 Hz to 10 kHz,” in *14th International Confererence on Harmonics and Power Quality*, Bergamo, 2010.

[143] R. Stigler, J. Meyer, J. Kilter and S. Konzelmann, “Assessment of Voltage Instrument Transformer Accuracy for Harmonic Measurements in Transmission Systems,” in *International Conference on Harmonics and Quality of Power (ICHQP),* Belo Horizonte, Brazil, 2016.

[144] M. I. Samesima, J. C. de Oliveira and E. M. Dias, “Frequency Response Analysis and Modeling of Measurement Transformers Under Distorted Current and Voltage Supply,” *IEEE Transactions on Power Delivery,* vol. 6, no. 4, pp. 1762-1768, 1991.

[145] J. Bak-Jensen, B. Bak-Jensen, S. D. Mikkelsen and C. G. Jensen, "Parametric Identification in Potential Transformer Modelling," *IEEE Transactions on Power Delivery*, vol. 7, no. 1, pp. 70-76, 1992.

[146] H. J. Vermeulen and P. Davel, "Voltage Harmonic Distortion Measurements Using Capacitive Voltage Transformers," in *IEEE AFRICON*, Stellenbosch, 1996.

[147] F. Ghassemi, P. Gale, T. Cumming and C. Coutts, "Harmonic Voltage Measurements Using CVTs," *IEEE Transactions on Power Delivery*, vol. 20, no. 1, pp. 443-449, 2005.

[148] L. Kadar, P. Hacksel and J. Wikston, "The Effect of Current and Voltage Transformers Accuracy on Harmonic Measurements in Electric Arc Furnaces," *IEEE Transactions on Industry Applications*, vol. 33, no. 3, pp. 780-783, 1997.

[149] J. C. Chen, B. T. Phung, D. M. Zhang and T. Blackburn, "Frequency response of MV current transformers," in *IEEE TENCON Spring Conference*, Sydney, 2013.

[150] L. Erning, J. M. MacAlpine and L. Yanbing, "On-line Identification of Frequency Response of Current Transformers Using a Correlation Method," in *Proceedings of 1997 IEEE International Symposium on Circuits and Systems*, Hong Kong, 1997.

[151] B. Vujičić, M. Sokola, Z. Mitrović, B. Santrač and V. Vujičić, "Coreless Current Measurement Transducer and Instrument for Distorted and," in *13th European Conference on Power Electronics and Applications*, Barcelona, 2009.

[152] "CTLAB," [Online]. Available: http://www.ctlab.com/products/impedoduo/. [Accessed 25 July 2015].

[153] "HIOKI," [Online]. Available: https://www.hioki.com/products/option/828. [Accessed 25 July 2015].

[154] A. Cataliotti, D. Di Cara, S. Nuccio and A. E. Emanuel, "Hall effect current transducer characterization under nonsinusoidal conditions," in *IEEE Instrumentation and Measurement Technology Conference*, Singapore, 2009.

[155] IEEE 037.11-2011, "IEEE Guide for the Application of Transient Recovery Voltage for AC High-Voltage Circuit Breakers".

[156] S. D. Cho, "Parameter Estimation for Transformer Modeling," PhD dissertation, Michigan Technological University, 2002.

[157] J. Barros, J. J. Gutiérrez, M. de Apráiz, P. Saiz, R. Diego and A. Lazkano, "Rapid Voltage Changes in the Power System Network and Their Effect on Flicker," *IEEE Transactions on Power Delivery,* vol. 31, no. 1, pp. 262-270, 2016.

[158] J. Meyer, A.-M. Blanco, M. Domagk and P. Schegner, "Assessment of Prevailing Harmonic Current Emission in Public Low-Voltage Networks," *IEEE Transactions on Power Delivery,* vol. 32, no. 2, pp. 962-970, 2017.

[159] E. Styvaktakis and M. Bollen, "Signatures of voltage dips: transformer saturation and multistage dips," *IEEE Transactions on Power Delivery,* vol. 18, no. 1, pp. 265-270, 2003.

[160] S. Hodder, B. Kasztenny, N. Fischer and Y. Xia, "Low second-harmonic content in transformer inrush currents - Analysis and practical solutions for protection security," in *Protective Relay Engineers,* College Station, 2014.

Appendix A Scatter plots of POC harmonic voltage and current vs active and reactive power

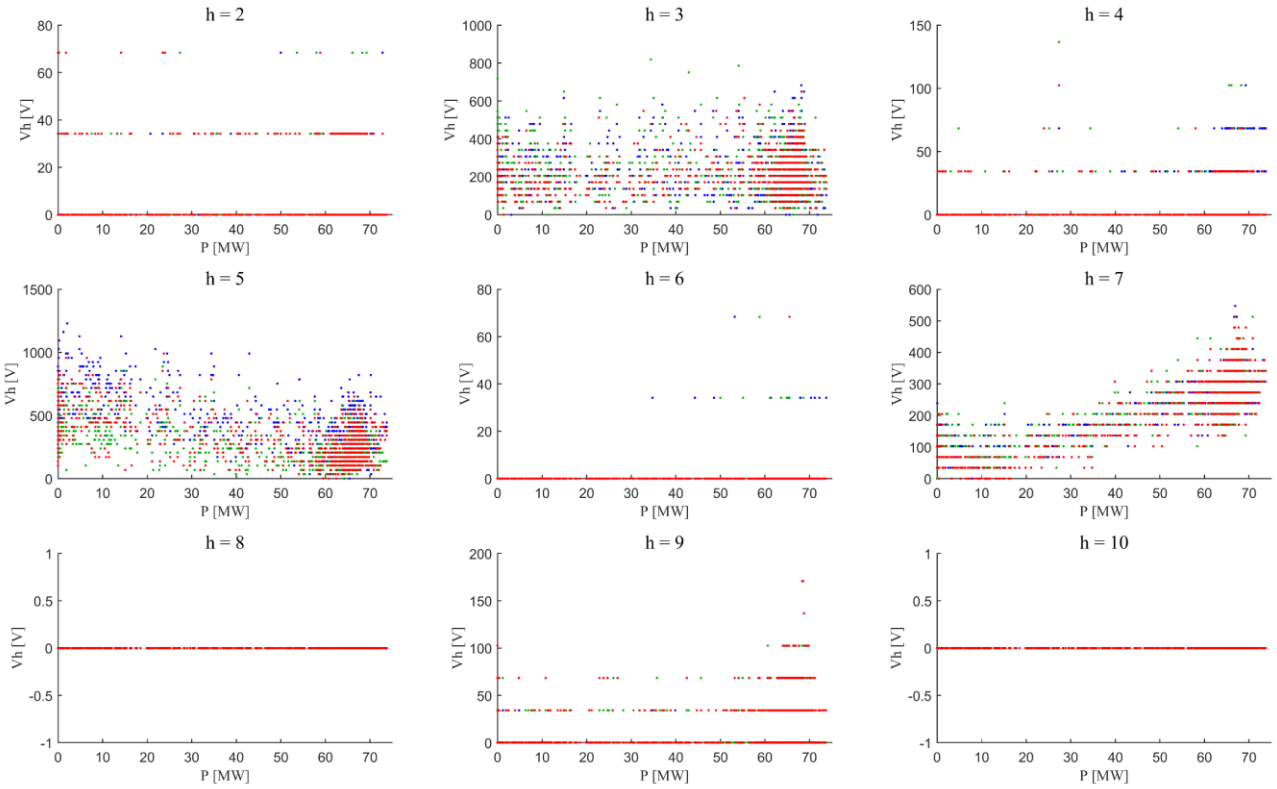

Figure A-1: 10-minute harmonic voltage emissions vs plant active power generation (h = 2 – 10) Red, white and blue phases represented by red, green and blue dots respectively.

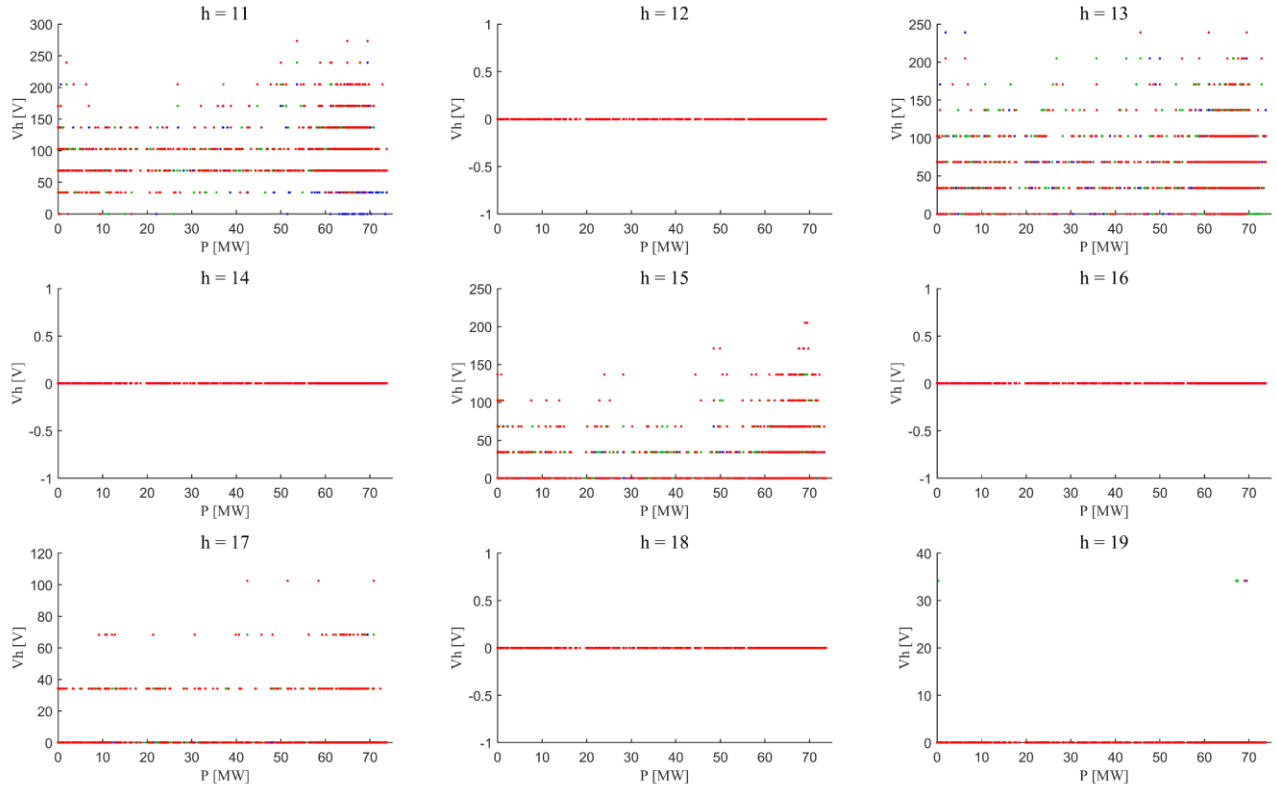

Figure A-2: 10-minute harmonic voltage emissions vs plant active power generation (h = 11 – 19) Red, white and blue phases represented by red, green and blue dots respectively.

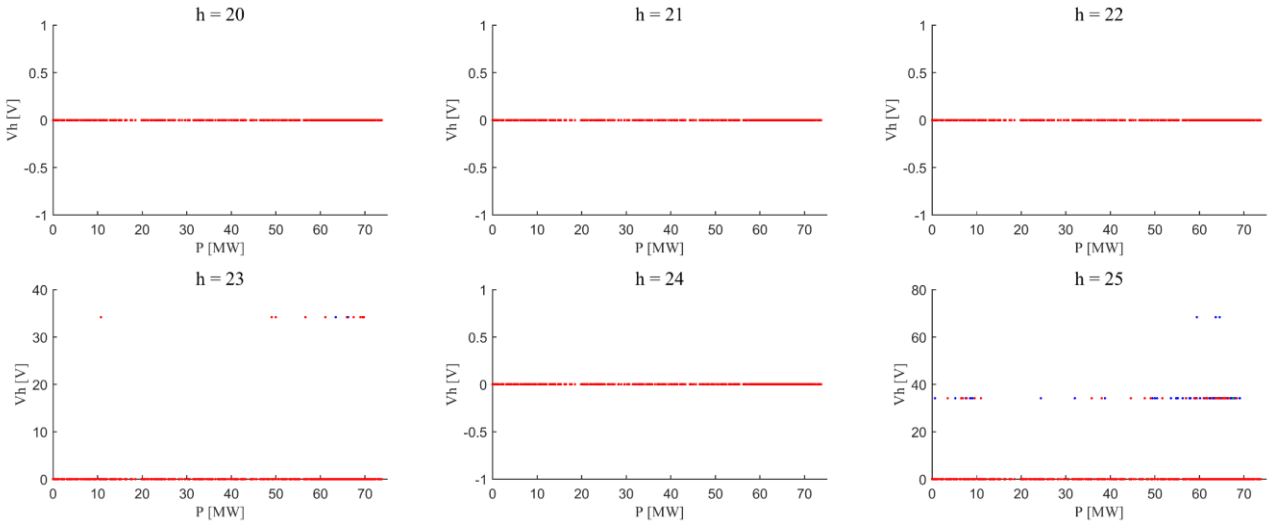

Figure A-3: 10-minute harmonic voltage emissions vs plant active power generation (h = 20 – 25) Red, white and blue phases represented by red, green and blue dots respectively.

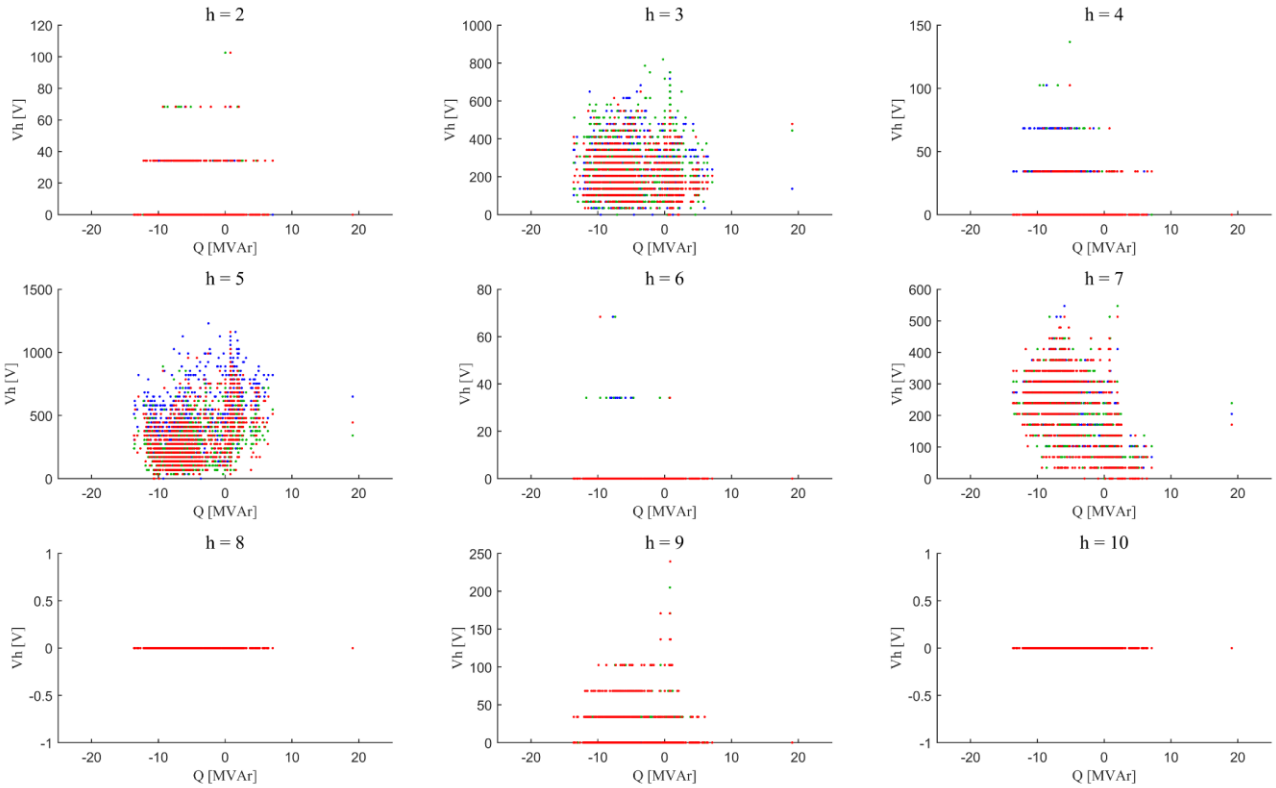

Figure A-4: 10-minute harmonic voltage emissions vs plant reactive power generation (h = 2 – 10) Red, white and blue phases represented by red, green and blue dots respectively.

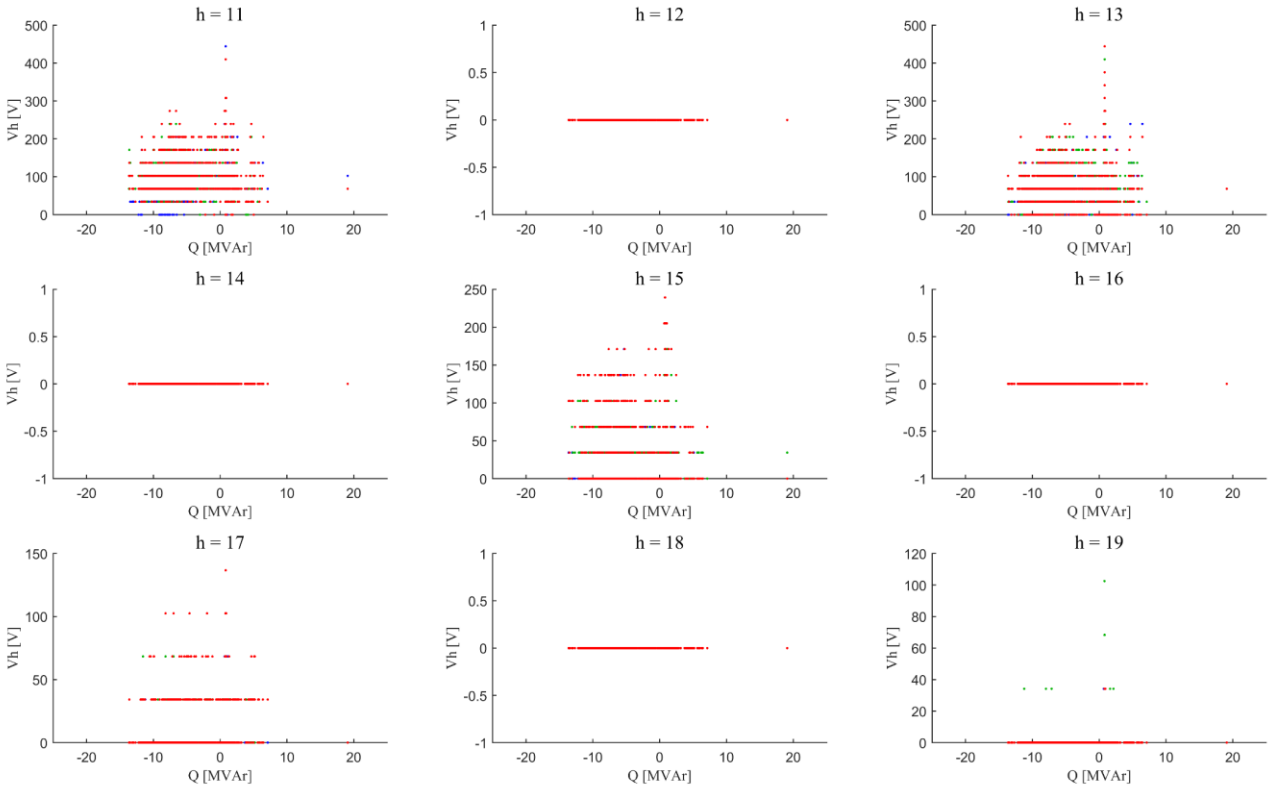

Figure A-5: 10-minute harmonic voltage emissions vs plant reactive power generation (h = 11 – 19) Red, white and blue phases represented by red, green and blue dots respectively.

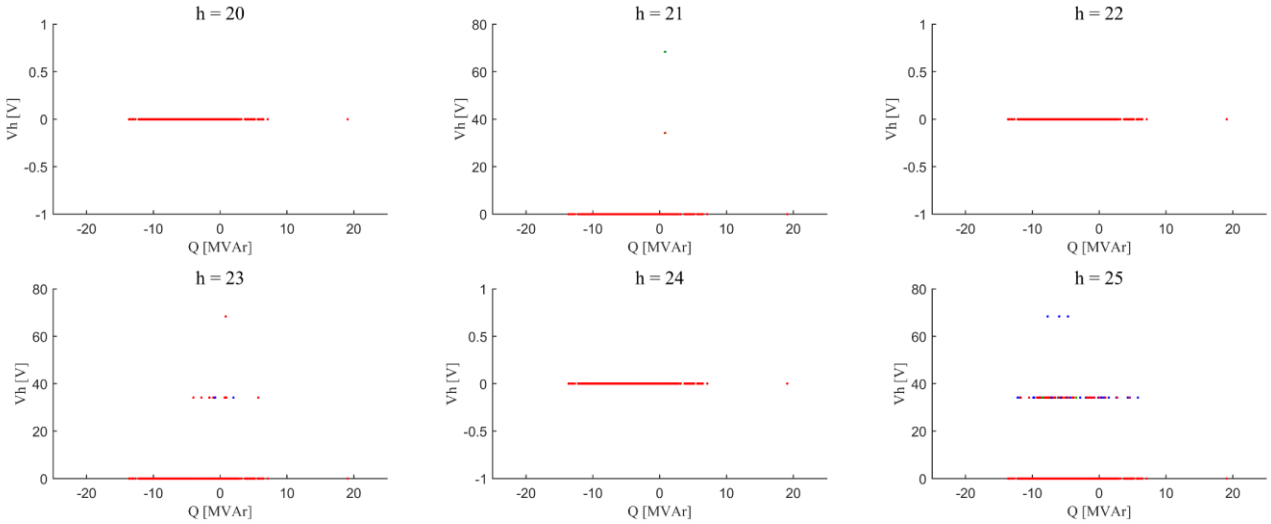

Figure A-6: 10-minute harmonic voltage emissions vs plant reactive power generation (h = 20 – 25) Red, white and blue phases represented by red, green and blue dots respectively.

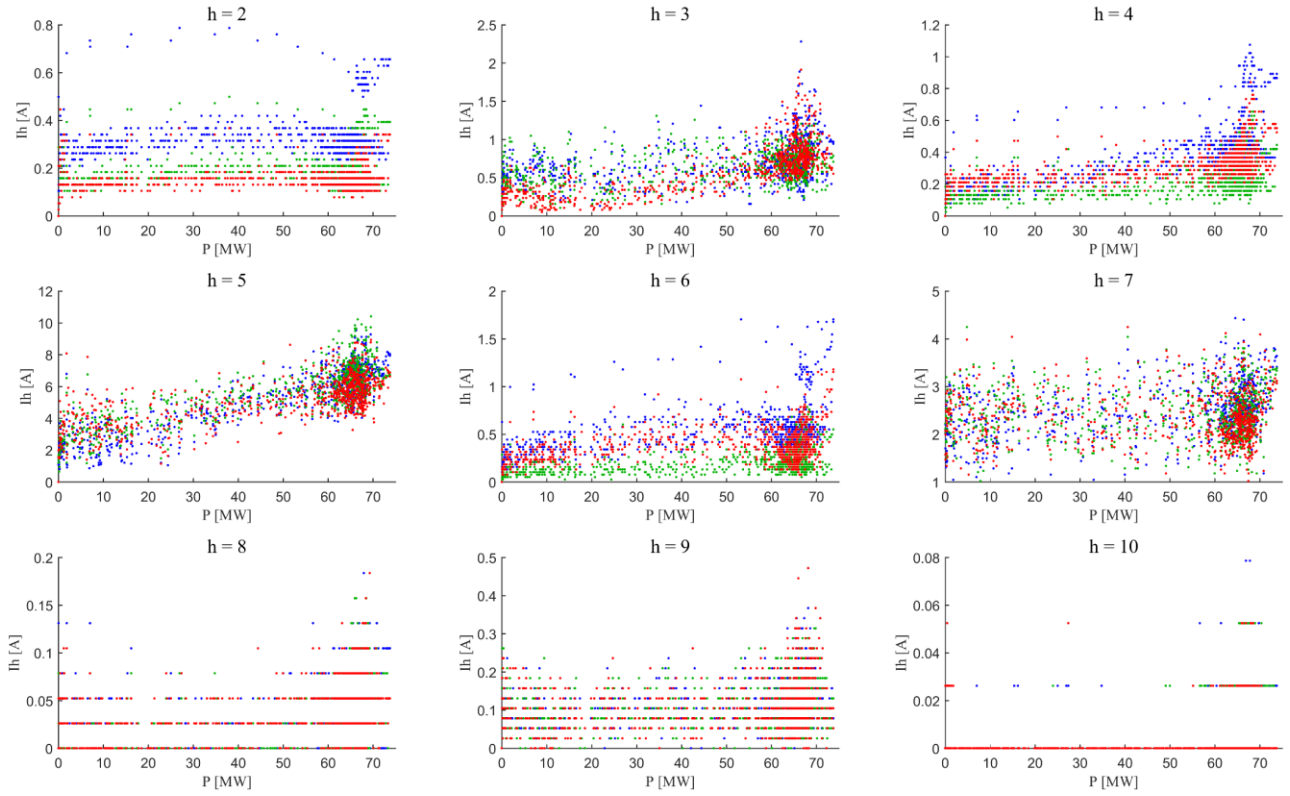

Figure A-7: 10-minute harmonic current emissions vs plant active power generation (h = 2 – 10) Red, white and blue phases represented by red, green and blue dots respectively.

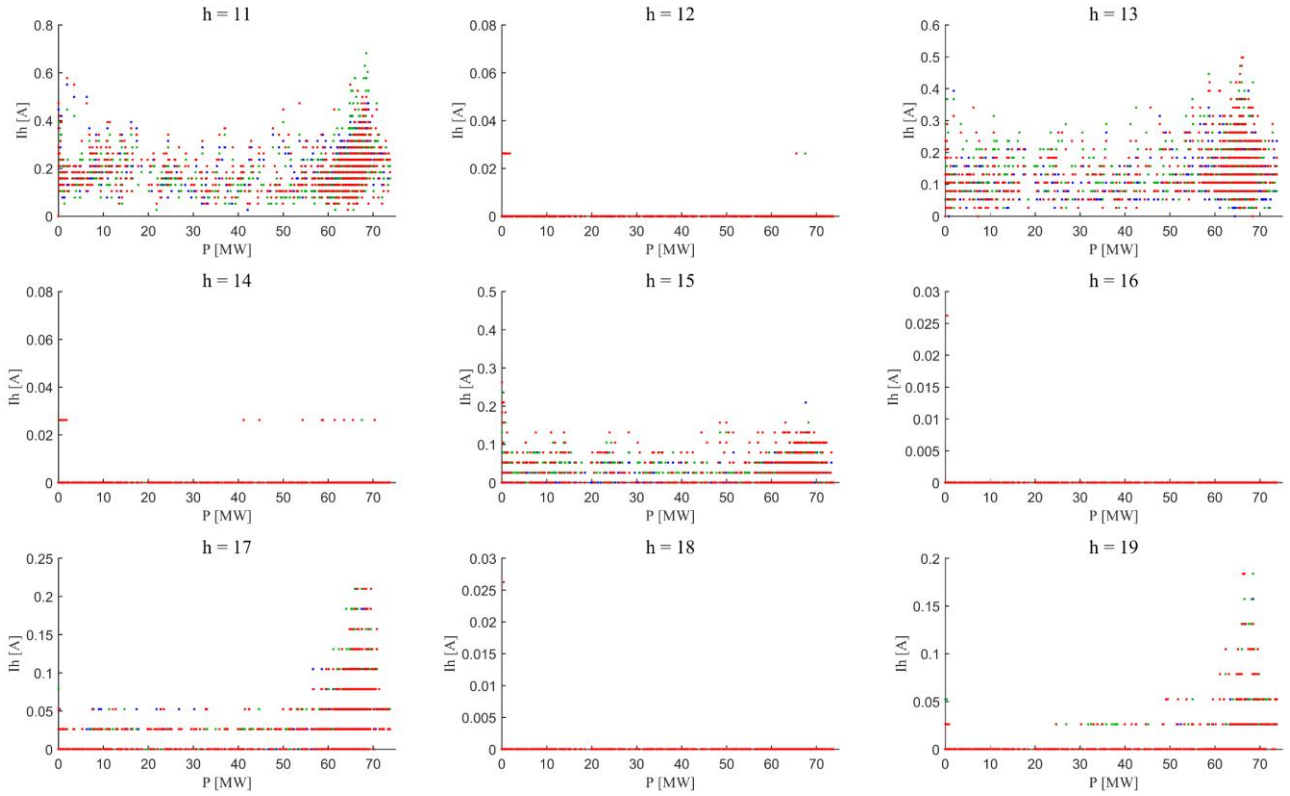

Figure A-8: 10-minute harmonic current emissions vs plant active power generation (h = 11 – 19) Red, white and blue phases represented by red, green and blue dots respectively.

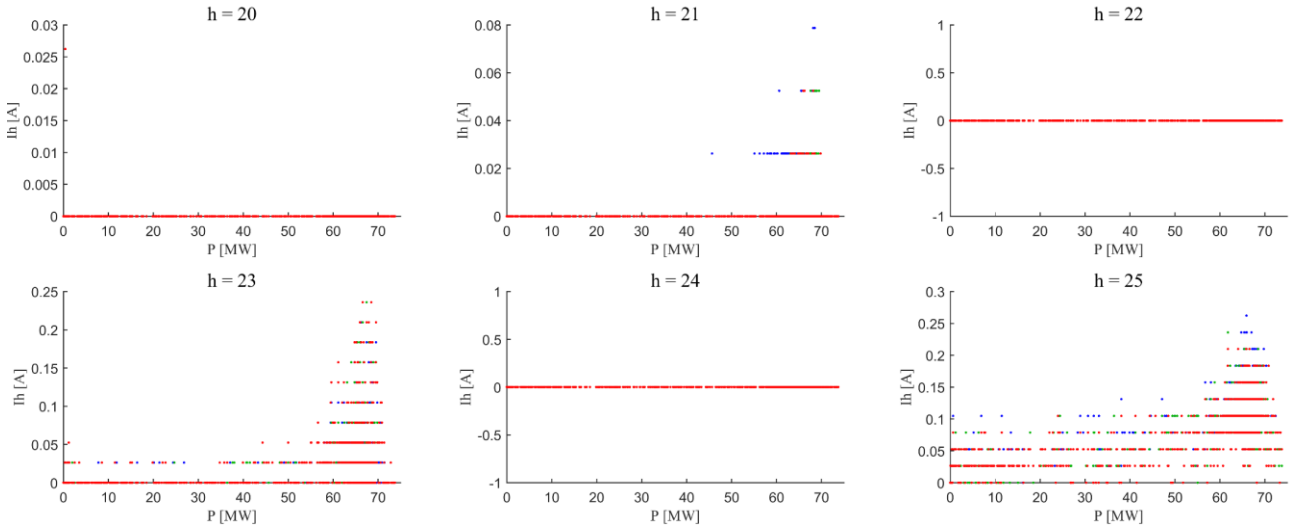

Figure A-9: 10-minute harmonic current emissions vs plant active power generation (h = 20 – 25) Red, white and blue phases represented by red, green and blue dots respectively.

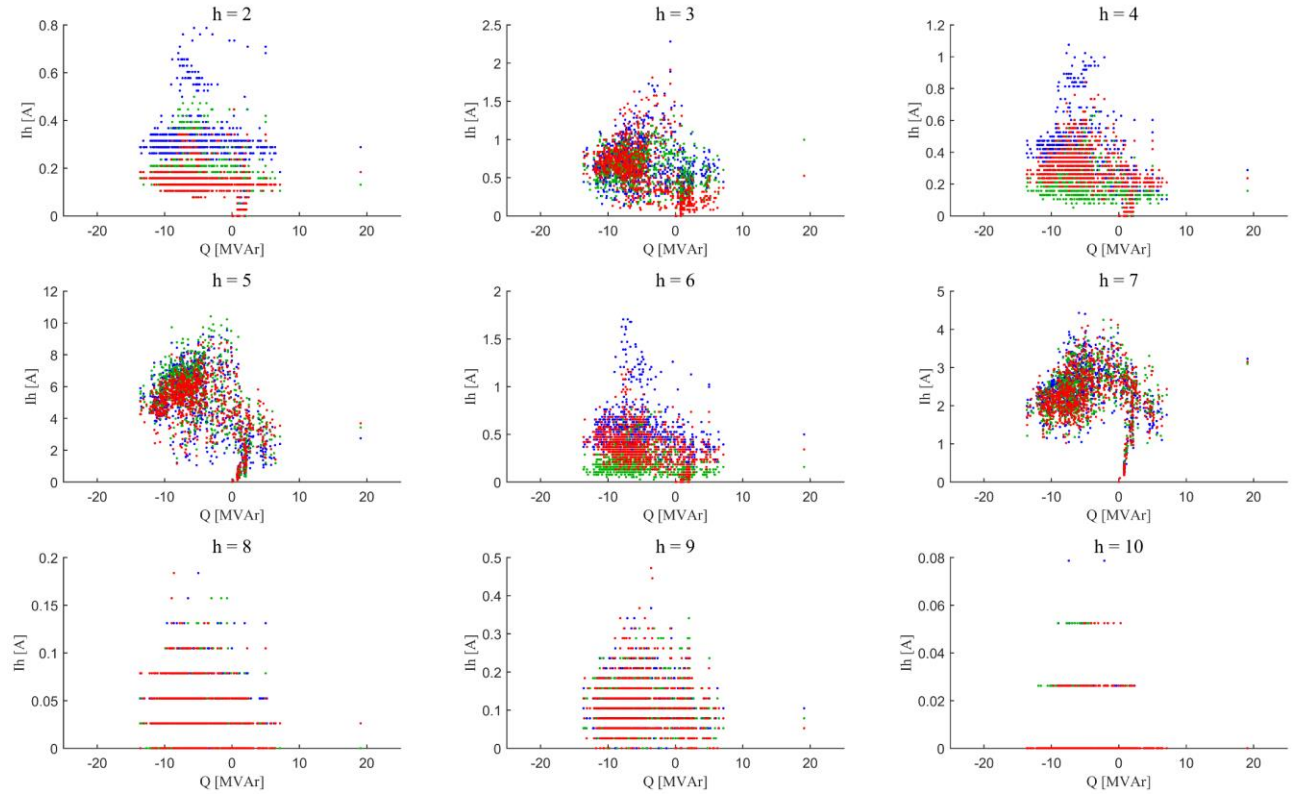

Figure A-10: 10-minute harmonic current emissions vs plant reactive power generation (h = 2 – 10) Red, white and blue phases represented by red, green and blue dots respectively.

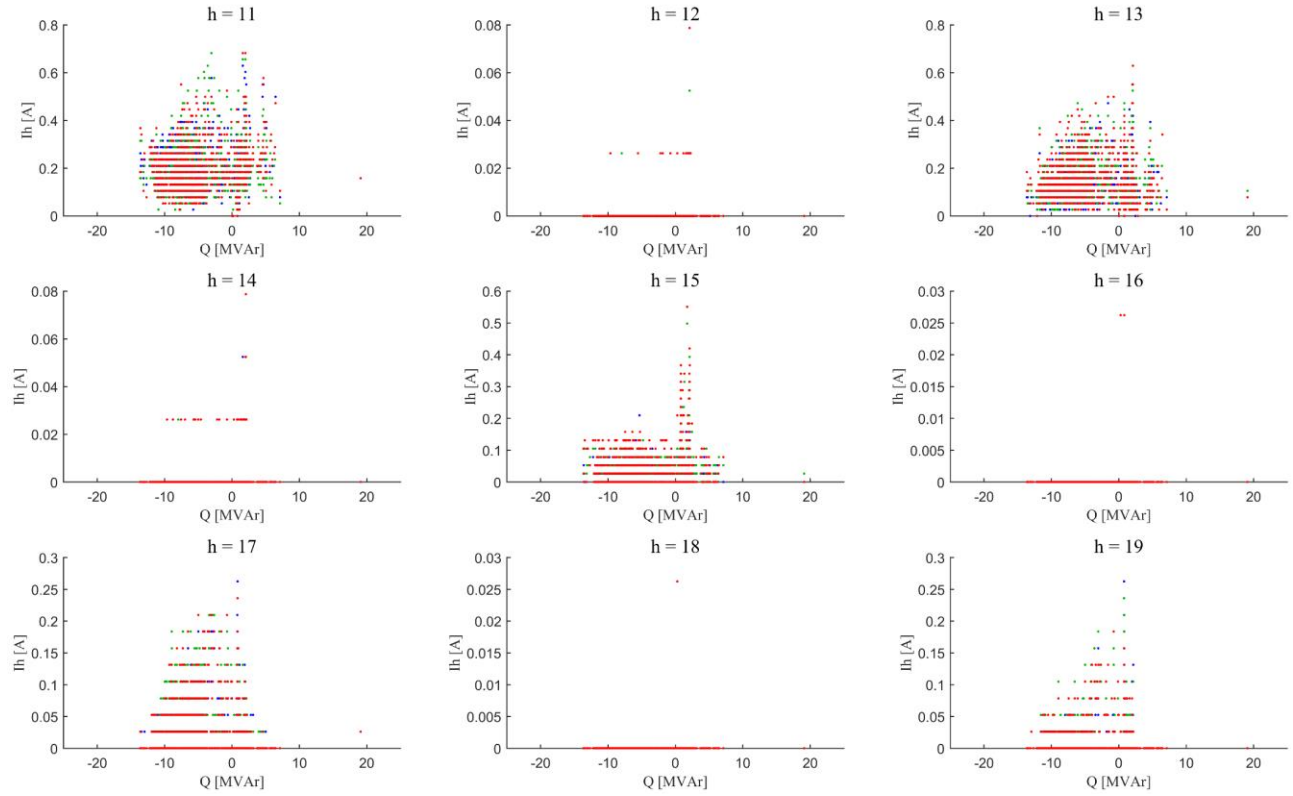

Figure A-11: 10-minute harmonic current emissions vs plant reactive power generation (h = 11 – 19) Red, white and blue phases represented by red, green and blue dots respectively.

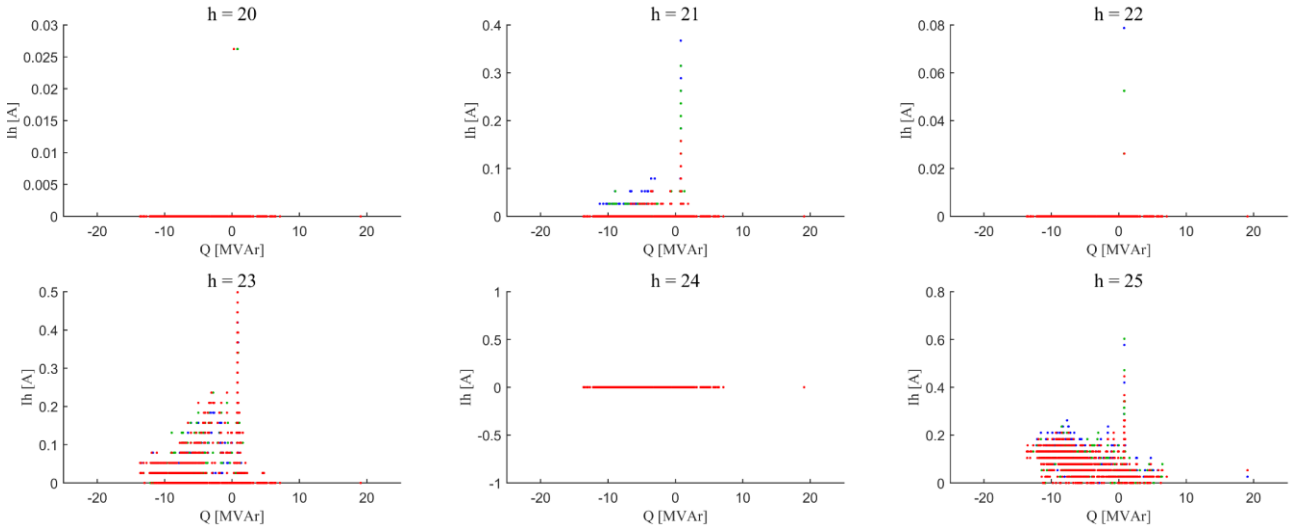

Figure A-12: 10-minute harmonic current emissions vs plant reactive power generation (h = 20 – 25) Red, white and blue phases represented by red, green and blue dots respectively.

Appendix B Scatter plots of POC harmonic voltage and current vs time of day

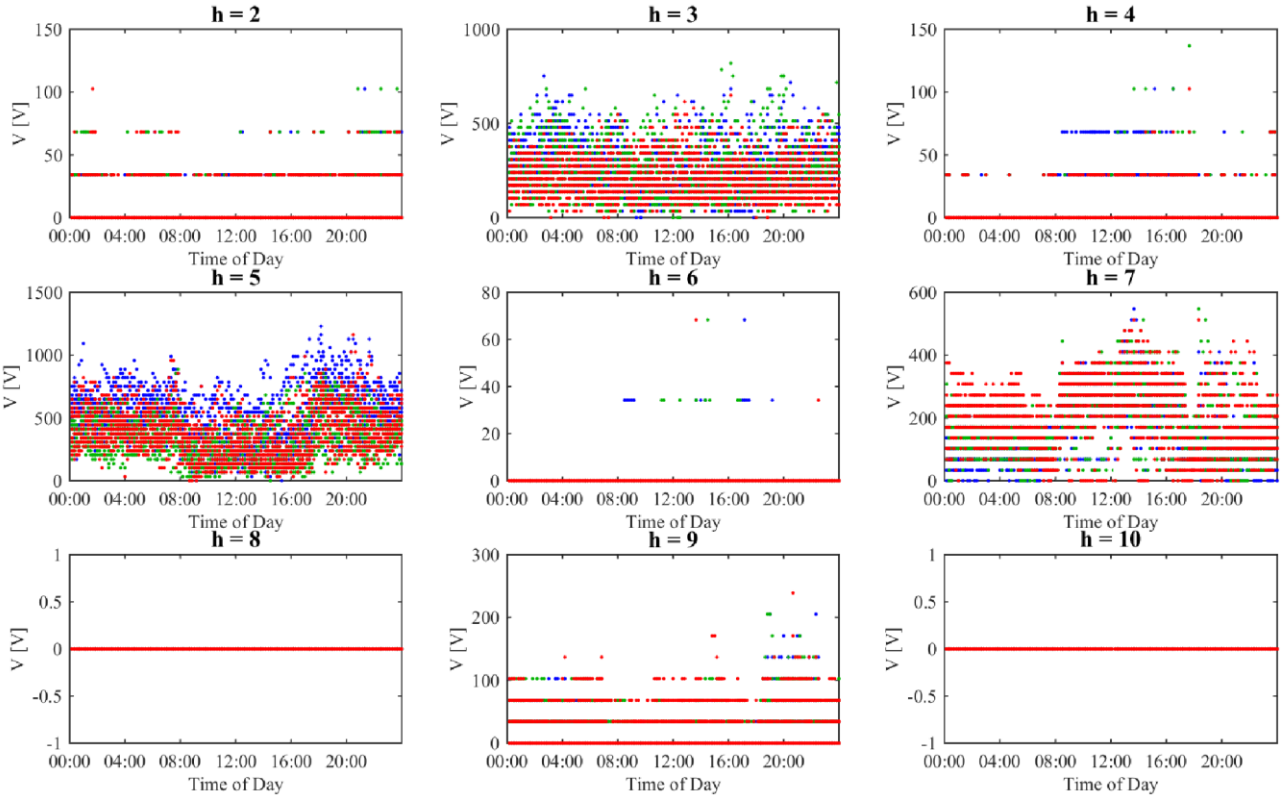

Figure B-1: 10-minute harmonic voltage emissions vs time of day (h = 2 – 10) Red, white and blue phases represented by red, green and blue dots respectively.

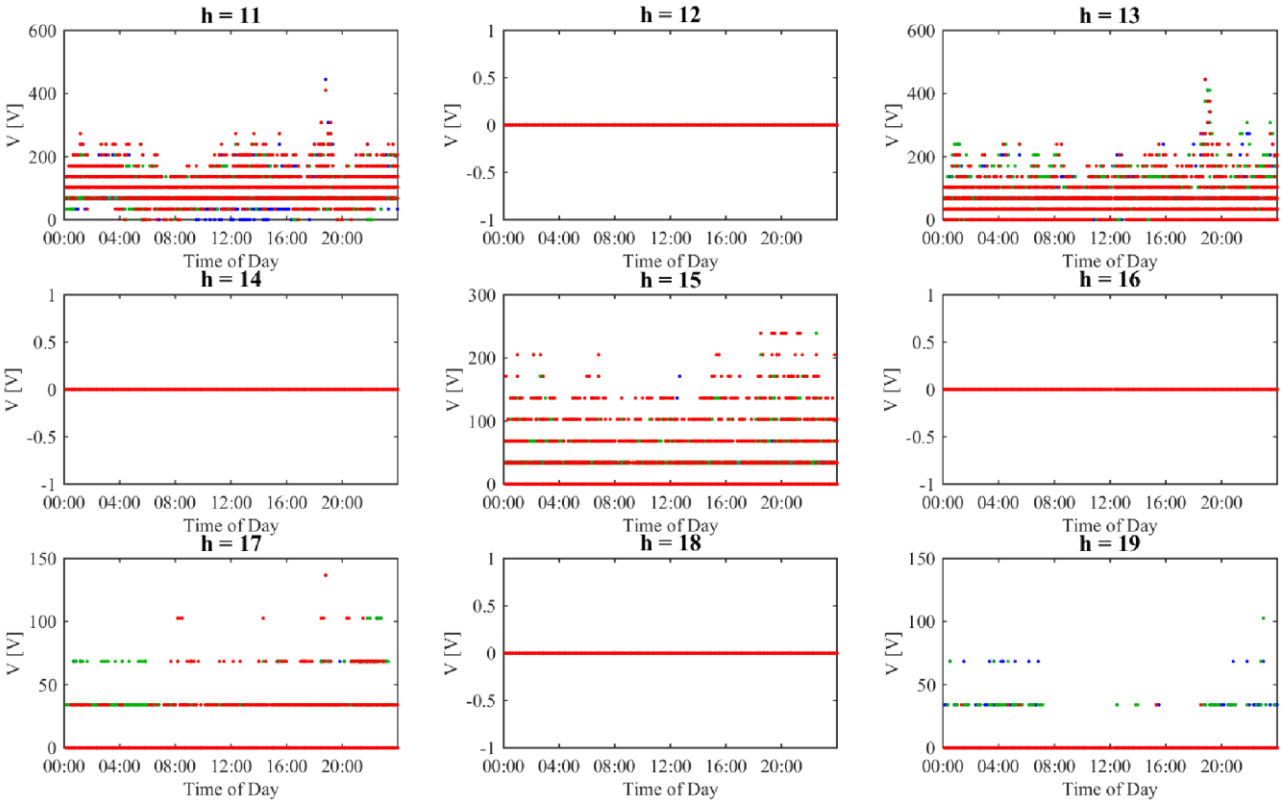

Figure B-2: 10-minute harmonic voltage emissions vs time of day (h = 11 – 19) Red, white and blue phases represented by red, green and blue dots respectively.

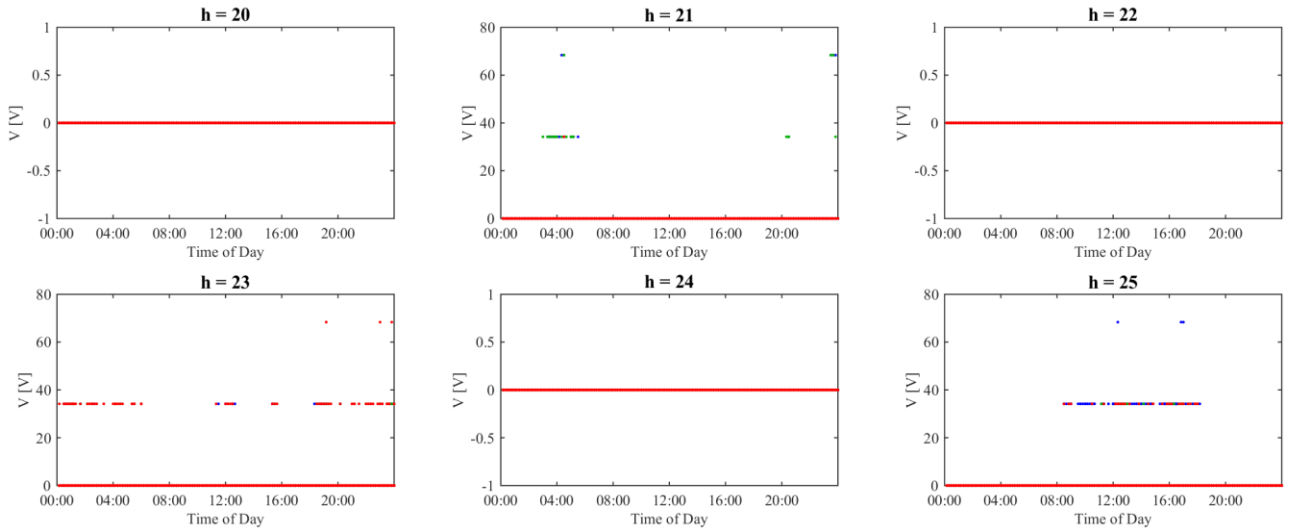

Figure B-3: 10-minute harmonic voltage emissions vs time of day (h = 20 – 25) Red, white and blue phases represented by red, green and blue dots respectively.

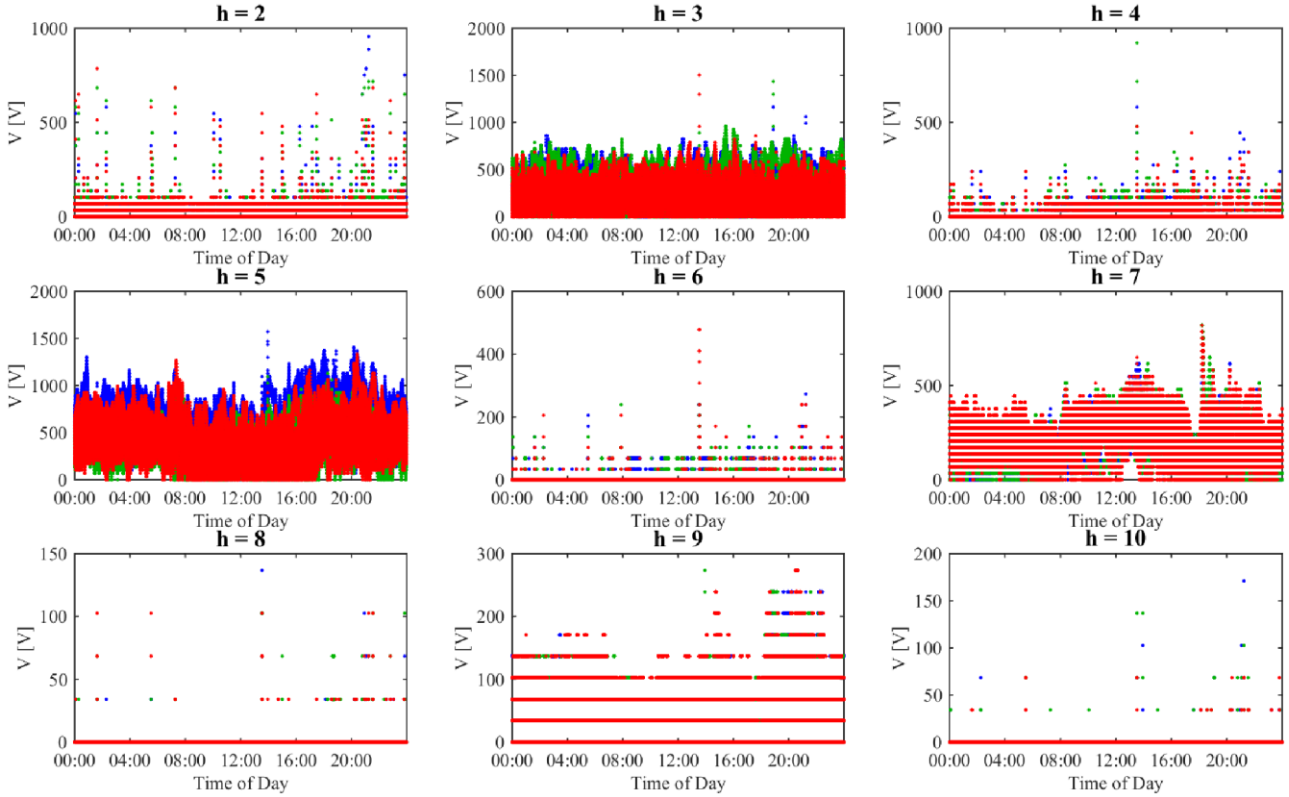

Figure B-4: 3-second harmonic voltage emissions vs time of day (h = 2 – 10) Red, white and blue phases represented by red, green and blue dots respectively.

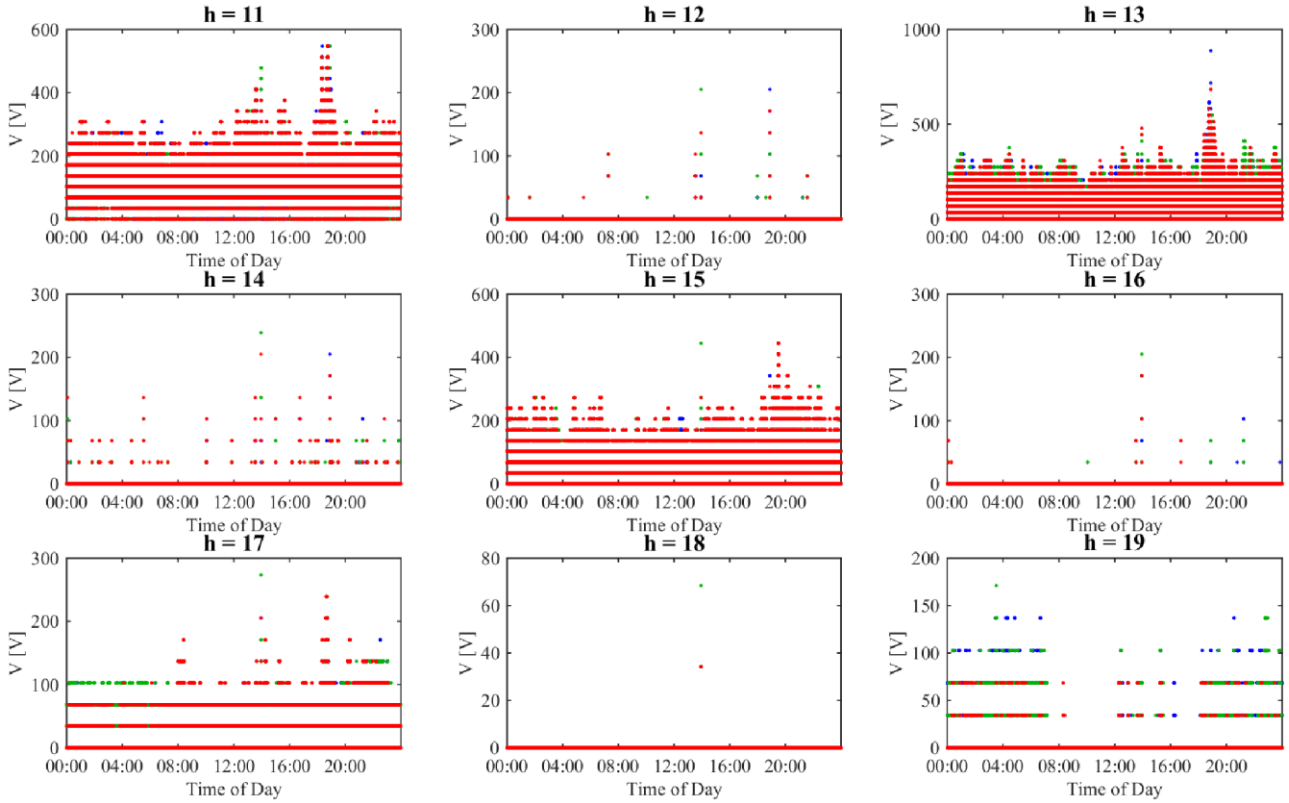

Figure B-5: 3-second harmonic voltage emissions vs time of day (h = 11 – 19) Red, white and blue phases represented by red, green and blue dots respectively.

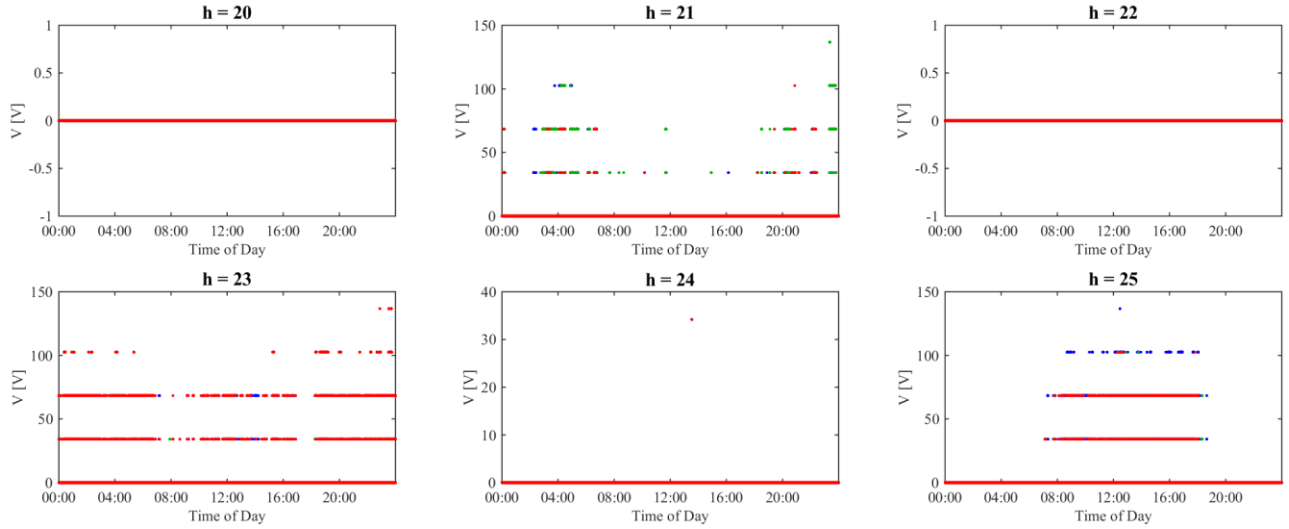

Figure B-6: 3-second harmonic voltage emissions vs time of day (h = 20 – 25) Red, white and blue phases represented by red, green and blue dots respectively.

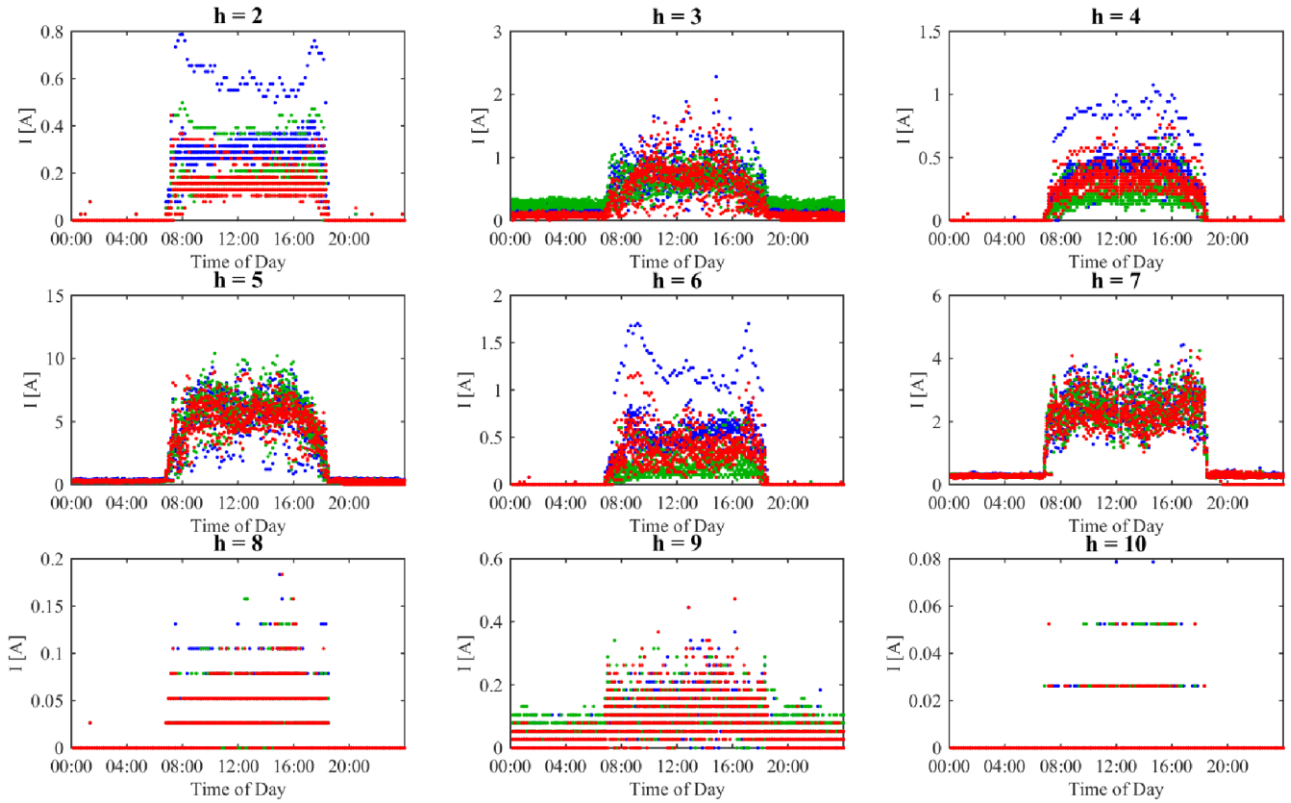

Figure B-7: 10-minute harmonic current emissions vs time of day (h = 2 – 10) Red, white and blue phases represented by red, green and blue dots respectively.

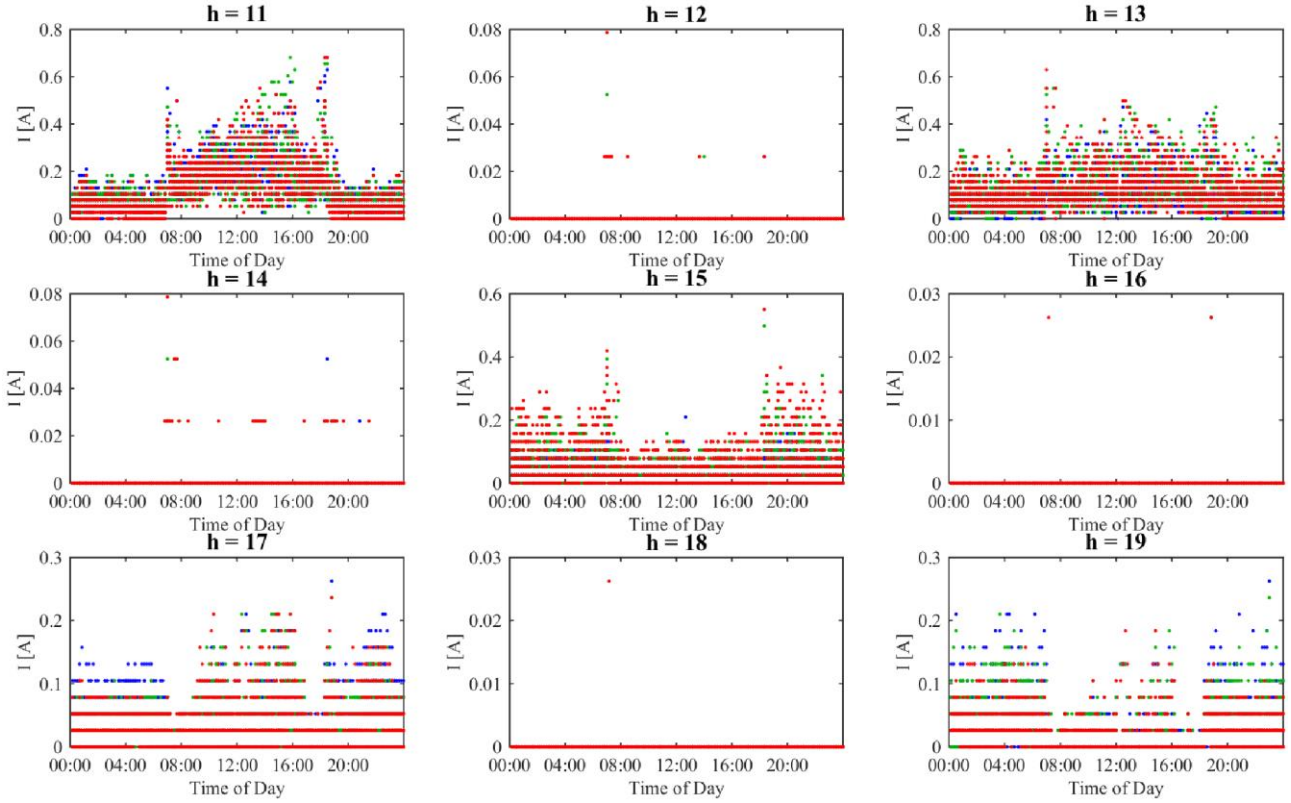

Figure B-8: 10-minute harmonic current emissions vs time of day (h = 11 – 19) Red, white and blue phases represented by red, green and blue dots respectively.

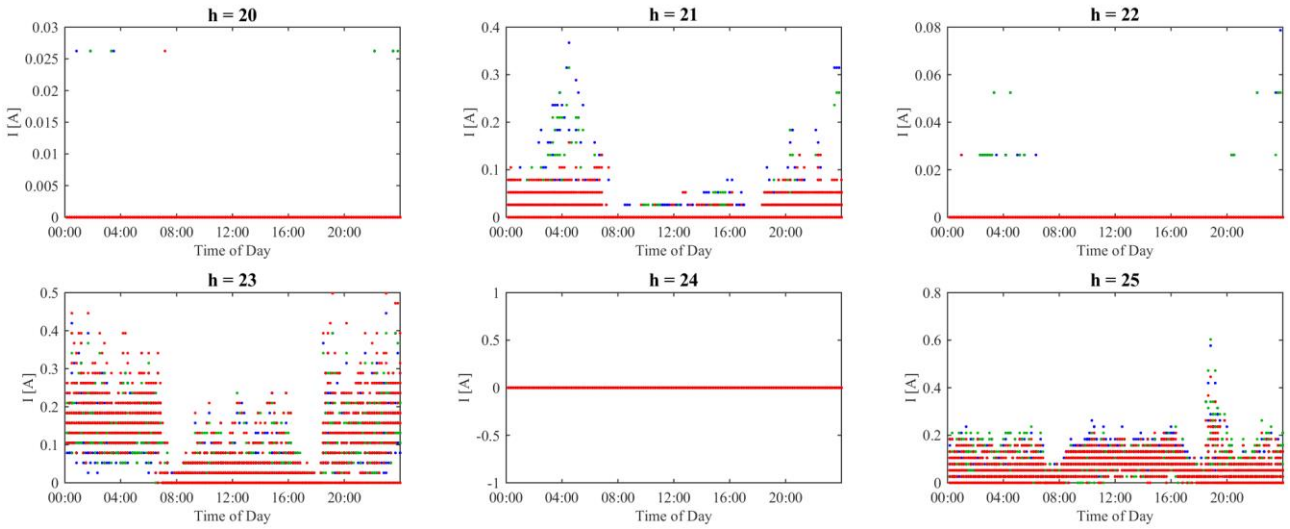

Figure B-9: 10-minute harmonic current emissions vs time of day (h = 20 – 25) Red, white and blue phases represented by red, green and blue dots respectively.

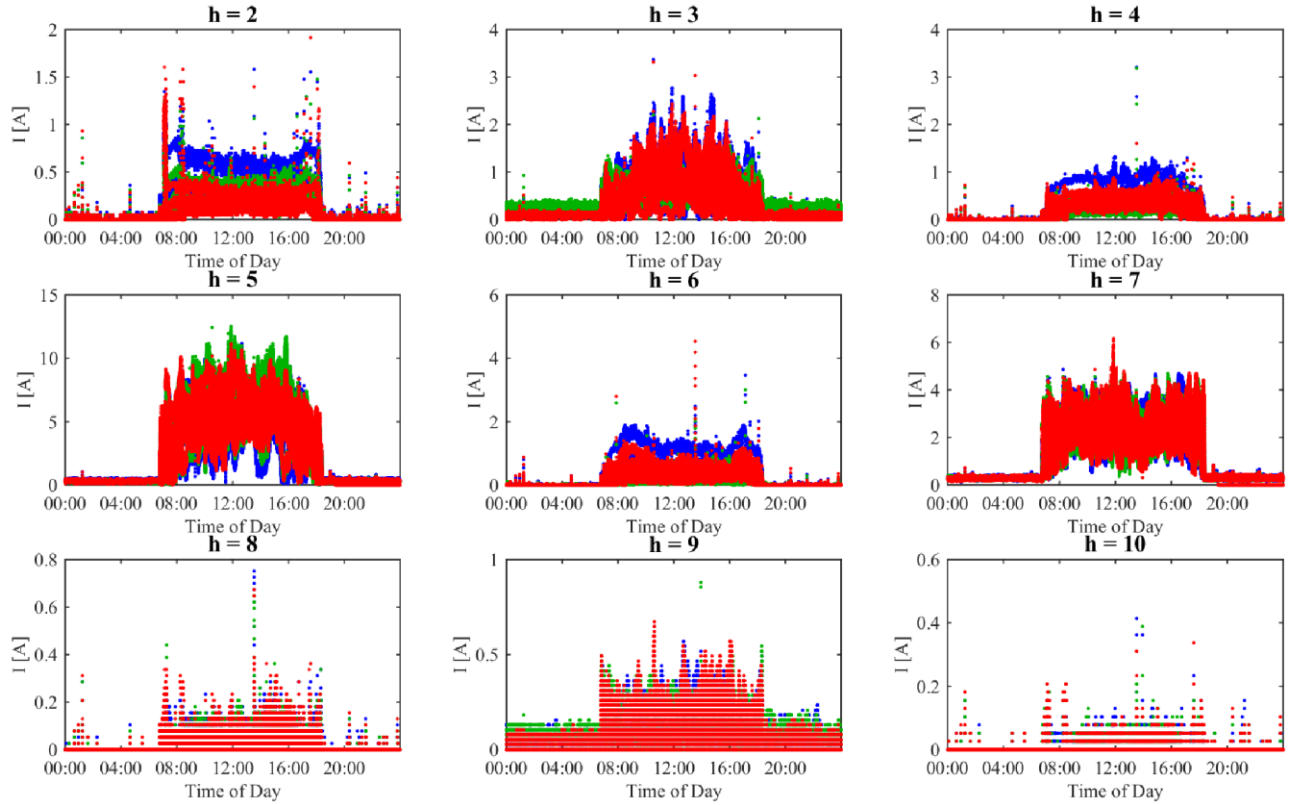

Figure B-10: 3-second harmonic current emissions vs time of day (h = 2 – 10) Red, white and blue phases represented by red, green and blue dots respectively.

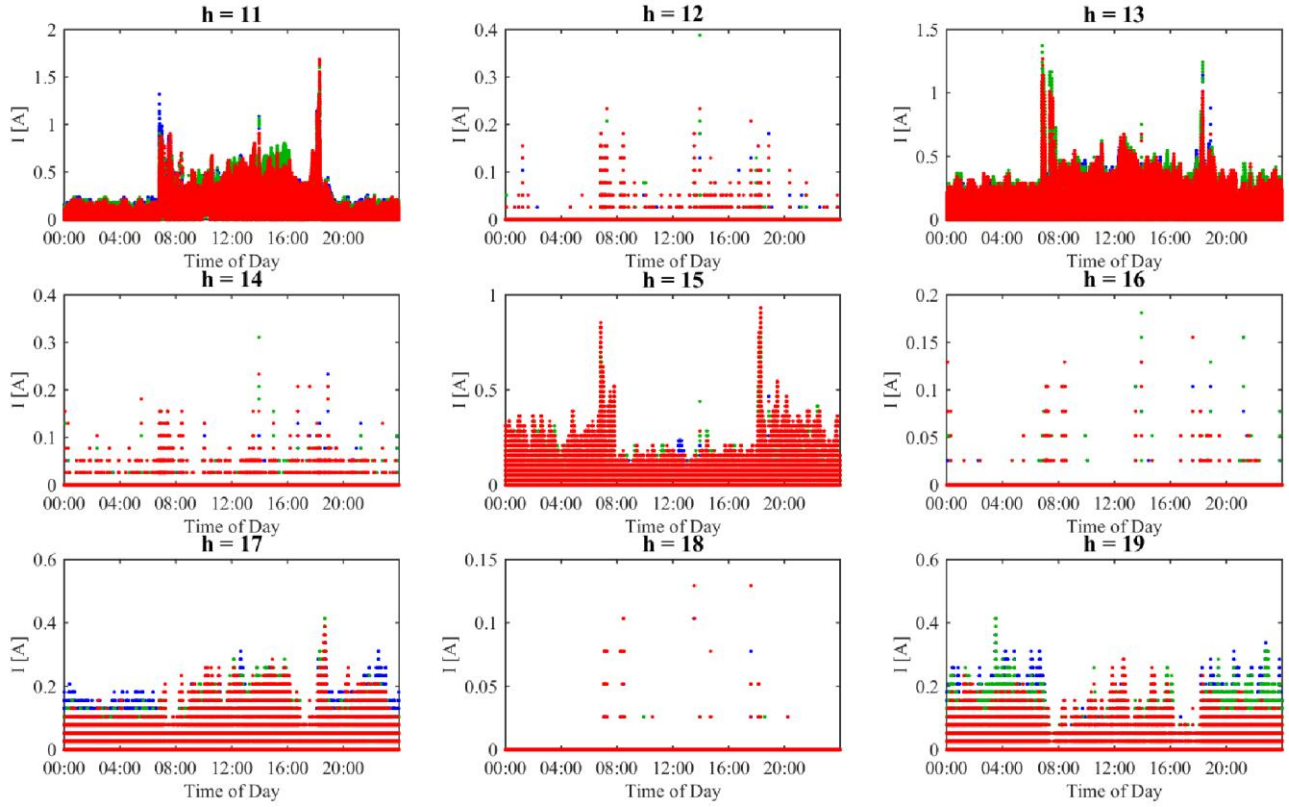

Figure B-11: 3-second harmonic current emissions vs time of day (h = 11 – 19) Red, white and blue phases represented by red, green and blue dots respectively.

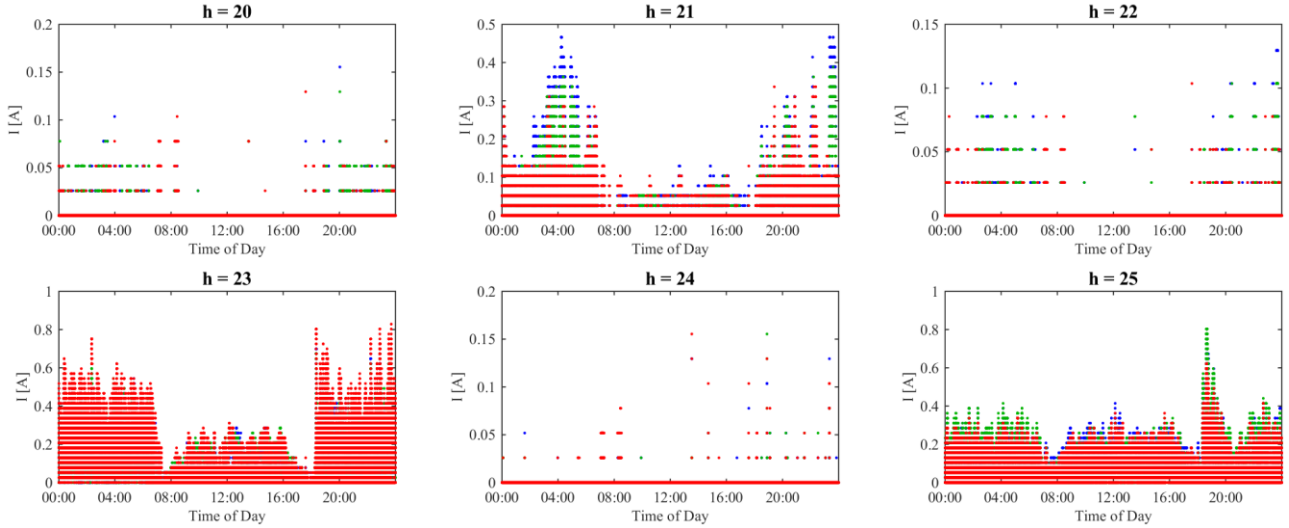

Figure B-12: 3-second harmonic current emissions vs time of day (h = 20 – 25) Red, white and blue phases represented by red, green and blue dots respectively.

Appendix C Bar plots of mean background and operating harmonic voltages and currents

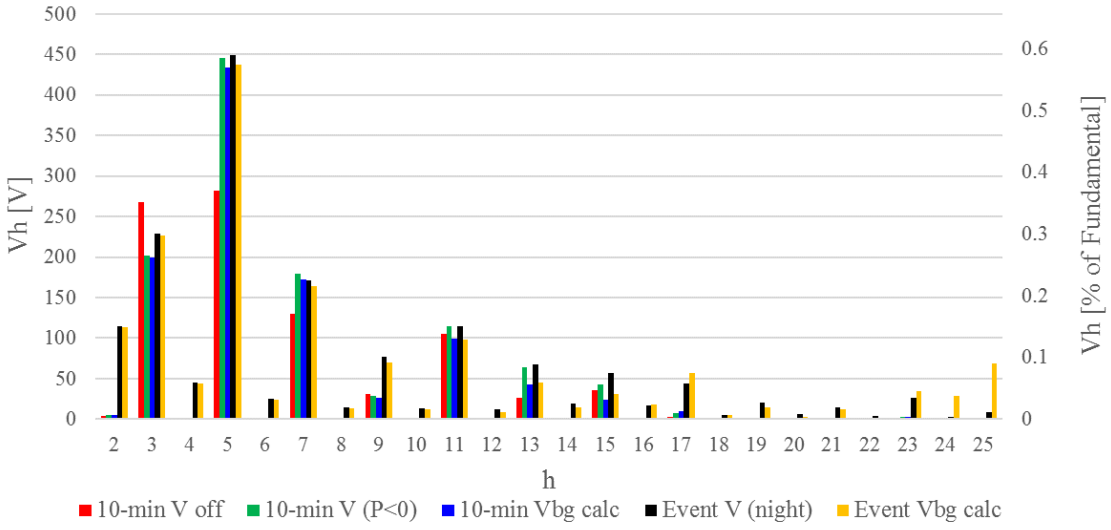

Figure C-1: Background harmonic voltage assessment results (Red Phase)

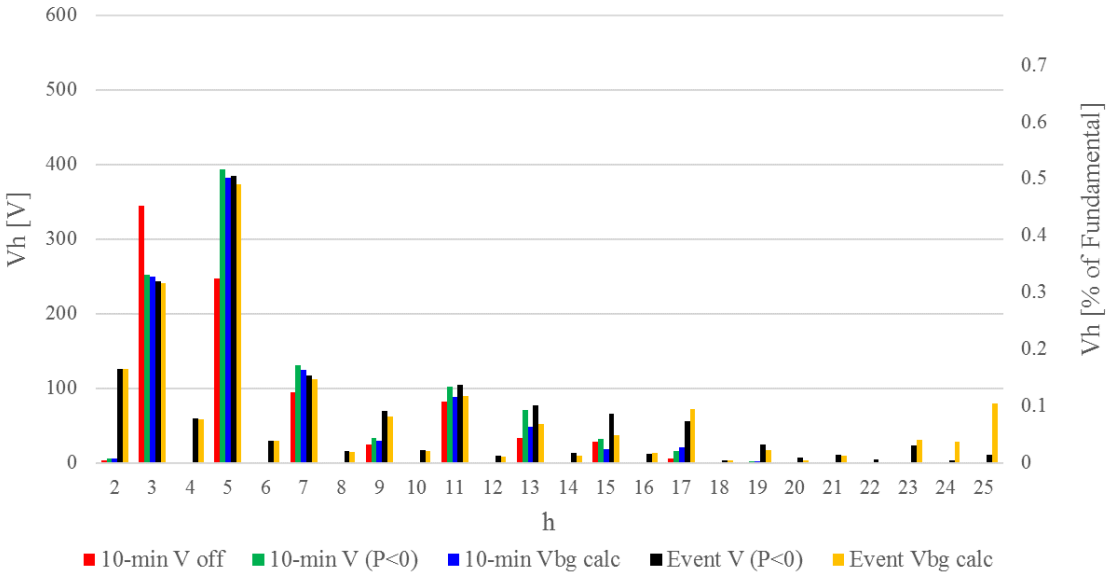

Figure C-2: Background harmonic voltage assessment results (White Phase)

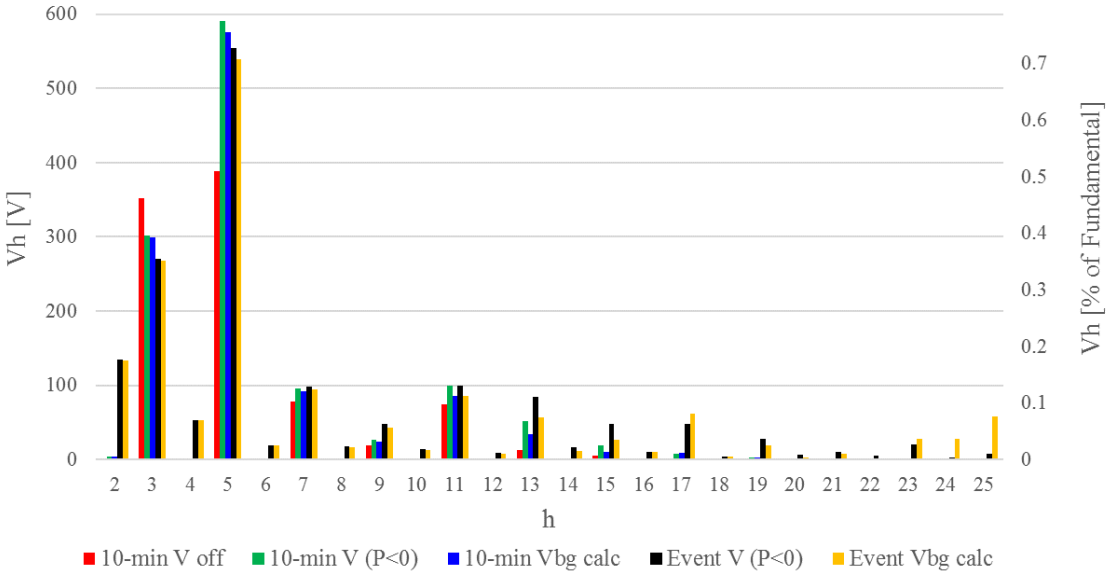

Figure C-3: Background harmonic voltage assessment results (Blue Phase)

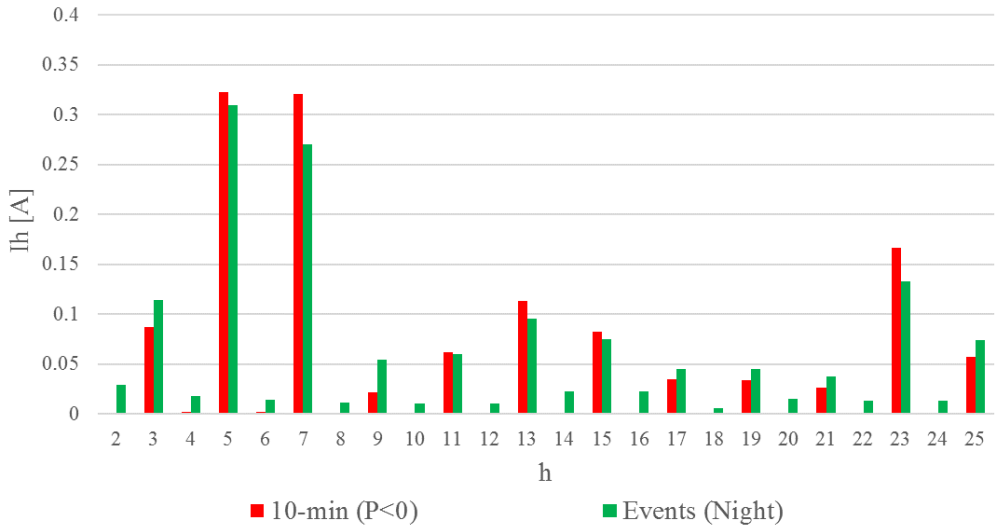

Figure C-4: Mean red phase harmonic currents measured at POC when plant is not operating

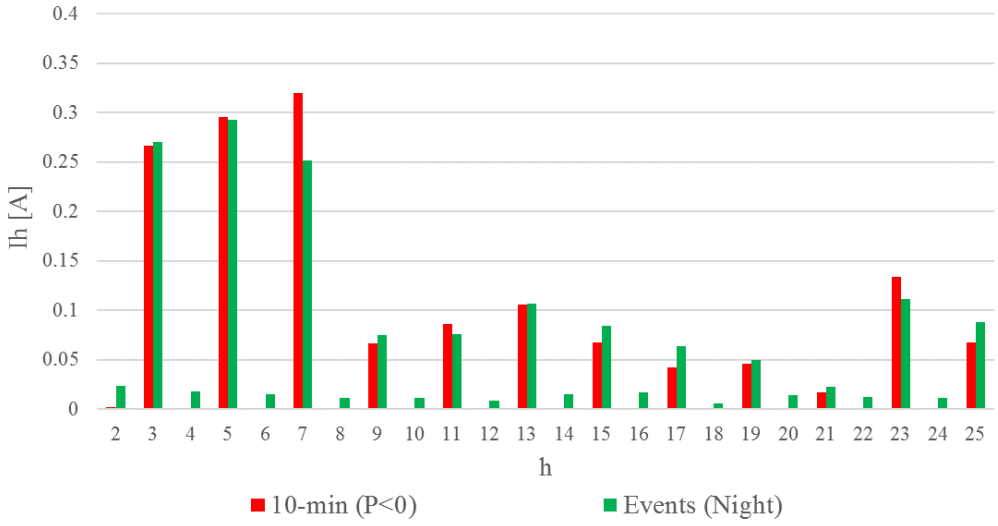

Figure C-5: Mean white phase harmonic currents measured at POC when plant is not operating

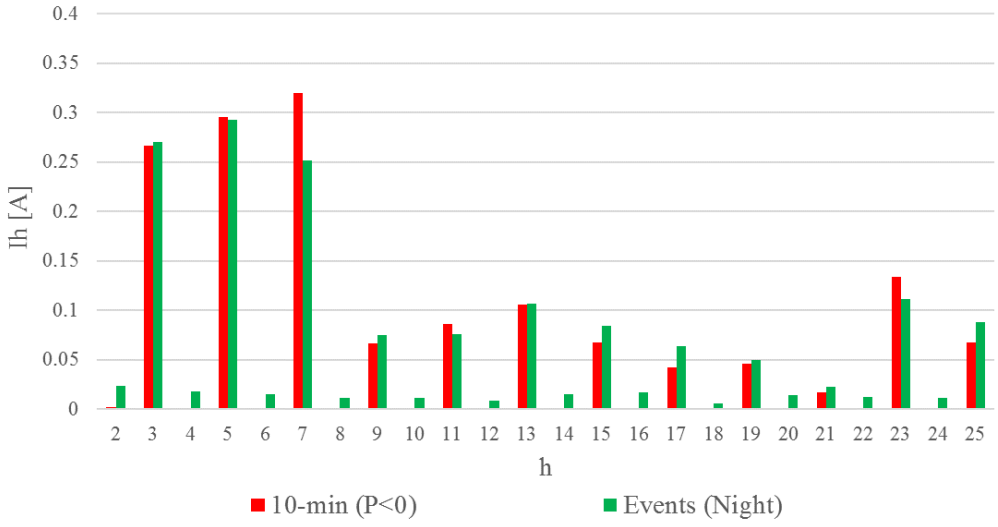

Figure C-6: Mean blue phase harmonic currents measured at POC when plant is not operating

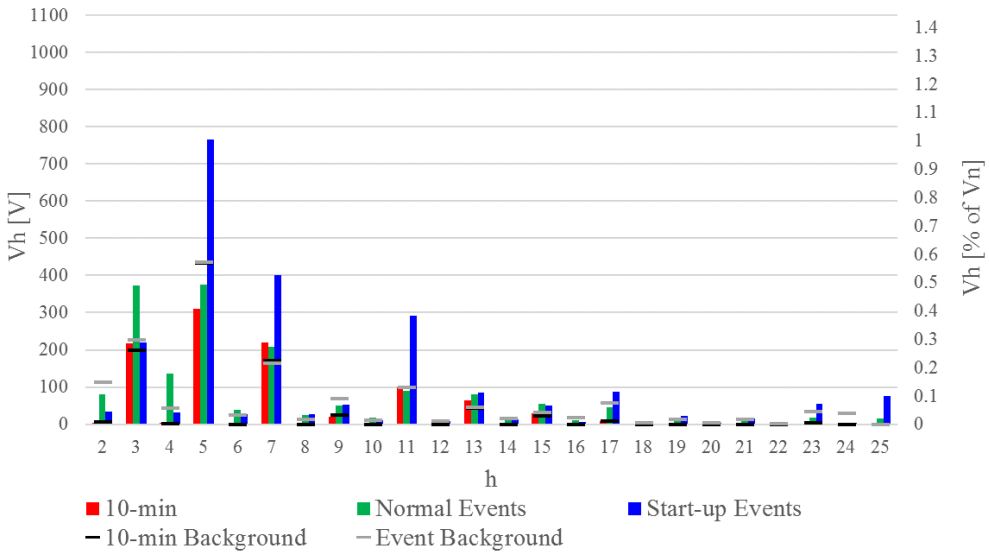

Figure C-7: Mean red phase harmonic voltages from daytime measurements

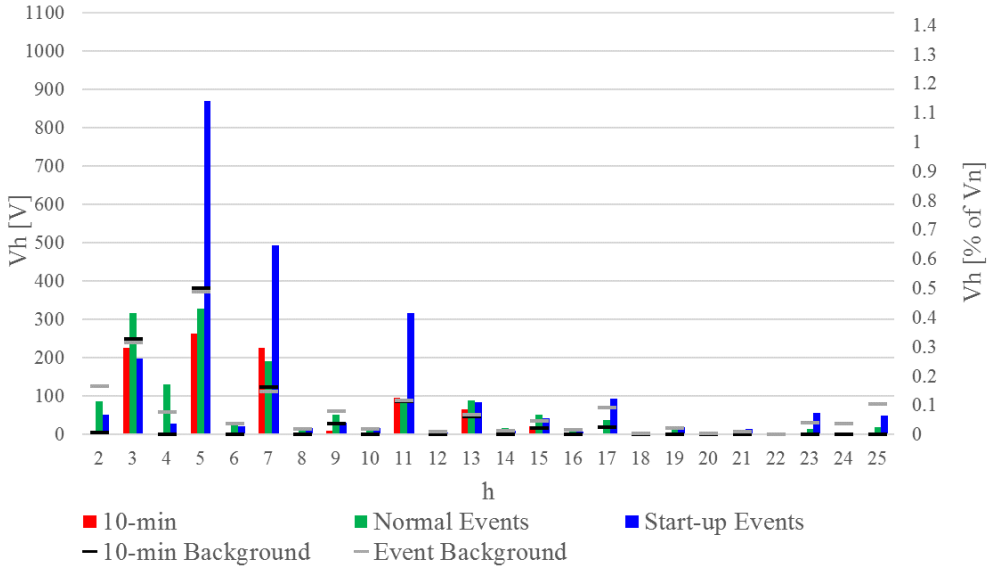

Figure C-8: Mean white phase harmonic voltages from daytime measurements

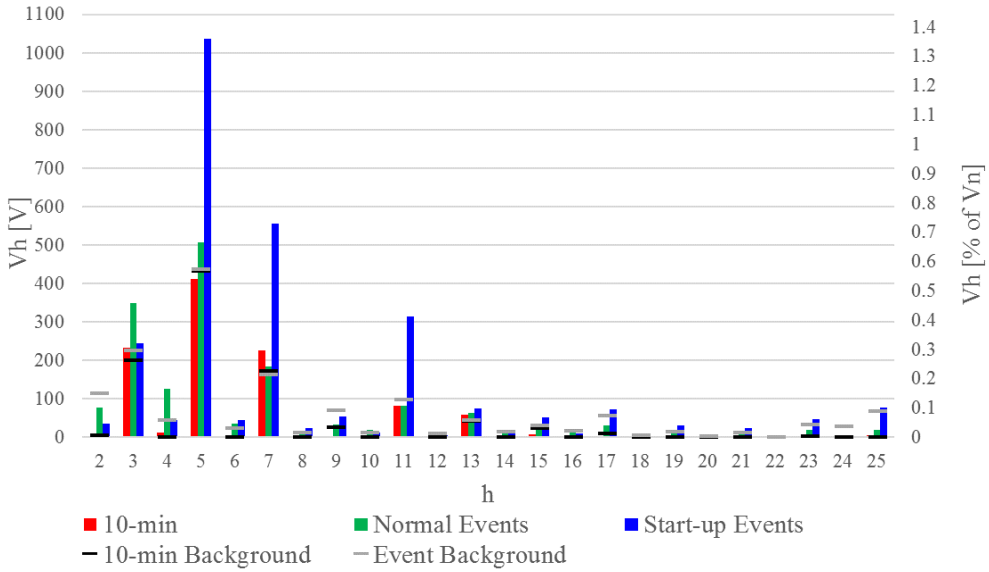

Figure C-9: Mean blue phase harmonic voltages from daytime measurements

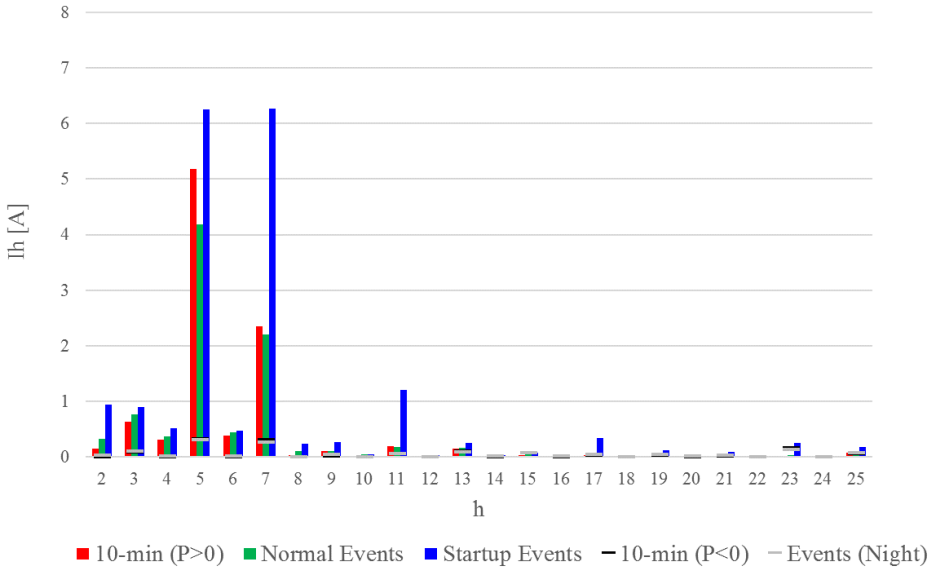

Figure C-10: Mean red phase harmonic currents from daytime measurements

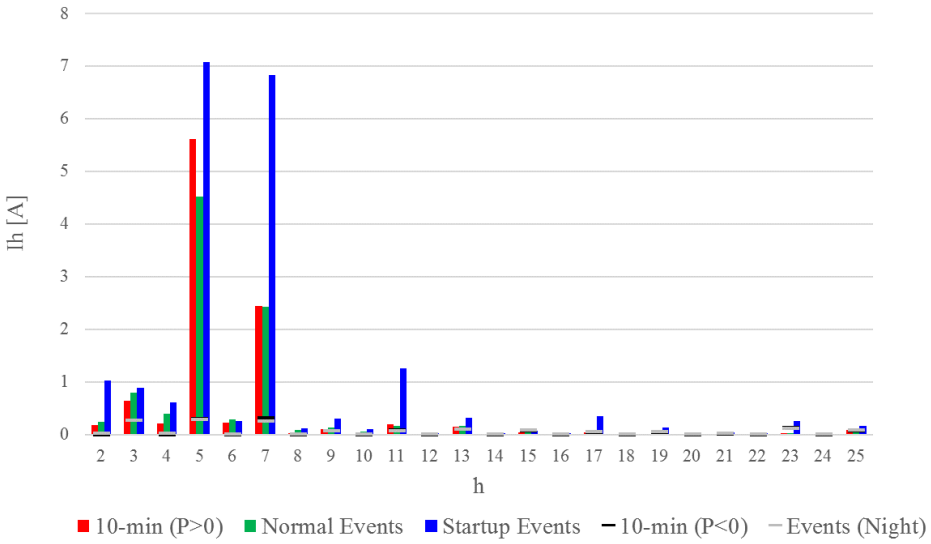

Figure C-11: Mean white phase harmonic currents from daytime measurements

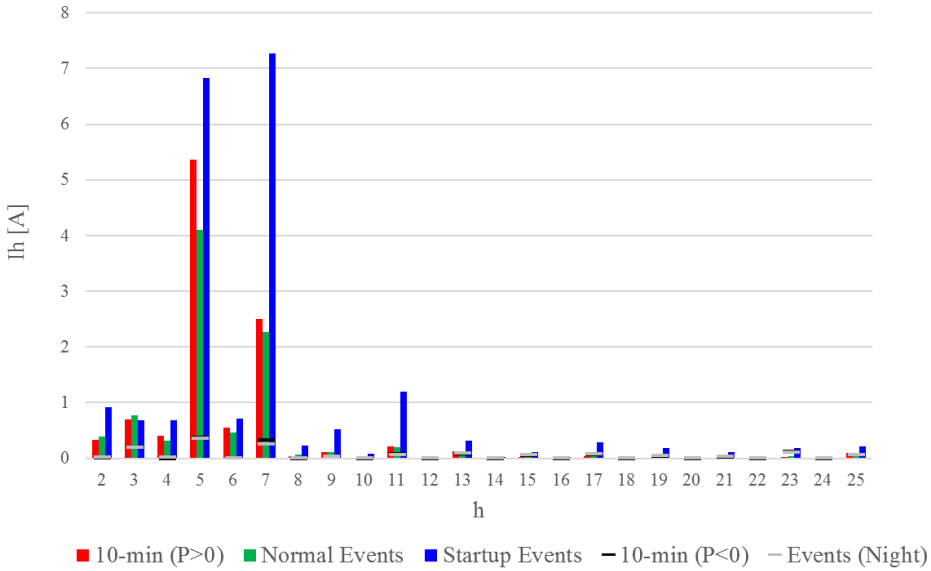

Figure C-12: Mean blue phase harmonic currents from daytime measurements

Appendix D Emissions calculation results for red, white and blue phases

D.1 Method 1: Reverse application of general summation law

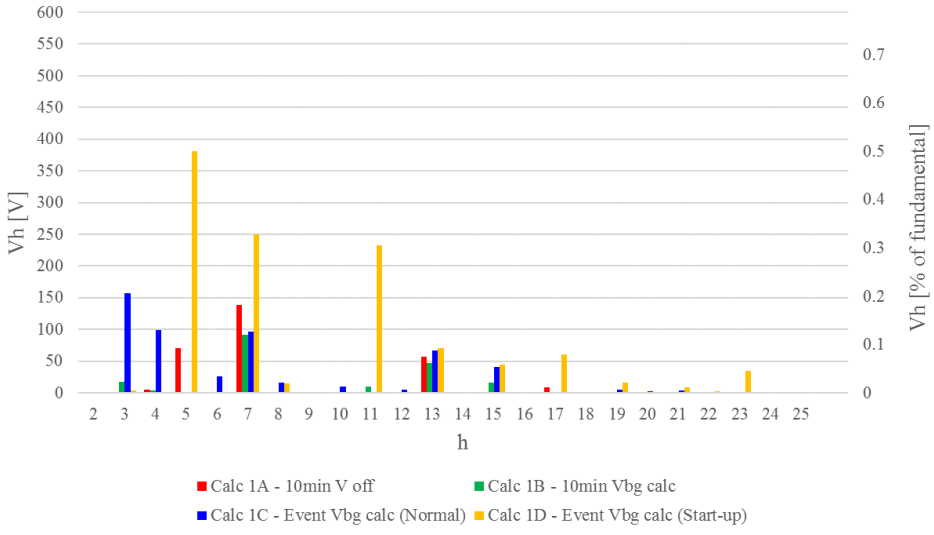

Figure D-1: Method 1 mean harmonic voltage emissions (red phase)

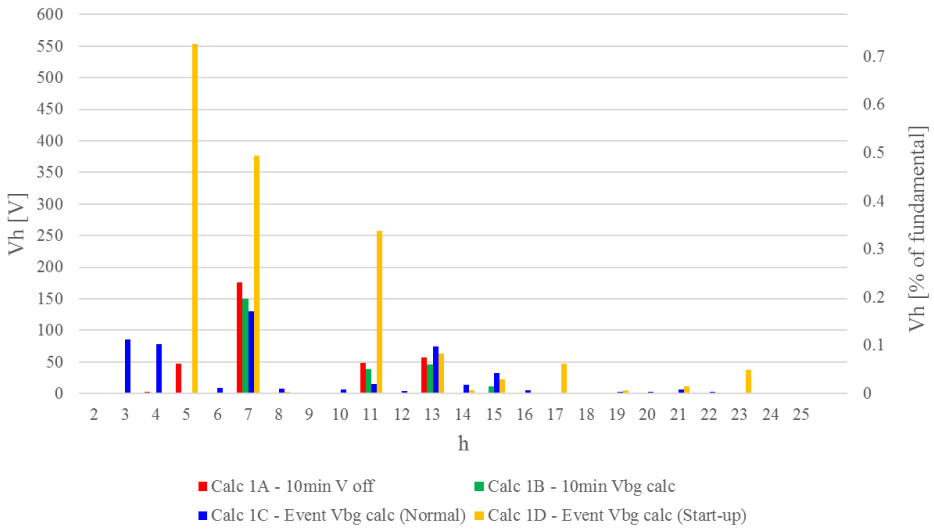

Figure D-2: Method 1 mean harmonic voltage emissions (white phase)

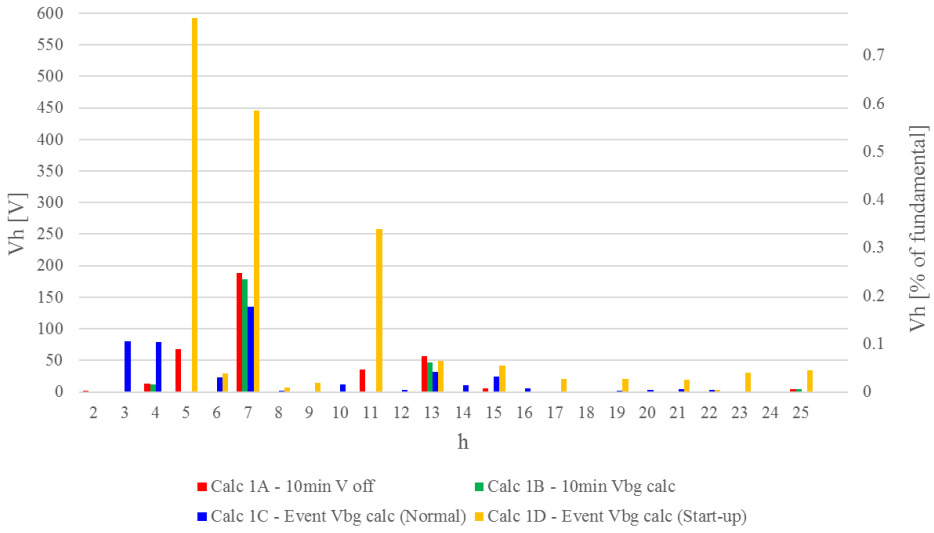

Figure D-3: Method 1 mean harmonic voltage emissions (blue phase)

D.2 Method 2: Harmonic voltage phasor method

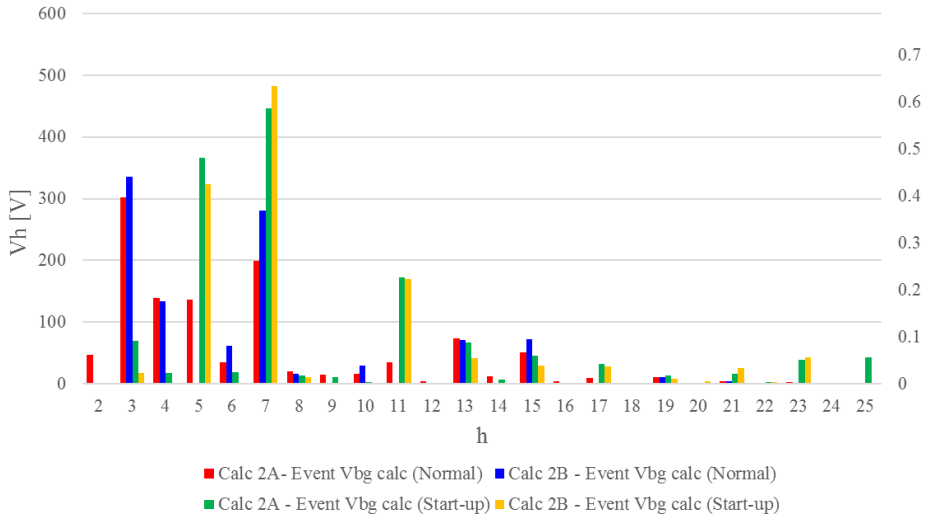

Figure D-4: Method 2 mean harmonic voltage emissions (red phase)

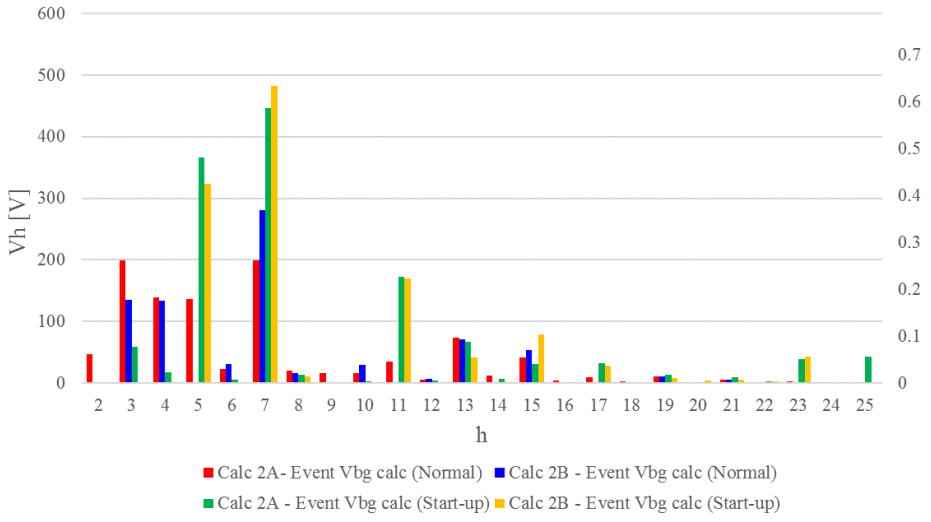

Figure D-5: Method 2 mean harmonic voltage emissions (white phase)

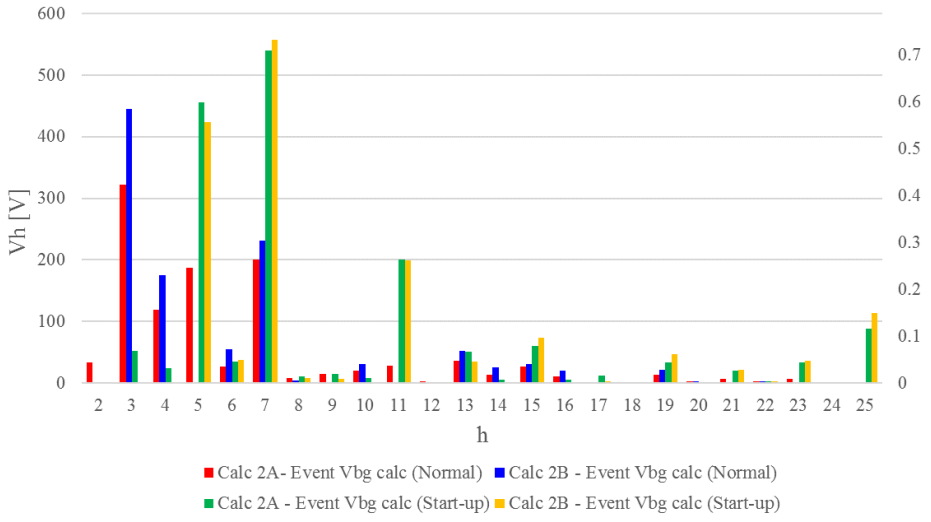

Figure D-6: Method 2 mean harmonic voltage emissions (blue phase)

D.3 Method 3: IEC 61000-3-6 Scatter Plots

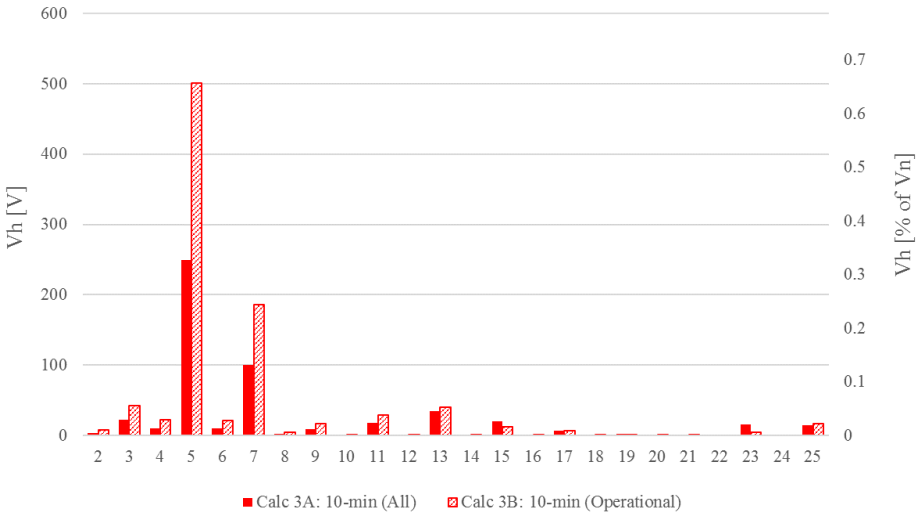

Figure D-7: Method 3 mean harmonic voltage emissions (red phase)

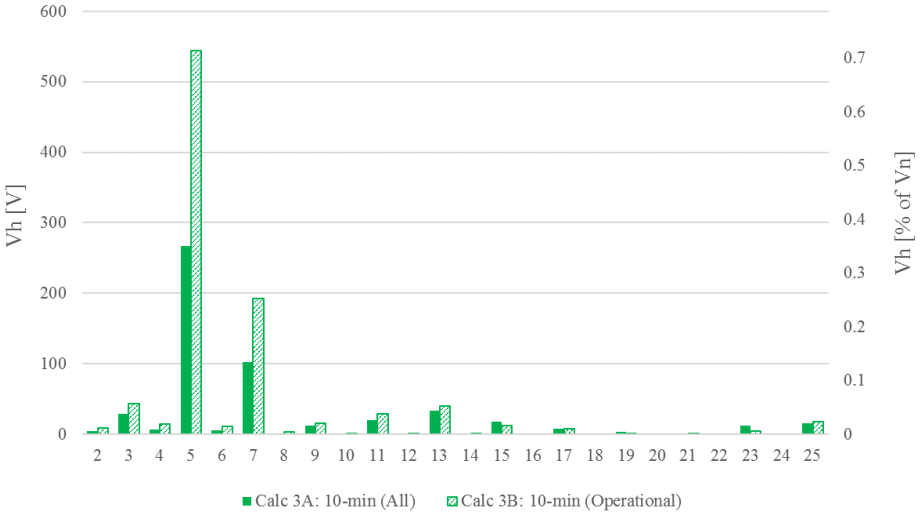

Figure D-8: Method 3 mean harmonic voltage emissions (white phase)

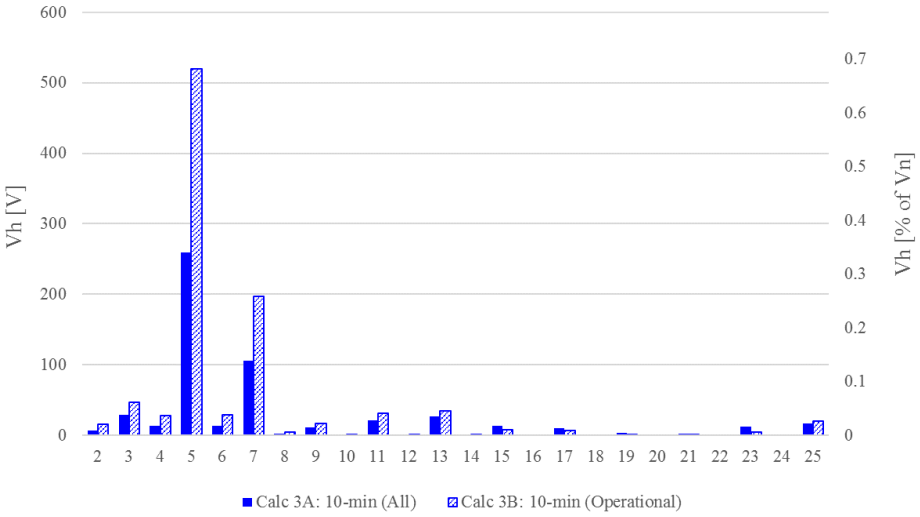

Figure D-9: Method 3 mean harmonic voltage emissions (blue phase)

D.4 Method 4: Harmonic vector method

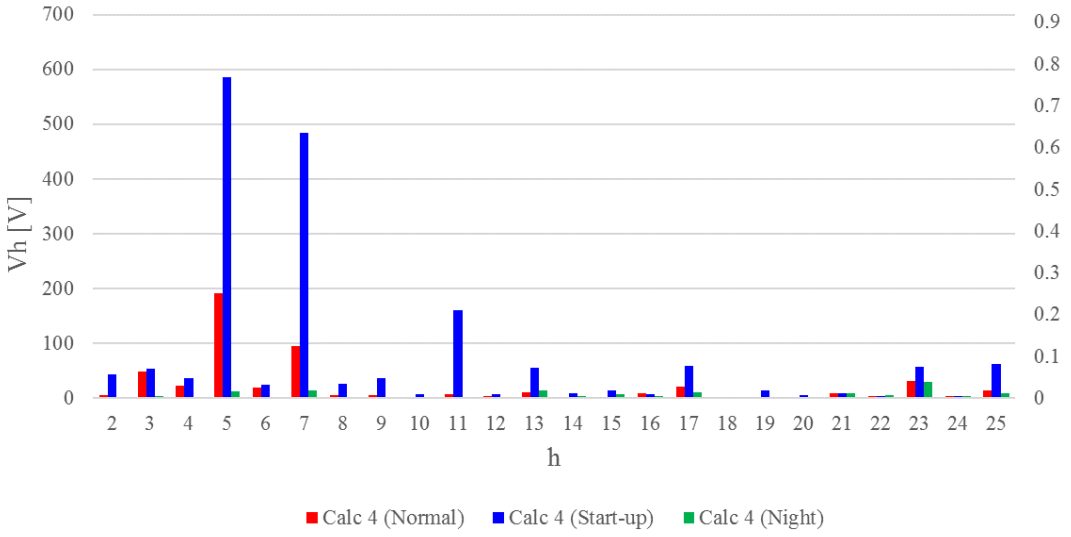

Figure D-10: Method 3 mean harmonic voltage emissions (red phase)

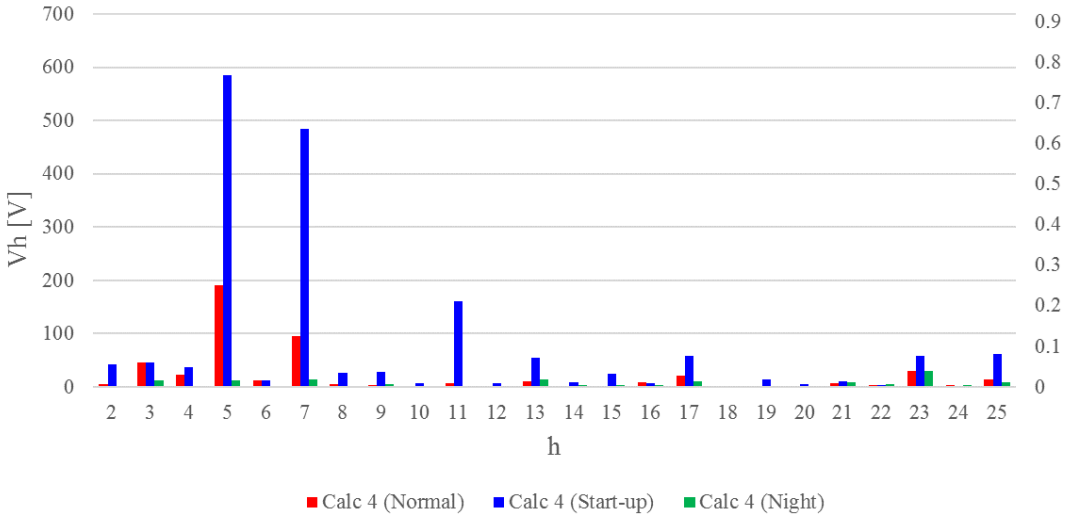

Figure D-11: Method 3 mean harmonic voltage emissions (white phase)

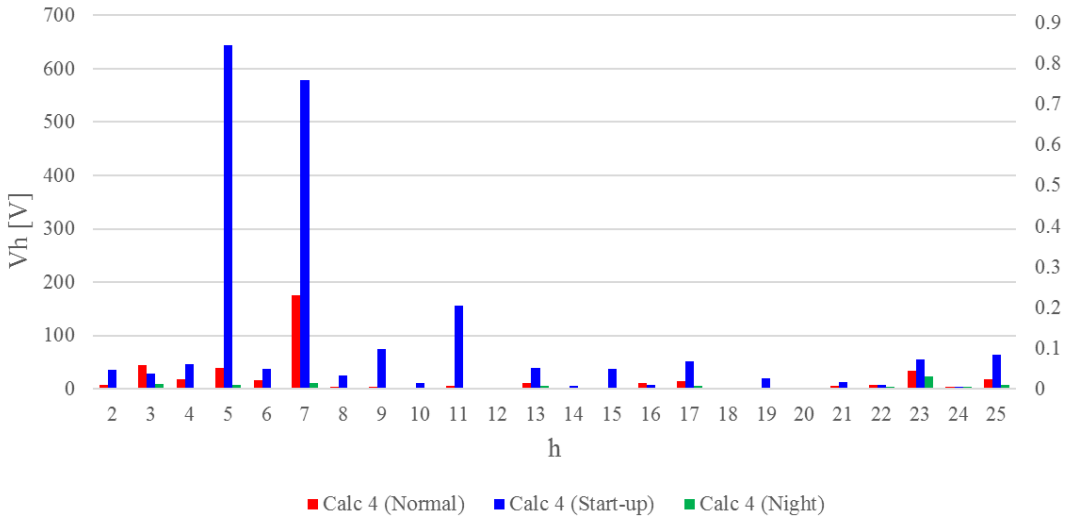

Figure D-12: Method 3 mean harmonic voltage emissions (blue phase)

D.5 Comparison of mean, P75 and P90 voltage emission calculations

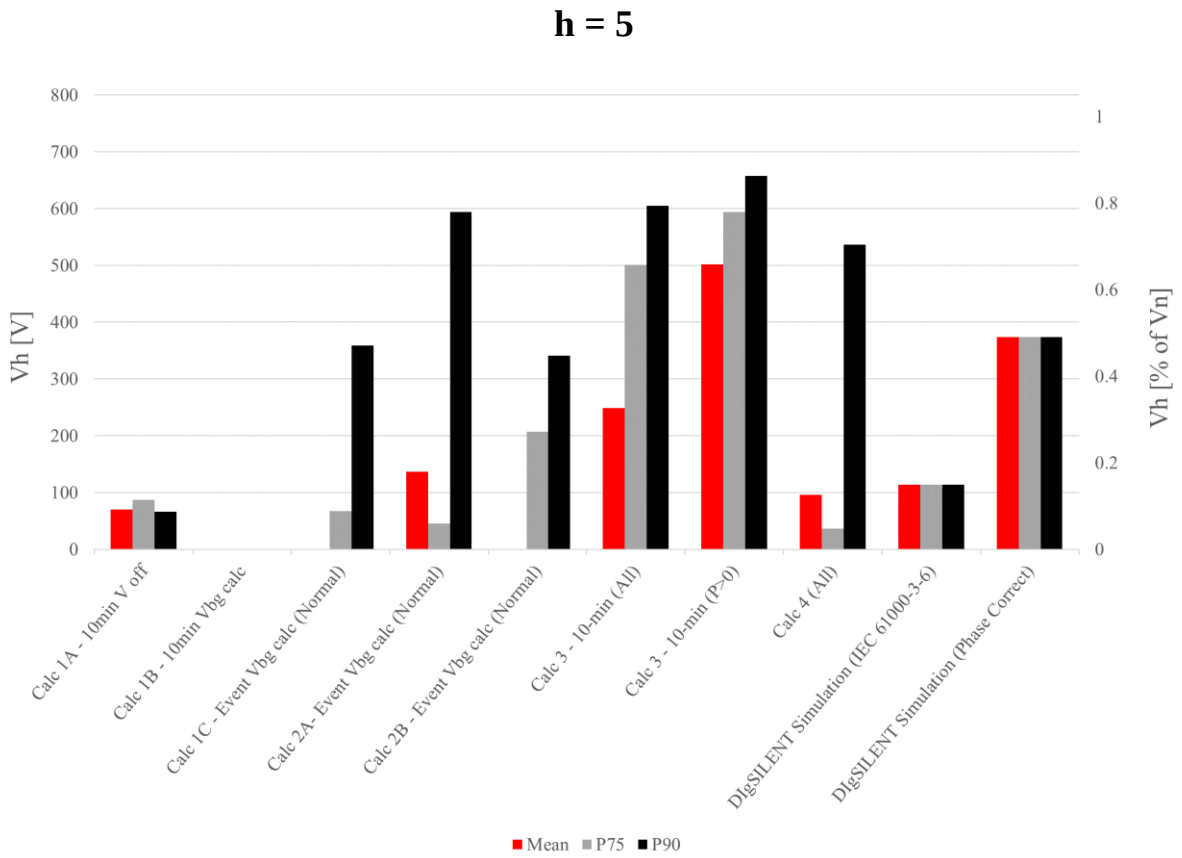

Figure D-13: Comparison of calculation methods for normal operation (h = 5, red phase)

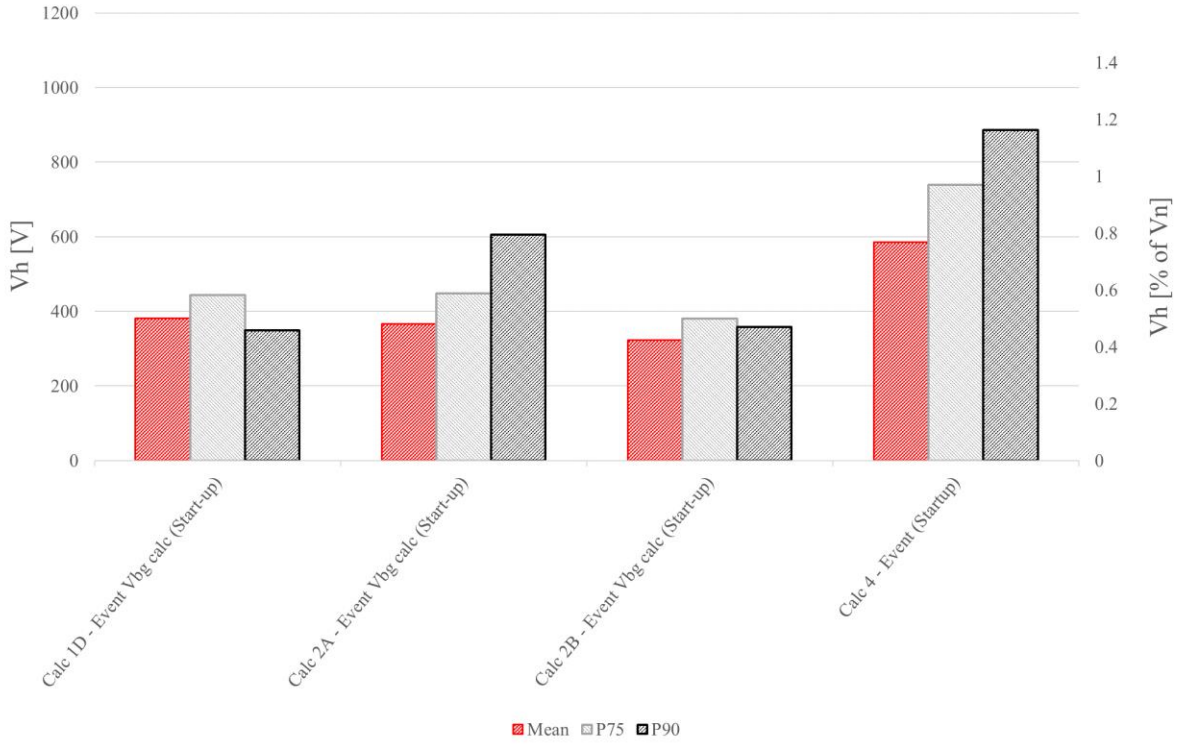

Figure D-14: Comparison of calculation methods for start-up operation (h = 5, red phase)

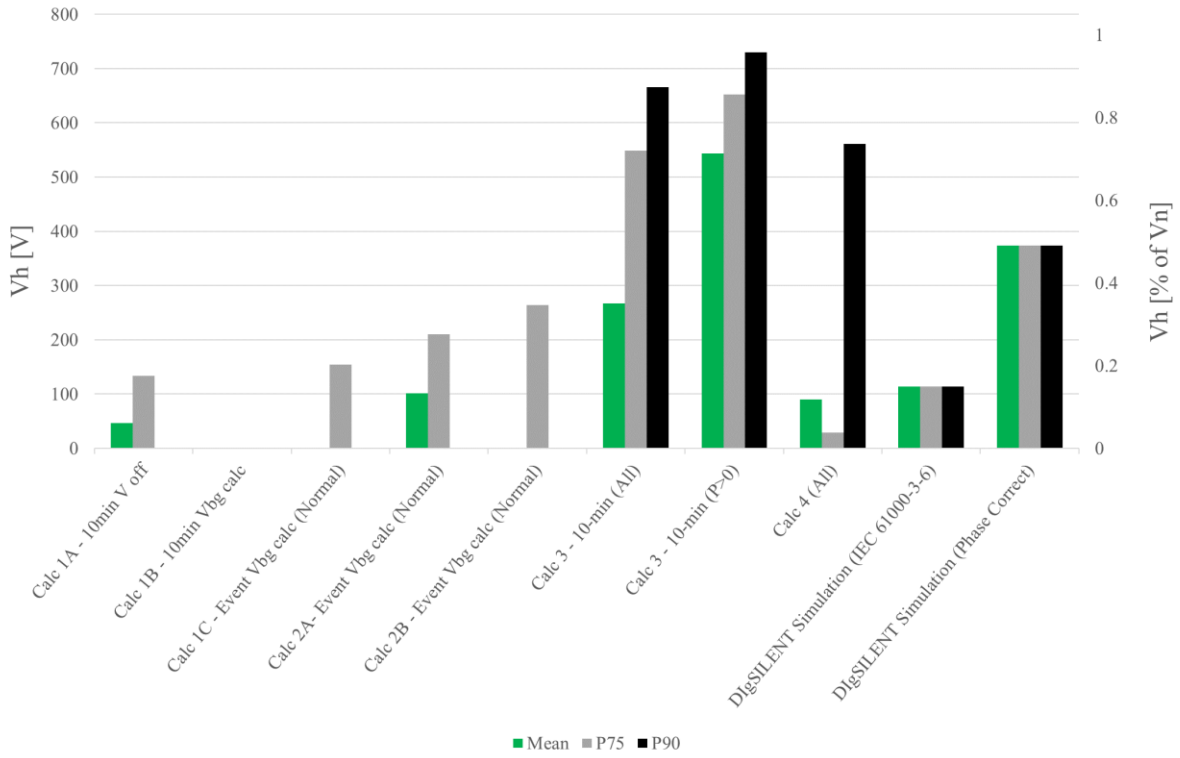

Figure D-15: Comparison of calculation methods for normal operation (h = 5, white phase)

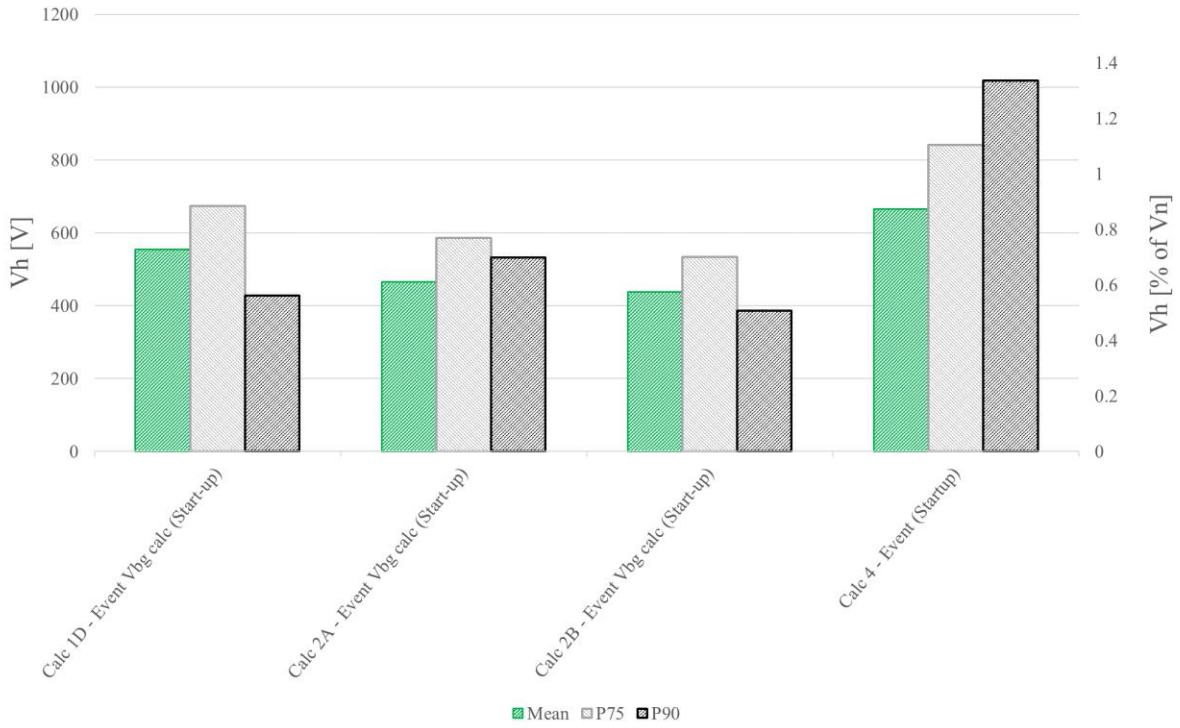

Figure D-16: Comparison of calculation methods for start-up operation (h = 5, white phase)

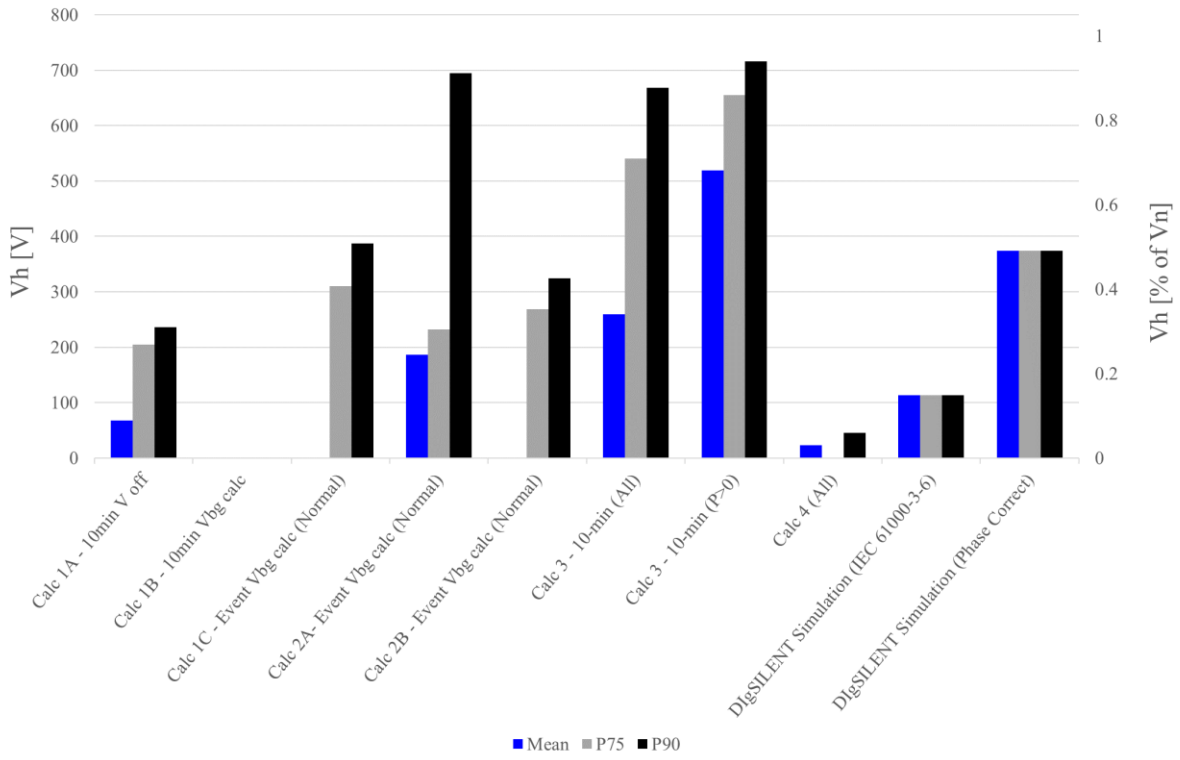

Figure D-17: Comparison of calculation methods for normal operation (h = 5, blue phase)

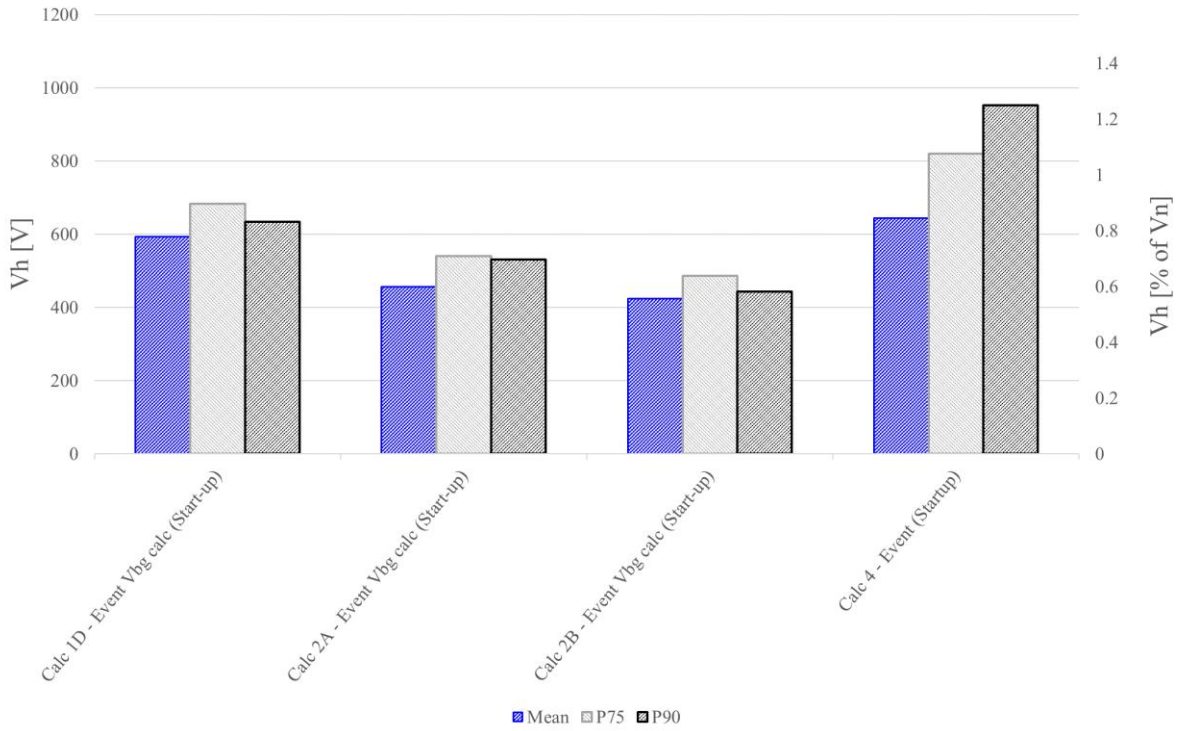

Figure D-18: Comparison of calculation methods for start-up operation (h = 5, blue phase)

h = 7

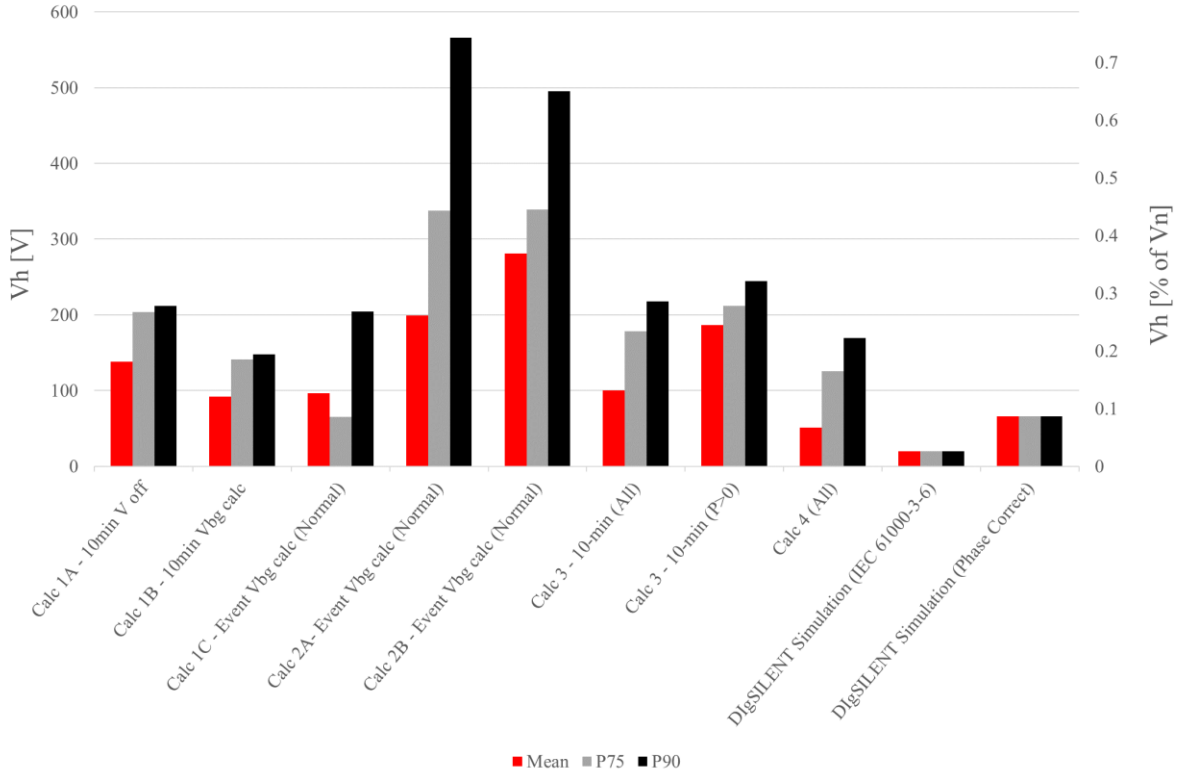

Figure D-19: Comparison of calculation methods for normal operation (h = 7, red phase)

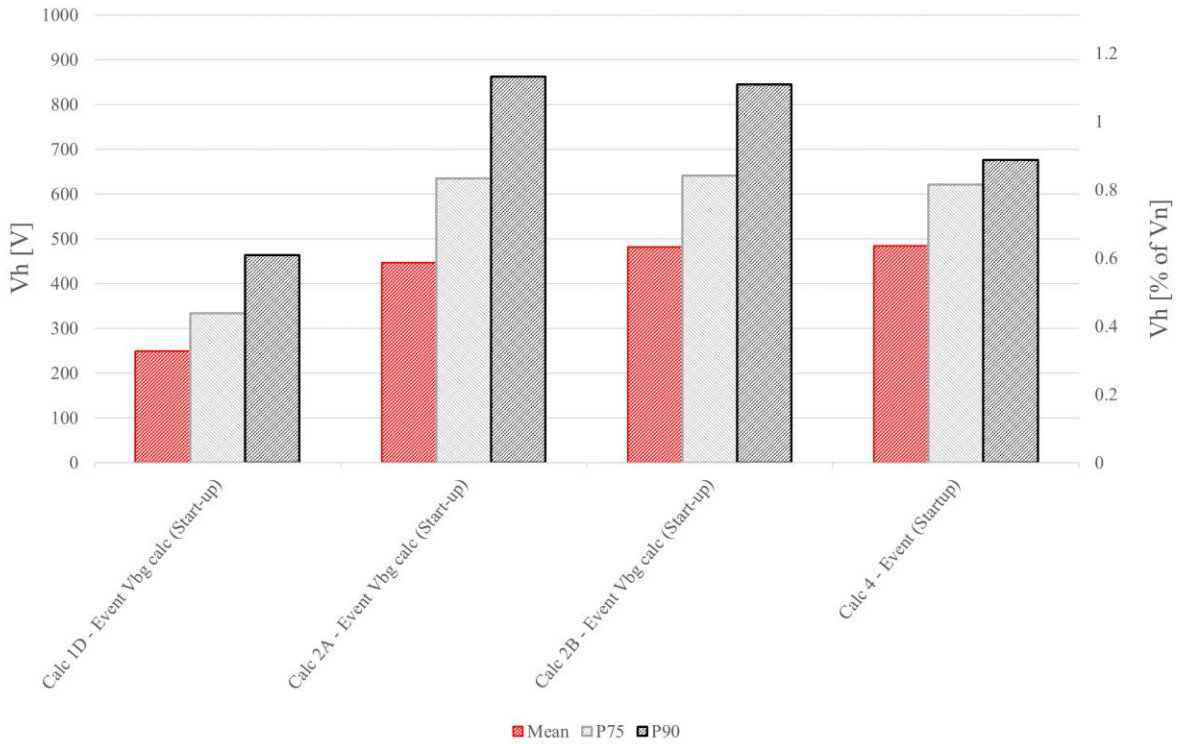

Figure D-20: Comparison of calculation methods for start-up operation (h = 7, red phase)

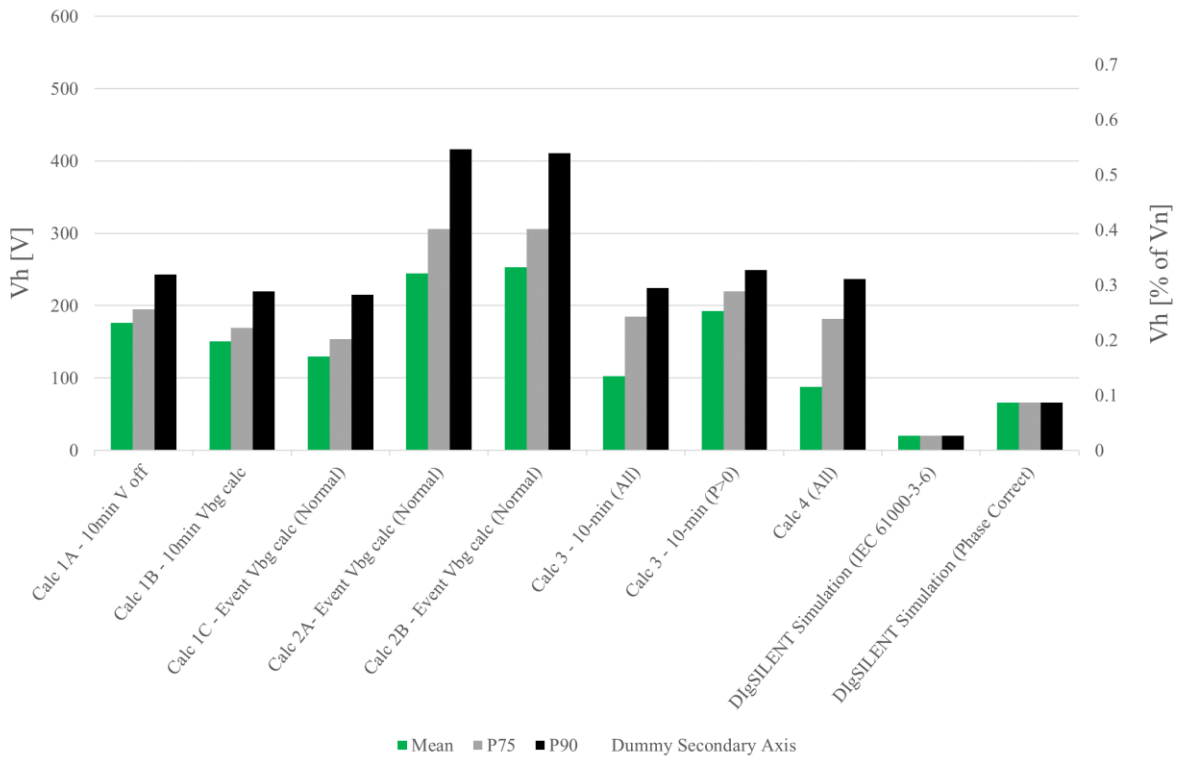

Figure D-21: Comparison of calculation methods for normal operation (h = 7, white phase)

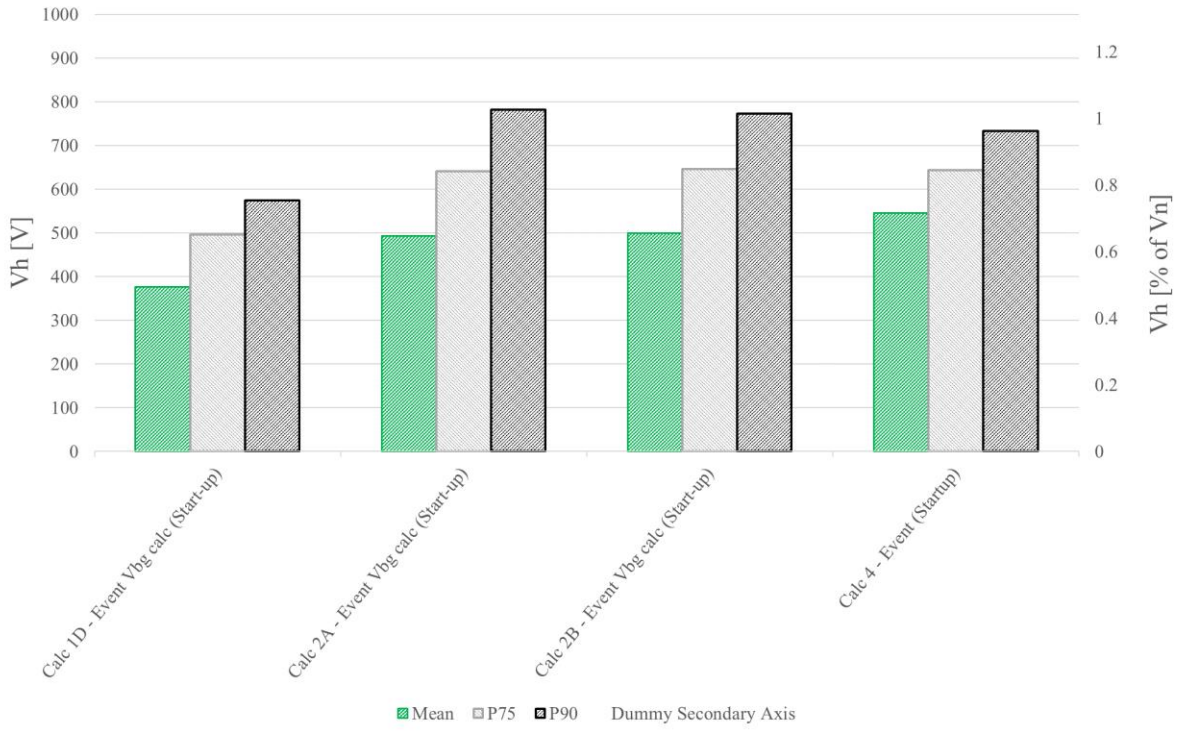

Figure D-22: Comparison of calculation methods for start-up operation (h = 7, white phase)

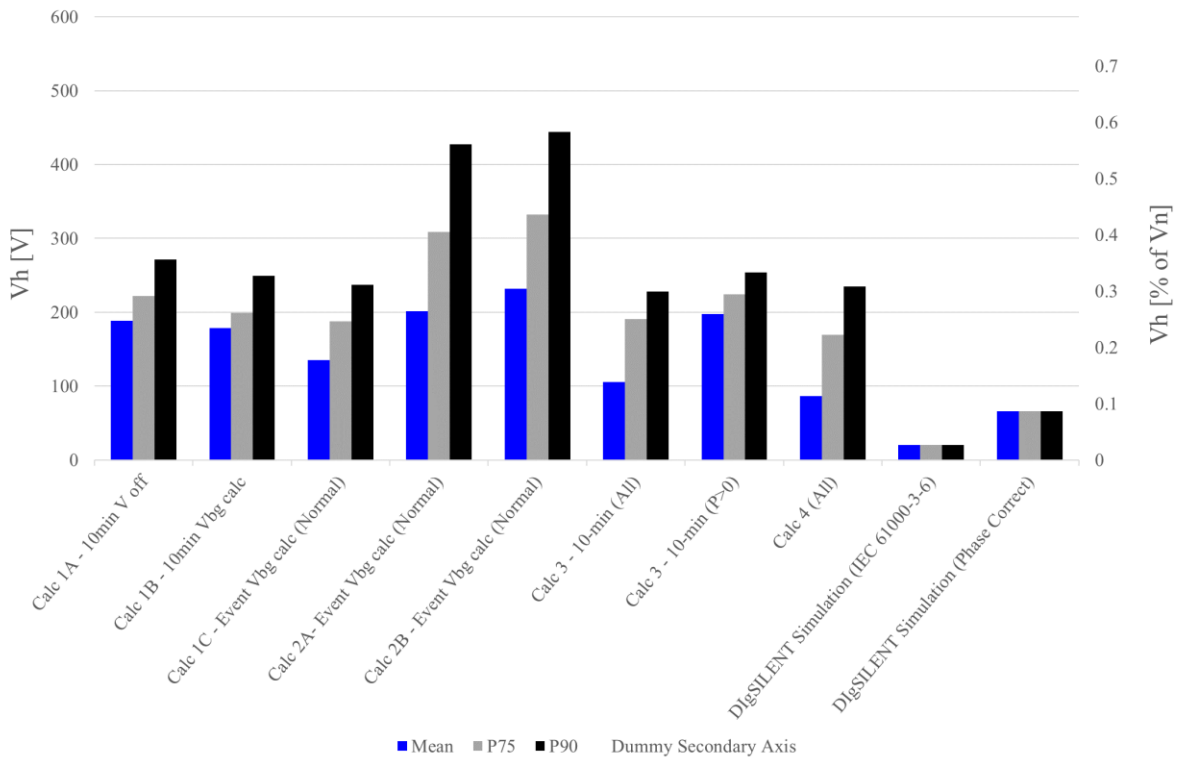

Figure D-23: Comparison of calculation methods for normal operation (h = 7, blue phase)

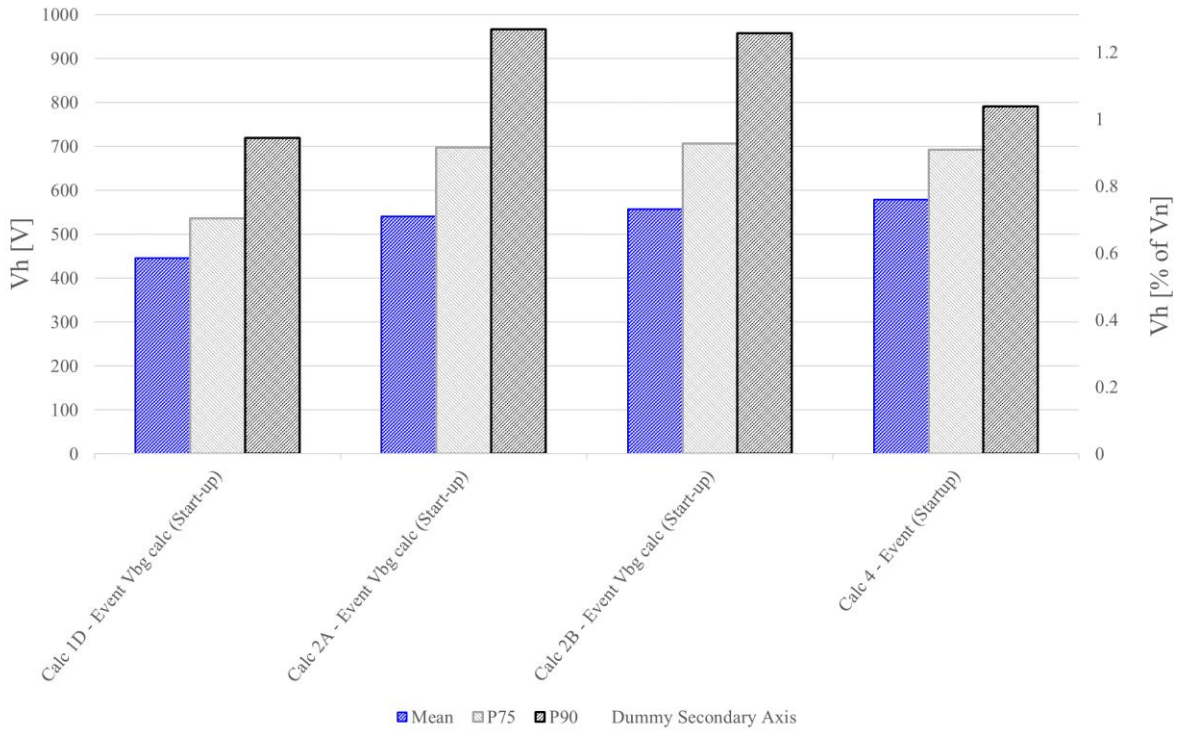

Figure D-24: Comparison of calculation methods for start-up operation (h = 7, blue phase)